CHARACTERIZATION OF THE CARBONATE MUD ROCKS OF THE MIDDLE JURASSIC TUWAIQ MOUNTAIN FORMATION, JAFURAH SUB-BASIN, SAUDI ARABIA; IMPLICATION FOR UNCONVENTIONAL RESERVOIR QUALITY PREDICTION

BY

AHMED MOHAMMED HUSSAIN HAKAMI

A Dissertation Presented to the

DEANSHIP OF GRADUATE STUDIES

KING FAHD UNIVERSITY OF PETROLEUM & MINERALS

DHAHRAN, SAUDI ARABIA

In Partial Fulfillment of the

Requirements for the Degree of

DOCTOR OF PHILOSOPHY

In

GEOLOGY

DECEMBER 2016

KING FAHD UNIVERSITY OF PETROLEUM & MINERALS

DHAHRAN- 31261, SAUDI ARABIA

DEANSHIP OF GRADUATE STUDIES

This thesis, written by **Ahmed Hakami** under the direction his thesis advisor and approved by his thesis committee, has been presented and accepted by the Dean of Graduate Studies, in partial fulfillment of the requirements for the degree of **DOCTOR OF PHILOSOPHY IN GEOLOGY**

Dr. Abdulaziz Al-Shaibani
Department Chairman

Prof. Salam A. Zummo
Dean of Graduate Studies

5/1/17
Date

Dr. Khalid Al- Ramadan
(Advisor)

Dr. Abdulaziz Al-Shaibani
(Co-Advisor)

Prof. Sidiqi Abu-Khamsin
(Member)

Prof. Michael Kaminski
(Member)

Dr. Sedat Inan
(Member)

DEDICATION

This work is dedicated to my parents whose continuous prayers and encouragement were behind achieving my goals, to my wife for being my inspiration, to my kids for bringing me joy and happiness, and finally to my brothers and sisters for always supporting me.

ACKNOWLEDGMENTS

First and foremost, all praises to Allah who helped me to finish this work. Second, I would like to express my sincere gratitude to my advisor Dr. Khalid Al-Ramadan for his continuous support of my Ph.D. research at the King Fahd University of Petroleum & Minerals. Beside my advisor, I would like to thank the rest of my research committee: Dr. Abdulaziz Al-Shaibani, Prof. Sidqi Abu-Khamsin, Dr. Sedat Inan and Prof. Michael Kaminski for their encouragement, insightful comments and valuable advice during my research. This thesis would not have been to a close without the immense help from Dr. Khalid Al-Ramadan and Dr. Sedat Inan, whose almost daily scientific comments were not limited to the bounds of this thesis, but rather extended to my better understanding of the geoscience subject in general. Many thanks for their valuable support throughout my research study.

I also would like to thank the entire Geosciences and Petroleum Engineering Departments for their constant guidance, support, and for creating a friendly environment for me to complete my work. A special thank you goes to my co-workers within the Jafurah asset team at Saudi Aramco for the stimulating discussions. I am also grateful to Saudi Aramco Oil Company Management for approving my residency program at the KFUPM and for providing me with the data used in the study. I look forward to contributing to the Company's continuing success.

Last but not the least, thanks are due to my parents for their prayers, to my wife and kids for their patience and support. Their continuous question "When are you going to finish?" has now found an answer.

TABLE OF CONTENTS

LIST OF TABLES

LIST OF FIGURES

LIST OF ABBREVIATIONS

TOC = Total organic carbon (in weight percent)

MWD GR = Measuring while drilling gamma ray (API)

GRI = Gas research institute

SEM = Scanning electron microscopy

XRD = X-ray diffraction

VSP = Vertical seismic profile

MRI = Magnetic resonance imaging

Ro = Vitrinite reflectance (in percent)

S1 = Free volatile hydrocarbons (in mg HC/g rock)

S2 = hydrocarbon products of kerogen cracking during pyrolysis (in mg HC/g rock)

Tmax = the temperature of peak evolution of S2 hydrocarbons (in ºC)

HI = Hydrogen index (S2/TOC)*100

VRo – eq = Vitrinite reflectance equivalent (in percent)

BitRo = Bitumen reflectance (in percent)

K = Permeability (mD)

SW = Water saturation (in percent)

AVO = Amplitude variation with offset

AI = Acoustic impedance (g.ft/ (cm^3.s)

SI = Shear impedance

LWD = Logging while drilling

Eh = Static Young's Modulus in horizontal direction

Ev = Static Young's Modulus in vertical direction

ν_h = Poisson ratio in in horizontal direction

ν_v = Poisson ratio in in vertical direction

DFIT = Diagnostic fracture injection test

PLT = Production logging test

PVT = Pressure volume temperature test

IP = Initial production

EUR = Estimated ultimate recovery

ABSTRACT

Name : Ahmed Mohammed Hussain Hakami

Thesis Titles : Characterization of the Carbonate Mud Rocks of the Middle Jurassic Tuwaiq Mountain Formation, Jafurah Sub-basin, Saudi Arabia; Implication for Unconventional Reservoir Quality Prediction.

Major Field : Geology

Date of Degree : December, 2016

The Jurassic organic-rich Tuwaiq Mountain source rock (TQMN) in the Central Arabian basin has long been recognized as the source of conventional hydrocarbons trapped in the supergiant Jurassic reservoirs. Renewed interest in these rocks has revealed major gaps in our understanding of the Tuwaiq Mountain as a reservoir. From unconventional resources standpoint, this research provided focus points for Unconventional resources evaluation through detailed geochemical and petrophysical characterization, multidiscipline data integration, and basin modeling. The focus of this research is on the Jafurah Sub-Basin, which is a new frontier unconventional exploration play equivalent in size to the successful Eagle Ford play in south Texas. The basin is located immediately east of the supergiant Ghawar Oil Field, east Saudi Arabia. The spatial distribution of Tuwaiq Mountain lithofacies in the Jafurah Sub-Basin was assessed at different scales, from an outcrop scale to a detailed core description by SEM and optical microscopy. Six distinct lithofacies in the Tuwaiq Mountain Formation have been recognized on the cores obtained from the five wells included in this study. Based on a detailed petrophysical characterization of the Tuwaiq Mountain Formation, the formation has been divided into three tiers possessing varying reservoir qualities. Of these tiers, the bottom Tier 1, which is composed of lime

mudstone with excellent shale gas characteristics such as high total organic carbon (TOC) content up to 10%, low clay content (3-5%) and high porosity. The formation is also in the proper maturity window for hydrocarbon generation and relatively shallow; making it attractive for an economic unconventional shale gas play. Tier 2 and Tier 3 are also potential unconventional reservoirs but of less quality. A workflow for characterizing the Tuwaiq Mountain Formation as a potential unconventional liquid rich gas play has been established. This includes the development of a reservoir quality predictive model for acreage grading, sweet spot identification and fracturing stage selection. This methodical approach is applicable to the evaluation of any emerging unconventional play. In addition, new mud gas isotope logging (MGIL) methodology was tested and revealed important gas characterization potential enabling clear distinction between Middle and Upper Jurassic source rocks gases based on their isotopic signature. New methane carbon isotopic maturity correlation for the main Tuwaiq Mountain source rock has been calibrated and successfully tested: $\mathbf{Vitrinite\ Reflectance\ Equivalent\ (Vre)} = \mathbf{0.069}\ \boldsymbol{X}\ \boldsymbol{\delta 13C1} + \mathbf{5.13} - \mathbf{0.3}$. This finding has permitted accurate maturity assessments providing identification of the best sweet spots predicted for optimal Tuwaiq Mountain production potential. In addition, a detailed Basin Modeling work has been conducted to investigate the burial and thermal maturity evolution and hydrocarbon generation from the Tuwaiq Mountain Formation. Modeling results suggest that high temperature gradient areas of the basin requires higher basement heat flow input, which leads to satisfactory match between measured and predicted maturity, as well as measured versus predicted temperature at present day. This increase of basement heat flow in areas of higher temperature gradient is supported by the interpreted change in crustal composition (e.g., granitic basement) with higher radiogenic

heat generation potential. The modeling results also suggest that TQMN source rocks started generating oil at about 100 Ma and they reached the peak oil generation at about 70 Ma, and at Present, they are at a wet gas generation window in warmer (≥28 °C/km) parts of the basin (the northern and eastern part of the Jafurah Sub-Basin). An integration of outputs from geoscience workflows with multidiscipline data such as microseismic and hydraulic fracturing modeling was conducted to characterize the Tuwaiq Mountain and to provide insights on drainage strategies. Completion optimization and field development scenarios for two possible development scenarios have been illustrated. Based on this research, it was realized that assuming improper fracture geometries, matrix permeability and reservoir drainage models has severe consequences on optimal and economic development of an unconventional field. To supplement planning of initial pilots for understanding completion design and well spacing, investigation of possible fracture half-length has been undertaken. Results from this effort suggest that fracture half-length ranges between 400 ft and 800 ft, which can be used as an initial consideration for field development planning.

ملخص الرسالة

الاسم الكامل: أحمد محمد حسين حكمي

عنوان الرسالة: دراسة جيولوجية لوصف وتقييم المكامن الغير تقليدية (الغاز الصخري) لصخور كربونات الطين – الجوراسي الأوسط، تكوين جبل طويق البترولي -حوض الجافوره الفرعي-شرق المملكة العربية السعودية.

التخصص: جيولوجيا

تاريخ الدرجة العلمية: ديسمبر 2016

منذ فترة طويلة تم التعرُّف على صخور جبل طويق المصدرية الغنية بالمواد العضوية من العصر الجوراسي في الحوض المتوسط للمنطقة العربية على أنَّها المصدر الرئيسي للهيدروكربونات المحتجزة في مكامن العصر الجوراسي العملاقة. ومع ذلك فإن تجديد الاهتمام بهذه الصخور كشفَ فجوات عميقة في فهمنا للطبيعة المكمنية لجبل طويق. عند محاولة النظر الى الأمر من وجهة الموارد الغير تقليدية (الغاز الصخري)، فإن هذا البحث يقدِّم نقاط مركزة لتقييم الموارد الغير تقليدية عن طريق دراسة تفصيلية للخصائص الجيوكيميائية، والأوصاف البتروفيزيائية، ودمج بيانات متعددة المجالات، وتصميم النماذج. تتركز الدراسة في هذا البحث على حوض الجافوره الفرعي، والذي يعتبر منطقة استكشافية جديدة للموارد الغير تقليدية (الغاز الصخري) في المملكة العربية السعودية. هذا الحوض الفرعي مطابق في الحجم لحوض الغاز الصخري إيقل فورد المنتج للغاز والزيت في جنوب تكساس في الولايات المتحدة الأمريكية. يقع حوض الجافوره في المنطقة الشرقية للمملكة العربية السعودية والى الشرق من حقل الغوَّار النفطي العملاق. تم تقييم التوزيع المكاني للسحن الطبقية لجبل طويق في حوض الجافوره على مستويات مختلفة، ابتداءً من التكشفات الصخرية الكبيرة فوق سطح الأرض وانتهاءً بالتوصيف المفصل للعينات الصخرية الصغيرة، والعينات المجهرية الرقيقة. تم التعرف على ست سحن طبقية في تشكيل جبل طويق ودالك من خلال العينات الصخرية التي تم الحصول عليها من الآبار المُدرجة في هذه الدراسة. كما تم اجراء توصيف بتروفيزيائي مفصَّل على تشكيل جبل طويق في حوض الجافوره. بناءً على هذه الدراسة تم تقسيم التشكيل الى ثلاثة مستويات تختلف في جودة المكمن. المستوى الأول في الجزء السفلي يمتلك أفضل صفات الغاز الصخري، مثل نسبة مجموع الكربونات العضوية (TOC) المرتفعة، ونسبة الطين المنخفضة، ونسبة المسامية المرتفعة ومع درجة نضوجه عالية نسبياً لتوليد الهيدروكربونات وفي عمق يعتبر ضحلاً نسبياً، مما يجعله جذاباً من الناحية الاقتصادية لموارد الغاز الصخري. المستوى الثاني والثالث يعتبران مكامن غير تقليدية أيضاً ولكن بنسبة وجودة أقل من المستوى الأول. تم وضع خطة محددة لسير العمل من أجل توصيف تشكيل جبل طويق كأحد الموارد الغير تقليدية للغاز والسوائل. تتضمن طريقة العمل تطوير نموذج مفترض لجودة المكمن، وتحديد المناطق المفضلة للتجمعات البترولية، واختيار مراحل التكسير المائي. هذه الطريقة المنهجية تعتبر من الطرق المستخدمة عالمياً لتقييم المكامن الغير تقليدية، بالإضافة الى ذلك، تم اختبار طريقة تسجيل نظائر الغاز الطيني (MGIL) الجديدة، وكشفت عن امكانية الفصل الواضح عن طريق البصمة المميزة لنظائر الكربون بين الجزئين الأوسط والأعلى للصخور المصدرية ذات العمر الجوراسي. شملت هذه الدراسة توصيف جديد لعلاقات نضوج نظائر

غاز الميثان على الصخور المصدرية لتشكيل جبل طويق، وتمت معايرة النتائج واستنتاج معادله حسابيه جديده واختبارها بنجاح:

$$\textbf{Vitrinite Reflectance Equivalent (Vre)} = 0.069\,X\,\delta 13C1 + 5.13 - 0.3.$$

هذه المعادلة سمحت بتقييم دقيق لدرجات النضوج، وحددت المواقع المفضلة والمقترحة لأقصى درجات الانتاج الممكنة. بالإضافة الى ذلك، تضمن هذا البحث عمل نموذج تفصيلي للحوض الرسوبي من أجل التحقيق في عملية الدفن وتطور النضوج الحراري في تشكيل جبل طويق خلال الزمن الجيولوجي. نتائج النموذج تقترح أن مناطق معدلات الحرارة المرتفعة تتطلب مدخلات تدفق حراري عالي في الحوض الرسوبي، وهذا يقود الى مخرجات مرضية متوافقة بين قيم النضوح المقاسة والمتوقعة، بالإضافة الى درجات الحرارة المقاسة والمتوقعة في الوقت الحاضر. زيادة قيم التدفق الحراري في الحوض الرسوبي في المناطق ذات معدلات الحرارة المرتفعة يتوافق مع تفسير التغير التركيبي في تركيب القشرة الأرضية في قاع حوض الجافوره (مثال: الجرانيت)، والذي يعني توليد المزيد من الحرارة الاشعاعية. نتائج النموذج تقترح أن الصخور المصدرية لتشكيل جبل طويق بدأت توليد النفط منذ حوالي مائة مليون سنة، ووصلت الى قمة توليدها منذ سبعين مليون سنة. في الوقت الحالي تتواجد هذه الصخور في النافذة الرطبة لتوليد الغاز في مناطق أدفأ بمعدل 28 درجة سيليزية في الكيلومتر الواحد من الحوض الرسوبي (المناطق الشمالية والشرقية من حوض الجافوره). دمج المعلومات والنتائج من الدراسة الجيوعلمية مع البيانات متعددة الأصول كالبيانات السيزمية الصغرى، ونموذج التكسير المائي ساعد على توصيف جبل طويق والحصول على بعض التنويرات على آليات الانتاج. وقد تم توضيح آلية التحسين وسيناريو تطوير الحقل لنموذجين مميزين للمكمن، هذان النموذجان يتطلبان نفاذية صخرية مختلفة. بناءً على هذا البحث تم إدراك أن افتراض مخططات هندسية خاطئة لآليات التكسير، والنفاذية الصخرية، ونماذج انتاج المكامن له عواقب انتاجية واقتصادية على حقول الموارد الغير تقليدية. لاستكمال التخطيط الحقلي والتمكن من فهم التصميم المثالي للمسافات بين الآبار، تم التحقيق في نماذج التكسير وتداخل الإنتاجية بين الآبار باستخدام نماذج محاكاة المكمن. نتائج هذه الدراسة وفرت مفاهيم منطقية لتصميم المسافات بين الآبار لتفادي التداخل في عمليات الانتاج.

CHAPTER 1

Introduction

The Middle-Upper Jurassic, organic-rich carbonate mudrocks, of Tuwaiq Mountain Formation of the Arabian Basin have long been recognized as a source of hydrocarbons trapped primarily in Upper Jurassic carbonate reservoirs. With the development of commercial hydrocarbon production of unconventional reservoirs in North America, these organic-rich, carbonate mudrocks (traditionally classified as shales or marls) are now recognized not only as source rocks and seals but also as potential reservoirs. This paradigm shift has changed our perception about what we call "peak oil" and the future of the oil industry. The definitions of unconventional gas reservoirs and resources has its origins in North America, where in the late 1970s the U.S. government applied a definition to tight (i.e., low-permeability) gas reservoirs (mainly sandstones) as those with expected reservoir-permeability of less than 0.1 md, and porosity of less than 10%, to determine which well operation would receive tax credits and/or higher gas prices. The first industry/academia definition for Unconventional reservoir was coined by Holditch (2006) who defined a tight gas reservoir as "the reservoir that cannot be produced at economic flow rates nor in economic volumes of natural gas unless the well is stimulated by a large hydraulic fracture treatment, a horizontal wellbore, or by using some other technique to expose more of the reservoir to the wellbore."

It is expected that the organic rich interval of the Tuwaiq Mountain Mudrocks may contain significant quantities of trapped hydrocarbons; similar to proven unconventional shale resources in North America. Research performed earlier was insufficient to determine the hydrocarbon resource potential of the Tuwaiq Mountain Mudrocks. This might be due to the limited subsurface data and, therefore, limited understanding of the rock characteristics. With the exception of some source rock data, detailed analytical data did not exist on the Tuwaiq Mountain mudrocks in the Jafurah Basin, East of the Ghawar field.

Accurate assessment of unconventional gas/oil resources or mudrocks requires multidisciplinary evaluation of many key variables that play a role in both the reservoir quality, as well as the completion quality. Organic matter type, richness, level of thermal maturity, clay type and content, matrix porosity, intra-kerogen porosity, permeability, brittleness, thickness, reservoir pressure, natural fractures, hydrocarbon viscosity and hydrocarbon saturations are some of the many essential attributes of given shale to qualify it as a potential gas/oil reservoir. In addition to the above, a pre-requisite for a commercially viable unconventional reservoir depends on the proper burial history and timing of hydrocarbon generation. This enables the estimation of the amount of hydrocarbons that have been expelled and retained.

It has been the aim of this research to conduct an integrated study that will enable understanding of the organic and inorganic controls on the Tuwaiq Mountain Mudrocks (shales); and its implications for Unconventional Reservoir Quality Prediction.

5.1 Thesis Summary

This section gives some general outline of this thesis:

CHAPTER TWO

This chapter reviewed the geological setting of the study area and assess the spatial distribution of Tuwaiq Mountain lithofacies in the Jafurah basin. Different scales of work were conducted, from an outcrop scale to a detailed core description, SEM and thin sections. Tectonically, the Mesozoic basins in the Arabian Plate were formed because of the Late Permian and Early Triassic opening of the adjacent Neo-Tethys Ocean and the subsequent development of localized passive margins. Differential subsidence within the shelf, combined with a relative increase in sea level, led to the formation of relatively short-lived intra-platform sub-basins that served as depocenters. These intra-shelf sub-basins, formed within the interior of a broad extensive shallow water carbonate platform that was separated from the open ocean to the east by a high-energy platform margin. Three sub-basins in the Arabian platform has been identified (Gotnia basin, Central Arabian basin, and South Arabian Gulf basin). The Jafurah sub-basin sits within the Central Arabia basin. The Jurassic succession of the Arabian Plate consists predominantly of marine carbonates that were deposited on the Arabian platform. Variation in the sedimentary facies throughout the Jurassic is attributed to eustatic sea level rise and fall. Six distinct lithofacies in the Tuwaiq Mountain Formation have been recognized on the cores obtained from the wells included in this study. From shallowest to deepest, the following lithofacies are recognized:

1- Shallow marine bioturbated lithofacies, oxic

2- Deep marine bioturbated lithofacies, oxic

3- Horizontal bioturbated lithofacies, dysoxic

4- Laminated lithofacies with storm ripples, anoxic

5- Laminated lithofacies without ripples, anoxic

6- Massive anoxic lithofacies

CHAPTER THREE

The Middle to Upper Jurassic organic-rich mudrocks are recognized as the source of oil in the Ghawar and many Jurassic oil fields in the eastern province of Saudi Arabia. These source rocks, notably the Jubaila and Tuwaiq Mountain, and to lesser extent Hanifa Formations possess excellent hydrocarbon attributes such as high total organic content (TOC), and sufficient maturity, combined with a relatively shallow burial depths, allowing for economical unconventional shale gas and shale oil exploitation. Mud gas isotope logging (MGIL) data obtained from wells used in this research revealed important gas characterization potential enabling clear distinction between Tuwaiq Mountain, Hanifa, and Jubaila Formation gases, based on their isotopic signature. A new methane carbon isotopic maturity correlation for the main Tuwaiq Mountain source rock has been calibrated and successfully tested: $\mathbf{Vitrinite\ Reflectance\ Equivalent\ (Vre) = 0.069\ X\ \delta 13C1 + 5.13 - 0.3}$. This finding has permitted accurate maturity assessments providing identification of the best sweet spots predicted for optimal Tuwaiq Mountain

production potential. This chapter reviewed the application of MGIL for gas characterization.

CHAPTER FOUR

This chapter provided a detailed Basin Modeling work that was conducted to investigate the burial and thermal maturity evolution and hydrocarbon generation from the Tuwaiq Mountain Formation. Five wells, representing the unconventional gas exploration wells drilled in the Jafurah Sub-Basin have been selected for 1D and 2D basin modeling work. The maturity of the Tuwaiq Mountain Formation intersected in five wells varies from 0.8 to 1.25 %VRE despite only slight differences in burial depths. Modeling results suggest that higher temperature gradient areas of the basin requires higher basement heat flow input, which leads to satisfactory match between measured and predicted maturity as well as measured versus predicted temperature at present day. This increase of basement heat flow in areas of higher temperature gradient matches the interpreted change in crustal composition (e.g., granitic basement) generating more radiogenic heat. The modeling results suggest that TQMN source rocks started generating oil at about 100 Ma and they reached the peak oil generation at about 70 Ma, and at present, they are at a wet gas generation window in warmer (≥28 °C/km) parts of the basin (the northern and eastern part of the Jafurah Sub-Basin). The central and southwestern part of the basin are cooler, and here, the TQMN source rocks are within the peak oil generation maturity window. The warmer parts of the basin have higher gas potential for the TQMN source rocks compared to cooler parts of the basin.

CHAPTER FIVE

This chapter provides a detailed petrophysical characterization of the Jurassic Tuwaiq Mountain Formation in the Jafurah Sub-Basin. Based on this research, the formation has been divided into three tiers possessing varying reservoir qualities. Of these tiers, the bottom Tier 1 possesses the most excellent shale gas characteristics such as high total organic content (TOC), low clay content and high porosity. Tier 2 and Tier 3 are also potential unconventional reservoirs but of less quality. The formation is also in the proper maturity window for hydrocarbon generation and relatively shallow, making it attractive for an economic unconventional shale gas play. Three wells, representing the first unconventional reservoir exploration wells drilled in the Jafurah Sub-Basin have been selected for detailed characterizations. The wells were drilled vertically, cored and logged. Wells were then sidetracked with 5,000 ft horizontal laterals and stimulated through multistage hydraulic fracturing. All stimulated wells flowed gas and condensate to surface. This chapter summarizes, with examples, a workflow for characterizing the Tuwaiq Mountain Formation as a potential unconventional liquid rich gas play. Crucial to this, is the development of a reservoir quality predictive model for acreage grading, sweet spot identification and fracturing stage selection. This methodical approach is applicable to the evaluation of any emerging unconventional play.

CHAPTER SIX

This chapter demonstrates how integration of outputs from geoscience workflows with multidiscipline data, such as microseismic, production logs, and hydraulic fracturing

modeling help to characterize an unconventional reservoir, and provide insights on drainage strategies. Completion optimization and field development scenarios for two ultra-low matrix permeability type have been illustrated. Based on this research, it was realized that assuming wrong fracture geometries, matrix permeability, and reservoir drainage models, impacts the optimal and economic development of an unconventional field. To supplement planning of initial pilots for understanding completion design and well spacing, investigation of fracture half-length using simulation models was undertaken. Results from this effort suggest that fracture half-length ranges between 400 ft and 800 ft, which can be used as initial considerations for field development planning.

5.2 Study Area

The Jafurah Sub-Basin, located east of the giant Ghawar oil field, is the primary focus of this research study. The basin is located within the shelf part of the Arabian Plate. The Jurassic Tuwaiq Mountain Formation in this basin possesses excellent shale gas characteristics, such as high total organic carbon (TOC) content and low clay content, and it is in the proper maturity window for hydrocarbon generation. The targeted formation is relatively shallow, making it attractive as an economical unconventional shale gas play. Five wells have been selected to represent the various vertical and lateral staking patterns as well as maturity windows to conduct a comprehensive Tuwaiq Mountain unconventional reservoir characterization within the study area (Figure 1-1). A key element of this research is to understand the relationship of the Tuwaiq Mountain Formation with the overlaying and underlying Formations. Therefore, outcrop of Tuwaiq Mountain type section, west of

Riyadh, along Darb Al-Hijaz, was measured by GR to construct a synthetic log from the outcrops for possible correlation with logs from wells used in the study.

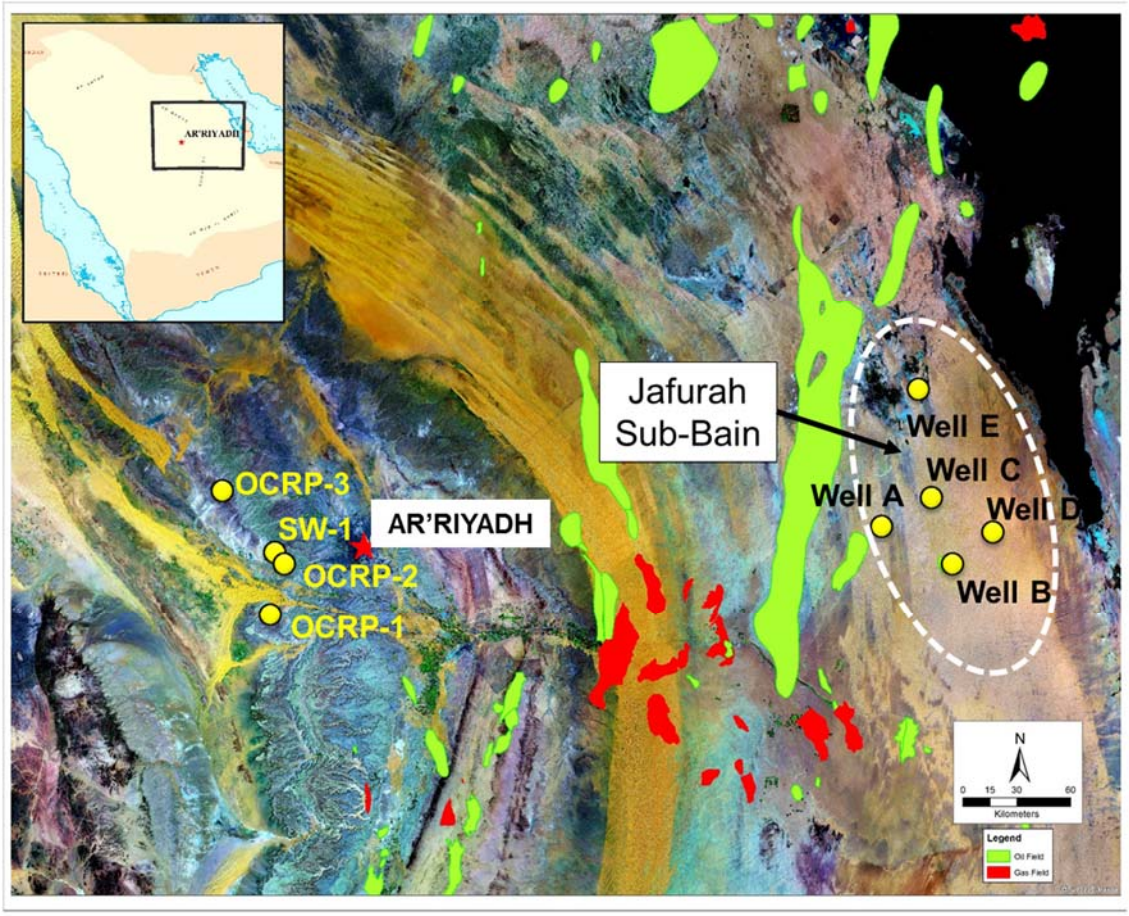

Figure 1-1 Landsat image of the East-Central Saudi Arabia, showing the Ghawar giant oil field, the approximate outline of Jafurah Sub-Basin (dashed white line), the five wells used in the study, the three outcrop locations (OCRP-1-3), and the shallow well (SW-1).

5.3 Problem Statement

Organic rich mud rocks are currently targeted for unconventional oil and gas exploration and development in many places around the world, including Saudi Arabia. These types of plays are very challenging to develop as they exhibit pronounced lithofacies heterogeneity,

both laterally and vertically. In addition, hydrocarbon resources associated with such plays are harder to access and extract when compared to conventional reservoirs. The Tuwaiq Mountain carbonate source rocks in the Jafurah Sub-Basin have become an important unconventional prospect in the Kingdom but the understanding of what rock properties are the drivers for this play are still unclear. It is the aim of this research to conduct an integrated study that will enable understanding of geological, geochemical, and petrophysical controls on the Tuwaiq Mountain Mudrocks (shales); and their implications for Unconventional reservoir quality prediction and drainage strategy.

5.4 Research Objectives

The purpose of this research is to provide a quantitative assessment of the Tuwaiq Mountain carbonate source rocks as a viable unconventional reservoir. This has been facilitated by the integration of the geological, geochemical, geomechanical and petrophysical data into a model for unconventional reservoir quality prediction and drainage strategy. The following objectives has been achieved throughout the course of this research study:

a) Construct a stratigraphic framework study to understand the spatial distribution of Tuwaiq Mountain lithofacies and rock characteristics. This has been facilitated at different scales from outcrop field-work to detailed core description, and finally to the investigation of the internal structure using SEM and thin sections. The work

include detailed bulk mineralogy by XRD to identify the mechanical behavior of different lithofacies.

b) Conduct a detailed petrophysical evaluation for Tuwaiq Mountain lithofacies using well logs and core data. This includes porosity, permeability, and hydrocarbon saturation measurements to identify the reservoir and non-reservoir facies.

c) Define the distribution of Tuwaiq Mountain source rocks by quantitative characterization of the organic matter type, richness and maturity variation. Use the observed data to develop a well calibrated model for maturity and Total Organic Carbon (TOC) prediction.

d) Conduct basin modeling work to constrain the burial history and model the thermal maturation history at and within the control wells.

e) Integrate the result from the Geoscience and Engineering data to identify the optimal stimulation and reservoir drainage strategy.

5.5 Unconventional Resources: Definition and Importance

Unlike conventional reservoirs that are of high porosity & high permeability and are easy to drain, the unconventional reservoirs are of low porosity (<10%), low permeability (<0.1 md) and they require stimulation to produce at economical flow rate (Holditch, 2006). The resource triangle (Figure 1-2), as described by Holditch (2006), illustrates that the high-quality reservoirs, which are easy to produce, are located at the top of the triangle. Moving away from the top, quality of the reservoirs gets worse where development of the reservoirs requires advance technology and high cost. This resource triangle can be summarized as follows:

- Almost all natural resources are distributed log normally in nature
- Hydrocarbons trapped within high quality reservoirs are small in size, difficult to find but easy to extract
- Toward the base of the triangle, resources become large in volume but require advance technology and cost to extract.

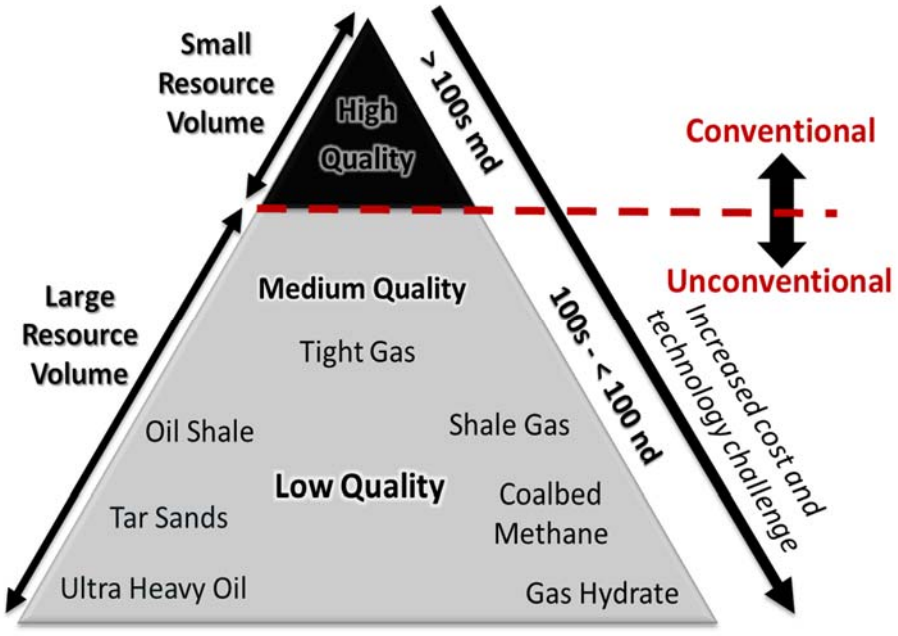

Figure 1-2 The hydrocarbon resource triangle (modified after Holditch, 2006).

According to this resource triangle concept (Figure 1.2), we should expect a log normal distribution of hydrocarbon resources in every basin that produced oil and gas. This concept of the resource triangle has been verified by a number of graduate students (in the Harold Department of Petroleum Engineering at Texas A&M University) who collected production data from over 25 basins in North America, where unconventional reservoirs have been under development for several decades. Results from the data analysis confirmed the resource distribution as suggested by the resource triangle concept (Holditch, 2013).

CHAPTER 2

Geological Setting, Regional Stratigraphic Correlation, Lithofacies, and Petroleum System

2.1 Geological Setting

The Mesozoic basins in the Arabian Plate were formed as a result of the Late Permian and Early Triassic opening of the adjacent Neo-Tethys Ocean (Figure 2-1) and the development of its margins -Tethys passive margins (Ayres et al., 1982; Droste, 1990; and Al-Husseini, 1997). During the Jurassic, the Arabian Plate was located closer to the Equator and differential subsidence within the shelf, combined with a relative increase in sea level, led to the formation of relatively short-lived intra-platform sub-basins that served as depocenters (Pollastro, 2003). These intra-shelf sub-basins formed within the interior of a broad extensive shallow water carbonate platform that was separated from the open ocean to the east by a high-energy platform margin (Ziegler, 2001). The schematic plate reconstruction and cross section in Figure 2-1, highlight the major Jurassic sub-basins in the Arabian platform (Gotnia basin, Central Arabian basin, and South Arabian Gulf basin). The Qatar Arch separates the Central Arabia basin from the Southern Arabian Gulf basin. The Rimthan Arch separates the Central Arabian basin from the Gotnia basin to the north. The focus of this study is on the Jafurah Sub-Basin, which is located within the Central Arabian Intra-shelf basin (Al-Husseini, 1997). Several Jurassic lithofacies have been identified within this basin. Each lithofacies represents a different depositional setting.

Understanding these lithofacies is essential to identifying the optimum unconventional target for the horizontal drilling program. The Jurassic section of interest for unconventional exploration in the Jafurah Sub-Basin is restricted to the organic-rich source-rocks facies of the Jubaila (early Kimmeridgian), Hanifa (Oxfordian to lower Kimmeridgian), and Tuwaiq Mountain (middle to late Callovian) Formations. These units in the Jafurah Sub-Basin represent the deepest sections of the Jurassic Central Arabian basin in Saudi Arabia. The organic-rich facies were deposited in a deep outer ramp setting, and they are better represented east of Ghawar, south of the Rimthan Arch toward the Qatar Arch. Although source rocks facies from the Tuwaiq Mountain and Hanifa Formations are also found outside the Jafurah Sub-Basin, they have never reach the maximum maturity that they exhibit in the Jafurah Sub-Basin in Saudi Arabia. Despite the presence of organic-rich source rocks within the Jubaila and Hanifa Formations, the Tuwaiq Mountains shows better source rock development in terms of thickness, maturity and lateral continuity, as to be considered a primary target for an unconventional play. For that same reason, most of the discussion in this research will concentrate on this Formation. The Hanifa and the Jubaila are present in the Jafurah Sub-Basin as a secondary target, especially where source rocks facies of the Hanifa are stacked directly above the Tuwaiq Mountain section of interest. The Jubaila source rock represents a separate target restricted to the depocenter of the Jafurah Sub-Basin.

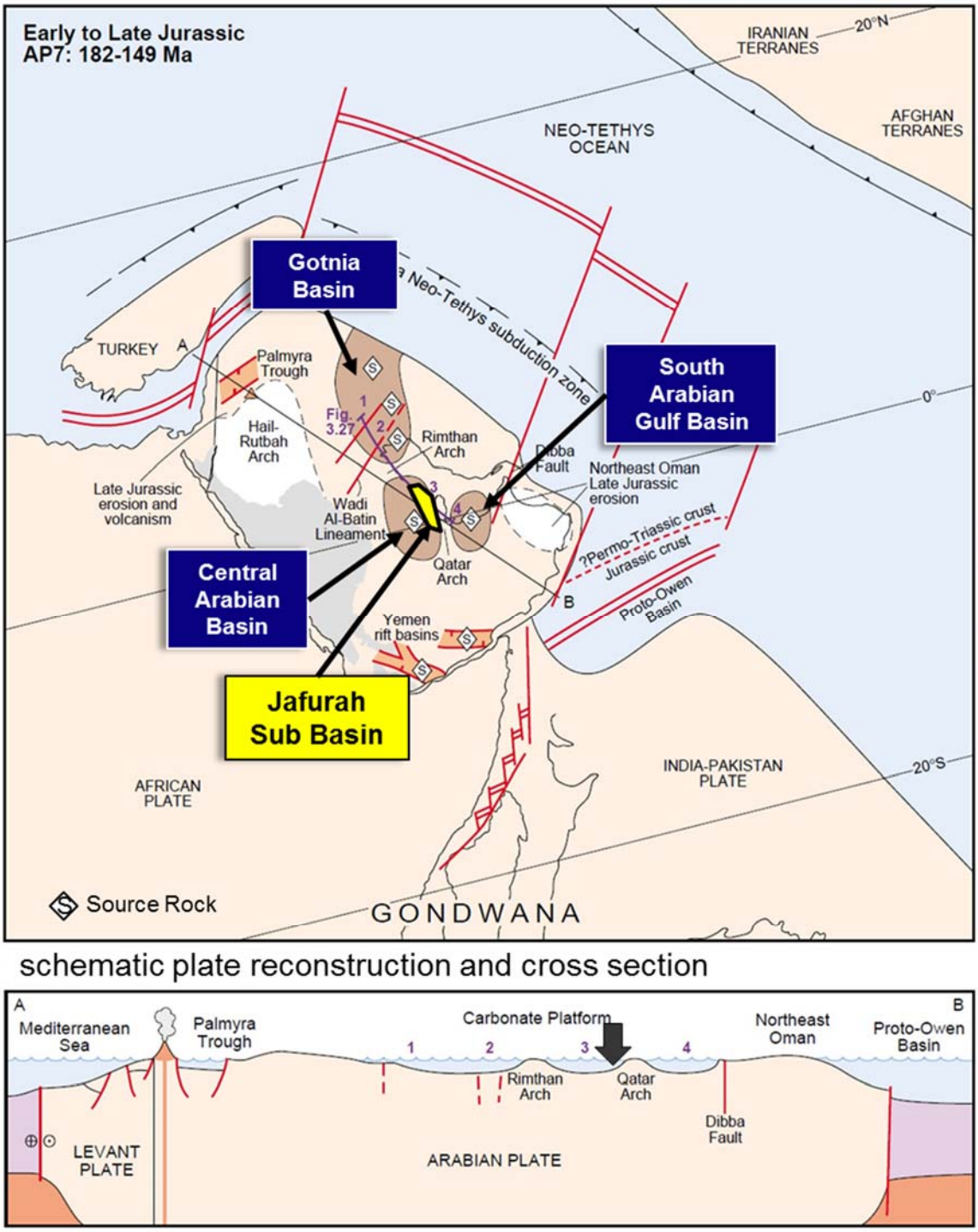

Figure 2-1 Schematic plate reconstruction and cross section for Early to Late Jurassic plate setting modified after Sharland et al., (2001). Major Jurassic sub-basins in the Arabian platform (1/2 Gotnia basin, 3-Central Arabian basin, and 4-South Arabian Gulf basin) are shown in brown color, whereas, the approximate outline of Jafurah sub-basin is shown in yellow.

2.2 Field Work and Regional Stratigraphic Correlation

The Jurassic source rocks intervals in the Jafurah Sub-Basin have originally been described in outcrops west of Riyadh along Darb Al-Hijaz. At the type section, the Jubaila, Hanifa and Tuwaiq Mountain Formations were deposited in a broad open platform ramp system (Murris, 1980). The interval of interest in this study is located some 380 km at the east of the type section, where these units are present in basinal, muddier facies, deposited on a deep outer ramp setting. The combined section for the Jubaila, Hanifa and Tuwaiq Mountain Formations west of Riyadh, has a thickness of approximately 430 meter and it represents a proximal setting. At the center of the Jafurah Sub-Basin, the same interval is only 150 meter, of which 70 to 100 meter correspond to the Tuwaiq Mountain organic-rich source-rock facies.

The Tuwaiq Mountain limestone was first described by Steineke in 1937 as a member of his Tuwaiq Mountain Group. It was redefined as a Formation by Berj et al., in a 1945 internal report of the Arabian American Oil Company, and this report has been since referred as being produced by Bramkamp, who was co-author and probably the person who did the ground work for the stratigraphic framework presented on that report.

The first published mention of the Tuwaiq Limestone was in Arkell, 1952, in a paper describing the Jurassic ammonites from Jebel Tuwaiq where the type section was described. The paper outlined the Jurassic stratigraphy of Saudi Arabia and described some of the type sections for the Jurassic with an introduction to the stratigraphy written by Steineke and Bramkamp. Based on faunal evidence, Arkell assigned a middle Callovian age to the base of the Tuwaiq Mountain Formation.

Powers et al, 1966, subdivided the Upper Dhruma (D7) in two distinct members, the Atash and Hisyan, based on lithological and faunal evidence (Figure 2-2). Powers et al indicate a probable late Bathonian age for the Atash Member citing Arkell, 1952, and mentioned that the fossils in the Hisyan Member were closely related to the lower part of the Tuwaiq Mountain Formation, concluding that the upper part of the Hisyan Member was not older than Callovian. Powers et al provide a detailed discussion on how the placement of the limit between the Dhruma and the Tuwaiq evolved in the early days of regional mapping by the Arabian American Oil Company and suggest that the contact between the Dhruma and the Tuwaiq Mountain is transitional, located between the Atash and the Hisyan Member and partially conformable from Qiba to Al Haddar.

In 1983, Vaslet et al., informally subdivided the Tuwaiq Mountain Formation into three members (from oldest to youngest); T1, T2 and T3 (Figure 2-2), which correspond to their informal names Baladiyah, Maysiyah, and Daddiyah. They considered the Atash and Hisyan Members as part of the upper Dhruma (D7) and assigned Early to Middle Callovian? age to the Upper Dhruma and Middle to Late Callovian to the Tuwaiq Mountain. They indicate that the whole Callovian sequence is transgressive. Le Nindre et al, 1983, points to a major sedimentological and paleontological break at the base of their unit D7 (Atash), but states that, at that moment, it is not possible to established whether or not there was a hiatus in the lower Callovian.

Le Nindre et al., 1990, added the Atash and Hisyan members to the Tuwaiq Mountain, as those two members together with T1 member make a third-order depositional sequence. This interpretation has been adopted by others including Al Husseini, 1997; Hughes, 2004; Hughes 2009; and Cantrell et al., 2014. Al Ibrahim, 2014, indicated that the Atash and

Hisyan represent the transgressive system track of a third-order depositional system and the T1 member represents the high stand systems tract. T2 and T3 members represent a younger third-order sequence.

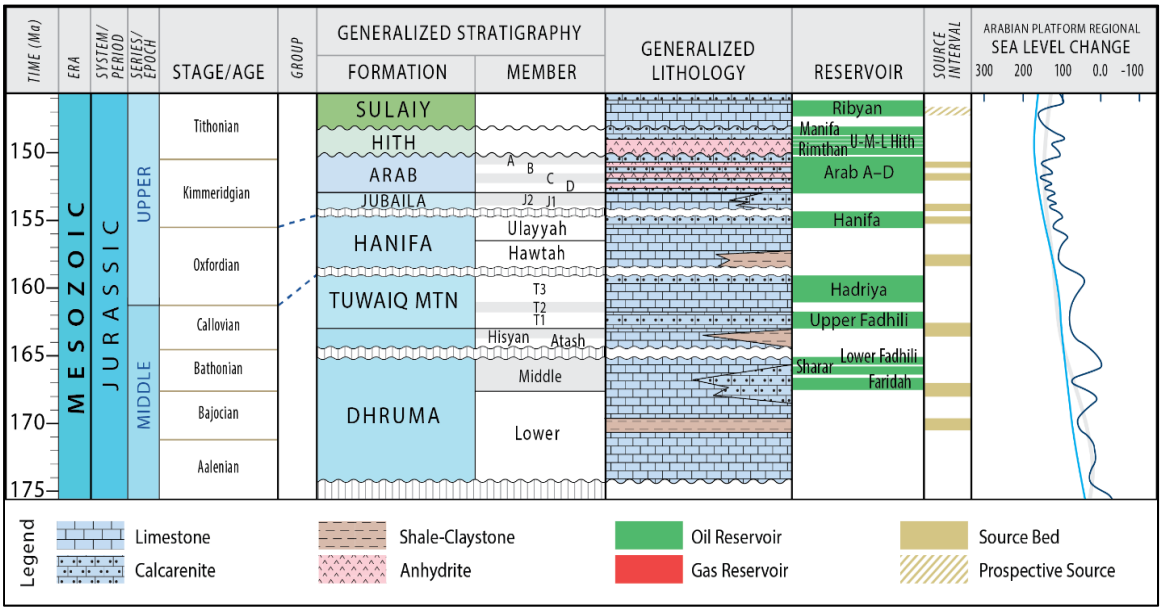

Figure 2-2 Generalized geologic column of the Middle and Upper Jurassic Epoch (after Cantrell et al., 2014).

2.3 The Relationship between TQMN and the Adjacent Formations

To better understand the relationship between the units described in the Jurassic type section and those in the subsurface of the Jafurah Sub-Basin, two field trips were conducted as part of this study. The first one took place in late May, and the second was carried out in October of 2015. The main objective of the field work was to construct a synthetic composite GR log of the Tuwaiq Mountain outcrops for possible correlation with the subsurface. Three outcrops locations were measured and logged with GR. These outcrops are White Cement Factory (OCRP-1); Makkah Road (OCRP-2); and End of the World (OCRP-3; Figure 2-3). The outcrop sections comprise the base of the Tuwaiq Mountain

(T1) down to the D6 Limestone of the Dhruma Formation. Fieldwork around the White Cement Factory (WCF; Figure 2-3b) helped to identify the basal contact between the D6 Limestone of the Dhruma Formation and the Atash Member. It is worth mentioning that an oyster bed was found above the base of the Hisyan member, which turned-out to be a regional marker. A complete section from the D6 to the middle of the Hisyan Member was measured and logged at the WCF with a clear indication of the stratigraphic position of the Oyster bed located 11.3 m (37 ft) above the contact between the Atash and Hisyan Members (Figure 2-4). At about 20 km northeast of the WCF, a second section (OCRP-2; Figure 2-3c) was measured from the lower of Tuwaiq Mountain Formation to the upper contact with Hanifa Formation. About 50 km north of the WCF, a third section (OCRP-3; Figure 2-3d) was measured from the Oyster bed up to what appears to be a maximum flooding surface in the logged section. A synthetic composite GR log from the top of Hanifa Formation all the way down to Dhruma Formation was built based on GR data collected at the three outcrop locations (Figure 2-5). This synthetic composite GR log was also refined using GR data obtained from a shallow well (SW-1) drilled closed to OCRP 2 (Figure 2-3a). The shallow wells have log and core data from the top of Hanifa all the way to the lower part of Tuwaiq Mountain Formation, without reaching Dhruma Formation. Using the synthetic composite GR log to drive a regional stratigraphic correlation between the outcrop and the subsurface wells was very challenging for several reasons. First, it is not a one-to-one correlation, as it represents correlating the proximal facies to the distal facies, which is not possible. Second, the distance between the outcrops and the subsurface wells in the Jafurah sub basin is large (~ 400 km), which increase the uncertainty in the correlation. Therefore, the regional stratigraphic correlation work for Tuwaiq Mountain

Formation was limited to the sub-surface wells. Figure 2-6 shows the stratigraphic cross section correlation between the Jafurah subsurface wells (Well A, Well B, Well C, Well D, and Well E). This cross section was constructed to understand the spatial distribution of the Tuwaiq Mountain Formation in the study area.

The correlation suggests that the thickness of the Tuwaiq Mountain Formation across the investigated wells is relatively uniform (100 ft. – 150 ft.), whereas, the Hanifa Formation is of various thickness between 50 ft in Well D to 200 ft thick in Well E. This formation is marked from the top by the presence of a thin anhydrite layer as indicated by the density logs. One interesting observation from this correlation is the identification of a source rock facies at the base of the Jubaila Formation, as shown by the high GR in Figure 2-6. The thickness of this potential source facies increases from 40 ft at well A to >200 ft. at Well E. This implies a potential shale gas target that worth to be evaluated.

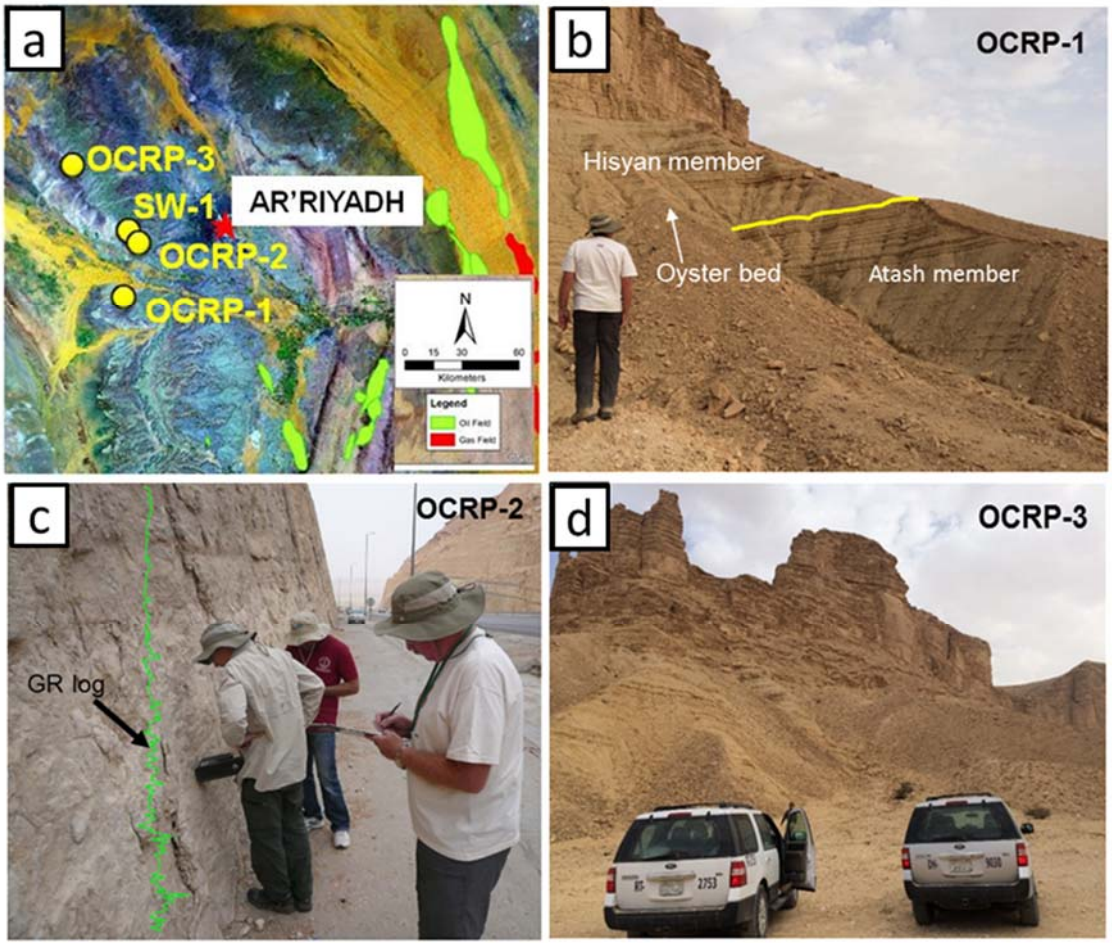

Figure 2-3 a) Map of the three outcrop locations, b) Field photo of the OCRP-1 north White Cement Factory, where the Atash and lower part of the Hisyan members were measured and described, c) Photo of the Tuwaiq Mountain Formation at OCRP-2 along Makkah Road, west of Riyadh, d) Field photo showing Tuwaiq Mountain in OCRP- 3 at the End of the World section.

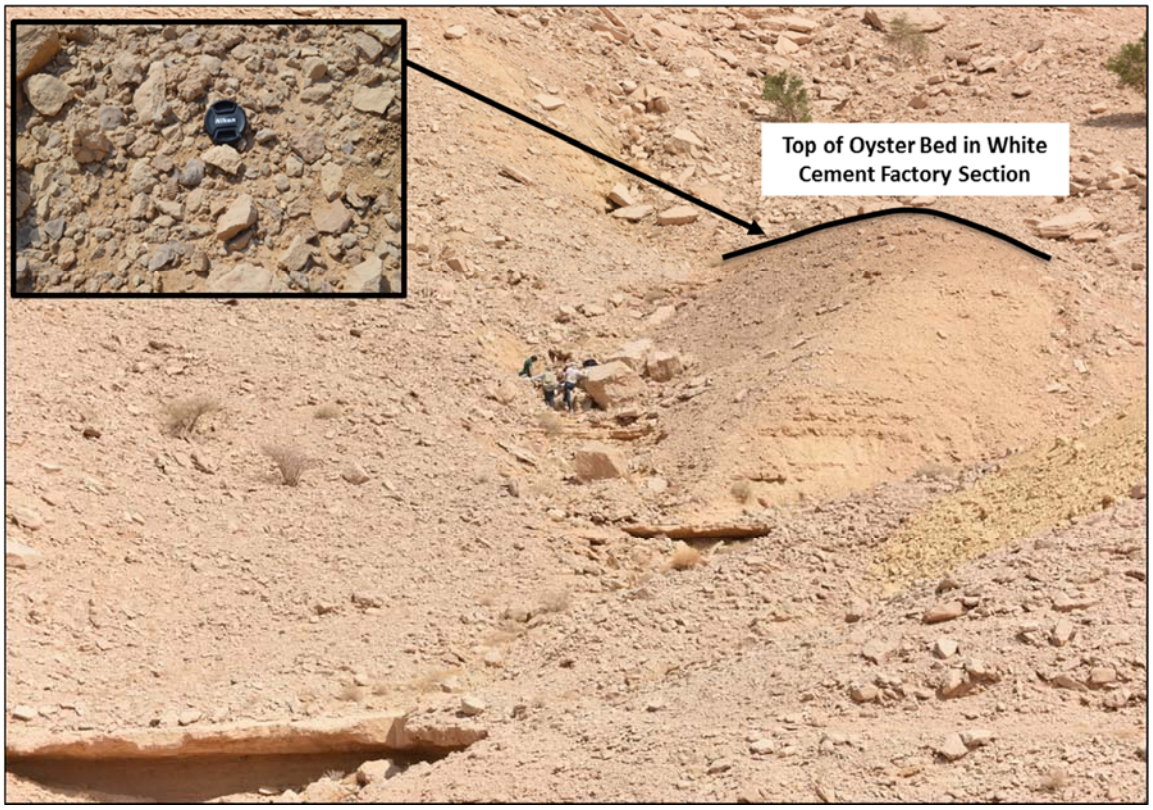

Figure 2-4 Filed photo outlining the stratigraphic position of the Oyster bed located 11.3 m (37 ft) above the contact between the Atash and Hisyan Members. North of the white cement factory

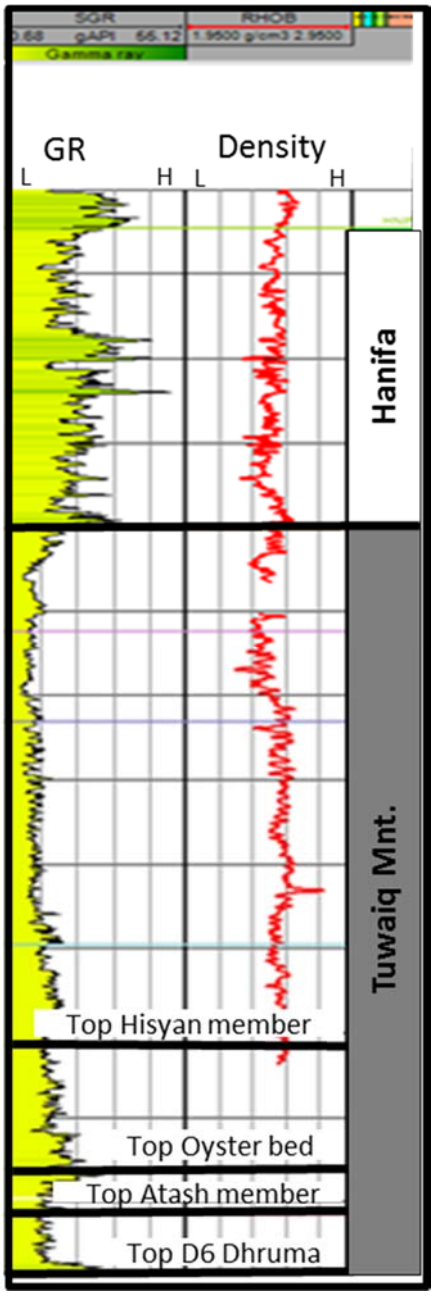

Figure 2-5 A synthetic composite GR log of the Middle Jurassic at the three outcrop locations, west of Riyadh.

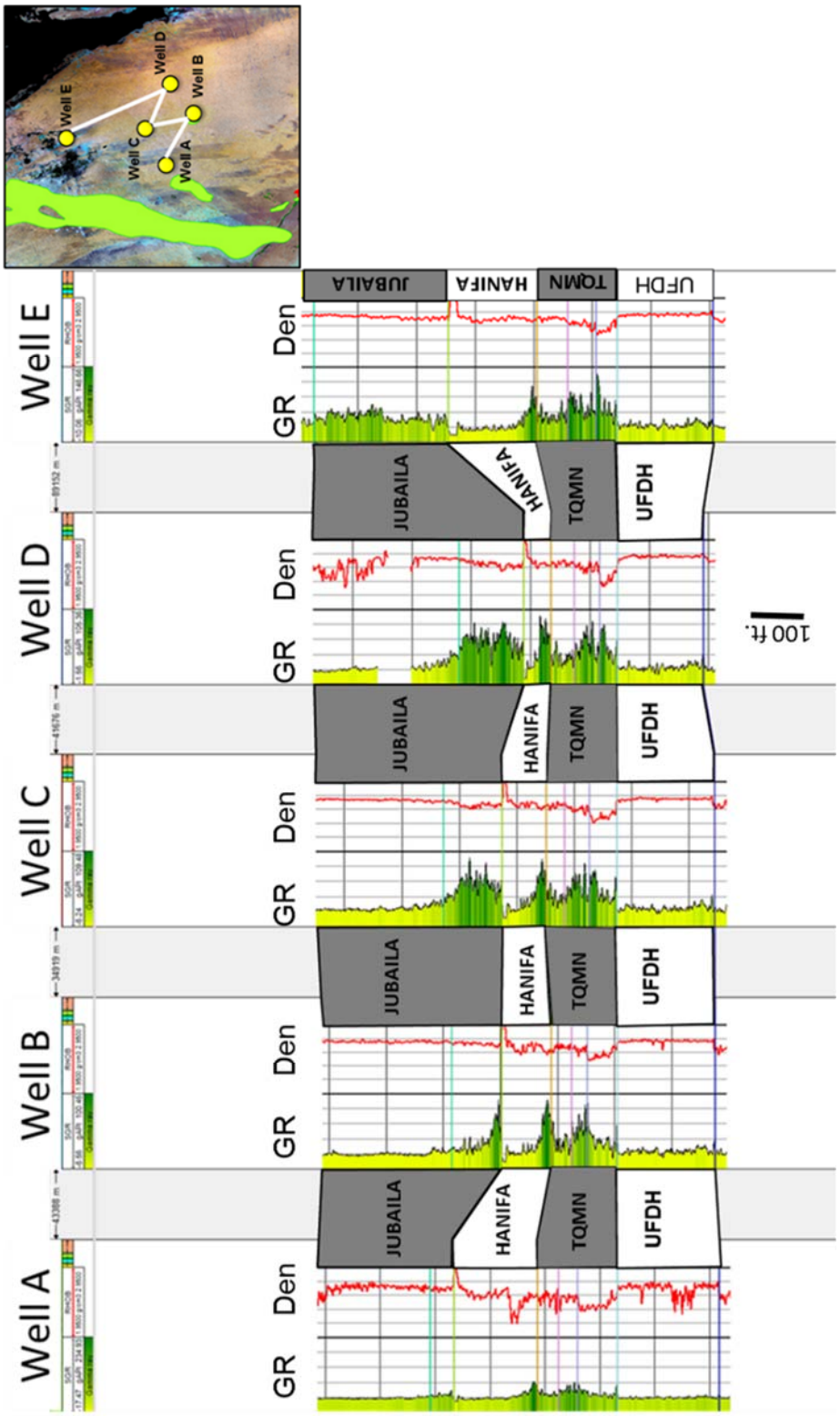

Figure 2-6 Stratigraphic cross section between the five wells used in the study, showing the lateral variation in formations thickness.

2.4 Lithofacies

The Jurassic succession of the Arabian Plate (Figure 2-2) consists predominantly of marine carbonates that were deposited on the Arabian carbonate platform. This carbonate platform developed in response to marine transgressions at the south-western margin of the Tethys Ocean (Murris, 1980; Al-Husseini, 1997). Variation in the sedimentary facies throughout the Jurassic is due to eustatic sea level rise and fall. The Middle Jurassic includes the Tuwaiq Mountain Formation, which is the main source rocks for the major oil and gas accumulations discovered in late Jurassic carbonate reservoirs in Saudi Arabia (Cole et al., 1994, and Carrigan et al., 1995). A representative core description for the Tuwaiq Mountain Formation based on this study is shown in Figure 2-7. Based on the core description, six distinct lithofacies were identified within the Tuwaiq Mountain Formation. These lithofacies were described based on its rock composition, degree of bioturbation, sedimentary structures and organic richness. From shallowest to deepest, the following lithofacies are recognized:

1- Shallow marine bioturbated lithofacies, Oxic

2- Relatively deeper marine bioturbated lithofacies, Oxic

3- Horizontal bioturbated lithofacies, Dysoxic

4- Laminated lithofacies with storm ripples, anoxic

5- Laminated lithofacies without ripples, anoxic

6- Massive anoxic lithofacies

The Tuwaiq Mountain Formation is generally calcareous and interpreted to have been deposited in a restricted marine environment within an intra-shelf basin (Al-Sharhan and Christopher, 1994). The basinal facies of Tuwaiq Mountain Formation consist of cycles of laminated, organic-rich, lime mud wackestones, deposited in an outer ramp/basin environment, beneath fair-weather wave base and above storm wave base. Storms swept sediments down-dip into the outer ramp/basin in a cyclical manner. Sedimentary structures include gently undulating parallel lamination or sinuous lamination; micro-hummocky cross lamination; ripple lamination; micro cut and fill lamination; and micro-topographic infill lamination. Lindsay et al., 2014, suggested that a pycnocline divided the water column into: (a) anoxic water beneath it; (b) dysoxic water at the contact; and (c) oxygenated water above it (Figure 2-8). This pycnocline was probably a dynamic boundary that moved up and down, possibly by sea level fluctuation or basin restriction, or a combination of both.

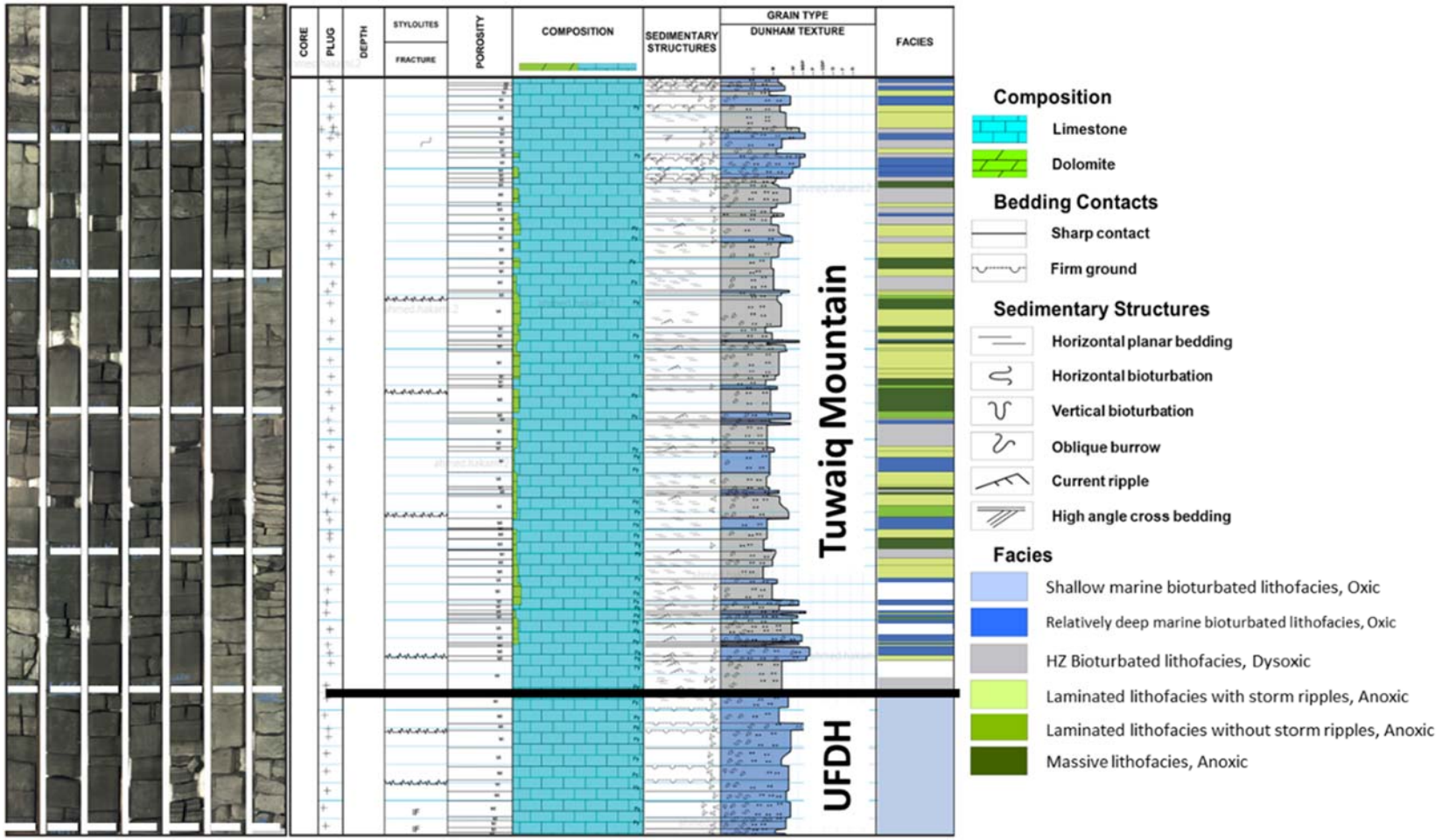

Figure 2-7 A representative core description for the Tuwaiq Mountain Formation at Well D.

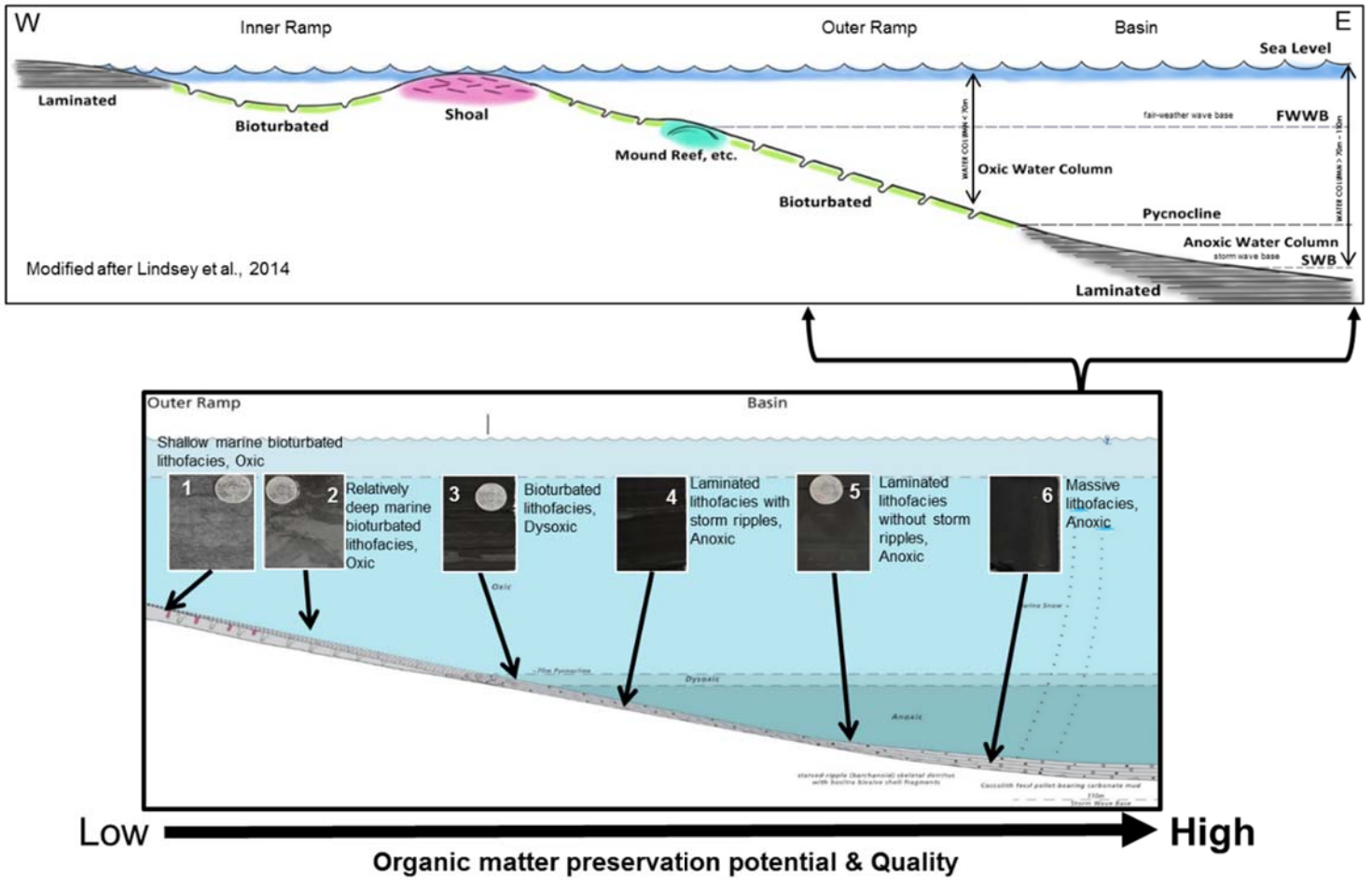

Figure 2-8 Schematic Ramp Profile showing the Tuwaiq Mountains Formation depositional environment. Modified after Lindsay et al., (2014). The pycnocline represent the layer in the water where density gradient is greatest.

The first two lithofacies (Figure 2-9) have generally less than 1% of TOC and are described as non-reservoir facies. On thin sections, facies 1 is mostly wackestone and mud-dominated packstone, with abundance of fossils, while facies 2 is also wackestone, and muddy dominated packstone/mudstone (Figure 2-10).

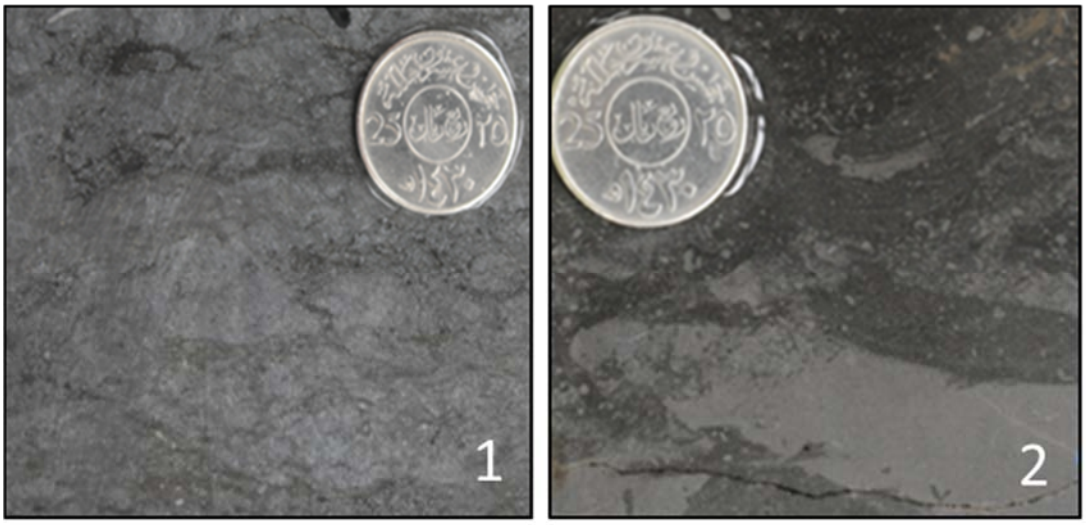

Figure 2-9 Slab core photos showing none-reservoir (organic lean) facies. Facies 1: Shallow marine bioturbated lithofacies and Facies 2: Relatively deeper marine bioturbated lithofacies.

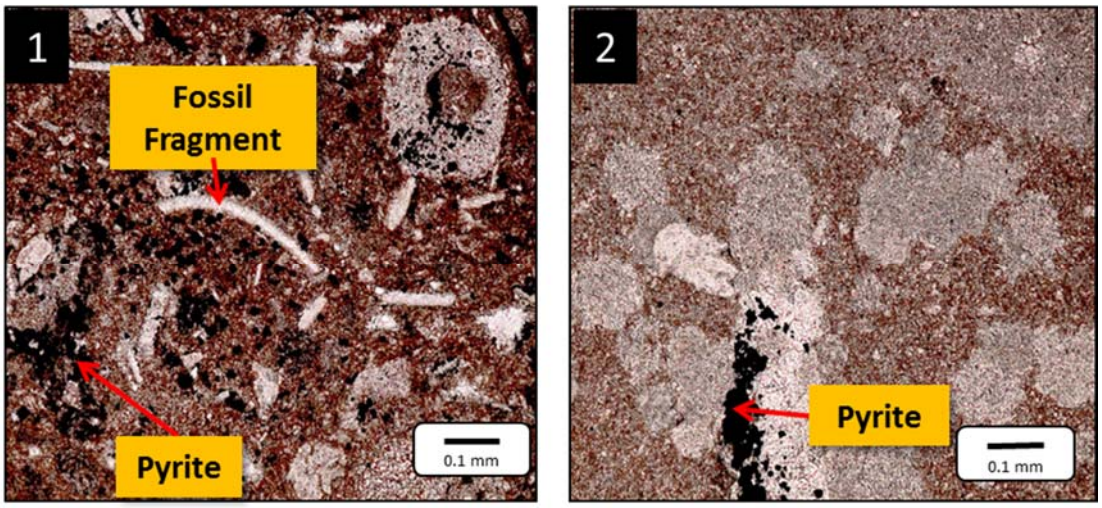

Figure 2-10 Thin sections images for none-reservoir (organic lean) facies 1 and 2. Facies 1: Shallow marine bioturbated facies, dark brown, argillaceous wackestone containing calcite and pyrite. Note abundance of fossil fragments. TOC content = 0.42 wt. %. Facies 2: Relatively deep marine bioturbated bed, massive, slightly argillaceous mudstone containing grain replacing calcite and pyrite. Note patchy distribution of calcite, TOC content = 0.5 wt. %.

The lower four lithofacies (Figure 2-11) are regarded as potential facies for unconventional reservoir targets. This is due to low clay (< 5%) and high organic matter (> 3%) content. In thin sections, facies 3 (Figure 2-12-3) mostly consists of wackestone containing scattered skeletal fragments and sparse dolomite. This facies is laminated with little bioturbation and is the most difficult to identify. It is assigned to a dysoxic environment, at the position of the pycnocline. Facies 4 (Figure 2-12-4) is a laminated wackestone to mud-dominated packstone with ripples. The ripples are support evidence that the basin floor was occasionally dragged by storms. The TOC content in this facies is variable, but high. Facies 5 (Figure 2-12-5) is a laminated organic-rich mud dominated packstone without ripples. TOC is generally high and it is common to observe the remnants of cocoliths, where most of the organic matter is concentrated. The organic matter is mostly present in the form of fecal pellets. Facies 6 (Figure 2-12-6) represents the massive source

rock, mostly wackestones, muddy packstones or mudstones. TOC content in this facies is very high, and may reach of up to 12% or more.

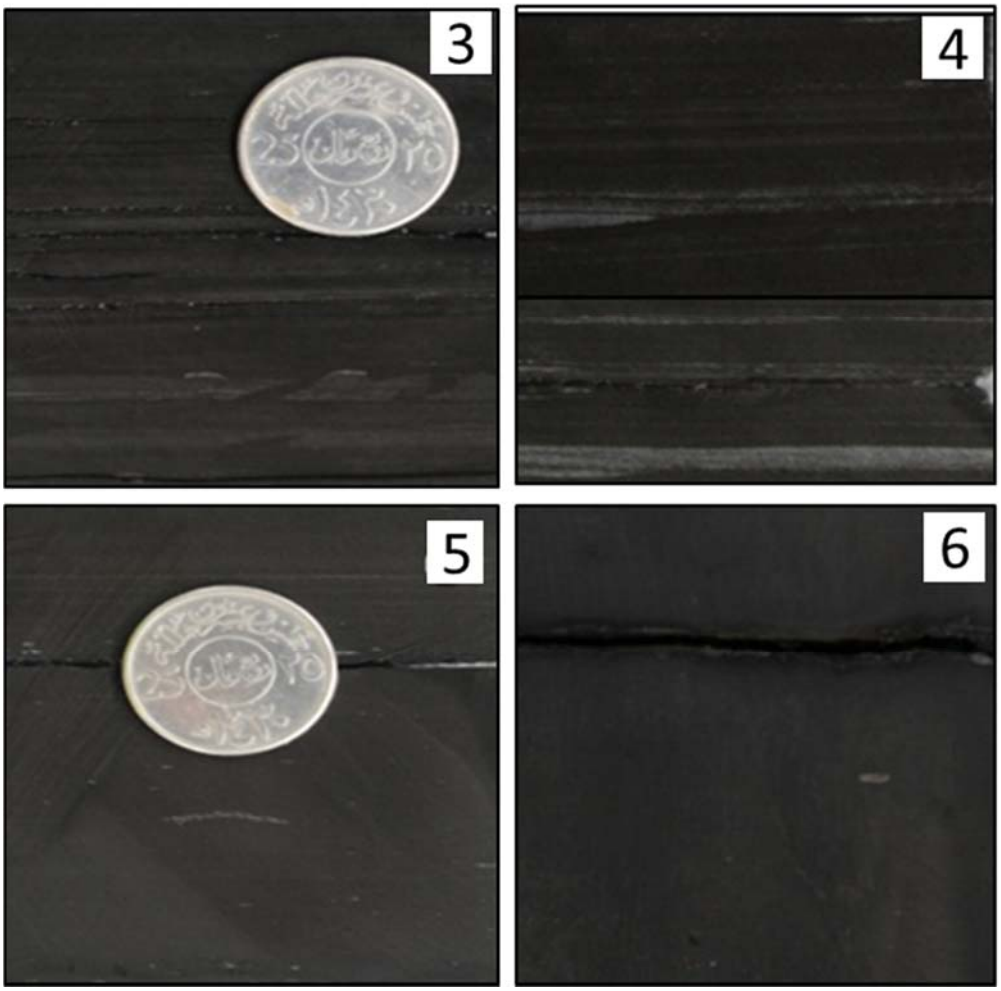

Figure 2-11 Slab core photos showing potential unconventional reservoir (organic rich) facies. Facies 3: Horizontal bioturbated lithofacies, Facies 4: Laminated lithofacies with storm ripples, Facies 5: Laminated lithofacies without ripples, and Facies 6: Massive anoxic lithofacies.

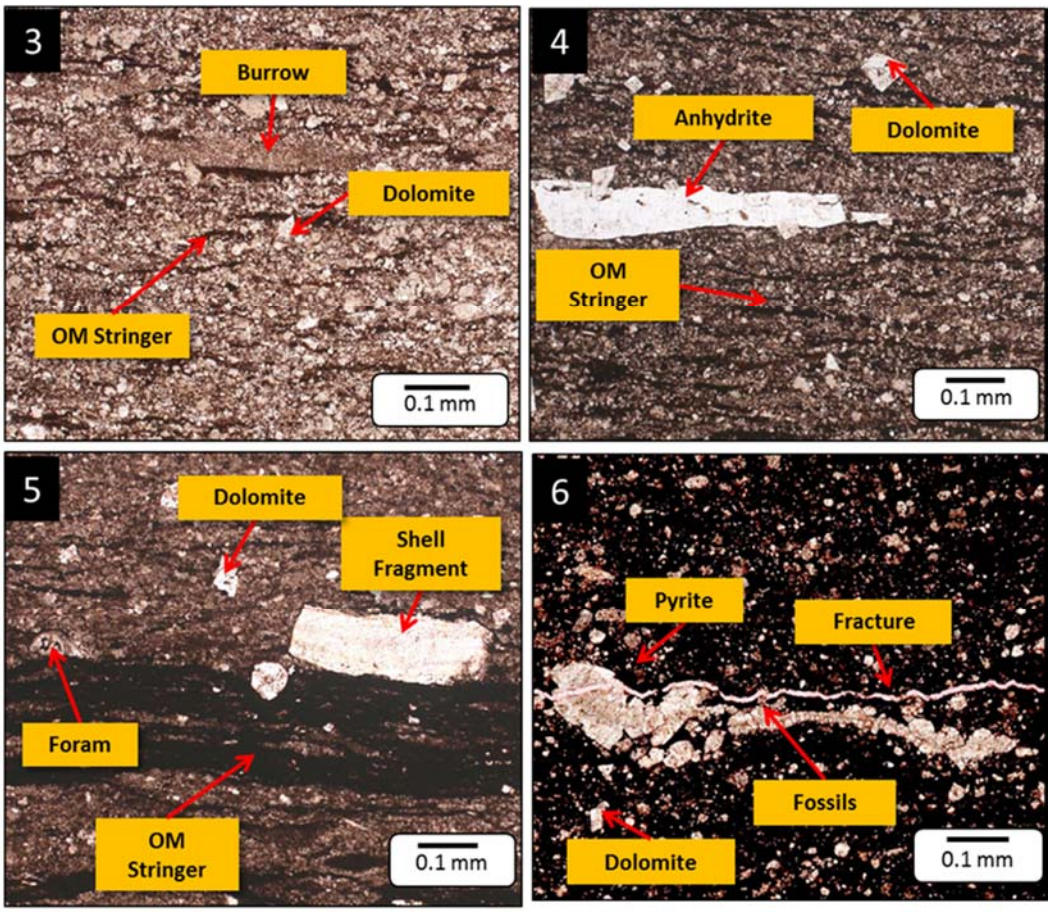

Figure 2-12 Thin sections images for the basinal reservoir (organic rich) facies. 3) Horizontally bioturbated facies: Dark brown to black, faintly-laminated, lime mudstone with minor anhydrite nodules. Horizontal microburrows occur locally. Organic matter appears mainly as bedding-oriented stringers. Dolomite rhombs disseminate throughout the sample. Rare fish bone fragments. Measured TOC is 3.56 wt. % for this sample. 4) Laminated with ripples: Dark brown, laminated, lime mudstone. This sample is characterized by many wavy organic-rich laminae, some of which are probably microstylolites in nature. Silt-sized, authigenic dolomite rhombs are dispersed throughout the sample. Note that shell fragments and anhydrite nodules are present as well. Except for the organic-rich laminae, discontinuous organic matter stringers are commonly seen within the micritic matrix. Measured TOC is 5.38 wt. % for this sample. 5) Laminated facies, no ripples: Dark brown, faintly-laminated, lime mudstone. Stratification is defined by bedding-oriented, organic matter stringers and elongate anhydrite nodules. Euhedral dolomite rhombs are sparsely distributed throughout the sample. Minor shell fragments are also observed. A couple of induced fractures can be seen. Measured TOC is 7.08 wt. % for this sample. 6) Massive facies: Dark brown, massive, dolomitic, recrystallized, argillaceous lime mudstone containing pyrite. Clay volume is 5.2% and consists of illite and illite/smectite. TOC content is 11.70 wt. %. Note microfracture and recrystallized fossils.

X-ray diffraction (XRD) and scanning electron microscopy (SEM) were also utilized to identify rock composition and morphology. Based on XRD measurements from cores collected from the five wells used in the study, calcite is the dominant component. The calcite distribution ranges from 59% to 89% by volume and averages 74%. Dolomite occurs in low amounts and ranges from 1% to 30%, with an average of 11%. The quartz content is relatively low, ranging from 1.7% to 5%, with a 3% average. The total clay content is extremely low, ranging from 2.8 to 7.6%, with averages of 5%; with illite and kaolinite predominant. The low volume of clays correlate with the low water saturation in the matrix of the rock measured in the laboratory. The high brittle calcite content along with the low ductile clay content makes the Tuwaiq Mountain Formation the ideal lithology for hydraulic fracturing stimulation. Figure 2-13 shows a Ternary and pie-chart plots of the Tuwaiq Mountain Formation whole rock and clay mineralogy for wells A through E. The rock classification for the bulk mineralogy is based on Helena et al. (2012) classifications for organic mudstone.

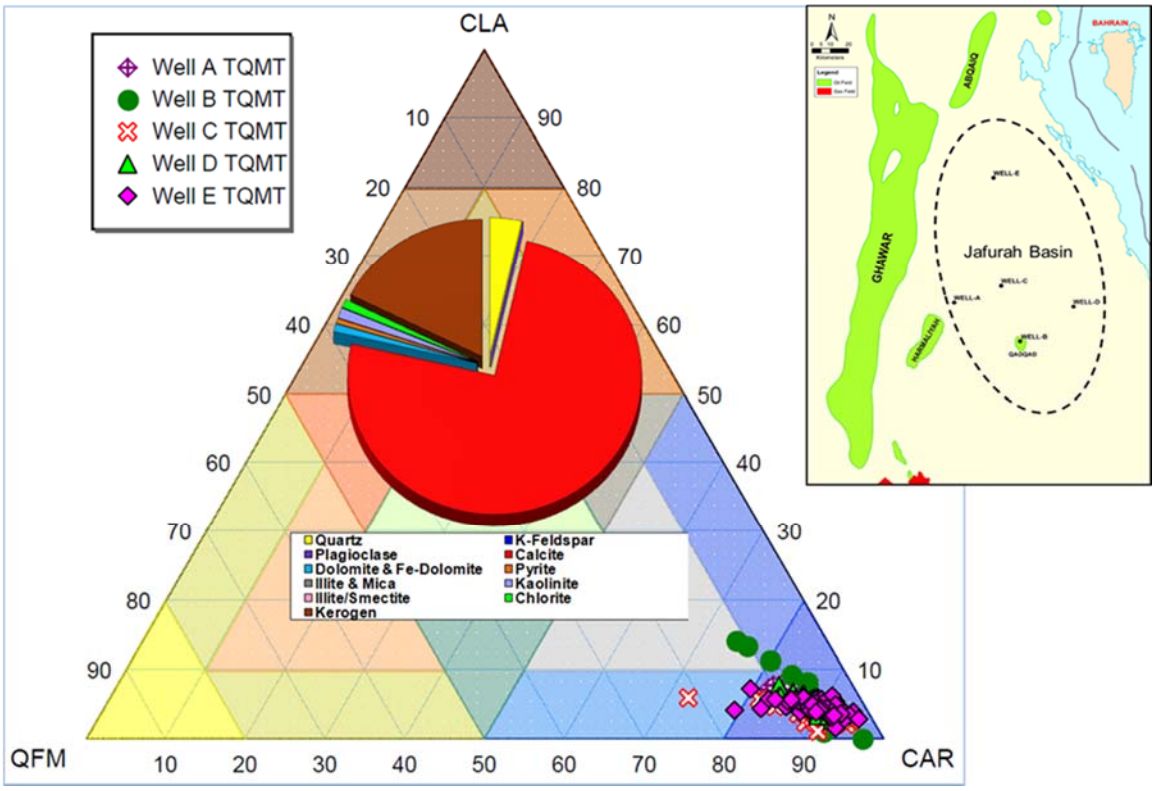

Figure 2-13 Ternary plot and pie-chart of Tuwaiq Mountain Formation whole rock and clay mineralogy for wells A through E. As illustrated by the pie chart, the kerogen is largely the second main component after calcite.

Scanning electron microscopy was used to characterize the pore types of the Tuwaiq Mountain source rock. As illustrated in (Figure 2-14), nanopores are common in the internal texture of the organic matter. This type of organic nanoporosity has been well described by Pommer and Milliken (2015), and it is the dominant pore type in shale gas plays like the Eagle Ford. The SEM images of reservoir facies from four different wells reveal a moderately to well-connected organic pore system in the matrix of the Tuwaiq Mountain Formation. The shapes of the pores are mostly irregular polygonal to spherical with predominant pore sizes less than 1µm (84% distribution) and the remaining fraction has micro pores greater than 1 µm. As a result, the pore network in the Tuwaiq Mountain play will be controlled by the abundance, distribution, and the thermal maturation levels of

the organic matter. It is noted that the pores show no evidence of compaction, and it is reasonable to conclude that the predominant calcite framework is very strong and prevents organic matter or pore compaction.

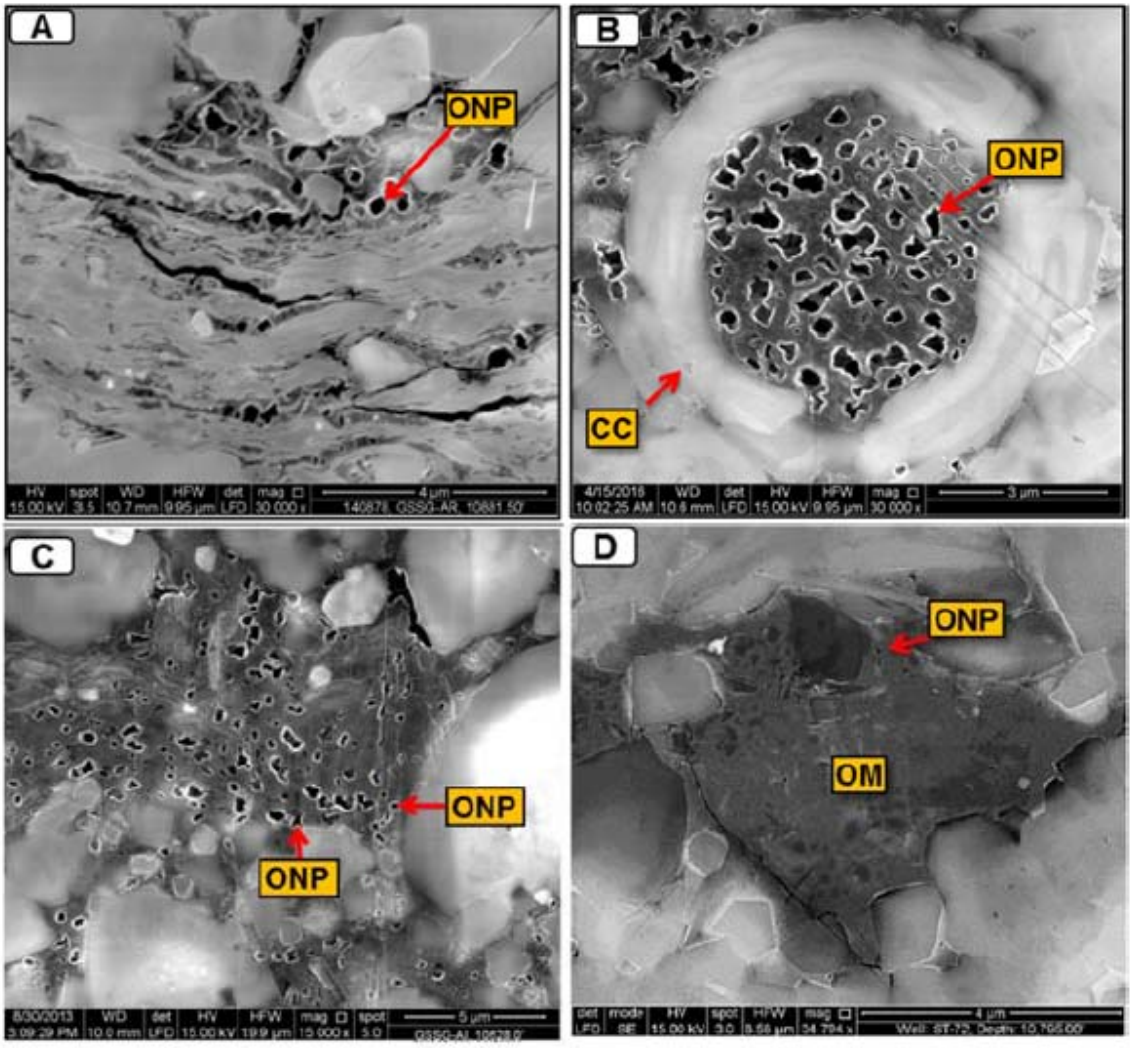

Figure 2-14 SEM images of representative Tuwaiq Mountain Fm. Samples. a) Well B, intergranular pores mostly filled by organic matter. Organic matter occupies most pores and displays abundant, well-developed organic nanopores (ONP). B) Well c, view of a coccolith plate (CC) filled with organic matter with common nano-sized pores. c) Well D, organic matter is filling intergranular pores and develop organic nanopores, typically along pore walls and smaller pores. d) Well E, organic matter is predominantly present as bitumen filling interparticle spaces. Some bituminous organic matter displays abundant development of organic nanoporosity.

2.5 Petroleum System

Two major Petroleum Systems occur in Eastern and Central Saudi Arabia (Abu-Ali et al., 1991, Abu-Ali et al., 1999, Cantrell et al., 2014). A "Paleozoic System" related to the Prototethys/Paleotethys, and a "Mesozoic System" associated with the Neo-Tethys. These petroleum systems, which are naturally segregated in time by the tectonic evolution of the Arabian Plate, also show distinct differences in reservoir properties and hydrocarbon content. The reservoir of the Paleozoic petroleum system are primarily siliciclastic-dominated and host both oil and gas, whereas the Mesozoic petroleum system is dominated by carbonate and mixed clastic-carbonate reservoirs, which are among the most prolific oil producers in the world. These two main petroleum systems are separated in geological time by the closure of the Paleo-Tethys and the amalgamation of Pangea, followed by subsequent breakup of Pangea and the opening of the Neo-Tethys during the Late Triassic to Early Jurassic (Figure 2-15).

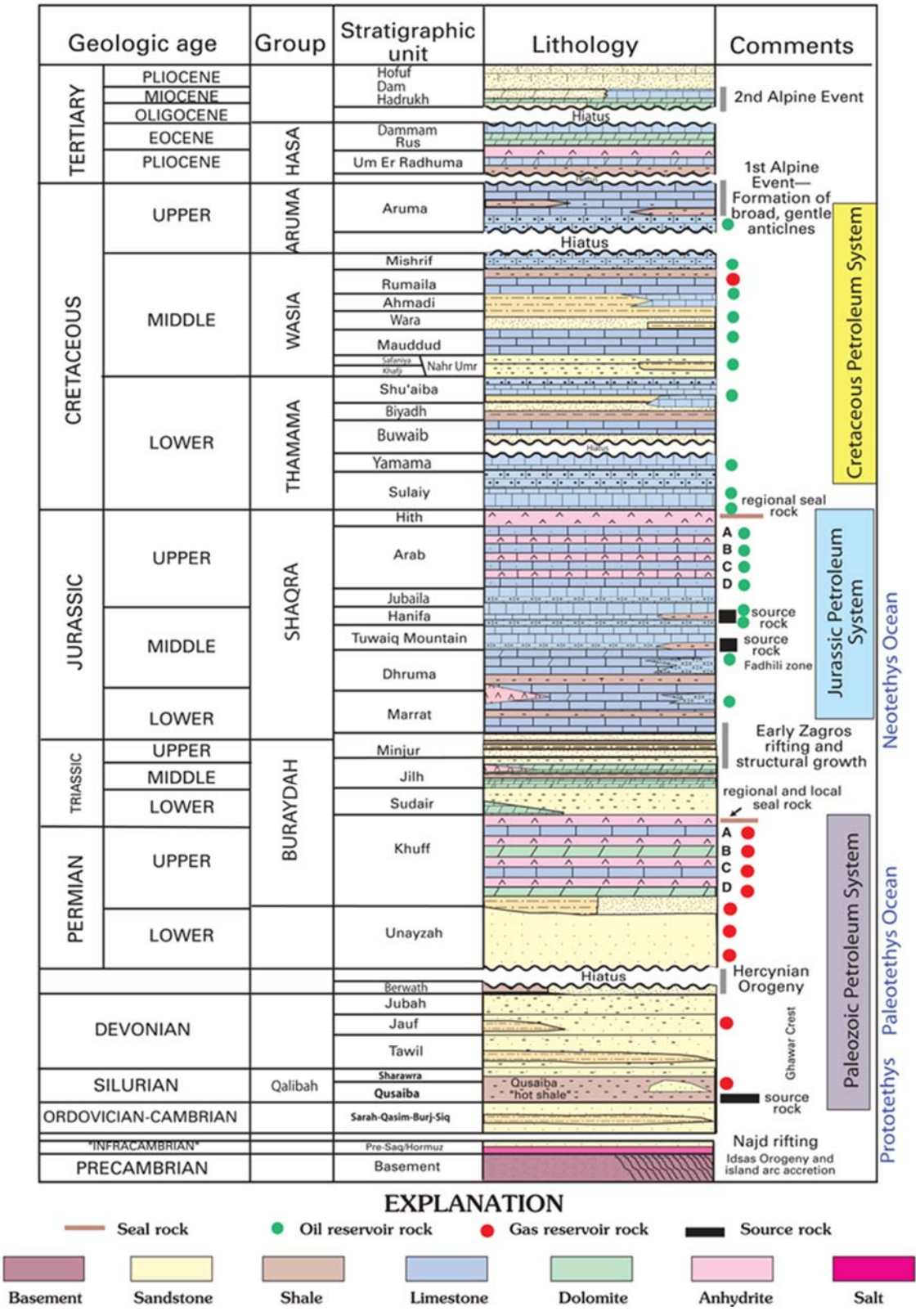

Figure 2-15 Major tectonic events and stratigraphic units that comprise the major Tethyan Petroleum Systems of Saudi Arabia (Pollastro, 2003; Cantrell et al., 2014).

2.5.1 Mesozoic Petroleum System

The Mesozoic petroleum system (Figure 2-16) is primarily sourced by the thermally mature, middle Jurassic Carbonate source rock of the Tuwaiq Mountain Formation (Ayres et al., 1982; Droste, 1990; Carrigan et al., 1994). The generated oil then migrated and was trapped in permeable and porous carbonate reservoirs. The Jurassic reservoirs are capped by highly efficient evaporate seals, which stopped further migration and warranted the entrapment of the oils in these large structural traps (e.g., Ghawar Oil Field). In the Cretaceous, traps are mainly sealed by low porosity and low permeability carbonates or shales, with Eocene evaporites acting as the regional top seal. The large size of the resulting oil and gas fields is not just a function of the size of the structures present, but also reflects the areal extent of the stacking source; reservoir, and seal, over an area that is almost continental in scale (Pollastro, 2003, Cantrell et al., 2014).

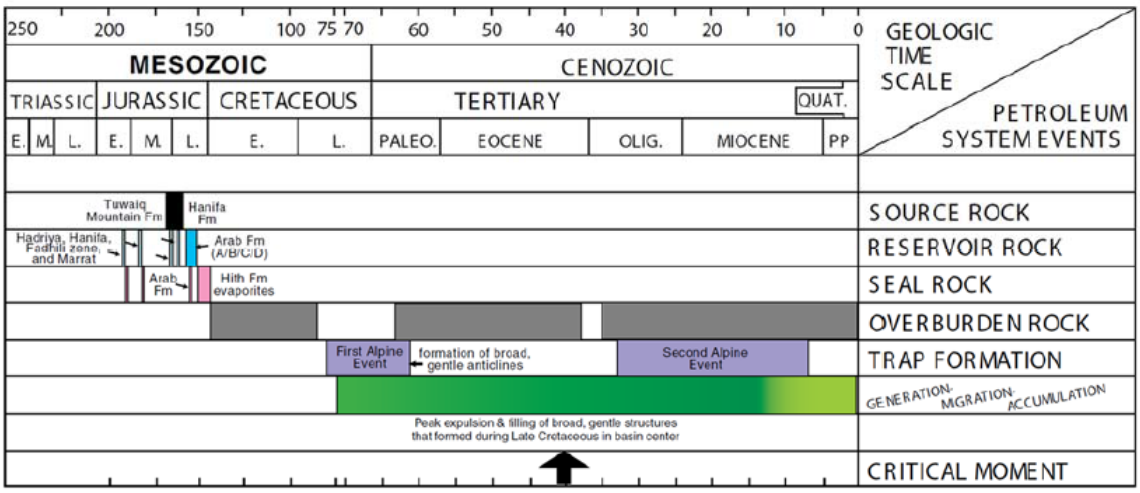

Figure 2-16 Event chart for the Mesozoic petroleum system in the Arabian Basin, Eastern Saudi Arabia (after Pollastro, 2003).

2.5.2 Tuwaiq Mountain Formation: Distribution, Richness and Maturation

The key play elements of the Mesozoic Petroleum System are shown in Figure 2-15. The Mesozoic system contains the Jurassic Tuwaiq Mountain Formations as the principle source rocks, with reservoirs extending from the Lower Jurassic to Upper Cretaceous and regional seals occurring in the Hith Formation and in the Wasia Group. The Tuwaiq Mountain Formation source rocks have an average TOC content of about 4.9%, and locally with content as high as 13.17% (Table 1). Total pyrolytic yield (SI + S2 from Rock-Eval) is as high as 30.84 mg HC/g rock and with and an average yield of 6.8 mg HC/g rock, representing excellent source rock potential. Hydrogen indices of thermally immature rocks are between 600 and 800 mg HC/g TOC, which indicate an oil-prone kerogen. Based on petrographic studies, it is known that the organic matter is dominantly fluorescing lamalginite, with subordinate amounts of vitrinite and inertinite (Carrigan et al., 1995). These results suggest that organic-rich units within the Tuwaiq Mountain Formations contain type II kerogen with an excellent oil generation potential. The Tuwaiq Mountain Formation source rock quality, type, and maturity are discussed in great detail in chapters 3 and 4. At present, the Tuwaiq Mountain source rocks to the east of the Ghawar structure have passed through the oil window, whereas, the source rocks in the center of the Arabian Basin (west of the Ghawar structure) are still in the oil generation window. In the western portion of the Arabian Basin, the source rocks are either immature or marginally mature with respect to the oil window. Results from basin modeling suggest that the Jurassic source rocks commenced hydrocarbon expulsion during the Late Cretaceous. The Tuwaiq Mountain Formation source rocks entered the early maturity stage for oil generation at about 100 Ma and reached the peak oil generation at about 70 Ma, and at Present, they are

at wet gas generation window in the basinal areas (Figure 2-16). Expelled hydrocarbon then starts to migrate to a wide range of structural and stratigraphic traps. More discussion on the basin evolution and modeling are provided in chapter 4.

Table 2-1 TOC and pyrolysis data for samples from the Tuwaiq Mountain, Hanifa and Jubaila Formations at the five wells used in the study.

Geochemical Attributes		Jurassic Formations		
		Jubaila 185 Samples	Hanifa 172 Samples	Tuwaiq Mountain 333 Samples
Total Organic Carbon Content (Wt. %)	Maximum	4.98	3.90	13.17
	Minimum	1.00	0.15	1.12
	Average	2.44	1.19	4.9
S1 Pyrolysis Yield (mg HC / g rock)	Maximum	4.69	4.58	12.04
	Minimum	0.32	0.02	0.39
	Average	1.05	0.77	3.4
S2 Pyrolysis Yield (mg HC / g rock)	Maximum	7.55	6.18	18.8
	Minimum	0.55	0.02	0.54
	Average	2.53	0.8	3.4
Hydrogen Index (S2*100/TOC)	Maximum	231	218	194
	Minimum	63	50	48
	Average	112	102	91
Tmax (ºC)	Maximum	476	479	493
	Minimum	434	456	455
	Average	462	471	475

2.6 References

Abu-Ali, M. A., J. L. L. Rudkiewicz, J. G. McGillivray, and F. Behar, 1999, Paleozoic petroleum system of central Saudi Arabia: GeoArabia, v. 4, p. 321–336.

Abu-Ali, M. A., U. A. Franz, J. Shen, F. Monnier, M. D. Mahmoud, and T. M. Chambers, 1991, Hydrocarbon Generation and Migration in the Paleozoic Sequence of Saudi Arabia. Society of Petroleum Engineers, Middle East Oil Show Bahrain, 16-19 November 1991. (SPE 21376), p. 345–356.

Al-Husseini, M., 1997, Jurassic sequence stratigraphy of the western and southern Arabian Gulf: GeoArabia, v. 2, no. 4, p. 361-382.

Al Ibrahim, Mustafa. A., 2014, Multi-scale sequence stratigraphy, cyclostratigraphy, and depositional environment of carbonate mudrocks in the Tuwaiq Mountain and Hanifa Formations, Saudi Arabia: Colorado School of Mines, PH.D. Dissertation, P. 1-181.

Alsharhan, A. S., and C. G. St. C. Kendall, 1994, Depositional setting of the Upper Jurassic Hith anhydrite of the Arabian Gulf: An analogue to Holocene evaporates of the United Arab Emirates and Lake MacLeod of Western Australia: AAPG Bull., v. 78, p. 1075-1096.

Alsharhan, A.S., and Christopher, G., Kendall ST. C., 1986, Precambrian to Jurassic Rocks of Arabian Gulf and Adjacent Areas: Their Facies, Depositional Setting, and Hydrocarbon Habitat. AAPG Bulletin, v. 70, no. 8, p. 977-1002.

Arkell, E. J., 1956, Jurassic Geology of the World, Oxford University Press, p. 1-565.

Ayres, M. G., M. Bilal, R. W. Jones, L. W. Slentz, M. Tartir, and A. O. Wilson, 1982, Hydrocarbon habitat in main producing areas, Saudi Arabia: AAPG Bull., v. 66, p. 1-9.

Cantrell, D.L., P.G. Nicholson, G.W. Hughes, M.A. Miller, A.G. Bhullar, S.T. Abdelbagi, A.K. Norton, 2014. Tethyan petroleum systems of Saudi Arabia, in L. Marlow, C. Kendall and L. Yose, eds., Petroleum systems of the Tethyan region: AAPG Memoir 106, p. 613-639.

Carrigan, W. J., G. A. Cole, E. L. Colling, and P. J. Jones, 1994, Geochemistry of the Upper Jurassic Tuwaiq Mountain and Hanifa Formation petroleum source rocks of Eastern Saudi Arabia, in B. J. Katz, ed., Petroleum Source Rocks: Springer-Verlag, New York, p. 67-87.

Cole, G. A., Carrigan, W. J., Colling E. L., Halpern, H. I., Al-Khadhrawi, M. R. and Jones, P. J., 1994, The organic Geochemistry of the Jurassic petroleum system in Eastern Saudi Arabia, Canadian Society of Petroleum Geologists Memoir 17, 413-438.

Droste, H. H. J., 1990, Depositional cycles and source rock development in an epeiric intra-platform basin, the Hanifia Formation of the Arabian Peninsula: Sedimentary Geology, v. 69, p. 281-296.

Grabowski, G. J. and Norton, I. O., 1995, Tectonic Controls on the Stratigraphic Architecture and Hydrocarbon Systems of the Arabian Plate. GeoArabia, v. 1, p. 413–430.

Helena, G. D., Camron, M., and Richard, L., (2012). sCore: A Classification for Organic Mudstones based on bulk mineralogy. Presented at AAPG 2012 Southwest Section Meeting, Ft Worth, Texas, 19-22 May 2012. Search and Discovery Article # 40951, posted June 11, 2012.

Holditch, S. A., 2006, Tight gas sands, SPE Journal of Petroleum Technology 58 (6), 86–93 (103356-MS).

Holditch, S. A., 2013, Unconventional oil and gas resource development – Let's do it right, Journal of Unconventional Oil and Gas Resources 1–2 (2013) 2–8

Hughes, G. W., 2004, Middle to Upper Jurassic Saudi Arabian carbonate petroleum reservoirs: Biostratigraphy, micropalaeontology and palaeoenvironments: GeoArabia, v. 9, no. 3, p. 79-114.

Hughes, G. W., 2009, Micropalaeontology and palaeoenvironments of Saudi Arabian Upper Permian carbonates and reservoirs, in D. Demchuk, and A. C. Gary, eds., Geologic problem solving with microfossils: A volume in honor of Garry D. Jones: Society for Sedimentary Geology, p. 111–126.

International Energy Agency (IEA), 2011

Le Nindre, Y-M., J. Manivit, H. Manivit, and D. Vaslet, 1990, Stratigraphie séquentielle du Jurassique et du Crétacé en Arabie Saoudite: Bulletin of the Geological Society of France, ser. 8, p. 1025-1034.

Lindsay, R.F., Khan S., Dhubeeb A., Davis R., 2014. Unconventional Jurassic carbonate source rocks, Saudi Arabia. International Conference & Exhibition, September 14-17, 2014, Istanbul, Turkey, AAPG article # 90194.

McGuire, M. D., R. B. Koepnick, J. R. Markello, M. L. Stockton, L. E. Waite, G. S. Kompanik, M. J. Al-Shammery, and M. O. Al-Amoudi, 1993, Importance of sequence

stratigraphic concepts in development of reservoir architecture in Upper Jurassic grainstones, Hadriya and Hanifa reservoirs, Saudi Arabia: Proceedings of 8th Middle East Oil Show, SPE #25578, p. 489-499.

Murris, R.J. 1980, Middle East Stratigraphic Evolution and Oil Habitat, AAPG Bulletin, v. 64, p. 597-618.

Pollastro, R. M., 2003, Total petroleum systems of the Paleozoic and Jurassic, greater Ghawar uplift and adjoining provinces of central Saudi Arabia and northern Arabian-Persian Gulf: U.S. Geological Survey Bulletin 2202-H, 100p.

Powers, R. W., L. F. Ramirez, D. D. Redmond, and E. L. Elberg Jr., 1966, Geology of the Arabian peninsula, sedimentary geology of Saudi Arabia: U. S. Geological Survey Professional Paper, 560-D, 150 p.

Powers, R. W., 1968, Lexique stratigraphique international, Paris, Centre Nationale de la Recherche Scientifique, v. 3, Asie, part 10b, 180 p.

Sharland, P. R., R. Archer, D. M. Casey, R. B. Davies, S. H. Hall, A. P. Heward, A. D. Horbury, and M. D. Simmons, 2001, Arabian Plate sequence stratigraphy: GeoArabia Special Publication 2, Gulf PetroLink, Bahrain, 371 p

Steineke, M., R. A. Bramkamp, and N. J. Sander, 1958, Stratigraphic relations of Arabian Jurassic oil: AAPG Symposium, Tulsa, OK, p. 1294-1329.

Vaslet, D., Manivit, J., Le Nindre, Y.-M., Brosse, J.-M., Fourniguet, J. and Delfour, J. 1983. Explanatory notes to the geologic map of the Ar Riyad Quadrangle, Sheet, sheet 23H, Kingdom of Saudi Arabia. Saudi Arabian Deputy Ministry for Mineral Resources Geoscience Map GM-63, scale 1:250,000, with text, 46 pp.

ww.eia.go/aer. Annual Enery Review 2011.

Ziegler, M. A., 2001, Late Permian to Holocene paleofacies evolution of the Arabian Plate and its hydrocarbon occurrences: GeoArabia, v. 6, no. 3, p. 445-504.

CHAPTER 3

Source rock Quality and Gas Origin

Mud Gas Isotope Logging Application for Sweet Spot Identification in an Unconventional Shale Gas Play, A Case Study from Jurassic Carbonate Source rock in the Jafurah Sub-Basin, Saudi Arabia

Ahmed Hakami [a,*], Leroy Ellis[a], Khalid Al-Ramadan[b], and Sami Abdelbagi [a]

[a] Saudi Aramco, Exploration Organization, 31311, Dhahran, Saudi Arabia
[b] Petroleum Engineering and Geosciences College, King Fahad University of Petroleum and Minerals

Published Paper in Marine and Petroleum Geology 76, May (2016) 133-147 (ELSEVIER)

Abstract

The Jafurah Sub-Basin is a new frontier unconventional exploration play equivalent in size to the successful Eagle Ford play in south Texas. The basin is located immediately east of the adjacent supergiant Ghawar Oil Field. The middle to upper Jurassic organic-rich mudrocks are recognized as the source of Ghawar hydrocarbons and are being extensively evaluated across the Jafurah Sub-Basin. These source rocks, notably the Jubaila and Tuwaiq Mountain, and to lesser extent Hanifa Formations possess excellent hydrocarbon attributes such as high total organic content (TOC), and sufficient maturity, combined with

a relatively shallow burial depth, allowing for economical unconventional shale gas and shale oil exploitation. Mud gas isotope logging (MGIL) data obtained from recent exploration wells revealed important characterization potential enabling clear distinction between Tuwaiq Mountain, Hanifa and Jubaila Formation gases based on their isotopic signature. A new methane carbon isotopic maturity correlation for the main Tuwaiq Mountain source rock has been calibrated and successfully tested:

$$\textbf{Vitrinite Reflectance Equivalent (Vre)} = \mathbf{0.069}\ \boldsymbol{X}\ \boldsymbol{\delta 13C1} + \mathbf{5.13.}$$

This finding has permitted accurate maturity assessments providing identification of the best sweet spots predicted for optimal Tuwaiq Mountain production potential. Next stage lateral drilling developments will leverage MGIL technology to assess the effectiveness of future hydraulic fracturing treatments in this formation and ensure maximum in zone completions for best production potential.

3.1 Introduction

The Jurassic organic-rich carbonate mudrocks in the Arabian basins have long been recognized as the source of conventional hydrocarbons trapped in the supergiant Jurassic carbonate reservoirs in Saudi Arabia (Cole et al., 1994). With the recent development of commercial hydrocarbon production from shale source rocks in North America, efforts are underway to assess the unconventional resource potential within the Jurassic source rocks intervals in Saudi Arabia. Mud Gas Isotope Logging (MGIL) is one of several technologies that are being utilized by Saudi Aramco for optimum unconventional play evaluation. Mud Gas Isotope Logging, a technique involving analysis of the carbon isotopic composition of hydrocarbon gas species (C1-C5) from circulating mud gas streams during drilling of a

well, has found considerable application in global hydrocarbon exploration and production operations (Ellis et al., 1999; Wilhelms et al., 2001; Ellis et al., 2003, Ellis, 2004; Ellis et al., 2007). It is the intent of this paper to document the first application of Mud Gas Isotope Logging (MGIL) in the context of shale gas evaluation in Saudi Arabia. The focus of this work is on the Jafurah frontier basin located east of Ghawar Oil Field (Figure 3-1). Five exploration wells were selected for this study. These wells were drilled vertically, cored, logged and sampled for MGIL analysis. The coring program was designed to collect enough core samples to enable detailed source rock and maturity characterization across the three potential targets; Tuwaiq Mountain, Hanifa and Jubaila Formations. MGIL and source rock data were used to assess type, origin and thermal maturity of hydrocarbon shows with integration of both datasets to develop and calibrate accurate geochemical tools for maturity estimation.

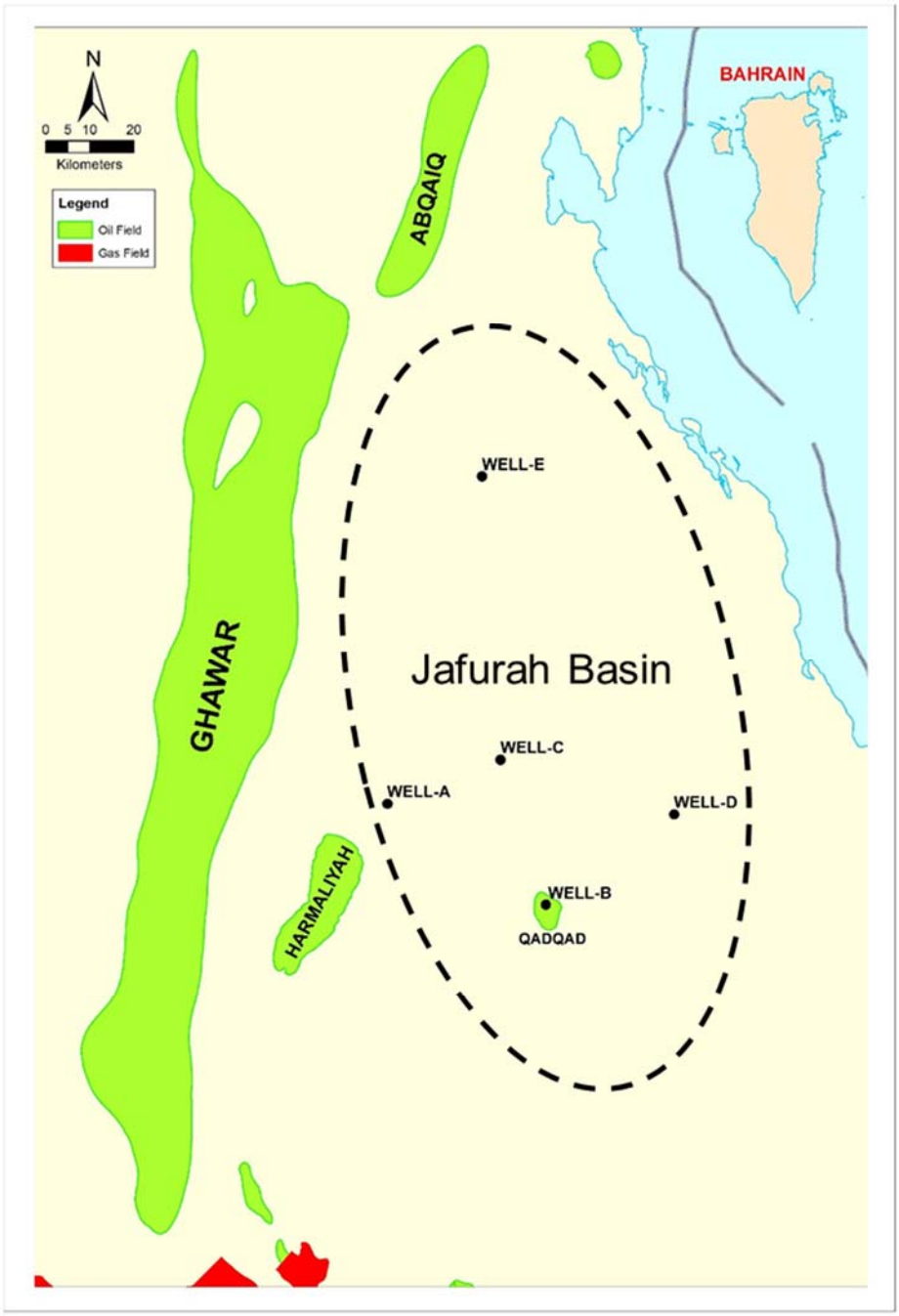

Figure 3-1 Location map of the study area, showing the Ghawar supergiant oil field in Saudi Arabia, the approximate outline of Jafurah Sub-Basin (dashed black line), and the five wells used in the study.

3.2 Lithofacies

The Jurassic succession of the Arabian Plate consists predominantly of marine carbonates that were deposited on the Arabian platform. This carbonate platform developed in response to marine transgressions at the south-western margin of the Tethys Ocean (Murris, 1980; Al-Husseini, 1997). At its zenith, stagnation of seawater and the formation of an extensive evaporitic platform occurred over much of the shelf during the Late Jurassic (Droste, 1990). Variation in the sedimentary facies throughout the Jurassic is attributed to eustatic sea level rise and fall. (Figure 3-2) shows the generalized geological column of the Middle and Upper Jurassic stratigraphy of Saudi Arabia (Cantrell et al., 2014). The Middle Jurassic organic-rich formations in the Arabian basins comprise the main calcareous source rocks for the major oil and gas accumulations occurring in late Jurassic carbonate reservoirs in Saudi Arabia (Cole et al., 1994 and Carrigan et al., 1995). Representative oils from these reservoirs show very similar chromatographic and biomarker geochemical fingerprints to bitumen extracted from the Tuwaiq Mountain and Hanifa Formations, suggesting that the oils can be correlated to these source rocks. Visual inspections of cores from these formations reveal cycles of laminated, organic-rich, lime mud Wackestone that has been deposited in a restricted marine environment within an intra-shelf basin (Cole et al., 1994 and Carrigan et al., 1995). Figure 3-3 shows a stratigraphic cross section between the five wells investigated, highlighting the lateral correlation of individual lithofacies within the middle and upper Jurassic source rock intervals. These laminated, organic-rich lime mudstone source rocks are relatively thick (up to 400 ft.) and extend over large geographical areas across the Arabian Basins. Cantrell et al., 2014 reported that the organic-rich facies in the Jubaila

Formation are of less significance as a source when compared to the organic-rich facies of Tuwaiq Mountain and Hanifa Formations. However, based on the source rock data obtained in this study as it will be discussed later, the Jubaila Formation in the Jafurah Sub-Basin possesses good source rock quality and may prove to be an important secondary contributor of hydrocarbons. Conversely, the Hanifa Formation in this basin shows poor organic facies. The thickness of the Tuwaiq Mountain Formation is relatively uniform between the wells used in this investigation, whereas, the Jubaila Formation thickness increased toward the north at Well-E (Figure 3-3). The Hanifa Formation is of various thickness and it is marked from top by the presence of a thin anhydrite layer (as indicated by the electric logs in Figure 3-3) approximately 5-15 feet in thickness.

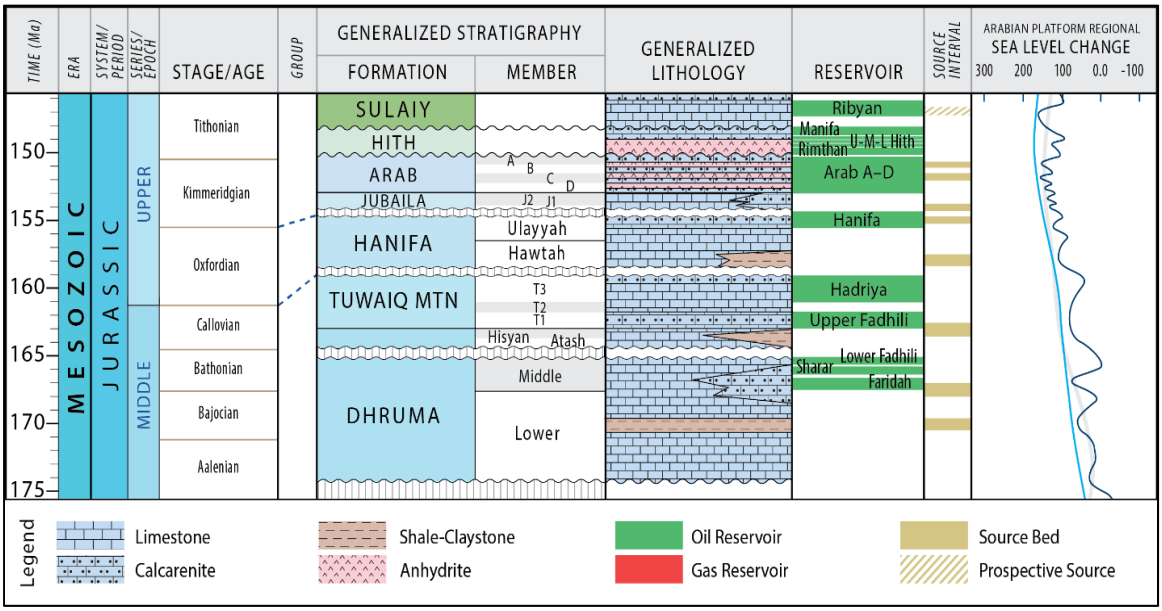

Figure 3-2 Generalized geologic column of the Middle and Upper Jurassic Epoch (after Cantrell et al., 2014).

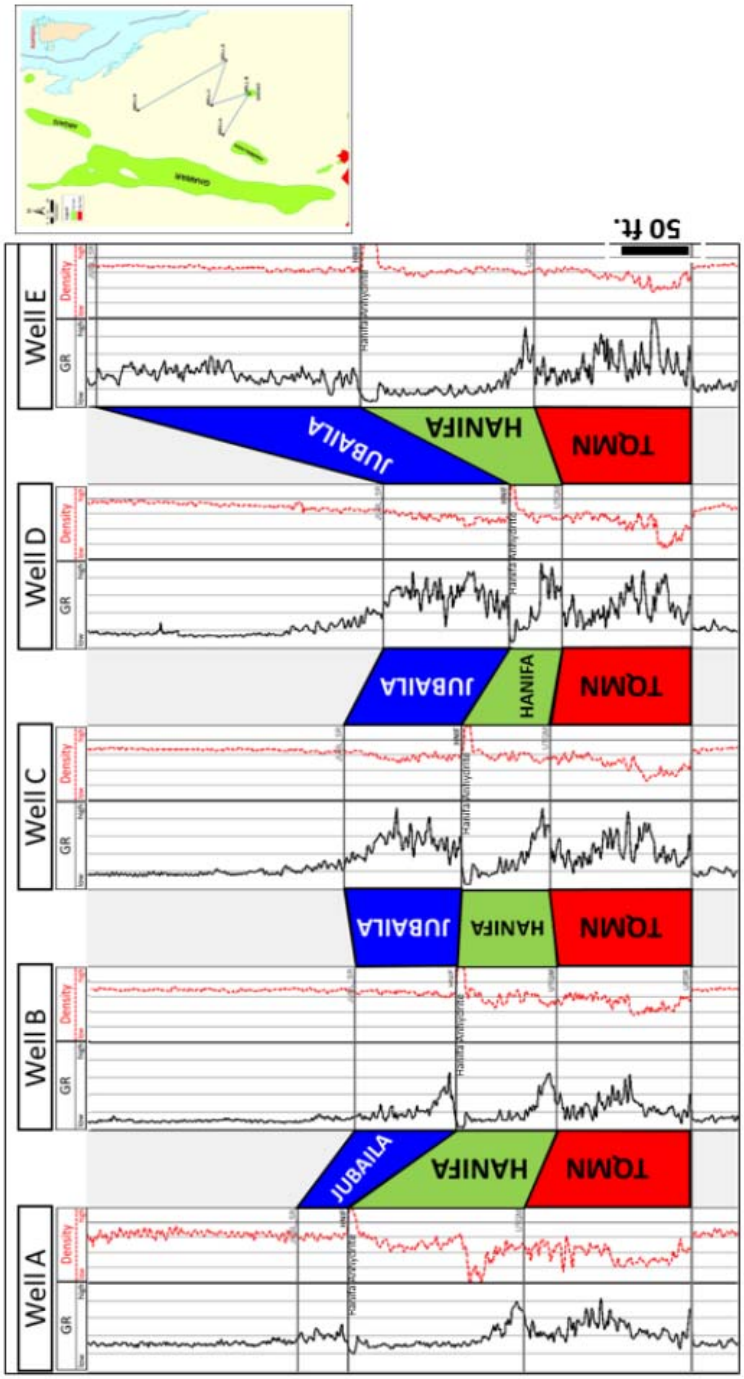

Figure 3-3 Stratigraphic cross section between the five wells, highlighting the lateral variation in formations thickness.

3.3 Data and Methods

A comprehensive data acquisition program was implemented to acquire core, mud-log and mud gas isotope data from targeted wells investigated in this study (Tables 3-1 and 3-2). The coring program was designed to capture full formation-thick cores across the three potential targets; Tuwaiq Mountain, Hanifa and Jubaila Formations to enable detailed source rock characterization. Mud-logs and mud gas isotope data were used to assess type, origin and thermal maturity of the hydrocarbon shows.

Table 3-1 Geochemical properties for Tuwaiq Mountain, Hanifa and Jubaila Formations for the five wells used in the study

Geochemical Attributes		Jurassic Formations		
		Jubaila 185 Samples	Hanifa 172 Samples	Tuwaiq Mountain 333 Samples
Total Organic Carbon Content (Wt. %)	Maximum	4.98	3.90	13.17
	Minimum	1.00	0.15	1.12
	Average	2.44	1.19	4.9
S1 Pyrolysis Yield (mg HC / g rock)	Maximum	4.69	4.58	12.04
	Minimum	0.32	0.02	0.39
	Average	1.05	0.77	3.4
S2 Pyrolysis Yield (mg HC / g rock)	Maximum	7.55	6.18	18.8
	Minimum	0.55	0.02	0.54
	Average	2.53	0.8	3.4
Hydrogen Index (S2*100/TOC)	Maximum	231	218	194
	Minimum	63	50	48
	Average	112	102	91
Tmax (ºC)	Maximum	476	479	493
	Minimum	434	456	455
	Average	462	471	475

Table 3-2 Carbon and deuterium isotope data for gas samples recovered from Jubaila, Hanifa and Tuwaiq Mountain Formations at Wells A through E.

Well	Sample No	Formation	$\delta^{13}C_1$	$\delta^{13}C_2$	$\delta^{13}C_3$	$\delta^{13}iC_4$	$\delta^{13}nC_4$	$\delta^{13}iC_5$	$\delta^{13}nC_5$	δDC_1	δDC_2	δDC_3
WELL-A	1	Hanifa	-59.6	-41.2	-30.9	-30.3	-27.8	-28.4	-28.4	-329	-148	-99
	2	Tuwaiq Mnt	-59.7	-41.1	-30.6	-30.0	-27.7	-28.7	-28.3	-336	-149	-103
	3	Tuwaiq Mnt	-60.1	-40.5	-30.4	-30.6	-27.6	-28.9	-27.9	-335	-147	-101
WELL-B	1	Jubaila	-56.1	-31.1	-25.8	-29.5	-25.1	-27.3	-25.9	-272		
	2	Hanifa	-56.3	-33.6	-27.8	-30.7	-26.9	-28.2	-25.9	-292	-118	-97
	3	Hanifa	-56.1	-32.1	-26.7	-30.5	-25.6	-27.2	-25.1			
	4	Tuwaiq Mnt	-56.0	-31.3	-25.6	-29.8	-24.9	-26.9	-24.2	-292	-118	-96
WELL-C	1	Jubaila	-52.8	-33.7	-28.0	-30.1	-26.9	-29.2	-33.4	-265		
	2	Jubaila	-53.2	-33.5	-28.0					-265		
	3	Jubaila	-56.2	-33.2	-27.8		-26.8	-28.4	-32.8	-266		
	4	Hanifa	-56.2	-31.7	-26.6	-30.5	-26.1	-28.6	-34.5	-290	-100	
	5	Hanifa	-56.4	-31.8	-26.8	-31.7	-26.7	-28.1	-34.3			
	6	Tuwaiq Mnt	-55.9	-30.5	-25.5					-310	-116	
	7	Tuwaiq Mnt	-55.5	-30.5	-25.5	-29.4	-24.7	-27.2	-30.1	-293	-105	-91
	8	Tuwaiq Mnt	-56.0	-30.7	-25.4	-30.1	-24.7	-27.0	-31.4	-294	-113	
	9	Tuwaiq Mnt	-55.7	-30.5	-25.3					-306	-118	
WELL-D	1	Jubaila	-50.2	-29.7	-26.8	-29.7	-26.1	-28.7	-25.2	-224	-128.0	-105
	2	Jubaila	-50.4	-30	-26.3	-29.4	-25.9	-27.7	-24.8	-220	-125.0	-103
	3	Jubaila	-50.2	-30	-26.3	-28.9	-25.6	-27.3	-24.1	-223	-130.0	-105
	4	Hanifa	-52.4	-30.2	-26.1	-29.4	-25.2	-27.1	-24.1	-256	-120.0	-103
	5	Tuwaiq Mnt	-53.8	-29.8	-25.9	-29.8	-24.8	-27.1	-23.9	-278	-110.0	-96
	6	Tuwaiq Mnt	-53.8	-29.4	-25.5	-29.4	-24.4	-26.5	-23.8	-281	-107.0	-98
	7	Tuwaiq Mnt	-54.1	-29.4	-25.1	-29.4	-24.2	-26.6	-23.9	-281	-109.0	-97
	8	Tuwaiq Mnt	-53.7	-30	-25.9	-30	-24.6	-26.6	-24	-279	-109.0	-93
WELL-E	1	Jubaila	-50.5	-30.5	-27.8	-31.0	-26.2	-29.3	-25.2	-225		
	2	Jubaila	-50.9	-29.6	-26.3	-30.1	-25.2	-28.5	-24.8	-233		
	3	Jubaila	-51.0	-29.1	-25.3	-29.2	-24.1	-27.7	-23.7	-229		
	4	Hanifa	-56.6	-28.6	-24.6	-30.4	-22.8	-26.9	-22.0	-267		
	5	Hanifa	-56.3	-28.2	-22.5	-30.2	-22.5	-26.7	-23.0	-273		
	6	Hanifa	-53.0	-26.5	-22.7	-28.8	-22.0	-25.9	-22.6	-280		
	7	Tuwaiq Mnt	-51.3	-25.4	-22.1	-28.3	-21.8	-25.5	-21.8	-277		
	8	Tuwaiq Mnt	-51.5	-25.3	-22.1	-28.3	-21.5	-25.3	-22.1	-269		
	9	Tuwaiq Mnt	-50.7	-24.4	-20.8					-270		

3.3.1 Coring and Analysis

The exact cored intervals were pre-determined by seismic data and through correlation with historical offset wells. While drilling, coring points were picked by utilizing near-bit Measuring While Drilling Gamma Ray (MWD GR) tools to precisely identify formation tops. This coring technique also allowed the capture of portions of the overlying and underlying formations to then accurately pick the transitions across formations, while at the same time, eliminating the risk of missing targeted Tuwaiq Mountain, Hanifa and Jubaila source intervals. In addition, these short cored transition intervals above and below formations of interest can provide valuable data for future sedimentological work to understand depositional history, and engineering information on fracture growth behavior. RockEval pyrolysis and LECO® were utilized to identify source rock intervals and assess their quality (generative potential) and thermal maturity (Table 3-1). Source rock maturity was also determined by direct organic microscope analysis. For microscope analysis, whole-rock pellets are prepared using cold epoxy and allowed to cure overnight. Pellets are polished and detrital Organic-matter fragments identified microscopically in reflected and fluorescent light. Depending on fragment size, one or more random reflectance measurements (Ro) made on each fragment using the standard technique of coal petrography and reflectance investigation (Bustin et al, 1985). The thermal maturity analysis system consist of a Zeiss Axiotech incident and transmitted light microscope equipped with mechanical stage and tungsten halogen and xenon gas discharge light sources. All analyses were conducted at 50X magnification under oil immersion. To measure reflectance, the microscope is equipped with a J&M Analytik's TIDAS S MSP 200 photomultiplier that perform fast and highly sensitive measurements in conjunction

with the powerful software that control the photometer and the microscope to record data, build histograms, and calculate statistical parameters. KB standards sapphire, YAG, and GGG used for calibration. A Zeiss AxioCam MRC digital camera is used to document and prepare high quality images of different organic particles under reflected white light and UV light.

3.3.2 Mud Gas Isotope Sampling and Analysis

Mud Gas Isotope Logging (MGIL) is an industry utilized formation evaluation logging technology involving direct isotopic and compositional measurements of formation gases sampled from the circulating mud-stream during drilling (Ellis et al., 2003). Information of this nature has been shown to provide direct benefits to exploration, including detection of missed pay zones, suppressed show recognition, seal evaluation, and petroleum system evaluation. Saudi Aramco started utilizing the MGIL technology in unconventional gas exploration programs (shale and tight sand). Benefits for unconventional gas exploration include identification of active source rocks, identification of sweet spots within tight reservoirs, identification of thermal maturity of hydrocarbons and indirect estimation of fracture height growth. The MGIL technique is relatively inexpensive and equipment is easily accommodated on drilling rigs. The MGIL technique samples the same gas stream from which standard mud gases are analyzed. The technique was developed to use existing onsite well mudlogging equipment, technology, and captures representative gases from the mudlogging gas flow-line. For a frontier basin such as Jafurah Sub-Basin, an MGIL sampling strategy was designed to collect one sample approximately every 150 ft. in the nonproductive zones to establish a background gas trend. Once a background is established in a field, the sampling interval is relaxed to 500 ft. or greater on subsequent wells. During

"shows," the sampling interval is increased to about one sample every 30 ft. of penetration. The isotopic ratio of the different gas components are analyzed using an Isotope Ratio Mass Spectrometer (IRMS) outlined in detail below (Ellis et al., 2003). The accuracy of the pre-drilling seismic estimated tops and formation thicknesses was compared to the actual depths encountered during drilling to determine the number of representative gas samples obtained. Since the Hanifa Formation was found to be predominantly a non-source facies, only a minimum number of samples to adequately cover the formation thickness were selected for subsequent isotopic analysis. For much thicker intervals the top, middle and bottom–third would be sampled. In cases such as the Jubaila Formation in Well-A and Well-B, the source interval (excluding poor or non-source facies) was found to be largely non-existent or insufficiently resolved. Missing data in (Table 3-2) was generally the result of non-selection, or typically as in the case of deuterium analyses, low gas component concentration (below analytical minimum required).

3.3.2.1 Procedure for Gas Isotope Analysis

For determination of the δ13C (methane through pentane) and δ2H (methane, ethane and propane) of a hydrocarbon gas component, the GC-C-IRMS technique is utilized. Individual gases must first be separated from other gases in the mud gas sample by injecting into the preparation system and GC column enough sample to yield a substantial peak on the IRMS. Solenoid valves are on the outlet of the GC column and either vent the GC carrier stream or channel it through a high temperature conversion furnace. For 13C analysis, any hydrocarbon component of interest is passed through a furnace containing a metal oxide catalyst, where high temperature oxidation to CO2 and H2O combustion products occurs. The CO2 and H2O are then passed through an interface where H2O is

removed via a water separator and the CO2 continues into the IRMS where the associated isotopic value is measured. For 2H analysis any hydrocarbon component of interest is passed through an inert furnace where high temperature conversion to H2 and H2O reductive products occurs. The H2 and H2O are then passed through an interface where H2O is removed via a water separator and the H2 continues into the IRMS where the associated isotopic value is measured. The IRMS produces reliable data within a predetermined sample signal range, and only samples that can produce an appropriate size signal are analyzed or reported. A minimum of 20% of all analyses on the IRMS are samples for quality control, either as duplicate sample analyses or analysis of laboratory reference gases. From these quality control samples reproducibility of the 13C isotope data within ± 0.3 ‰ is required. Samples that contain low concentrations of hydrocarbon gases required an enrichment technique using liquid nitrogen. Isotopic compositions are reported relative to Peedee belemnite (VPDB) standard for carbon and relative to standard mean ocean water (SMOW) for hydrogen. Precisions for individual components in the molecular analysis are ±2% and ±0.1‰ for δ13C by cryogenic separation and ±0.3‰ for δ13C by on-line continuous flow gas chromatography–isotope ratio– mass spectrometry. Precisions for δ2H measurements are ±2‰ by off-line cryogenic separation and ±5‰ by on-line continuous flow methods.

3.4 Results and Discussion

3.4.1 Source Rock Characterization

For this study, Rock Eval pyrolysis (Tissot and Welte 1984) was used to characterize the source rock quality within the Middle and Upper Jurassic Formations in the Jafurah frontier basin. The analyses were performed on around 700 core samples collected from five unconventional exploration wells (Well-A, -B, -C, -D and -E). Table 3-1 summarizes the average geochemical properties for the Tuwaiq Mountain, Hanifa and Jubaila Formations. The distribution of total organic carbon (wt. % TOC) content for the three Formations is shown in (Figure 3-4). Based on the average geochemical attribute obtain for this study (Table 3-1), both the Tuwaiq Mountain and Jubaila Formations in the Jafurah Sub-Basin possess excellent hydrocarbon attributes, such as high total organic carbon (TOC) content and sufficient maturity combined with a relatively shallow burial depth to allow for an economical unconventional shale gas and hydrocarbon liquids development. These intervals, especially the Tuwaiq Mountain, have similar petrophysical characteristics (i.e. organic richness and maturity) to proven unconventional shale gas reservoirs in North America. On the other hand, the Hanifa Formation in the Jafurah Sub-Basin shows relatively low source rock quality and limited unconventional potential. Discussion in this paper will therefore focus on the Tuwaiq Mountain and Jubaila Formations, as they are the primary and the secondary targets for unconventional shale gas exploration in the Jafurah Sub-Basin.

3.4.1.1 Tuwaiq Mountain Formation Source Rock Potential

High total organic carbon (TOC) content, predicted by Gamma Ray (GR) logs across the Tuwaiq Mountain Formation source rock tend to be cyclical, probably due to fluctuations in relative sea level (Carrigan et. al., 1995). The observed cyclicity can easily be seen from well logs (Figure 3-3). Average TOC values of 4.9% together with maximum values recorded as high as 13.17% confirm excellent source rock potential (Figure 3-4). At present depth and present-day thermal maturity, this Formation has hydrogen indices (HI) of 48 to 194 mg HC/ g TOC. At shallower depth and lower maturities, Tuwaiq Mountain source rock to the west of the study area shows hydrogen indices (HI) of 500 - 650 mg HC/ g TOC, typical of Type IIS kerogen (Ayres et al., 1982, Carrigan et. al., 1995). In the stratigraphic cross section in (Figure 3-3), the thickness of the Tuwaiq Mountain Formation is relatively uniform between the wells used in this investigation with a slight increase in thickness noted toward the west at Well-A. Thermal maturity level determines the source rock generative potential. Several methods exist that may estimate the maturity level of a source rock (Jarvie et al., 2001). One of the most accepted and accurate methods of determining thermal maturity is vitrinite reflectance (%Ro). Vitrinite is a type of maceral that originate from the woody tissue of higher plants. In cases where no vitrinite is available or rare as the case in carbonate depositional environments, reflectance of solid bitumen or other vitrinite-like macerals is used, and then the measurements are converted to a normalized 'equivalent' reflectance value (VRo- eq).

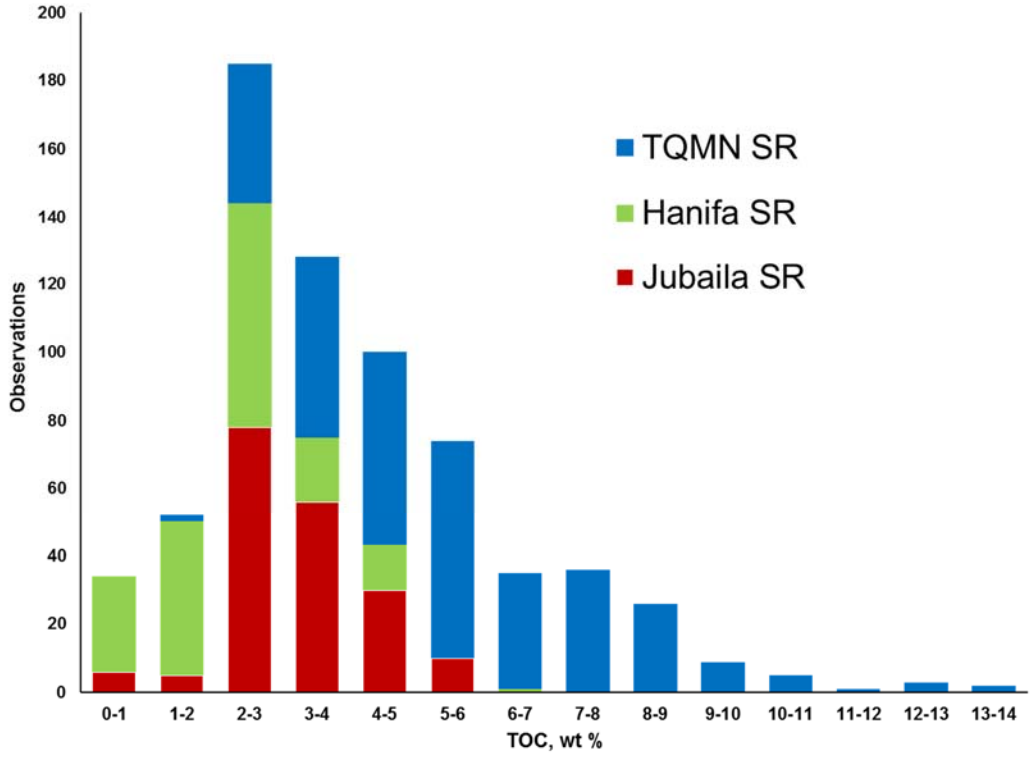

Figure 3-4 Distribution of total organic carbon (wt. %TOC) content for Tuwaiq Mountain, Hanifa and Jubaila Formations.

Solid bitumen reflectance has been used successfully in Lower Paleozoic rocks and in younger rocks that lack vitrinite (Jacob, 1989; Schoenherr et al., 2007; Petersen et al., 2013). Alternatively, organic matter type and maturity may also be assessed using Rock Eval or other pyrolysis techniques. In this paper, present day thermal maturity was measured and calculated for all samples using both Rock Eval and solid bitumen reflectance.

The average Tmax value for the Tuwaiq Mountain source rock is 475 °C, with values as low as 455 °C in Well A in the west and values as high as 493 °C in Well E in the north (Figure 3-1). The data suggest that the Tuwaiq Mountain Formation source rock maturity

ranges from late oil to early dry gas maturity window. In this investigation, we used Jarvie's conversion formula (Equation 1) to estimate VRe from Tmax data (Jarvie et al., 2001). The Jarvie Equation was developed using Ro and Tmax data from the Barnett shale, and has found extensive use in estimating thermal maturity in basins worldwide.

$$VRo - eq = 0.018\ X\ Tmax - 7.16$$ …….. **Equation 1**

The Vitrinite reflectance equivalent (%VRe), calculated for Tuwaiq Mountain samples based on Jarvie's conversion formula was estimated to range from 1.0% in Well-A to 1.55% in Well-E and with an average VRe of 1.39% (Figure 3-5). A clear increase with depth is observed.

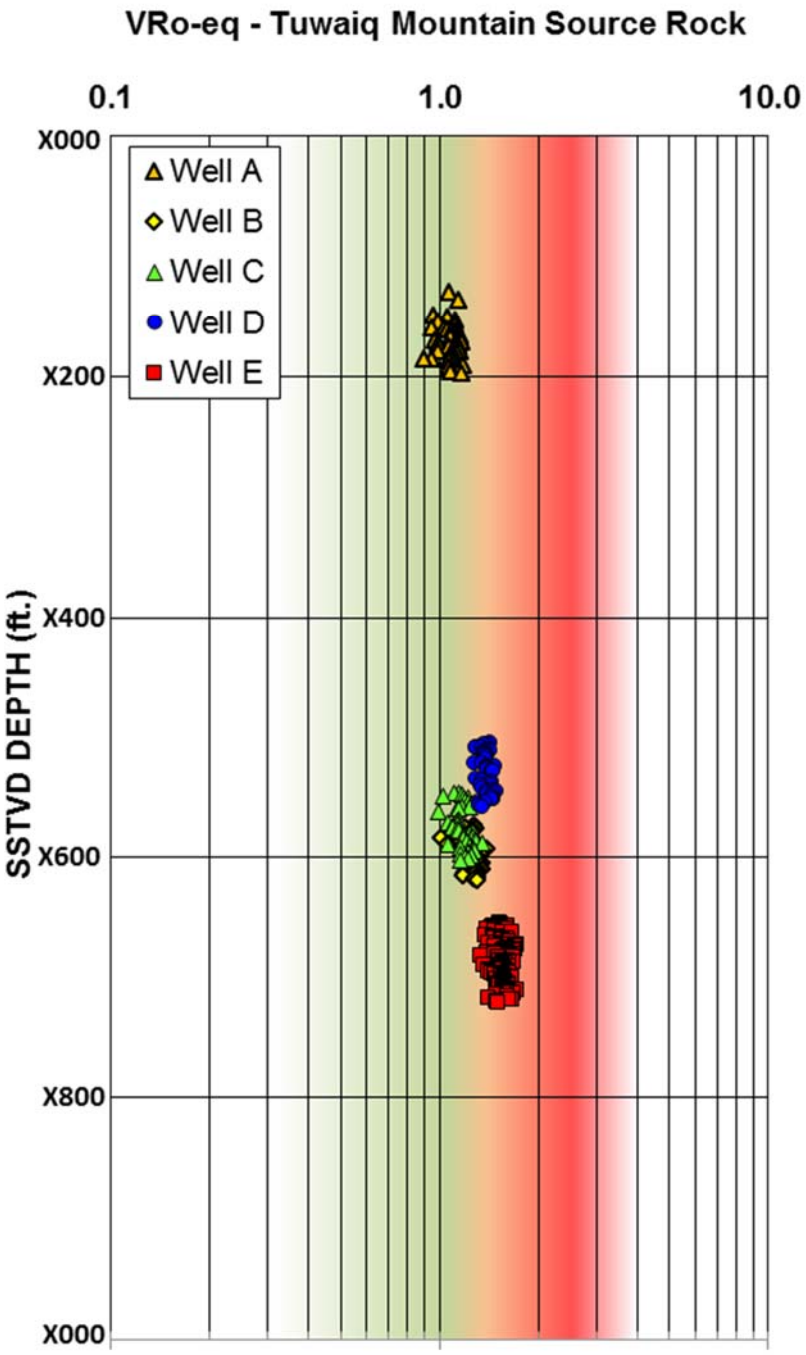

Figure 3-5 Maturity (VRo-equivalent) and depth profile for Tuwaiq Mountain source rocks at Wells A through - E. VRe calculated from Tmax using Jarvie's conversion formula (Jarvie et al., 2001).

To compare maturity estimates obtained using Jarvie's method, maturity also measured on reliable solid bitumen (BitRo) fragments from Tuwaiq Mountain core samples. Vitrinite equivalent (VRe) was estimated from measured solid bitumen reflectance (BitRo) using Jacob's conversion formula (Equation 2), (Jacob, 1989).

$$VRo - eq = 0.618\ X\ BitRo + 0.4$$ …….. .....**Equation 2**

(Figure 3-6, a, b, c, d and e) shows the bitumen reflectance data and images of representative Tuwaiq Mountain core samples from Well-A through Well-E. In general, measured samples are rich in organic matter and consist of solid bitumen having various forms, co-deposition with carbonate grains, and in association with framboidal pyrite in some cases. A network of amorphous bituminite and traces of inertinite were also observed in the matrix. Figure 3-7 shows a cross plot of Tmax-derived VRE versus Bitumen-derived VRE. The relationship between the two calculated VRE is very close with an average correlation coefficient of 0.93, suggesting that both methods are reliable to use.

The mean solid bitumen reflectance (BitRo) recorded for a Tuwaiq Mountain core sample at Well-A was 1.01% based on 28 readings (Figure 3-6a), which resulted in a VRe of 1.02% using Jacob's conversion formula. This value is in excellent agreement with the 1.03 % VRe calculated from Tmax using Jarvie's equation (Figure 3-7). Both maturity calculation methods suggest the Tuwaiq Mountain organic matter in Well-A is presently at a maturity corresponding to the oil window of hydrocarbon generation.

In Well-B, the mean solid bitumen reflectance (BitRo) recorded for a Tuwaiq Mountain core sample was 1.5% based on 38 readings (Figure 3-6b), which resulted in a VRe of

1.33% using Jacob's conversion formula. This value is also in excellent agreement with Vre calculated from Tmax (1.34) using Jarvie's equation (Figure 3-7).

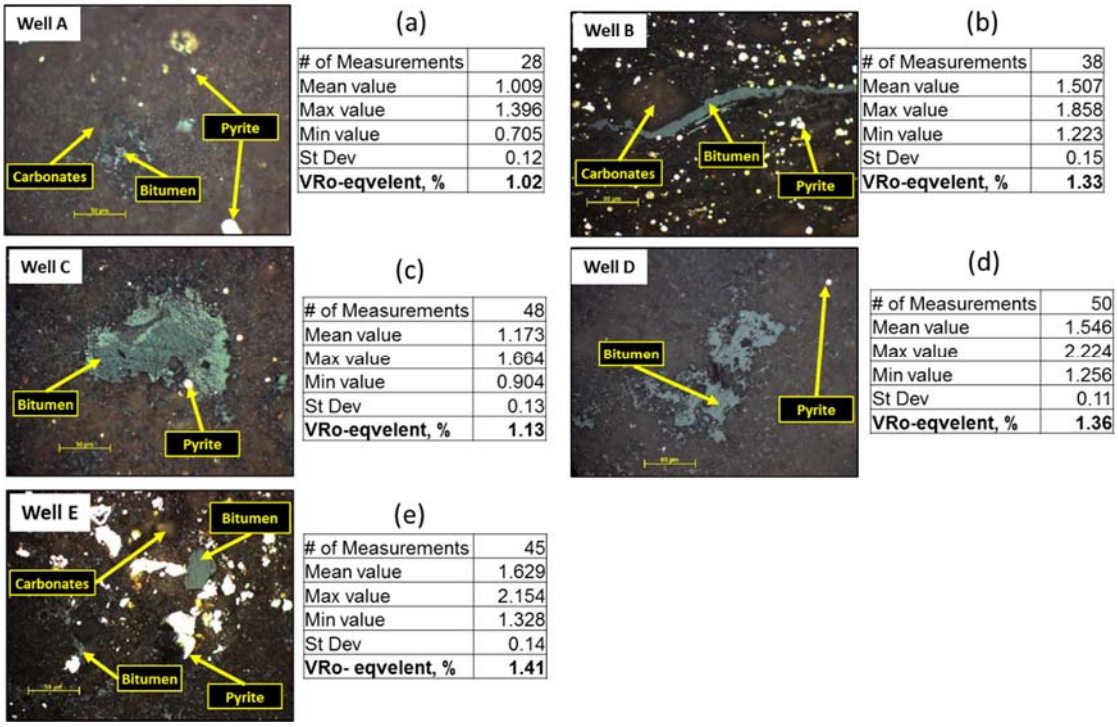

Figure 3-6 Bitumen and vitrinite reflectance data and images of representative Tuwaiq Mountain core samples for Wells A through E. VRe was calculated based on Jacob's conversion formula: VRo - eq = (0.618 (BitRo) + 0.4).

Both maturity calculation methods suggest that Tuwaiq Mountain organic matter in Well-B is mature and is at the wet gas generation window maturity. The mean solid bitumen reflectance (BitRo) recorded for a Tuwaiq Mountain core sample at Well-C was 1.2% based on 48 readings (Figure 3-6c), a VRe of 1.12% was calculated using Jacob's conversion formula. This value is comparable with VRe 1.21% calculated from Tmax using the Jarvei formula (Figure 3-7). Both calculation methods suggest that Tuwaiq Mountain organic matter in Well-C is mature and is at the late oil generation window.

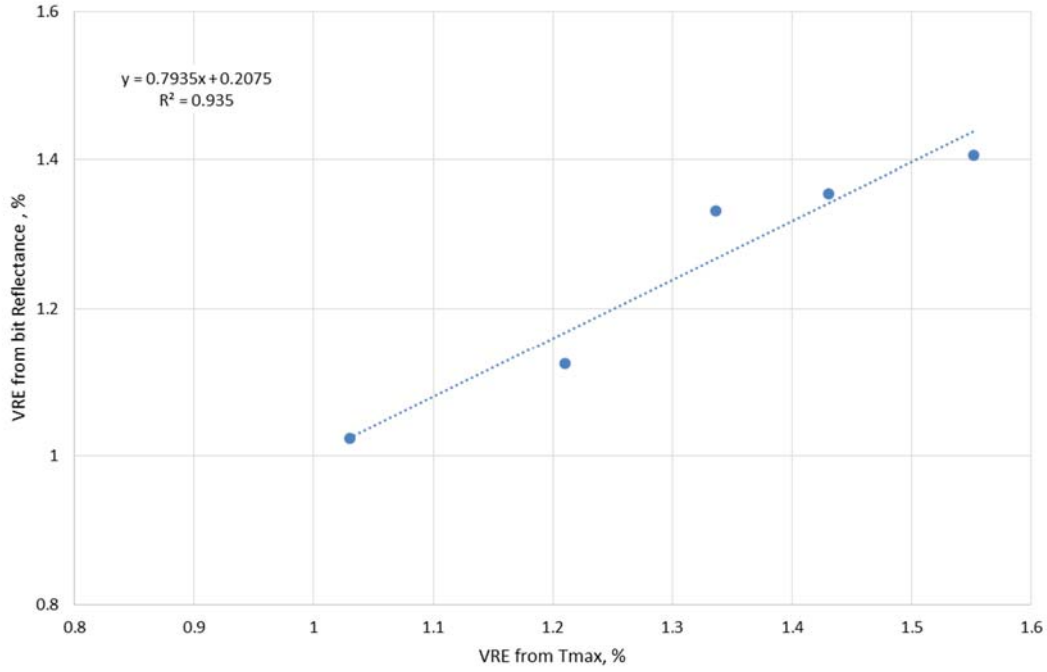

Figure 3-7 Cross plot of Tmax-derived VRE versus Bitumen-derived VRE.

For Well-D, the mean solid bitumen reflectance (BitRo) recorded for a Tuwaiq Mountain core sample was 1.54% based on 50 readings (Figure 3-6d), which resulted in a VRe of 1.36% using Jacob's conversion formula. This value agrees very well with a VRe value of 1.43% calculated from Tmax, using Jarvie's equation (Figure 3-7). Both maturity calculations suggest that Tuwaiq Mountain organic matter in Well-D is very mature and in the late wet gas generation window.

The measured mean bitumen reflectance (BitRo) for a Tuwaiq Mountain core sample at Well-E was 1.63% based on 45 readings (Figure 3-6e); the VRe was calculated to be 1.41% using Jacob's conversion formula. However, %VRe calculated from Tmax for this well is found to be 1.55% slightly different than the VRe calculated from bitumen reflectance

(Figure 3-7). At present, maturity measured on vitrinite and maturity calculated from Tmax (Jarvie's formula), that the Tuwaiq Mountain organic matter in Well-E is slightly more mature and is at the dry gas generation window. It can be concluded that the slight disparity observed between these techniques for this sample may suggest that one of these methods (Tmax-derived VRE versus Bitumen-derived VRE) is less sensitive at slightly higher maturity. However, the carbon isotope data as will be discussed later is in a better agreement with the Tmax-derived VRE.

3.4.1.2 Jubaila Formation Source Rock Potential

The Jubaila source rock shows an average TOC value of 2.44% with a maximum of 4.98% (Table 3-1). The average Tmax values recorded for the Jubaila source rock was 462 °C, with values as low as 453 °C for Well-A in the west, which corresponds to an oil generation maturity window. At this maturity level, Hydrogen indices of the samples are between 63 and 231 mg HC/g TOC suggesting a type II kerogen; possibly with minor contribution of type III kerogen. The Jubaila source rock maturity increases to the east reaching a maximum average Tmax value of 469 °C in Well-E, which at present corresponds to a wet gas generation maturity window. Very similar results were achieved using Jarvie's conversion formula, the Vitrinite reflectance equivalent (VRo -eq) for the Jubaila source rock was estimated to range from 0.99% at Well-A to 1.28% at Well-E and with an average VRo -eq of 1.1% (Figure 3-8).

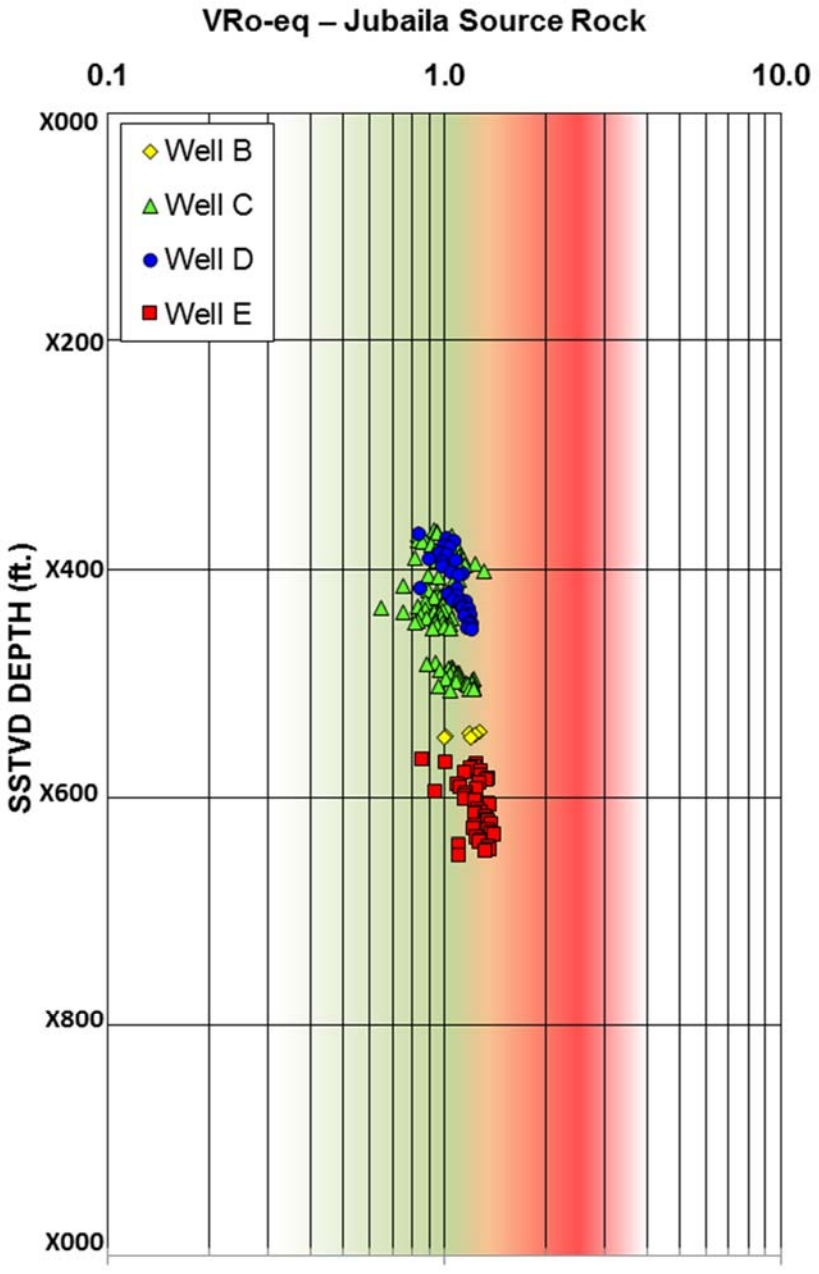

Figure 3-8 Maturity (VRo-equivalent) and depth profile for Jubaila source rocks at Wells A through E. VRe was calculated from Tmax using Jarvie's conversion formula (Jarvie et al., 2001).

3.5 Mud Gas Isotope Data Interpretation

For the five selected Jafurah Sub-Basin wells shown in (Figure 3-1) (Wells A through E), MGIL sampling programs were developed to enable capture of representative gases from the Jubaila, Hanifa and Tuwaiq Mountain Formations (Table 3-2). Figure 3-9 shows depth plots for Well-D and Well-E selected as type examples illustrating general geological data together with gas sampling locations. The vertical depth y-axis covers 550' (from the same starting depth) encompassing all three formations for each well. The plot reveals the present day depth variations between the two wells across more than 80 km of the basin, for which the depth differential in the Tuwaiq Mountain formation is only approximately 170' suggesting a wide smooth subsidence in the basin. The lower x-axis shows the recorded well site drilling mud gas measurements (C1-C5 total gas), which for each Jubaila and Tuwaiq Mountain source rock reveal stronger gas shows towards the basal sections. This is typical of transgressive depositional cycles where the high concentration of organic matter, and consequently, high gas shows can be found toward the base of each formation. It is not possible to directly compare gas abundances between wells as Well-E was drilled significantly more overbalanced than Well-D. The upper x-axis in (Figure 3-9) shows the measured methane carbon isotopic values (‰) for each gas sampling location and the interpolated trend. Interestingly, for Well-D the shallower Jubaila methane carbon isotopic values are significantly are heavier than that of the deeper Tuwaiq Mountain Formation. This is highly unusual as isotopic trends with increasing depth generally result in heavier isotopic values due to progressive generation of isotopically heavier methane gas via thermal cracking of indigenous kerogen. For the limited depth range covered here, no significant differences would be expected.

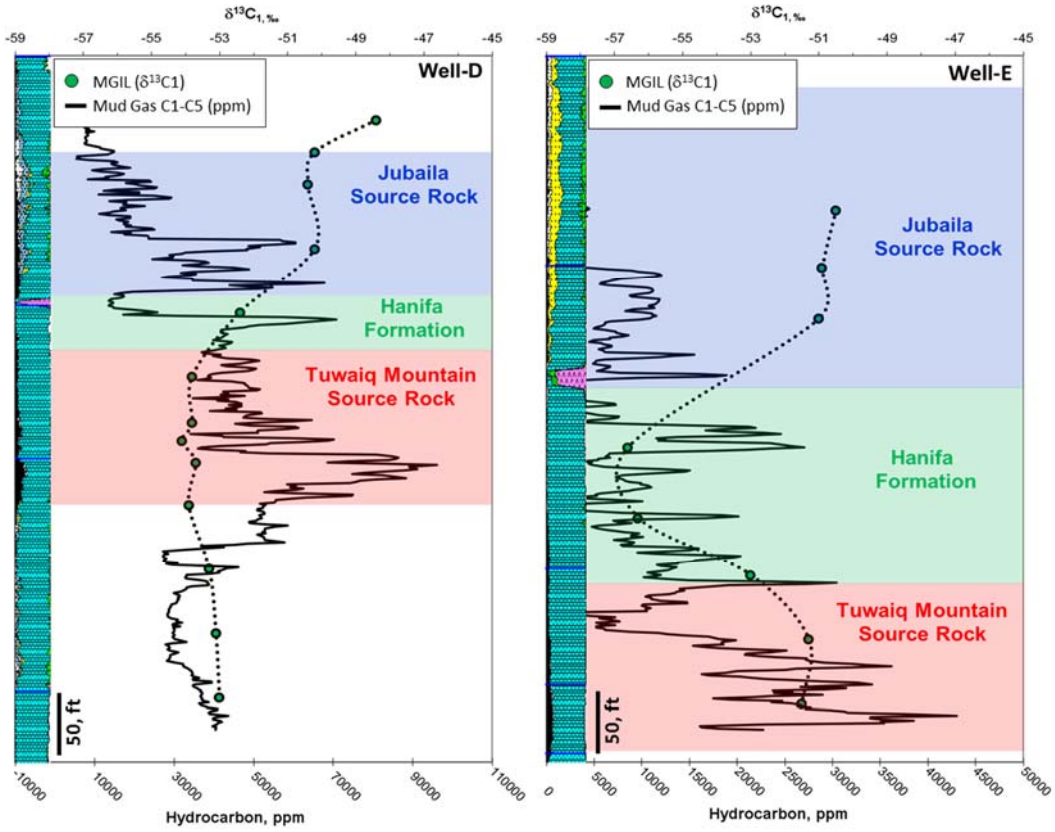

Figure 3-9 Lithofacies, carbon isotope and gas composition profiles for wells D and E.

What the values may suggest is that the Jubaila Formation source organic matter may be distinctly different than that of the underlying Tuwaiq Mountain formation. For Well-E, no significant carbon isotopic differences between the two source rock formations were observed. Interestingly, since the Jubaila Formation isotopic signatures in both Well-D and Well-E are very similar, the Tuwaiq Mountain methane gas isotopic values in Well-E appear to have disproportionately increased. This apparent significant increase in Well-E Tuwaiq Mountain maturity appears to be a result of the higher geothermal gradient observed near Well-E. Figure 3-10 illustrates a simplified reconstructed geothermal

gradient map for the eastern Saudi Arabia. Temperature gradients were calculated from corrected bottom hole temperature measurements at wells across the Arabian Basin. The map shows an increase in geothermal gradient in the Jafurah Sub-Basin from south to north. This increase is attributed to possible different basement rock composition (Aramco Internal and confidential data. As discussed in the next section, measured isotopic values for samples collected in the Hanifa reservoir formation also exhibited different trends. For Well-D, the one sample collected recorded a value in between that of both source rocks suggesting possible mixing, while in Well-E the three measured values were more negative than either source formations suggesting indigenous gas or early hydrocarbon expulsion from one or both adjacent source rocks.

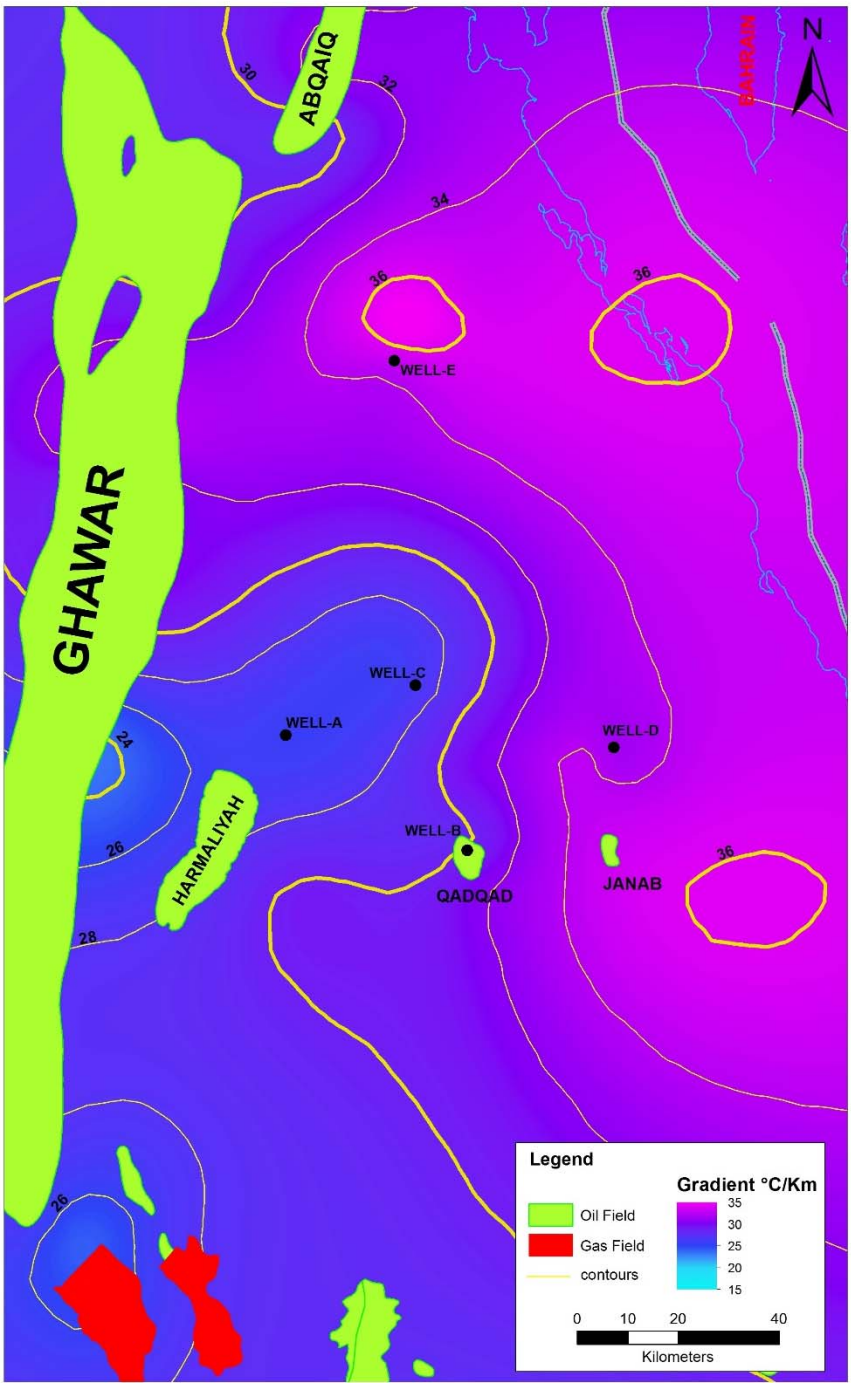

Figure 3-10 Simplified geothermal gradient map of eastern Saudi Arabia showing the Ghawar giant oil field in Saudi Arabia, showing the five wells used in the study.

3.5.1 Gas Origin

Gases sampled directly from unconventional shales are unique in that the gases generated from source rock organic matter as a result of deep burial and associated subsurface heating are purely thermogenic in composition. The direct sampling of gases in source rocks and absence of any secondary sourced component that could be scavenged, as experienced during conventional system migration phases permits accurate source typing and maturity calibration. (Figure 3-11) shows a plot of methane carbon and hydrogen (deuterium) isotopic data for each of the gases sampled from Wells A through E (Table 3-2). It is apparent that gases sampled from the Jubaila, Tuwaiq Mountain source rocks are isotopically distinct, and individual parallel trends separating the two source rocks are clearly established. While the methane carbon isotopic character of both source rock gases significantly overlap, the deuterium values are well separated. This observation may for the first time, permit the accurate identification of hydrocarbons generated from these sources in regional Saudi Arabian petroleum systems. The two source rocks are only geologically separated by a few million years and were deposited under similar depositional conditions, therefore 'not surprisingly'; oil geochemistry has yet to yield any useful tools for separation. It is important to note that no reliable oil known to originate from the Jubaila Formation has ever been targeted or identified. It has been assumed that the organically richer Tuwaiq Mountain formation has been the dominant, if not only, oil-generating source rock (Carrigan et al. 1995). Further gas isotopic work involving many more regional wells will continue to consolidate and define these observed relationships. The gas samples collected and analyzed from the Hanifa Formation plot with wide variation. Interestingly, some data plot along the identified proposed source rock trends,

while others plot in between these trends. The Hanifa formation averages only 92' thick (+/- 38') across the five wells sampled in the Jafurah Sub-Basin. Data from Well-A (Table 3-2) reveals the single Hanifa gas sample 1 (approximately 27' below Jubaila Formation) in the 100' thick Hanifa interval plots directly with an underlying representative sample from the Tuwaiq Mountain formation.

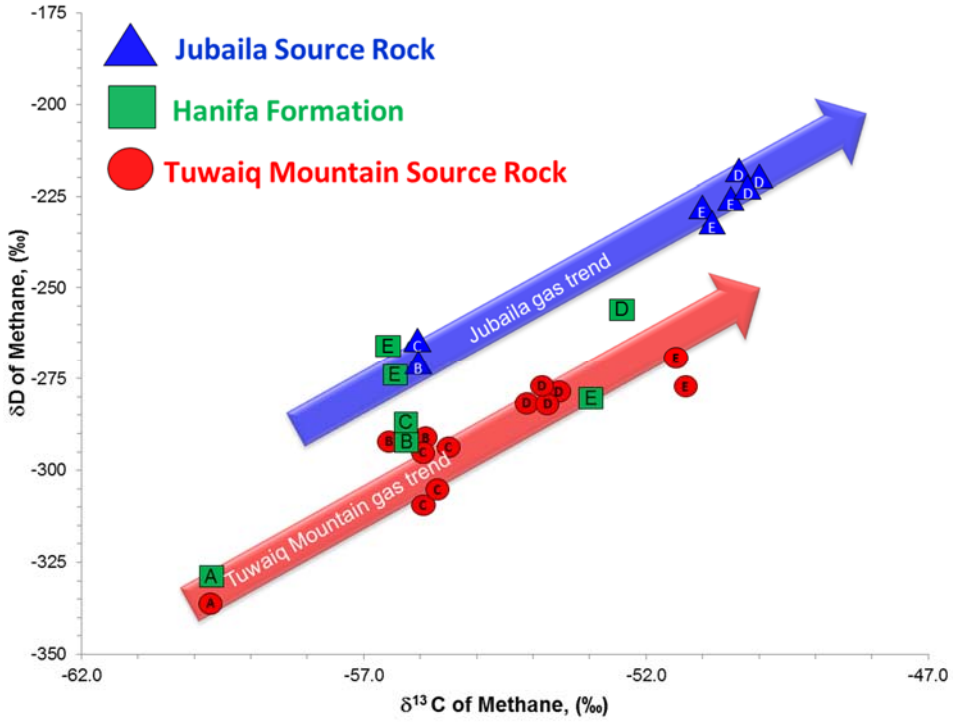

Figure 3-11 Cross plot of methane carbon and deuterium isotopes of mud gas samples collected from Jubaila, Hanifa and Tuwaiq Mountain Formations at Wells -A, -B, -C, -D, and -E. Jubaila gas is distinct in isotopic character to Tuwaiq Mountain, whereas, Hanifa gases reveal mixing.

Table 3-3 Tuwaiq Mountain Formation Maturity Calibration data for Well A, B, C, D and E.

Well	Tmax (C°)	Vitrinite Reflectance Equivalent from Tmax VRo-eq= (0.018*Tmax-7.16)* (%)	Vitrinite Reflectance Equivalent from solid bitumen (BitRo) VRo-eq= (0.618*BitRo + 0.4)** (%)	$\delta^{13}C_1$	2H1
Well A	455	1.03	1.02	-59.7	-336
Well C	465	1.21	1.12	-55.8	-301
Well B	472	1.34	1.33	-56.3	-292
Well D	477	1.43	1.36	-53.9	-280
Well E	484	1.55	1.41	-51.4	-273

* Jarvie et al., 2001
** Jacob, 1989

As both these samples plot along the identified Tuwaiq Mountain trend it can be concluded that gases sampled from the Hanifa Formation in Well-A are derived solely from that underlying source formation. A similar explanation can be applied to gases sampled from the Hanifa formation in Well-B. For Well-C, a gas sampled in the Hanifa formation (sample 5) appears to plot midway between the two source rock trends suggesting that gas mixing is occurring with expelled hydrocarbons contributions from both source rocks. (Figures 3-11 and 3-12) explore these mixing and sole source observations in more detail and in turn highlight a valuable application of the MGIL technology for charge assessment in reservoirs. (Figures 3-12 and 3-13) show an expanded plot for gases sampled from Well-D and Well-E, respectively, across the Jubaila, Hanifa and Tuwaiq Mountain Formations. Also included are the source rock trends (dotted lines) used as a calibration line derived from the averaged gas isotopic data for samples within each formation and for each well. A linear least squares regression analysis (see tables in Figures 3-12 and 3-13) is shown for each Jubaila and Tuwaiq Mountain trend and reveals reasonable correlation coefficients (r2) of 0.83 and 0.87 respectively. While further data will refine and likely improve the confidence in these values, this is considered a very promising fit when taking into account the limited number of exploration wells covering this large frontier basin. For Well-D, the

averaged isotopic data for representative gases from each Jubaila and Tuwaiq Mountain source formation plot as expected along the established trend lines (Figure 3-12). The significant difference in the source trends may be the result of differences in the organic matter content, maturity, or both. Regardless, as the data for the gas sampled from the Hanifa formation falls in between each of these source rock end- members, a simple two component-mixing model is the plausible explanation.

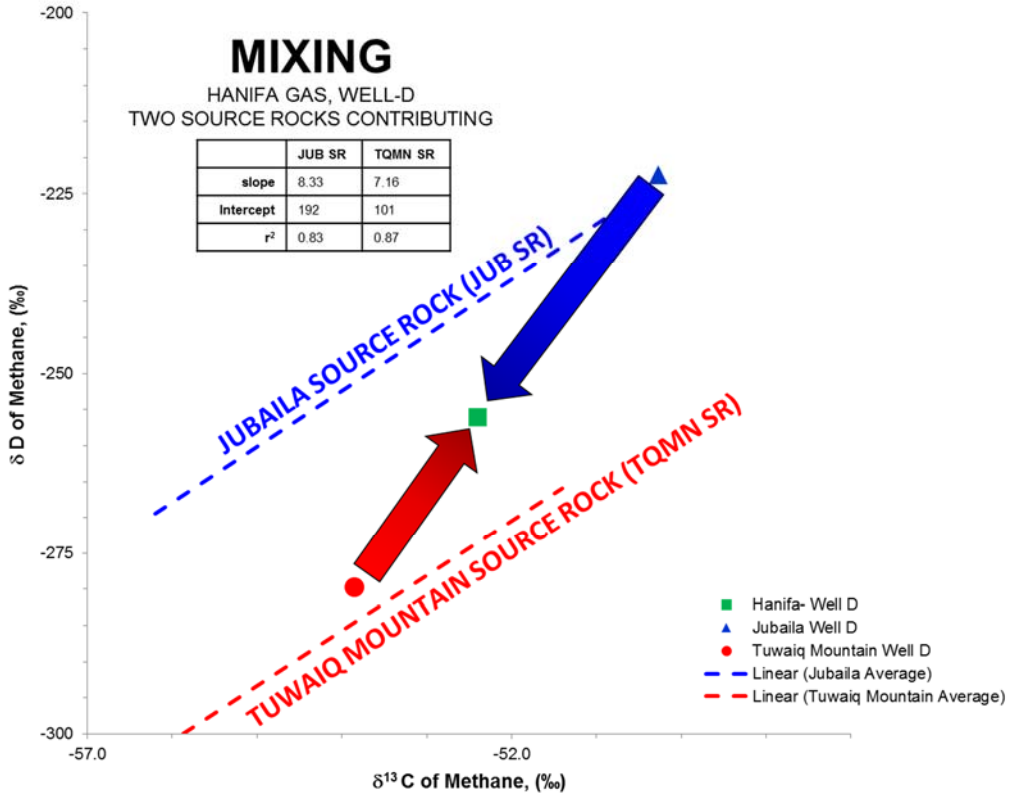

Figure 3-12 Cross plot of methane carbon and deuterium isotope showing the average trend for Jubaila and Tuwaiq Mountain gases in dashed lines. Jubaila gas in Well-D is distinct in isotopic character to Tuwaiq Mountain, whereas, Hanifa gas reveals mixing.

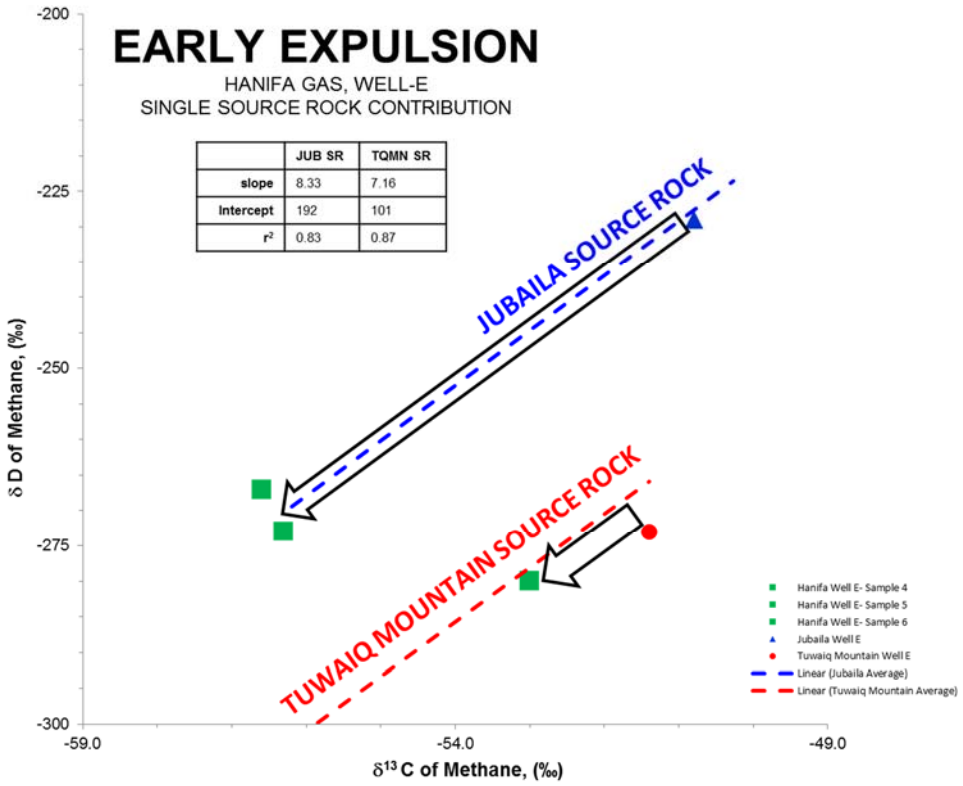

Figure 3-13 Cross plot of methane carbon and deuterium isotope showing the average trend for Jubaila and Tuwaiq Mountain gases in blue and red lines respectively. Hanifa gases in Well-E reveal early expulsion from either Jubaila or Tuwaiq Mountain source rocks.

The anhydrite layer in this location is very thin (< 5 ft) and not considered to represent a strong barrier to hydrocarbon communication from the Jubaila Fm. directly above. Further discussion in the next section explores this model in detail. Well-E sampled source rock gases also plot on the established source trends; however, the three sampled Hanifa formation gases do not plot in between as observed in Well-D, but separately along the source rock trend lines (Figure 3-13). The two uppermost Hanifa Formation sampled gases plot along the Jubaila Formation source trend suggesting they may represent early expelled Jubaila sourced hydrocarbon gases. In contrast, the lowermost Hanifa Formation sampled gas plots along the Tuwaiq Mountain source trend suggesting gases in this zone are also

examples of earlier expelled gases, but in this case derived from the Tuwaiq Mountain source rock. Interestingly the much greater distance along the Jubaila source trend line observed for the uppermost Jubaila sourced Hanifa gases compared to the distance observed for the lowermost Tuwaiq Mountain sourced Hanifa gases suggests that due to the increased anhydrite thickness in this immediate location (15 ft), that the lower maturity Jubaila gases in the Hanifa formation are not directly sourced from the overlying Jubaila, but may have been sourced further downdip where the anhydrite may not present as a significant barrier. The sampling depth for the lowermost Tuwaiq Mountain sourced Hanifa gas is directly above the parent source rock and of more similar maturity suggesting a direct vertical expulsion. With further study on future wells surrounding the Well-E location, more accurate explanations may become possible.

3.5.2 Gas Mixing Model

The identification, in this paper, of a significant Jubaila source rock that has expelled hydrocarbons highlights a critical need to further evaluate potential hydrocarbon contributions from this secondary source to the regional Jafurah Sub-Basin petroleum system. The Hanifa formation, given its appropriate thickness and stratigraphic position between the two source rocks, represents an ideal subsurface laboratory to explore more detailed two component multi-variable mixing models. (Figure 3-14) shows a natural gas plot of the averaged carbon isotopic data for each normal gas species (methane through n-pentane) from each formation for Well-D. As previously mentioned, the range of carbon

isotopic values for each source rock hydrocarbon gas overlap so the resulting profiles are not observed to be considerably different.

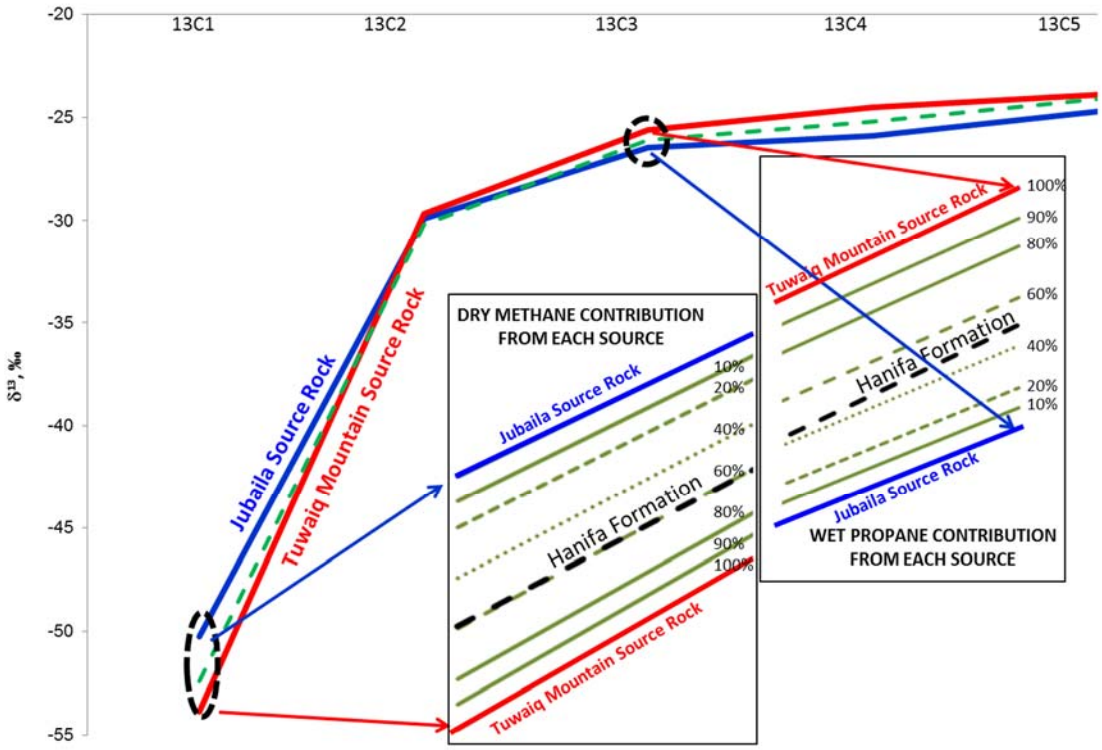

Figure 3-14 Mixing model of Well-D δ13C1- δ13C5 endmembers for Tuwaiq Mountain and Jubaila gases.

Even so, it is clear that gas sampled from the Hanifa formation plots suitably between the Jubaila and Tuwaiq Mountain end members. Mathematical modeling of two component mixing using dual variable gas compositional and carbon isotopic averaged data from the end members permits an estimate of relative hydrocarbon contributions. For methane (dry), the model would suggest 60% of that Hanifa gas is from the Tuwaiq Mountain formation, while for propane gases (wet) the relative contributions appear evenly split between the two source rocks. The greater Tuwaiq Mountain methane gas contribution is expected since this source rock has much higher organic matter composition.

Notwithstanding the importance of identifying any Jubaila source rock hydrocarbon contributions, the suggestion that hydrocarbon liquids, typically associated with wetter gas species such as propane, may be coming from the Jubaila source rock is of major importance. To further support the above estimates, a similar dual variable two component-mixing model was applied to the Well-D deuterium isotopic data (Figure 3-15). As shown in Figure 3-11, deuterium data uniquely separates the two source rocks and the resulting plot in Figure 3-15 for methane, ethane and propane reveals significantly greater spatial separation between the two source rock end members. Mathematical modeling of two component mixing using dual variable gas compositional and deuterium isotopic averaged data from the end members permits a potentially more accurate estimate of relative hydrocarbon contributions. For methane (dry), the model would suggest 60% of that Hanifa gas is from the Tuwaiq Mountain formation, exactly the same value as determined using carbon isotopes. For propane gases (wet), the model suggests that 80% of the contribution comes from the Jubaila formation. This result, although surprising, certainly unequivocally establishes the Jubaila formation as a potentially significant hydrocarbon contributor in this well while further work will assist in supporting the efficacy of this approach when applied in a regional context.

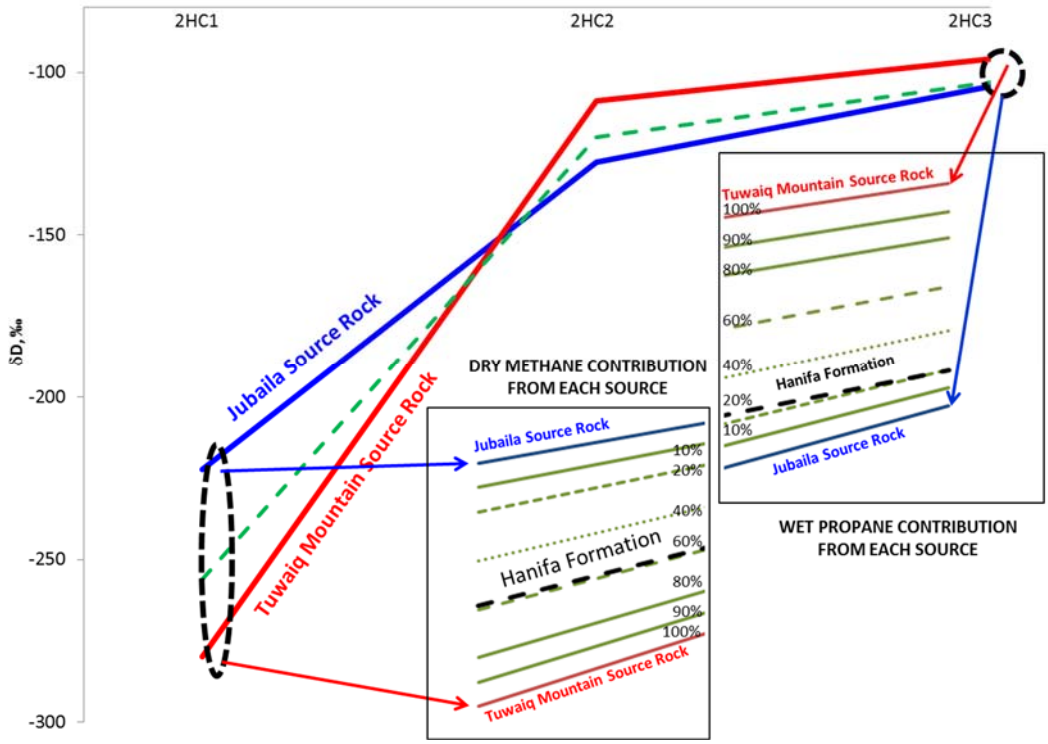

Figure 3-15 Mixing model of Well-D 2HC1-2HC3 endmembers for Tuwaiq Mountain and Jubaila gases.

3.5.3 Gas Maturity Model

Once the provenance of a sampled subsurface gas is determined, the ultimate aim of any geochemical tool is to as accurately as possible estimate the maximum thermal maturity that the parent source rock attained. With conventional petroleum systems, this is extremely difficult to estimate once hydrocarbons expelled from the source rock and begin to migrate along porous conduits from a few tens of meters to hundreds of kilometers in extreme cases, many geochemical signatures of the hydrocarbons are irreversibly altered. These changes are often the result of many different processes, including; mixing with secondary contributors, gravity/density segregation and even distillation physical processes. New fields of science such as those attempting to derive hydrocarbon

generation kinetics from laboratory pyrolysis experiments of source rocks attempt to model subsurface conditions and quantify resultant hydrocarbon products generated. These techniques however require difficult to obtain representative source rock examples and in many cases are required to use poor quality analogues. Since with conventional petroleum systems it is nearly impossible to fact check the model accuracy against real field data from the source rock itself, these approaches are understandably viewed with caution. With unconventional shale petroleum systems and mud gas isotope logging field data it is relatively easy to correlate in situ source rock maturity with the compositional and isotopic products of associated hydrocarbon generation. These reservoir samples are truly representative and self-sourcing.

Using Tuwaiq Mountain source rock data (Table 3-1) and gas isotope data (Table 3-2) from nearly equivalent depth intervals, it is possible to establish accurate thermal maturity relationships between the data (Table 3-3). Source rock maturity in terms of vitrinite reflectance has been derived from Tmax and bitumen reflectance measurements as discussed above. Comparison of data from the two different techniques (Tmax-derived VRE and Bitumen-derived) revealed values in excellent agreement adding good confidence in the maturity estimation. Together with the measured gas isotopic values of entrained generated hydrocarbon gases, these relationships can be mathematically defined to create specific source-maturity isotopic calibrations. (Figure 3-16) shows such a relationship between methane carbon and hydrogen isotopic data with that of estimated thermal maturity vitrinite equivalent data.

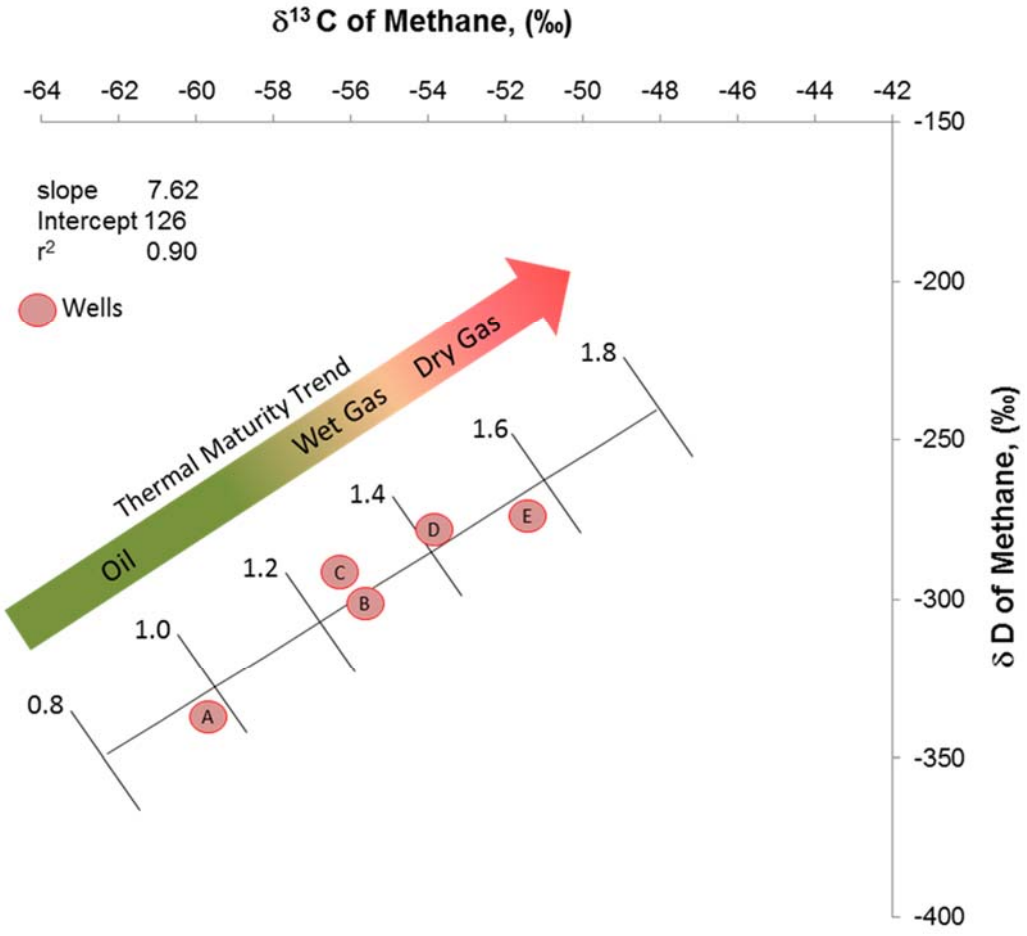

Figure 3-16 Tuwaiq Mountain Formation maturity model based on calibrated carbon and deuterium isotope data.

A least squares regression analysis yielded a correlation coefficient (r2) value of 0.9, permitting strong confidence in establishing a unique Tuwaiq Mountain gas isotopic maturity equation (see below);

$$\textbf{Tuwaiq Mountain vitrinite equivalent} = \mathbf{0.069}\ \boldsymbol{X}\ \boldsymbol{\delta 13C1} + \mathbf{5.13}. \ldots .\textbf{Equation 3}$$

It was observed that for Vre data calculated from isolated kerogen Tmax values (as opposed to whole rock pyrolysis) a correction factor of **-0.3** Vre was required to be applied to the

above equation. While it was noted that Tmax peaks on pyrograms of kerogen isolates appear sharper and easier to define, the cause of the apparent lower Tmax measurements for kerogen isolates or higher Tmax for raw sample is under investigation and will be the subject of future research. This new geochemical tool for estimating Tuwaiq Mountain source rock and expelled hydrocarbon maturity will be critically important in focusing exploration efforts to identify sweet spot areas for drilling. In cases where no or few reliable source rock samples are available, or indeed in situations (e.g. tight gas plays) where only captured hydrocarbon gases are feasible, application of this new tool will be vitally important for evaluation of thermal maturities and potentially the production potential of development wells.

3.6 Conclusion

- The Jurassic play in the Jafurah Sub-Basin represents a new unconventional shale gas play in Saudi Arabia covering an area equivalent in size to Eagle Ford play in south Texas.
- A comprehensive formation evaluation and data acquisition program was implemented to acquire a full complement of cores, well logs, and mud gas isotope data from wells investigated in this study.
- Excellent source rock intervals were identified within the Jubaila and Tuwaiq Mountain Formations; Hanifa Formation present less potential. These source rocks possess excellent shale gas attributes, such as high TOC and associated sufficient maturity combined with a relatively shallow burial depth to allow for an economical unconventional shale gas and hydrocarbon liquids development.Mud gas isotope logging (MGIL) data obtained from the studied wells reveal important

characterization potential enabling clear distinction between Tuwaiq Mountain, Hanifa and Jubaila Formation gases based on their isotopic signatures.

- A gas isotope maturity calibration and correlation equation has been driven to permit accurate VRE maturity assessments identifying the best exploration sweet spot locations that may be tied to future optimal Tuwaiq Mountain production.
- This investigation confirmed that the Hanifa Formation is predominantly a non-source facies in the study area, but one in which expelled hydrocarbons from the adjacent Jubaila and Tuwaiq Mountain source formations could accurately been deconvoluted and identified via MGIL technology which holds good potential for charge identification and assessment in potential reservoirs.
- Next stage lateral drilling developments will leverage MGIL technology to assess the effectiveness of future hydraulic fracturing treatments in this formation and ensure maximum in zone completions for best production potential.

3.7 References

Al-Husseini, M., 1997, Jurassic sequence stratigraphy of the western and southern Arabian Gulf: GeoArabia, v. 2, no. 4, p. 361-382.

Ayres, M. G., Bilal, M., Jones, R. W., Slentz, L. W., Tartir, M. and Wilson, A. O., 1982, Hydrocarbon habitat in main producing areas, Saudi Arabia: AAPG Bull., v. 66, p. 1-9.

Bustin, R.M., Cameron, A., Grieve, D., Kalkreuth, W., 1985. Coal petrology, its principles, methods and applications. Short Course Notes, 2nd edn. Geological Association of Canada, Victoria, 273 pp.

Cantrell, D.L., Nicholson, P.G., Hughes, G.W., Miller, M.A., Bhullar, A.G., Abdelbagi, S.T., Norton, A.K., 2014, Tethyan petroleum systems of Saudi Arabia, in L. Marlow, C. Kendall and L. Yose, eds., Petroleum systems of the Tethyan region: AAPG Memoir 106, p. 613-639.

Carrigan, W. J., Cole, G. A., Colling, E. L., and Jones, P. J., 1995, Geochemistry of the Upper Jurassic Tuwaiq Mountain and Hanifa Formation petroleum source rocks of Eastern Saudi Arabia, in B. J. Katz, ed., Petroleum Source Rocks: Springer-Verlag, New York, p. 67-87.

Cole, G. A., Carrigan, W. J., Colling E. L., Halpern, H. I., Al-Khadhrawi, M. R. and Jones, P. J., 1994, The organic Geochemistry of the Jurassic petroleum system in Eastern Saudi Arabia, Canadian Society of Petroleum Geologists, memoir 17, p. 413-438.

Droste, H. H. J., 1990, Depositional cycles and source rock development in an empiric intra-platform basin, the Hanifa Formation of the Arabian Peninsula: Sedimentary Geology, v. 69, p. 281-296.

Ellis, L., 2004, MGIL maximizes value of mud logging. Special Report: Drilling Technology, American Oil & Gas Reporter, April 127-131.

Ellis, L., Brown, A., Schoell, M. and Haught M., 1999, Mudgas isotope logging while drilling: A new field technique for exploration and production. 19th International Meeting on Organic Geochemistry, 6-10 September 1999, Istanbul, Turkey, Abstracts Part 1, p. 67-68.

Ellis, L., Brown, A., Schoell, M., and Uchytil, S., 2003, Mud Gas Isotope Logging (MGIL) assists in oil and gas drilling operations: Oil&Gas Journal, special report- New Views of Subsurface, May 26, 2003, p. 32-41.

Ellis, L., Berkman, T., Uchytil, S and Dzou, L., 2007, Integration of mud gas isotope logging (MGIL) with field appraisal at Horn Mountain Field, deep-water Gulf of Mexico. Journal of Petroleum Science and Engineering Special Issue, Volume 58, Issue 3-4, pages 444-464.

Jacob, H., 1989, Classification, structure, genesis, and practical importance of natural solid bitumen ("migrabitumen"): International Journal of Coal Geology, v.11 (1), p.65-79

Jarvie, D. M., B. L. Claxton, F. Henk, and J. T. Breyer, 2001, Oil and shale gas from the Barnett Shale, Fort Worth Basin, Texas: AAPG Annual Meeting Program, v. 10, p. A100.

Murris, R.J. 1980, Middle East stratigraphic evolution and oil habitat, AAPG Bulletin, v. 64, p. 597-618.

Petersen, H.I, Schovsbo, N. H., and Nielsen, A. T., 2013, Reflectance measurements of Zooclasts and solid bitumen in Lower Paleozoic shales, Southern Scandinavia: Correlation to vitrinite reflectance. International Journal of Coal Geology v. 114, p.1-18.

Pollastro, R. M., 2003, Total petroleum systems of the Paleozoic and Jurassic, greater Ghawar uplift and adjoining provinces of central Saudi Arabia and northern Arabian-Persian Gulf: U.S. Geological Survey Bulletin 2202-H, 100p.

Schoenherr, J., Littke, R., Urai, J.L., Kukla, P.A., Rawahi, Z., 2007, Polyphase thermal evolution in the Infra-Cambrian Ara Group (South Oman Salt Basin) as deduced by maturity of solid reservoir bitumen. Organic Geochemistry v. 38, p. 1293–1318.

Sharland, P. R., Archer, R., Casey, D. M., Davies, R. B., Hall, S. H., Heward, A. P., Horbury, A. D., and Simmons, M. D., 2001, Arabian Plate sequence stratigraphy: GeoArabia Special Publication 2, Gulf PetroLink, Bahrain, p. 371.

Tissot, B. P. and Welte, D. H., 1984, Petroleum Formation and Occurrences. Second revised and enlarged edition, Springer Verlag Berlin Heidelberg New York Tokyo 1984.

Wilhelms, A., Rein, E., Zwach, C., Steen, A.S., 2001, Application and implication of horizontal well geochemistry. Pet. Geosci. 7, p. 75–79.

Ziegler, M. A., 2001, Late Permian to Holocene paleofacies evolution of the Arabian Plate and its hydrocarbon occurrences: GeoArabia, v. 6, no. 3, p. 445-504.

CHAPTER 4

Basin Modeling

A Basin Modeling Study of Jafurah Sub-Basin, Saudi Arabia; Implications for Unconventional Hydrocarbon Potential of the Jurassic Tuwaiq Mountain Formation

Ahmed Hakami [a] and Sedat Inan [b]

[a] Saudi Aramco, Exploration Organization, 31311, Dhahran, Saudi Arabia

[b] Saudi Aramco, EXPEC Advanced Research Center, Dhahran 31311, Saudi Arabia

Published Paper in International Journal of Coal Geology 165, August (2016) 201-222 (ELSEVIER)

Abstract

The Middle-Upper Jurassic, organic-rich carbonate mudrocks, of the Tuwaiq Mountain Formation in the Jafurah Sub-Basin have long been recognized as a source of hydrocarbons trapped primarily in Upper Jurassic carbonate reservoirs (e.g. Giant Ghawar field). With the recent development of commercial hydrocarbon production of unconventional reservoirs in North America, these organic-rich, carbonate mudrocks are now recognized as productive zones. Three source rock intervals are being evaluated for shale gas potential;

namely, the Tuwaiq Mountain, Hanifa and Jubaila Formations. These source rocks, notably the Tuwaiq Mountain possesses excellent unconventional gas characteristics, such as high total organic content (TOC) and low clay content, and it is in the proper maturity window for oil and gas generation. Five wells, representing the first unconventional gas exploration wells drilled in the Jafurah Sub-Basin have been selected for 1D and 2D basin modeling work. The work was performed to investigate the burial and thermal maturity evolution of the Tuwaiq Mountain Formation. The maturity of the Tuwaiq Mountain Formation intersected in five wells varies from 0.8 to 1.25 %VRE despite only slight differences in burial depths. The present day temperature gradients have been calculated to be higher at well locations where the source rock is at higher maturity. Modeling results suggest that higher temperature gradient areas of the basin requires higher basement heat flow input which leads to satisfactory match between measured and predicted maturity as well as measured versus predicted temperature at present day. This increase of basement heat flow in areas of higher temperature gradient matches the interpreted change in crustal composition (e.g., granitic basement) generating more radiogenic heat. The modeling results suggest that TQMN source rocks started generating oil at about 100 Ma and they reached the peak oil generation at about 70 Ma, and at Present, they are at wet gas generation window in warmer (≥28 °C/km) parts of the basin (the northern and eastern part of the Jafurah Sub-Basin). The central and southwestern part of the basin are cooler, and here, the TQMN source rocks are within the peak oil generation maturity window. The warmer parts of the basin have higher gas potential for the TQMN source rocks compared to cooler parts of the basin. We conclude that for proper modeling and estimations of gas content in source rocks, some skilled modifications in basin modeling parameters are

necessary. For example, variations of the oil saturation threshold is necessary until a gas saturation level equal to or higher than the gas adsorption capacity of the source rock is obtained, otherwise, modeling will lead to overestimation of the oil migration out of the source rock and thus amount of the oil that can be cracked to gas, and thus amount of eventual gas content, will be underestimated. Following our basin modeling study, we note that improvement of the present day subsurface temperature data will be nearly sufficient in future to estimate the maturity and also gas potential of the TQMN source rocks in the Jafurah Sub-Basin.

4.1 Introduction

Organically rich mudrocks are currently targeted for unconventional oil and gas exploration and development in many places around the world, including Saudi Arabia. These types of plays are very challenging to develop as they exhibit great lithofacies heterogeneity, both laterally and vertically. In addition, hydrocarbon resources associated with such plays are difficult to access and extract when compared to conventional reservoirs. The Jafurah Sub-Basin, located east of the giant Ghawar oil field (Figure 4-1), is the primary focus of this paper. The basin is located within the shelf part of the Arabian Plate. (Figure 4-2) depicts the generalized geologic column of the East Central Arabian basin for the Middle- Upper Jurassic Period (Cantrell et al., 2014). The Jurassic organic-rich carbonate mudrocks (Tuwaiq Mountain, Hanifa and Jubaila Formations) have long been recognized as the source of conventional hydrocarbons trapped in the supergiant Jurassic carbonate reservoirs of the Ghawar Field in Saudi Arabia (Cole et al., 1994;

Cantrell et al., 2014). With the recent development of commercial hydrocarbon production from shale source rocks in North America (Montgomery et al., 2005; Jarvie et al., 2007; Alexander et al., 2011), efforts are underway to assess the unconventional resource potential within the Jurassic source rocks in Saudi Arabia.

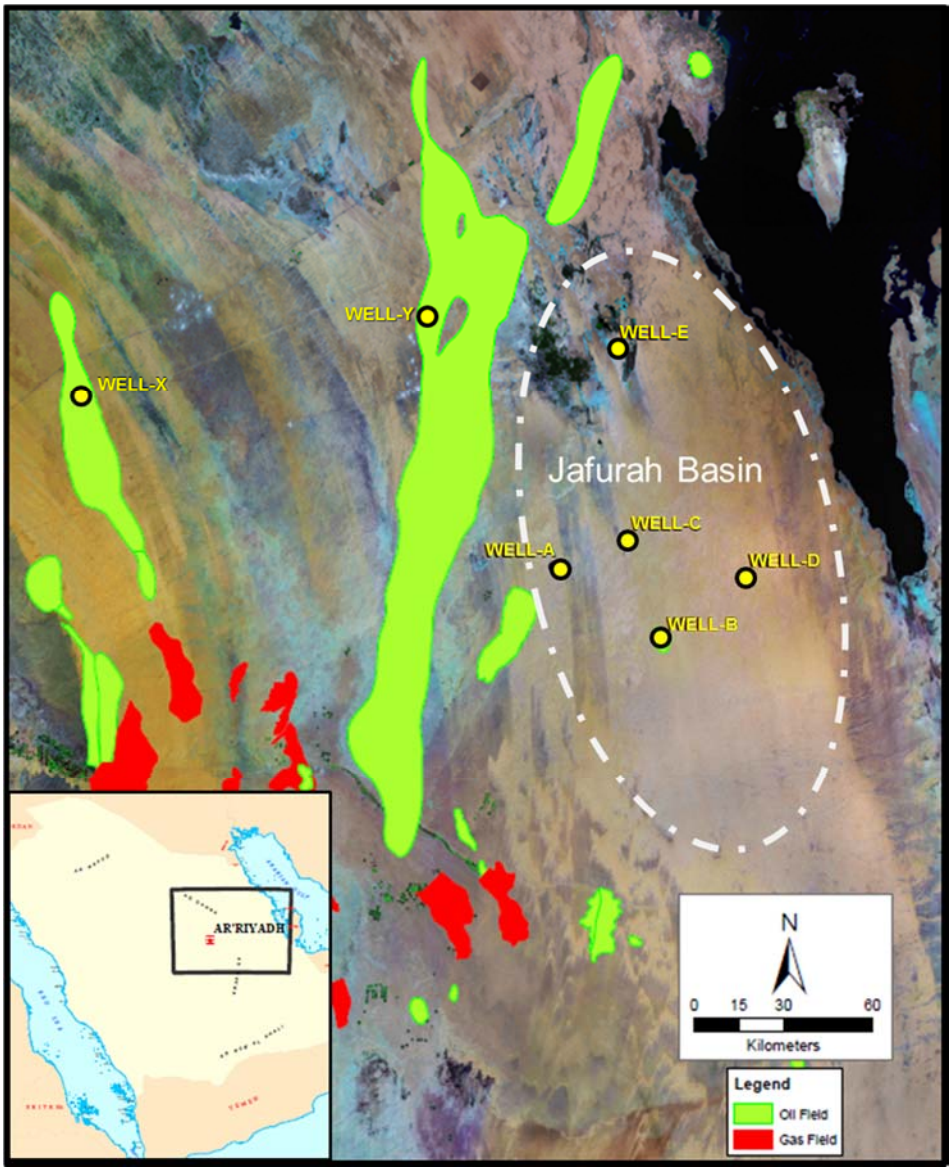

Figure 4-1 Location map of the study area, showing the Ghawar giant oil field in Saudi Arabia, the approximate outline of Jafurah Sub-Basin (dashed white line), and the five wells used in the study. Wells X and Y show the location of immature and marginally mature Tuwaiq Mountain source rock.

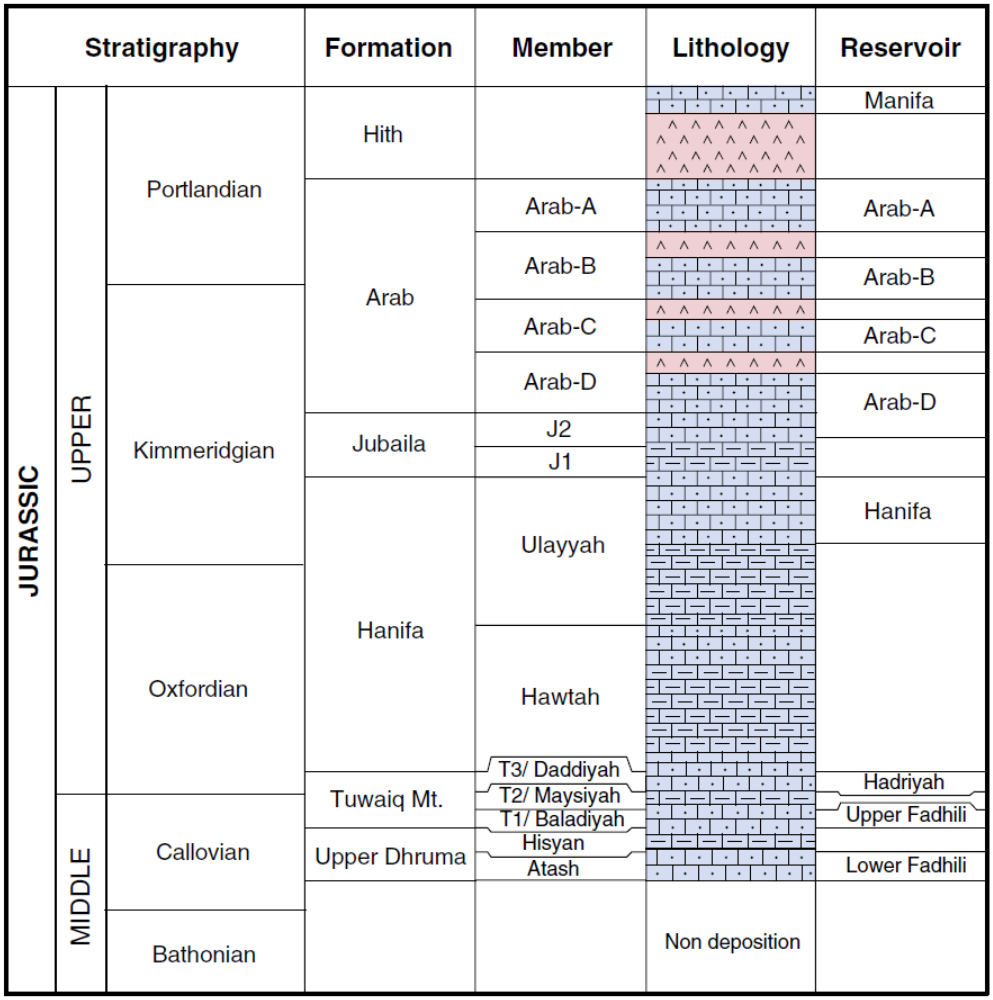

Figure 4-2 Generalized geologic column of the Middle and Late Jurassic Epoch (after Sharland et al., 2001).

It is expected that the organic-rich interval of the Jurassic Tuwaiq Mountain (TQMN) source rock within the Jafurah Sub-Basin may contain significant quantities of trapped hydrocarbons; similar to proven unconventional shale resources in North America (Montgomery et al., 2005; Jarvie et al., 2007). However, research performed in this frontier basin is insufficient to determine the hydrocarbon resource potential of the TQMN source rocks. This might be due to the limited subsurface data and, therefore, limited understanding of the rock characteristics. With the exception of some source rock data,

burial and maturity evolution studies based on basin modeling does not exist on the Jurassic in the Jafurah Sub-Basin. The aim of this study is to demonstrate the usefulness of basin modeling tool in the assessment of unconventional gas potential within Jafurah frontier basin. Five exploration wells were selected for this study (Figure 4-1); these wells were drilled vertically, cored and logged. A basin modeling software (PetroMod© 1D suite v.2013.1 and PetroMod© 2D suite v.2014.1 (Schlumberger) was utilized to reconstruct a burial history and model maturity and hydrocarbon generation of the TQMN source rocks in order to estimate gas potential at each well location. Then, we use the results from the modeling to critically evaluate the relationships between geological history, maturation, hydrocarbon generation and retention trends for the TQMN source rock gas play in the Jafurah Sub-Basin.

4.2 Data and Methods

A comprehensive formation evaluation and data acquisition program was implemented to acquire a wealth of core and well-log data from the five wells used in Hakami et al. (2016) and in this study. The coring program was designed to collect enough core samples across the three potential source rock intervals; Tuwaiq Mountain, Hanifa and Jubaila Formations to enable detailed source rock characterization. The wireline logging program was designed to collect complete log datasets to assist in well-to-well correlation and in rock characterization. The details of the samples and data acquisition are given in Hakami et al. (2016). Data on subsurface depth and temperature cannot be provided due to company rules and confidentiality purposes. Pyrolysis data used in this study has been taken from Hakami et al. (2016) and are based on Source Rock Analysis (SRA – Weatherford) and LECO®

analyses. The data were utilized to identify source rock intervals and assess their quality (generative potential) and thermal maturity (Table 4-1). Source rock maturity was also evaluated based on bitumen reflectance data of Hakami et al. (2016). For a better quality pyrolysis-based maturity data, kerogen isolation from TQMN source rock samples were done following USGS method (Love, 1982). The samples were ground to less than 250 μm (micronmeter) and solvent extracted by using MAC (methanol, acetone, chloroform mixture: 70:15:15 v/v). Then the samples were rinsed with water and dried at 50 °C oven overnight. The ground samples were treated first with HCl followed by HF. The kerogen residue was added into heavy liquid (ZnBr) and centrifuged (4500 rpm for 15 minutes) to segregate and remove any inorganic left from acidification process. Later the kerogen fraction was collected from the top of the centrifuge tube and filtered and washed with distilled water to obtain clean sample. The isolated kerogen samples were analyzed by Hawk pyrolysis instrument (WILDCAT Technologies Inc.) to determine maturity based on Pyrolysis Tmax. To ascertain kerogen type and its sulfur content, elemental analyses of two isolated kerogen samples from TQMN Formation were conducted using a Vario Macro Cube Analyzer. Instrument uses TCD (thermal conductivity detector) for CHN and infrared detector (IR) for sulfur detection. Kerogen isolation was done following the procedure described for Jafurah Sub-Basin samples. The instrument's combustion reactor was operated at 1150 °C and the reduction reactor was set at 850 °C.

4.3 Hydrocarbon Source Rock Characterization of the TQMN Formation

Hakami et al. (2016) have analyzed by Source Rock Analyzer (SRA) around 700 core samples collected from the TQMN, Hanifa and Jubaila Formations intersected in five unconventional exploration wells (wells A, B, C, D and E of this study) to characterize the source rock quality within the Middle and Upper Jurassic Formations in the Jafurah Sub-Basin. Table 4-1 summarizes the screening analyses results for the TQMN, Hanifa and Jubaila Formations. The distribution of total organic carbon content (wt. % TOC) for all three formations are given in Figure 4-3a and HI versus Tmax plot for the TQMN Formation is shown in Figure 4-3b. It is important to note that most of the samples represent peak oil or wet-gas maturity window based on their Tmax data, and therefore, the measured TOC, S2 and HI values are less than that of an immature kerogen. The TQMN Formation in the Jafurah Sub-Basin holds excellent hydrocarbon generating potential with high total organic carbon (TOC) content and sufficient maturity (Table 4-1). On the other hand, the Jubaila and Hanifa Formations in the Jafurah Sub-Basin show relatively average source rock quality. Since among the three source rocks, the TQMN source rock is the richest, it is the primary target for unconventional gas exploration in the Jafurah Sub-Basin. As a result, we have focused on the TQMN in this study.

Table 4-1 TOC and pyrolysis data for total 690 core samples obtained from the Tuwaiq Mountain, Hanifa and Jubaila Formations in Wells A through E (after Hakami et al., 2016). The data are plotted in Figures 4-3a and 4-3b

Geochemical Attributes		Jurassic Formations		
		Jubaila 185 Samples	Hanifa 172 Samples	Tuwaiq Mountain 333 Samples
Total Organic Carbon Content (wt.%)	Maximum	4.98	3.90	13.17
	Minimum	1.00	0.15	1.12
	Average	2.44	1.19	4.9
S1 Pyrolysis Yield (mg HC / g rock)	Maximum	4.69	4.58	12.04
	Minimum	0.32	0.02	0.39
	Average	1.05	0.77	3.4
S2 Pyrolysis Yield (mg HC / g rock)	Maximum	7.55	6.18	18.8
	Minimum	0.55	0.02	0.54
	Average	2.53	0.8	3.4
Hydrogen Index (mg HC / g TOC)	Maximum	231	218	194
	Minimum	63	50	48
	Average	112	102	91
Tmax (°C)	Maximum	476	479	493
	Minimum	434	456	455
	Average	462	471	475
Pyrolysis Tmax from isolated kerogen analysis (few samples for each formation)(This study)				
*Tmax (°C)	Maximum	440	457	467
	Minimum	436	451	442

*The Tmax values are based on the analyses of isolated kerogen samples conducted in this study.

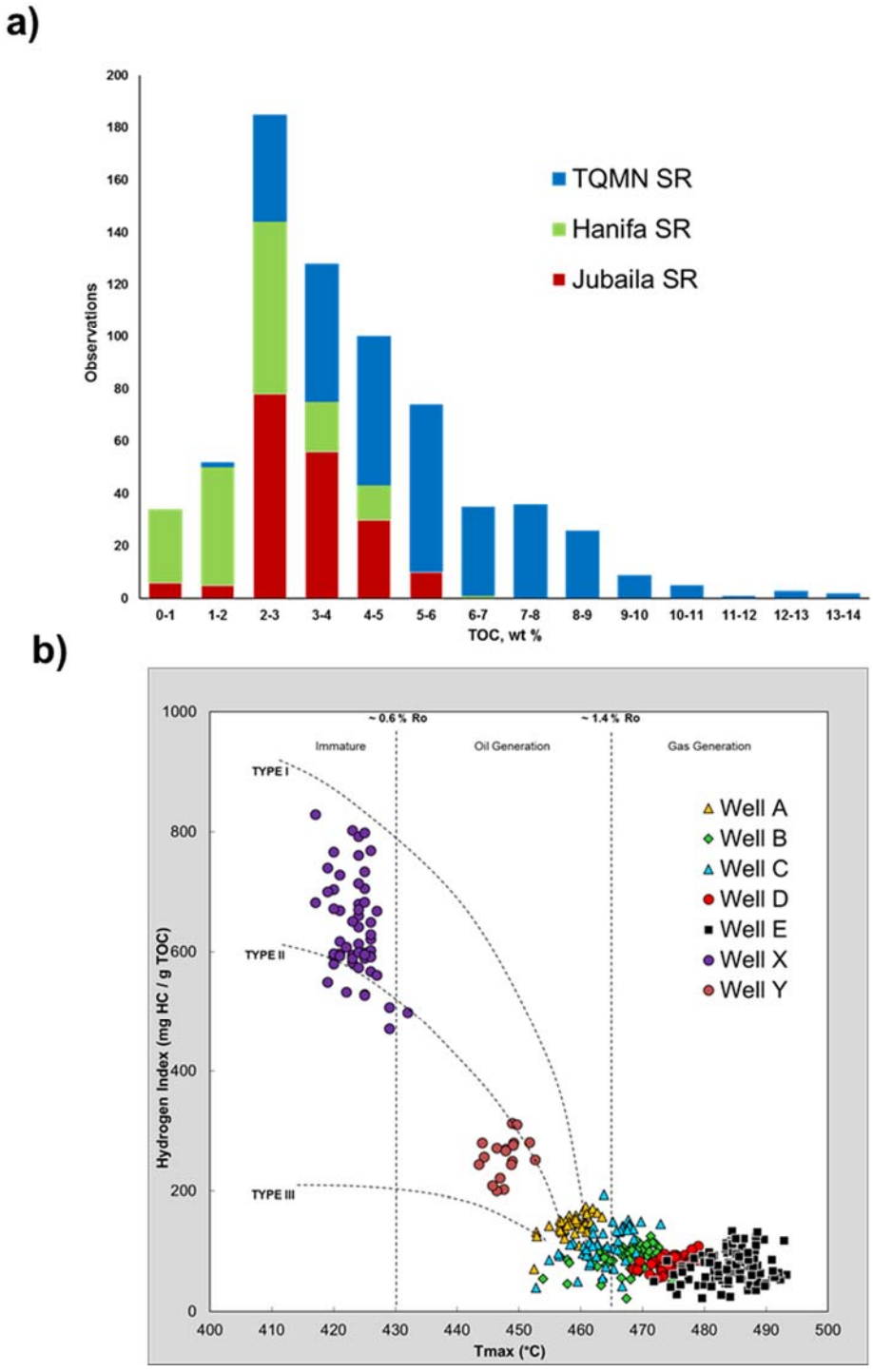

Figure 4-3 a) Distribution of total organic carbon (wt. % TOC) content for Tuwaiq Mountain, Hanifa and Jubaila Formations. b) Cross plot of Tuwaiq Mountain source rock Tmax versus HI for Wells A through E. Tuwaiq Mountain source rocks to the west of the study area (Wells X and Y) show hydrogen indices (HI) of 450 to 820 mg HC/g TOC, typical of Type II and Type I kerogen. Elemental analyses of isolated kerogen from immature TQMN source rock yielded atomic S/C ratio of 0.06, which suggests sulfur rich Type IIS kerogen (Orr, 1986).

Kerogen quantity will be discussed in this Section. The kerogen type in the TQMN source rocks is inferred to be Type II and Type I from the plot of HI vs. Tmax (Figure 4-3b). Ayres et al. (1981), Carrigan et al. (1995), and Hakami et al. (2016) have provided further discussion on kerogen type. The fact that oils from Jurassic reservoirs are known to be sulfur rich (2 to 4+ wt. % S; Carrigan et al., 1995), it has been therefore presumed that the kerogen of the main source rock, the TQMN, is/was sulfur rich. For this study, we isolated kerogen from two immature TQMN (obtained from a relatively shallow depth in well west of Ghawar field) and run elemental analyses. The results show that atomic S/C ratio is between 0.06 and 0.07, which is higher than the 0.04 value reported to be minimum for a kerogen to be considered Type II-S kerogen (Orr, 1986). Type II-S kerogen is compatible with the anoxic carbonate depositional environment where Fe input was negligible (Carrigan et al., 1995) and thus, sulfur incorporation into organic matter was a relatively easy process. Moreover, to input the best hydrocarbon generation kinetics, we utilized Aramco internal kinetic data obtained on an immature TQMN source rock kerogen, as it will be discussed later. Data from samples acquired from Wells X and Y located to the west of the study area are also added to the plot in Figure 4-3b. Immature TQMN source rock samples from Well X suggest that the kerogen is Type I and II, whereas, samples from Well Y plots on the same trend but are in oil generation window. Data from all five wells of this study show mature kerogen with respect to oil generation. It is worth noting that the TQMN maturity spread for a given well is quite high (Table 4-1 and Figure 4-3b). Therefore, for obtaining refined and better-constrained maturity data for calibration of the modeling, we extracted and isolated kerogen from the TQMN Formations from each well and run pyrolysis. The pyrolysis Tmax values obtained on isolated kerogens are given in

Table 4-2. The data suggest that the TQMN source rock maturity is lowest at Well A and highest at Well E. In Table 4-2, we included VRE calculations based on different Tmax – VRE relations given in previous studies. We also included VRE calculation based on bitumen reflectance from Hakami et al. (2016). The data of Hakami et al. (2016) listed in Table 4-1 and plotted in Figure 4-3 are only for displaying general characteristics of the Jurassic source rocks. The maturity data we have used for basin modeling calibration is from the pyrolysis analyses we have conducted on isolated and solvent-extracted kerogen; the results are given in Table 4-2.

Table 4-2 Pyrolysis Tmax data on isolated kerogen samples from the TQMN Formation in each well. Vitrinite reflectance equivalent (VRE) values derived from various Tmax –VRE relations are also given. VRE values derived from bitumen reflectance data is from Hakami et al. (2016).

WELL	1-Tmax (°C)	2-VRE %	3-VRE %	4-VRE %	5-VRE%	6-VRE%
Well A	443	0.81	0.86	0.97	0.62	0.91
Well C	442	0.80	0.84	0.95	0.72	0.97
Well B	455	1.03	1.05	1.12	1.04	1.15
Well D	457	1.07	1.08	1.15	1.10	1.19
Well E	467	1.25	1.24	1.28	1.21	1.26

1-Pyrolysis Tmax (°C) on isolated kerogen samples from this study.
2-VRE % = (Tmax*0.018)-7.16 (Jarvie et al., 2001) obtained on US shales.
3-VRE % = (Tmax-389.11)/ 63.03 (Petersen, 2006) obtained on coal samples.
4-VRE % = (Tmax*0.0134)-4.9706 (İnan et al., 2016) obtained on Silurian Qusaiba of Saudi Arabia.
5-VRE% = 1.0495*BR- 0.2443 (Schoenherr et al., 2007).
6-VRE% = 0.618*BR+ 0.4 (Jacob, 1989); reported in Hakami et al. (2016)

4.4 Basin Modeling

This study has utilized petroleum system and basin modeling approach to conduct a quantitative assessment of shale-gas and shale-oil potential of the carbonate mudrocks of the Upper Jurassic TQMN Formation. In this context, it is essential to provide information about the basin modeling approach and its initial assumptions and limitations. First, we will briefly explain these issues. Later, the input and calibration data will be described and finally, the simulation results will be discussed.

4.4.1 Basin Modeling Approach and Assumptions

We performed basin modeling using the PetroMod© software suite v.2013.1 and suite v.2014.1 (Schlumberger). Different approaches and assumptions in model simulations of geological and geochemical processes that are calculated during basin modeling are described below.

4.4.1.1 Burial and Thermal Evolution

The simulation starts with the deposition of the oldest layer and continues until the present-day geometry is reached. During simulation, various geological, geochemical and petrophysical processes are handled and updated at each defined time step and for each model grid cell. This simulation takes into account mechanical compaction, porosity reduction, and pore pressure calculations. Subsurface temperature calculations are based on assumed basal heat flow and dynamic values of thermal conductivities, computed by taking into account the thermal conductivity of the rock matrix and pore-filling fluid. Once

the temperature evolution of all sedimentary layers has been confidently established (by comparing measured and calculated maturity and present-day/corrected bore hole temperatures), modeling of hydrocarbon generation from organic rich source rocks can be achieved based on Arrhenius law kinetics using a source rock specific kinetic data sets which are sufficiently representative to the source rock under investigation (Tissot and Welte, 1984; Yalcin et al., 1997; Hantschel & Kauerauf, 2009).

4.4.1.2 Fluid Flow

The modeling software employs a so-called hybrid model, which combines both Darcy flow and Flow-path for simulation of fluid flow. Darcy flow describes multi-component three-phase flow based on relative permeability and capillary pressure. The carrier and non-carrier units are based on permeability and porosity thresholds (10−2 mD permeability and 30% porosity). Fluid migration through low permeability, non-carrier, and units is calculated assuming Darcy flow. In the flow path part of the modeling, migration of fluids through porous and permeable carrier units is assumed as instantaneous, and all fluids in a carrier are moved to the structurally highest position, or leaking into the next sedimentary unit (Hantschel and Kauerauf, 2009).

4.4.1.3 Maturation and Hydrocarbon Generation

The model provides many alternatives for computation of maturity of the potential hydrocarbon source rock(s) through time. Most widely used is the %Ro method of Sweeney and Burnham (1990), which provides calculations of vitrinite reflectance, based on kinetic approach of vitrinite maturation. Oil and gas generation is based on the kinetic

data obtained from various source rocks in the world that are selectable from the modeling software's archive. Alternatively, user defined kinetic data sets can be introduced if kinetic data sets are available for the source rock(s) under investigation. In either case, the values for initial TOC and hydrogen index (HI) values for the source rock(s) need to be defined. Hydrocarbon generation is calculated through time based on Arrhenius law assuming first order kinetics.

4.4.1.4 Hydrocarbon Expulsion and Primary Migration

When modeling for the purpose of shale-gas and shale oil resource estimations, it is very critical that careful selections of the governing physical laws and assumptions regarding oil expulsion and migration are made because these options will later determine the final hydrocarbon content of the source rock. It is quite clear that a selection of the default simple oil saturation threshold in Petro Mod (<5% as default value) for primary migration of the oil will not be representing the complexity and will most likely result in overestimation of migrated oil and underestimation of hydrocarbons retained in the source rock. The software provides some sophisticated options that can be used to obtain better approximations in regard to some complex processes like hydrocarbon migration from and retention within the hydrocarbon source rocks. More advanced understanding defines oil expulsion as release of oil from the kerogen network into inorganic volume (Stainforth and Reinders, 1990; Sandvik et al., 1992; Pepper and Corvi, 1995; İnan et al., 1998). As summarized by Mann et al. (1997), primary migration of oil within the source rock is a result of successive processes 1) generated oil is diffused through the kerogen network (Stainforth and Reinders, 1990), 2) once the system overcome adsorption capacity, oil is desorbed from

kerogen network (Sandvik et al., 1992; Pepper and Corvi, 1995) into the inorganic pore network of the source rock, 3) oil starts to aggregate and when a sufficient relative permeability (saturation threshold) is reached, 4) oil starts to flow within and out of the source rock. Here, internal pressure (or overpressure) of the source rock is considered to facilitate and/or enhance oil expulsion. Release of oil from kerogen seems to be an important step because kerogen is reported to sorb (by absorption + adsorption + Physical trapping) as much as 100 mg oil/ g of TOC (Sandvik et al., 1992). Pepper and Corvi (1995) calculated that sorption capacity of kerogen could reach up to 200 mg oil/ g TOC.

In modeling exercise, we followed the option of oil retention within the residual kerogen network. Accordingly, the adsorption potential (0.1 g generated HCs/g TOC equivalent to 10% of the remaining TOC) applies to sum of all components generated (Pepper and Corvi, 1995). In the applied model, all HCs in excess of 10% of the remaining TOC will be expelled into inorganic pore/fracture volume and that cracking of the adsorbed HCs (only the liquid compounds from C6 onwards) with increasing temperature results in the generation of methane. As a result, we selected the kerogen retention option and delay of oil migration was then successfully achieved in the simulation. Considering that the software default value for oil migration out of the source rock to commence is only 5% oil saturation, modeling oil migration from the source rock is very efficient and thus only a small fraction of generated oil resides (retained) in the source rock to be later cracked to gas at higher temperatures. Thus, in estimating source rock's oil and/or gas content using default values for critical oil saturation, modeling software will always overestimate the expulsion and underestimate the hydrocarbons left behind within the source rock. As a

partial remedy to the problem of overestimated expulsion efficiency of oil from organic rich source rock, the following two-step approach has been considered in this study. First, we assumed a 10% (100 mg oil/g TOC) retention of oil within the kerogen network. This yields more meaningful results as up to 10% of generated oil (0.1 g oil/g TOC) can be allowed to be retained/ entrapped within the remaining kerogen network and get cracked to gas at higher temperatures. A 0.1 g oil retention per g TOC will lead to 0.01 g oil/g of sample assuming a TOC content of 10 wt.%. When this oil is cracked to gas at higher temperatures in the gas generation window (oil to gas conversion factor of 0.7; Behar et al., 1997), it will lead to generation of about 7 m^3 methane per ton of source rock or about 250 standard cubic feet (scf) of methane per ton of source rock; taking the density of methane to be 0.656 kg/m3 at STP conditions. This amount of methane is sufficient to meet and exceed most organic rich source rocks' adsorption capacity (Heller and Zoback, 2014). Methane gas adsorption capacity measurements on shale source rocks (with TOC contents between 1.2 and 5.3 wt. % and at gas maturity level) from North America have been reported to range from12 to 74 standard cubic feet of methane gas per ton of rock (scf/ton) at 10,000 PSI (Heller and Zoback, 2014), which were found to be comparable with methane adsorption capacities (40 to 75 scf/ton at 10,000 PSI) reported earlier for Barnett shales (Montgomery et al., 2005). European shales, with higher TOC content (about 7.7 wt.%) and higher maturities in the gas window, have been reported to have methane adsorption capacity up to 275 scf/ton at about 3600 PSI (Gasparik et al., 2014). Based on gas adsorption experiments of organic rich (up to 10 wt. %) TQMN source rock samples, the methane adsorption capacity of the TQMN source rocks is in the same range as the American and European shales, for similar pressure and temperature conditions. Second,

we varied the oil saturation threshold incrementally from 5% to 10%, 20%, 50%, and 100% then attempted a match between model's predictions of gas content for the TQMN with the measured gas adsorption capacity. Essentially, the predicted gas content should not be lower than the adsorption capacity when sufficient gas has been generated and the formation pressure is sufficient to keep the gas in adsorbed state. Then based on the best match, we decided to use a 20% oil saturation threshold for oil migration out of the source rock.

4.4.1.5 Organic Porosity

As the modeling takes into account formation of organic matter porosity with increasing maturation, this creates more volume for the generated gas (from kerogen or cracked from oil) to be stored within the organic matter. Organic porosity becomes volumetrically significant only at advanced stage of maturity and plays important role for gas adsorption (e.g., Curtis, 2002; Chalmers et al., 2012; Zhang et al., 2012; Hao et al., 2013; Milliken et al., 2013; Romero-Sarmiento et al., 2014). The model also allows inputting Langmuir adsorption capacity for the source rock (determined for a source rock sample of known maturity at its subsurface pressure and temperature conditions) so that available gas can be adsorbed (up to adsorption capacity) within the source rock provided that formation pressure is adequately high. Ideally, modeling should account for and recalculate adsorption capacity based on changes in subsurface temperature and moisture. However, modeling is capable of only adjusting adsorption capacity for residual TOC. Therefore, adsorbed gas calculations of modeling can be viewed at best as qualitative. In any case, modeling considers the generated gas as adsorbed gas up to the adsorption capacity, and

when the generated gas exceeds this capacity, only then, the excess gas is considered as free gas in the inorganic void space. Depending on the subsurface pressure and temperature conditions, modeling may overestimate one gas type or the other. This assumption-based calculations and definitions of adsorbed- and free-gas will not cause significant errors in calculation of the total gas content, which is the sum of adsorbed and free gas. The examples provided above show that capability of recent modeling software(s) have been improved to such an extent that they are now also useful tools for assessments of unconventional resources. The possible shortcomings always exist in basin modeling, as is the case for any other modeling process. The success or even relevance of modeling exercise and its results will no doubt depend on 1) the quality of input data, 2) the success and sufficiency of model calibration by measurements and 3) the selection of most appropriate and most advanced physical models that can account for various processes and 4) success of mathematics describing and handling the physical processes.

4.4.2 Input and Calibration

This modeling exercise has benefitted from conceptual approaches of previous basin modeling studies targeting Paleozoic Qusaiba hot shales to the west of the study area (e.g., AbuAli and Littke, 2005, İnan et al., in press) and the model has been calibrated by using all available corrected borehole temperature and maturity data. These data were mostly available for the source rock intervals thus they were inevitably from a narrow depth range. Borehole temperatures were corrected using Horner correction method; data were then used to calibrate model predictions of present- day temperature gradients. Present-day temperature gradient map is shown in Figure 4-4. In this study, maturity measurements

used for calibration were obtained based on pyrolysis Tmax data. Then, these data were converted to vitrinite reflectance equivalent (VRE) as shown in Table 4-2. Measured maturity was compared to model predicted maturity and the best match was used to derive paleo- temperature through time for the TQMN source rock. Present-day and paleo-temperatures computed for each layer takes into account the heat flow input and matrix thermal conductivity value assigned by the model for each layer based on user defined lithology. Table 4-3 summarizes the input parameters for the basin modeling work at Well E. Thickness estimations of eroded sections at major unconformity(ies) are based on the studies of AbuAli and Littke (2005) and İnan et al. (in press). Both studies concluded that erosional unconformities (the regional Cretaceous and Oligocene erosional events) in the East-Central Arabian Basin did not lead to more than a few hundred feet of removed section.

Table 4-3 Input parameters for the 1D basin modeling at location of Well E.

Event No	Event Name	Age at base (Ma)	Lithology	Thickness (m) X Factor	Water Depth (m)	SWI (°C)	HF (mW/m2)
38	Pliocene_Q	5	Sandstone-shale-siltstone	18 (TE)	10	24	66
37	Neogene	23	Limestone_sandstone	278	20	22	66
36	Pre_Neogene	35	Limestone_sandstone	20 (TE)	40	22	66
35	Dammam	49	Limestone_sandstone	112	66	22	66
34	Rus	54	Dolomite_limest_anhydrite	290	60	22	66
33	Umm Er Radhum	64	Limestone (micrite)	595	50	22	66
32	Aruma	72	Limestone_with_shale	820	60	22	66
31	Lams	82	Shale_major_LS	565	155	24	66
30	Pamu	92	Shale (typical)	160	150	24	66
29	Ruml	93.5	Limestone (shaly)	212	145	24	66
28	Ahmd	97	Shale_major_LS	77	140	24	66
27	Wara	101.5	Shale_major_LS	10	135	24	66
26	Mddd	107.5	Sandstone-shale-siltstone	110	130	24	66
25	Safania	111	Sandstone (typical)	399	125	24	66
24	Pre_Wasia	114	Limestone (ooid grainstone)	10 (TE)	50	22	66
23	Shuabia	127	Limestone (shaly)	150	80	22	66
22	Bydh	134	Marl	445	100	22	66
21	Pre_Bydh	137	Marl	45 (TE)	100	22	66
20	Mdtm	143	Limestone (micrite)	263	10	20	66
19	Sulaiy	149	Limestone (micrite)	267	40	20	66
18	Hith	150	Anhydrite_minor_LS	196	60	20	66
17	Arab	150.38	Limestone_anhydrite	47	50	20	66
16	Abar	150.75	Limestone (ooid grainstone)	18	50	22	66
15	Arab	151.12	Limestone (ooid grainstone)	28	50	22	66
14	Abbr	151.5	Limestone (ooid grainstone)	9	50	22	66
13	Arbc	151.88	Limestone_anhydrite	67	50	22	66
12	Abcr	152.25	Limestone (ooid grainstone)	20	50	22	66
11	Arbd	152.62	Limestone_anhydrite	55	50	22	66
10	Abdr	153	Limestone (ooid grainstone)	26	50	22	66
9	Jubaila	153.5	Limestone (ooid grainstone)	355	50	22	66
8	Jubaila_SR	154	Marl	115	80	20	66
7	Hanifa_Anhyd	155	Anhydrite_minor_LS	10	50	22	66
6	Hanifa_LS	159	Limestone (micrite)	50	50	22	66
5	Hanifa_SR	161	Marl	15	100	20	66
4	Upper TQMN	163	Marl	50	100	20	66
3	Lower TQMN	165	Limestone (micrite)	18	50	22	66
2	Upper Fadhili	168	Limestone (micrite)	65	50	22	66
1	Dhruma	171	Limestone (micrite)	16	50	22	66

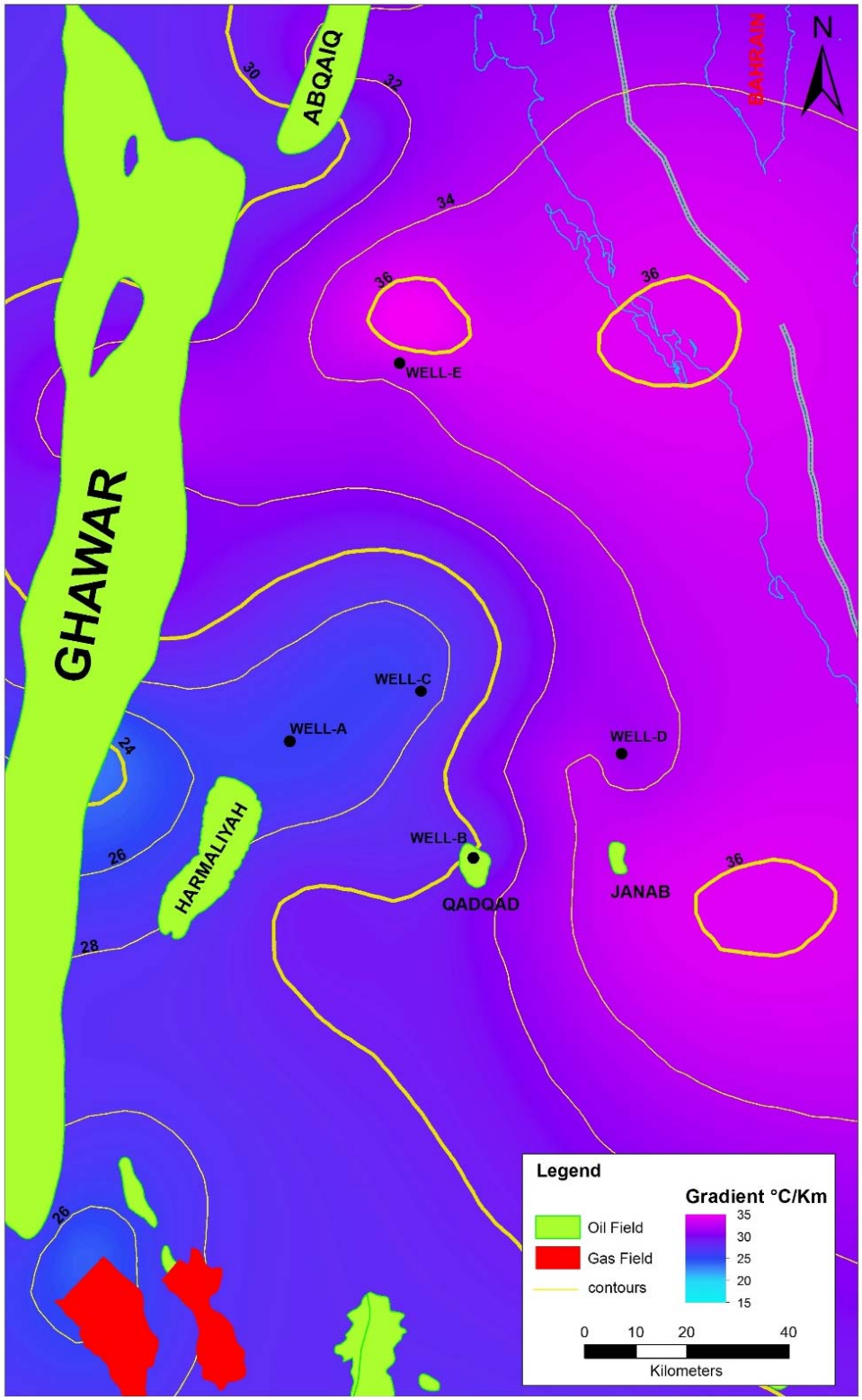

Figure 4-4 Simplified geothermal gradient map of eastern Saudi Arabia showing the Ghawar giant oil field in Saudi Arabia and the five wells used in the study (modified after Hakami et al., 2016).

The Jafurah Sub-Basin has developed more or less as a continuously subsiding basin. Eroded thicknesses were estimated from seismic sections and were used in the model but, as it will be shown later in burial history curves, influence of these breaks in burial history are not significant, and they have negligible effects on present day maturity and hydrocarbon generating potential of the source rocks. Compaction trends are also used as calibration. The simulation is run successively until the difference between calculated and present day thicknesses of all layers is within an acceptable range (e.g., <1%). For 2D basin modeling purposes, a geologically representative cross section (A–A') from southeast to northwest has been constructed in the Jafurah Sub-Basin (Figure 4-5) to simulate fluid flow that will provide better estimations of the hydrocarbons that migrate out of and/or get retained within the TQMN source rock. This cross section was prepared based on regional geological cross sections correlated and calibrated based on seismic and well data. The section does not involve structural discontinuities (e.g., faults) and geology is quite simple as rock layers are gently dipping to the east (average dip angle of 2°; Konert et al., 2001). The depth to the base of the TQMN Formation does not show much variations between the five wells (A, B, C, D, and E) modeled in this study. The model consists of different stratigraphic layers, covering a present- day depth interval from the top of the sedimentary pile down to the Middle Jurassic Dhruma formation underlying the target Middle- Upper Jurassic TQMN Formation. Age and lithology of each layer were entered by selecting appropriate lithology provided and/or user defined lithology in the software. Cross section A–A' (Figure 4-5) extends about 170 km and the lateral grid spacing is 1000 m.

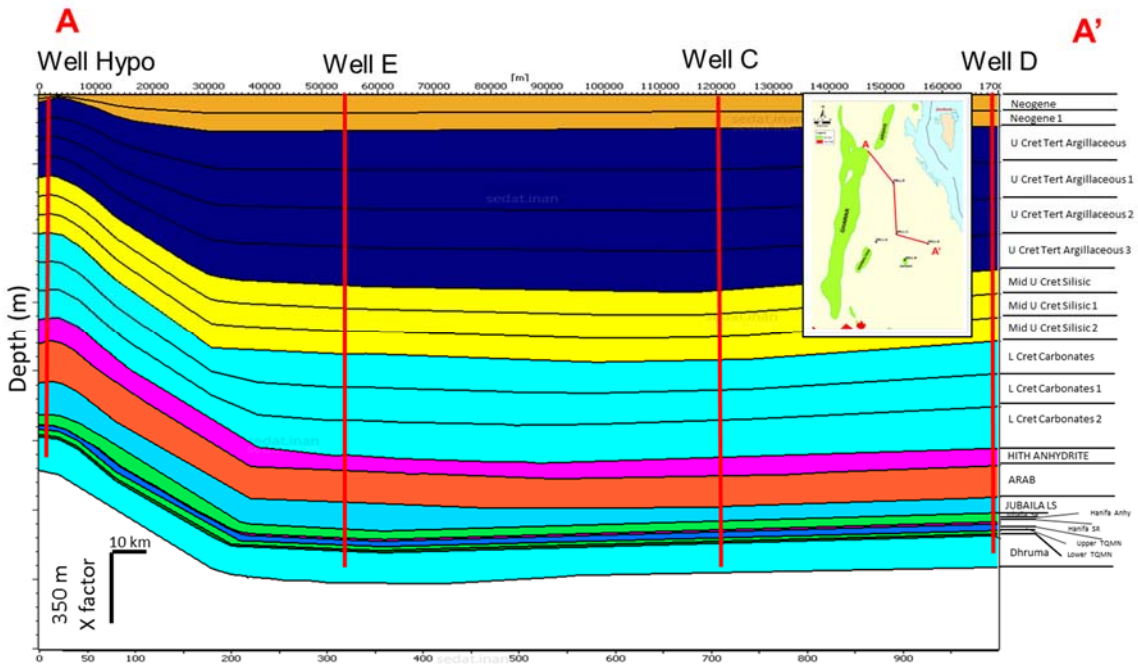

Figure 4-5 Constructed geological cross section (A-A') for 2D basin modeling in the Jafurah Sub-Basin

4.5 Results and Discussion

In this section, we will present the results for burial and thermal history evolution, followed by hydrocarbon generation, migration and retention through time. Finally, we will discuss how these processes led to variations in the present day gas potential of the TQMN source rock in the Jafurah Sub-Basin.

4.5.1 Burial and Thermal History

1D burial history reconstructions for the five wells were constructed as an example burial history for Well A is shown in Figure 4-6. Actual depth values cannot be given for confidentiality reasons; however, a proper depth scale multiplied by a hidden factor is displayed for each figure. Generally, it can be said that total depths for all wells are similar

except well A where the base of the TQMN source rock is about 1000 ft. shallower compared to other wells. With the exceptions of few minor uplift and erosional episodes, the basin is almost continuously subsiding and that present depths are the maximum burial depths that TQMN has been exposed to throughout the burial history.

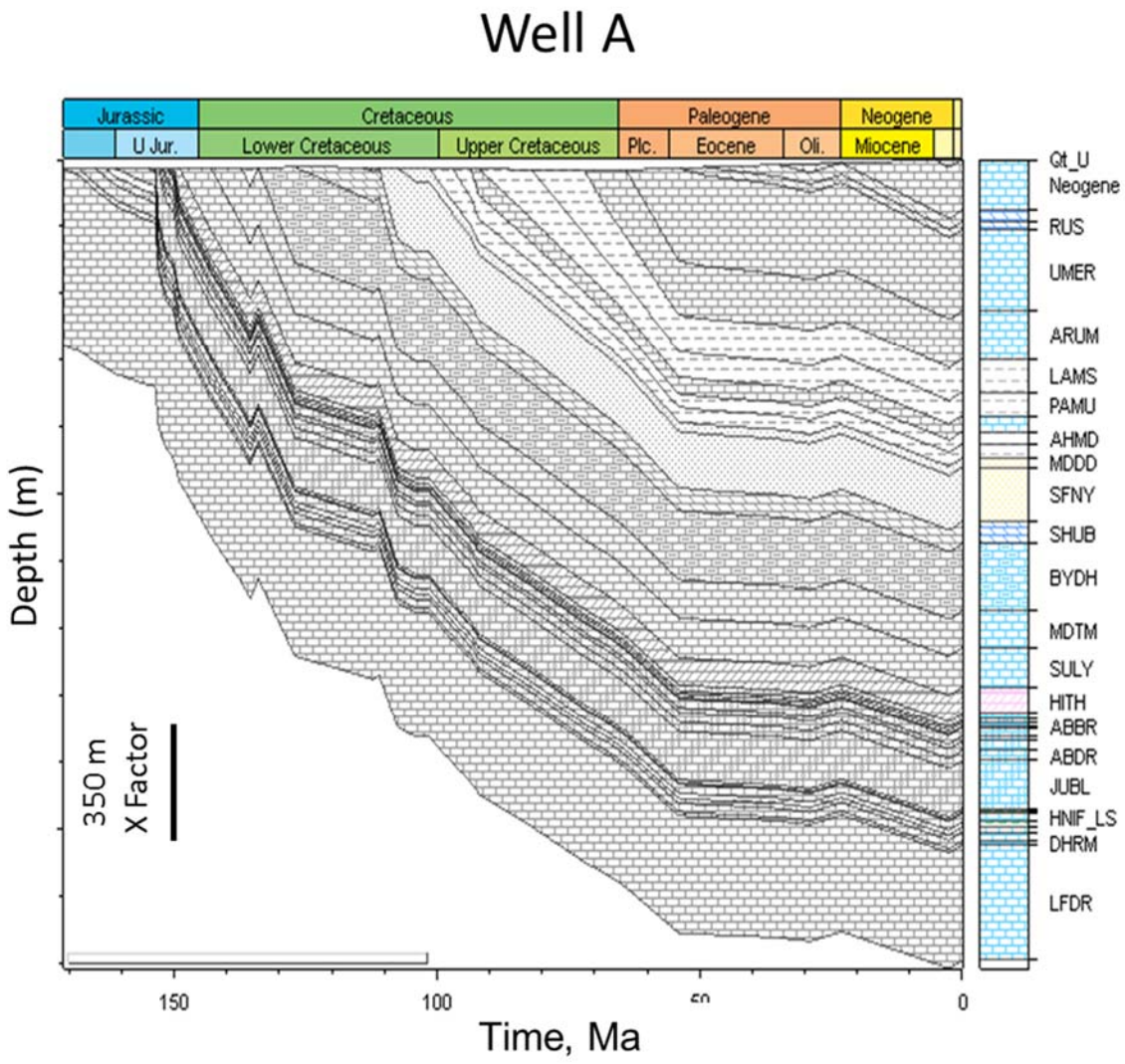

Figure 4-6 Reconstructed burial history for the sedimentary succession intersected in Well A.

In Figure 4-7a, measured versus computed temperatures, based on 1D modeling, are plotted for the five well locations. Data from thermal log was available for Well E and it has been shown. Solid circles are measured temperatures whereas continuous lines are predicted temperatures. The average surface temperature is assumed to be 24 °C. In Figure 4-7b, calculated temperature gradients for each well based on the approximation though red dashed lines are also shown. Figure 4-7c shows a schematic presentation of the temperature gradients calculated for each well. Note that the temperature gradient increases from locations of Well A to C, B, D, and to Well E. Based on the match between predicted and measured temperatures shown in Figure 4-7, the temperature gradients and present day heat flow values and average thermal conductivity values for entire section were calculated and given in Table 4-4. The differences in heat flow values are related to geothermal gradient variations from one well location to the other, which is in conformity with variations shown in the temperature gradient map (Figure 4-4). Calculated average thermal conductivity over the entire section suggest a value of about 2 W M−1 K−1 and does not show significant variations from one well to the other. This is not surprising because the lithology of the layers intersected in all wells are remarkably similar in all well locations. The variation of the temperature gradient in the Jafurah Sub-Basin is interpreted to reflect the variations in the basal heat flow, which in turn has different contribution of radiogenic heat from granitic basement in the eastern and northern Jafurah Sub-Basin (FragTech 2007 internal report to Aramco); lower temperature gradient areas are inferred to be underlain by more mafic basement that contributes less radiogenic heat.

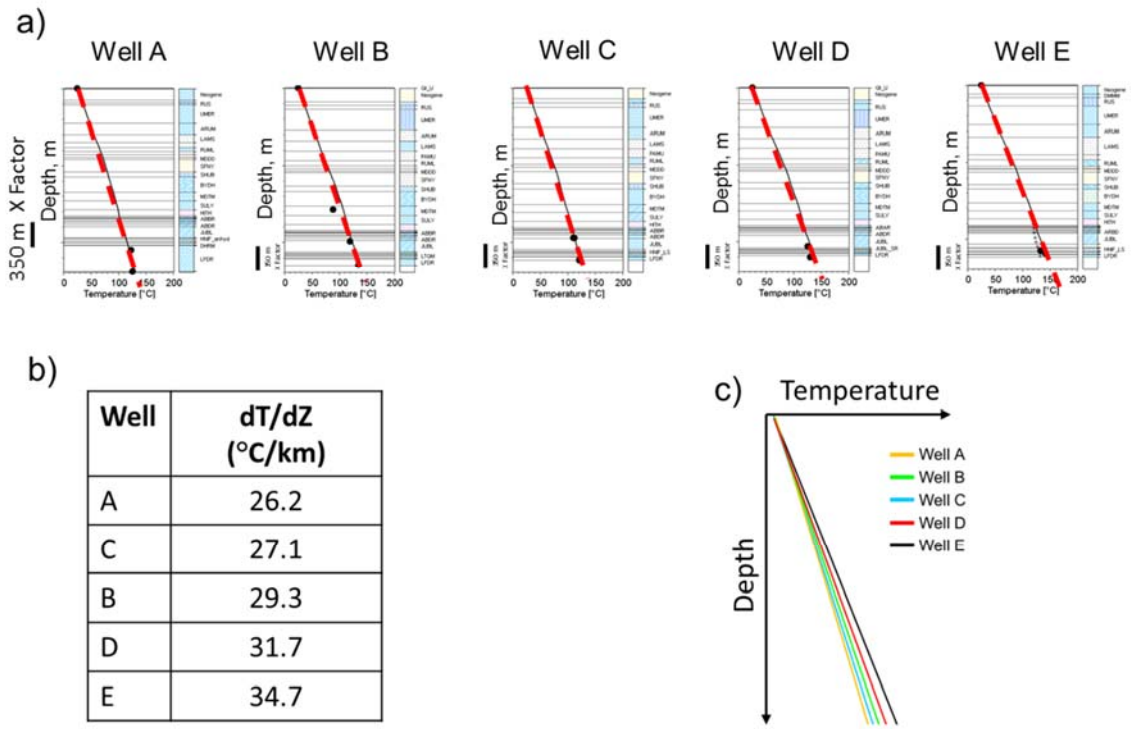

Well	dT/dZ (°C/km)
A	26.2
C	27.1
B	29.3
D	31.7
E	34.7

Figure 4-7 Measured versus computed subsurface temperature data for five wells (a), calculated temperature gradients for each well (b) and schematic presentation of the temperature gradients calculated for each well (c). Note that the temperature gradient increases from locations of Well A to C, B, D, and to Well E. Solid circles are measured temperatures (corrected by Horner approach) whereas continuous lines are predicted temperatures. Depth scale is the same for all temperature-depth profiles.

1D modeling results for measured versus computed maturity data for each well are given in Figure 4-8. Vitrinite reflectance equivalent (VRE) values are obtained from pyrolysis Tmax data. Bitumen reflectance measurements were also correlated with pyrolysis Tmax data to obtain the most reliable maturity data for calibration (Table 4-4). Various Tmax-VRE relations from previous studies have been used to convert pyrolysis Tmax values obtained on isolated kerogens. The VRE predictions are quite similar; however, all relations provide even stronger similarity between predicted VRE at relatively high maturity levels (e.g., above pyrolysis Tmax values of about 455 °C). At lower maturity

levels (e.g., Tmax 440 °C), some relations are predicting higher VRE compared to others. The reason for this slight discrepancy between different Tmax-VRE relations at peak oil generation maturity levels may be due to that the relations are established on pyrolysis analyses of source rocks containing different types of kerogen and some of the differences could be attributed to small sample population used to report the relations. At higher maturity level (e.g., pyrolysis Tmax values of 460+° C), all relations from previous studies provide very similar VRE calculations. It is worth noting that VRE derived from bitumen reflectance data also seems to over predict VRE at peak oil generation maturity level (e.g., Tmax 440 °C) when compared to Tmax-VRE relations; except the one reported by Inan et al. (2016). The reason for close similarity of VRE prediction of Tmax-VRE relation of Inan et al. (2016) and Bitumen- VRE relation of Hakami et al. (2016) needs to be investigated further. In fact, selection of any of the relations given in Table 4-2 will not affect the results significantly. Therefore, the pyrolysis Tmax-VRE relation of Jarvie et al. (2001) was used since it is based on more data points. We note that at present the TQMN Formation is at peak oil generation stage in localities of Wells A and C and late oil to wet gas generation stage at localities of Wells B, D, and E. The maturity data come only from the Jurassic source rocks as given in Tables 4-1 and 4-2. High confidence is placed on the appropriateness of the measured maturity on the isolated kerogen from TQMN source rocks as plotted in Figure 4-8. Maturity data available only from the TQMN Formation may be considered as a weakness in calibration. However, we are quite confident that the maturity data we have obtained for the TQMN are quite reliable and is suitable for calibration of the model for predicting maturity in this almost continuously subsiding Basin (Figure 4-6). If the basin had undergone inversion (e.g., uplift and erosion), then more

maturity data points covering greater depth range especially from across unconformity(ies) would have been necessary. In fact, we received two cutting samples from shallower intervals at Wells A and E and %VRE was calculated from the pyrolysis Tmax and superimposed on the respective plots (Figure 4-8). The fact that these two data points from shallower intervals fall on the computed maturity trends, lends strong support to our inference that available maturity data from the TQMN source rocks in each well are sufficient for maturity calibration. Thermal maturity predictions suggest that thermal maturity profiles are continuous; these profiles do not contain any breaks. The maturity evolution for the TQMN at Wells A and E; low maturity and high maturity, respectively, are superimposed on the burial history curves and shown in Figure 4-9. The prediction of maturity of TQMN source rock is higher (1.0 to 1.25% Ro) for Well E (and Wells B and D not shown) compared to Well A (and Well C not shown) where the TQMN maturity suggest peak oil generation window (0.8% Ro). Higher maturity predictions for localities of Wells B, D and E (TQMN being in late oil/wet gas generation zone) are in agreement with higher temperature gradients calculated at these well locations. In this context, this is a confirmation of the validity of using present-day heat flow as constant heat flow through time as listed in Table 4-4 for each well location. This is not surprising because the basin has almost been continuously subsiding and the organic rich TQMN source rock has been exposed to maximum temperatures and has attained present day maturity level in last 10 to 20Ma.We suggest that what controls the present day maturity of the source rock is in fact the temperature-time history of the source rock mainly throughout the last 20 million years.

Table 4-4 Heat flow through time based on acceptable matches between measured and computed temperatures and measured and computed maturity for five wells. Also given is the computed average temperature gradients from measured subsurface temperatures and the model-computed average thermal conductivity (K) of the lithological section intersected in each well. These heat flow values have been assumed to be constant through geologic time

Well	Heat Flow (mWM^{-2})	$\Delta T/\Delta Z$ (°C/km)	Computed average thermal conductivity (K) of the intersected lithology in each well ($WM^{-1}K^{-1}$)
Well A	55	26.2	2.10
Well C	55	27.1	2.03
Well B	60	29.3	2.05
Well D	62	31.7	1.96
Well E	66	34.7	1.90

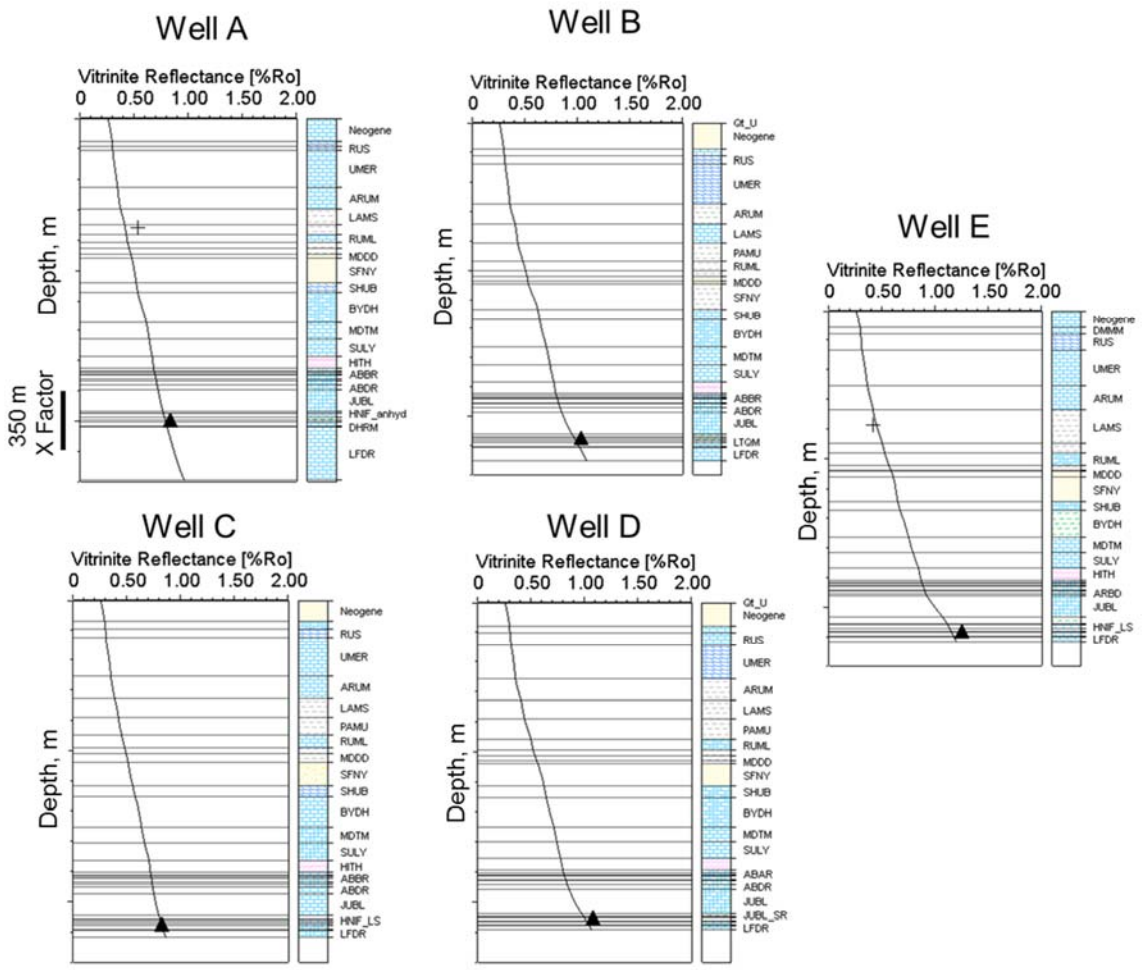

Figure 4-8 Measured versus computed maturity data for each well. Vitrinite reflectance equivalent values are obtained from pyrolysis Tmax data as shown in Table 4-2. Depth scale is the same for all maturity-depth profiles

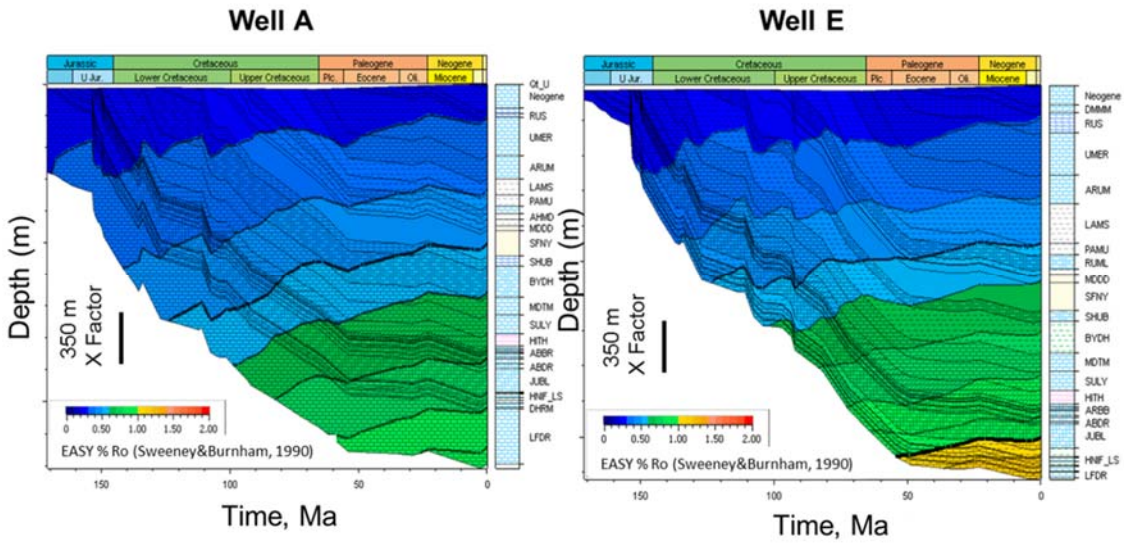

Figure 4-9 Examples of burial history curves for Wells A and E, a low TQMN maturity and a high TQMN maturity well, respectively. Maturity evolution (vitrinite reflectance) is superimposed. At present day, the TQMN is at peak oil and late oil-early gas generation maturity at Well A and Well E, respectively.

As shown in Figure 4-10, the burial evolution and present day depth to the base of the TQMN source rock at all well locations, except Well A, are quite similar (Figure 4-10a). A plot of TQMN Formation maturity versus depth for the five wells is given in Figure 4-10b; showing a variation of maturity from 0.8 to 1.25%VRE (covering roughly peak oil generation to wet gas generation maturity) in about 400 ft. of vertical distance (compare maturity of Well C and Well E) and it is clear that the maturity difference cannot be related to burial depth alone. Figure 4-10c depicts thermal maturity evolution of the TQMN Formation through time at five well locations. Here, the predicted thermal maturity results indicate that the differences are related to varying temperature gradients among locations, and that differences in thermal regimes are the most probable cause for the present day maturity variation of the source rock.

2D modeling results of the section A–A', utilizing the same temperature and maturity calibration as in 1D modeling discussed above, are shown in Figure 4-11 and Figure 4-12, respectively. Present-day heat flow values as determined for each well site through 1D modeling (Table 4-4) were used for the 2D modeling of the section A–A'. At calibration well locations, the heat flow values were taken as is from Table 4-4. For areas between the lines, interpolation was made respecting the temperature gradient map shown in Figure 4-5. Results of calibrated subsurface temperature distribution suggest that temperatures are depressed at location of Well C compared to the locations of Wells E and D (Figure 4-11). The higher temperature gradients for areas of Well D and E are probably caused by higher basal heat flow as mentioned above. According to the calibrated maturity (% Ro) distribution along section A–A, (Figure 4-12), the maturity of the TQMN Formation is higher in areas of wells D and E due to higher temperature gradients brought about higher paleo- and present-day heat flow; due probably to radiogenic heat flow contribution of granitic basement. At location of Well D and E, the maturity of the TQMN source rock is higher than 1.0% Ro indicating that the source rock is actively in late oil wet-gas generation window. At locality of Well C, which represents relatively cooler areas of the basin, the TQMN source rock is within peak oil generation window (e.g., 0.8%Ro).

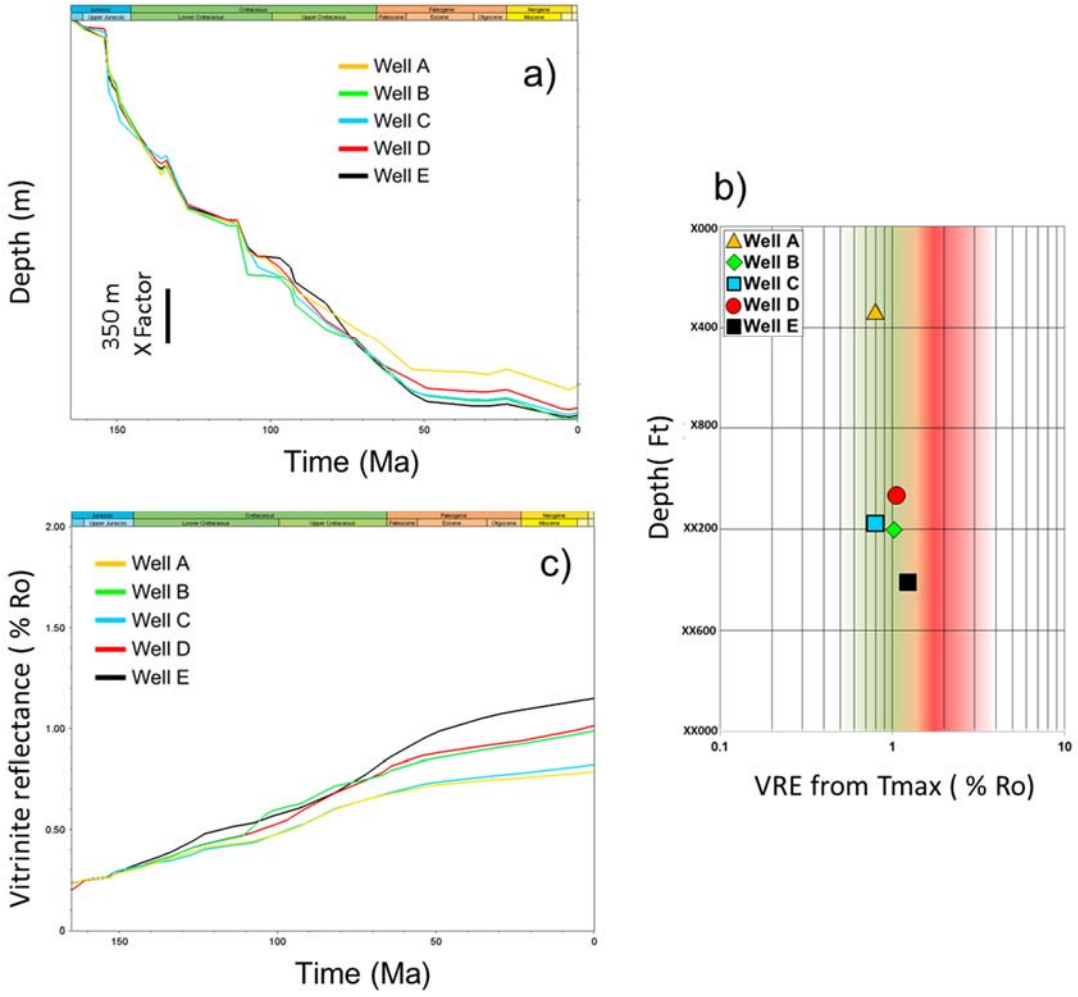

Figure 4-10 a) Burial history, b) present day maturity based on pyrolysis of extracted and isolated samples, and c) thermal maturity evolution curves for the TQMN Formation intersected in the five studied wells. Note that although the burial depth through time are almost identical for TQMN Formation at five well locations (except well A where the TQMN Formation is somewhat shallower), the present day maturity ranges from 0.8 to 1.25% Ro. See text for discussion.

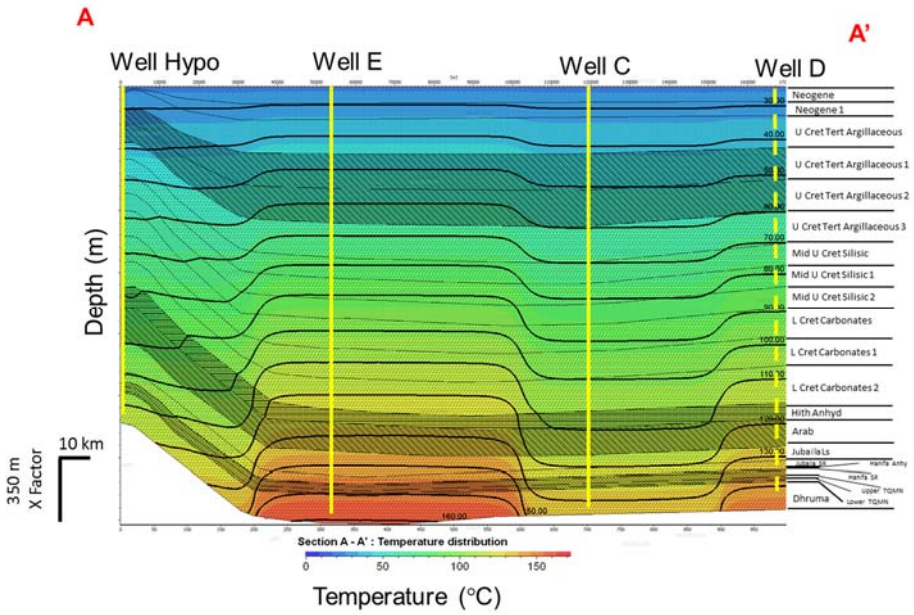

Figure 4-11 Calibrated temperature distribution along Section A-A'. The subsurface temperatures are depressed at location of Well C compared to the locations of Wells E and D. The higher temperature gradients for areas of Well D and E are most likely caused by higher basal heat flow

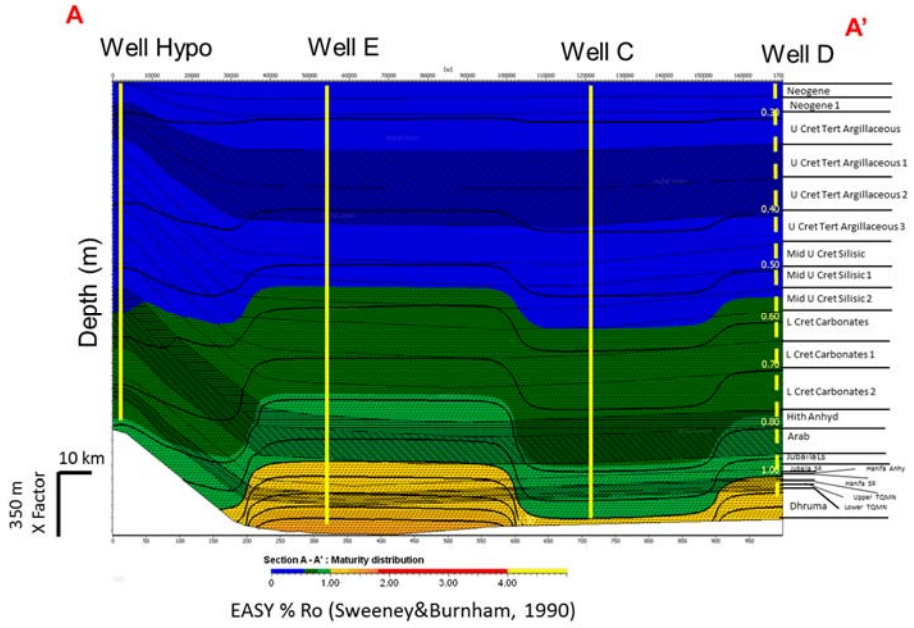

Figure 4-12 Calibrated maturity (% Ro) distribution along Section A-A'. The maturity of the TQMN Formation is higher in areas of wells D and E due to higher temperature gradients brought about higher paleo- and present-day heat flow. See text for discussion.

4.5.2 Hydrocarbon Generation and Migration

For modeling the hydrocarbon generation from the TQMN source rock, initial TOC content was assigned a 12 wt. % in accordance with the results of analysis of immature TQMN source rock in Well X and also considering the remaining TOC content within late oil mature levels reaching 4–5 wt. % TOC. The average present day TOC content for the TQMN samples from all wells representing a maturity range from 0.8 to 1.25% Ro is 4.9wt. % (Table 4-2). The maturity level on average translate to a transformation ratio of a 60% for the organic matter. Simple calculation indicate that present day average value of 4.9% TOC is about 40% of the initial TOC content of the TQMN at immature stage; leading to calculation of about 12 wt.% TOC as initial value for modeling hydrocarbon generation. An initial Hydrogen Index (HI) of 775 mg HC/g TOC was assumed, based on the kinetic analysis of an immature TQMN samples (Table 4-5). Present-day HI values for the samples from TQMN Formation vary from 48 to 196 mg HC/g TOC depending upon maturity across the Jafurah Sub-Basin.

Hydrocarbon generation was simulated using the kinetic model based on analysis of immature TQMN kerogen (Chen, 1995, Aramco Internal Report). The kinetic data given in Table 4-5 is for total petroleum generation potential of the TQMN kerogen. Therefore, ratio of oil and gas of the total petroleum generation potential was assumed based on ratios of oil and gas generation potential for Type II-S kerogen reported by Behar et al. (1997); namely 87.5% of the total petroleum potential was taken as for oil generation potential and 12.5% of the total petroleum potential was assigned for gas potential. Moreover, activation energy distribution for gas generation from the TQMN source rock kerogen was also taken

from Behar et al. (1997). For the modeling HC generation, as mentioned earlier, we assumed an initial TOC of 12 wt. % and initial HI of 775 mg HC/g TOC. Hydrocarbon generation from the TQMN source rock, at location of Well E, started at about 100 Ma and reached its peak about 70 Ma (Figure 4-13). This figure demonstrates that peak oil generation took place at about 0.82% Ro maturity of the TQMN source rock, which is expected for a Type II S kerogen generating oil at relatively early maturity due to S\\C bonding, these values are consistent with the results of Carrigan et al. (1995). In fact, we have proven that the kerogen isolated from immature TQMN source rock provided atomic S/C ratio between 0.06 and 0.07, which are higher than the threshold of 0.04 considered for sulfur rich kerogen (Orr, 1986).

Table 4-5 Kinetics data generated from pyrolysis of an immature TQMN isolated kerogen and used in modeling hydrocarbon generation. TOC= 4.36 wt %, HI= 775 mg HC/g TOC, Tmax=418 °C, Total petroleum potential (S2) =33.8 mg HC/g sample. Oil generation potential = 29.6 mg HC/g

	Oil	Gas
Ratio= 100.0 (%)	87.5**	12.5**
Sorption (g oil /g organic carbon)*	0.1	0
Frequency factor (1e+26/Ma)	5.23	5.23
Activation Energy (kcal/mol)	Fractions (%)	Fractions (%)
44	0.20	1.10
46	0.60	3.90
47	1.20	7.00
48	5.60	8.00
49	9.80	10.00
50	13.40	10.00
51	23.70	11.00
52	22.90	12.00
53	11.10	11.00
54	6.40	10.00
56	4.50	7.00
58	0.40	5.00
60	0.20	3.00
62	0.00	0.90
64	0.00	0.10
Total	100%	100%

*We assumed that 10 % of the generated oil is retained within the kerogen network as previously assumed (Stainforth and Reinders, 1990; Sandvik et al., 1992; Pepper and Corvi, 1995). This amount of oil will not leave the kerogen and will crack to gas at higher temperatures.

** Since the kinetics data for total petroleum potential of the TQMN kerogen has been given by Chen (1995, in the Aramco Internal Report), we took ratios of oil and gas from Type II-S kerogen kinetics (Behar et al., 1997) as approximation and distribute the generation potential for oil and gas accordingly.

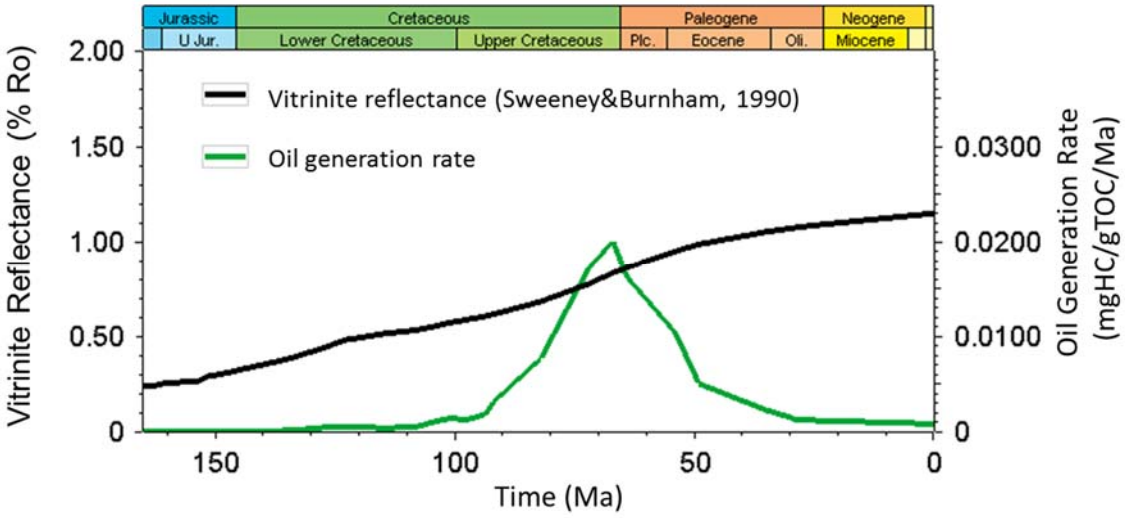

Figure 4-13 Oil generation rate versus thermal maturity evolution for the TQMN Formation at location of Well E. This figure demonstrates that peak oil generation took place at about 0.82% Ro maturity, which is expected for a Type II S kerogen, which generates oil at relatively early maturity due to S C bonding. See text for discussion.

Figure 4-14 shows cumulative hydrocarbon (oil and gas) generation from the TQMN formation at five well locations. Solid lines depict oil generation and dashed lines depict gas generation. As expected, the maximum generation took place at location of Well E where the TQMN formation has the highest maturity where TQMN has generated about 600 mg HC/ g TOC; about 77% of its initial potential, which was defined as 775 mg HC/g TOC. Gas generation from the TQMN at location of Well E has reached about 75 mg HC/g TOC at present. Concerning migration of generated oil from the source rock, as discussed in Section 4.5.2., modeling software takes a default value of oil saturation threshold (<5%) for primary migration of oil from the source rock. In such a case, most of the generated oil gets expelled and very little oil remains within the source rock for cracking to gas at higher burial temperatures. This assumption seems to overestimate oil expulsion at low oil saturation thresholds; meaning that oil can start leaving the source rock as a single phase

at oil saturations as low as 5%. We have simulated oil migration by varying the oil saturation (critical oil saturation after which oil starts to be expelled) thresholds (Figure 4-15) and compared the "oil gas cracking" and resultant "in-source gas estimations" compared to source rock's gas adsorption capacity (which has been measured to higher than 50 scf/ton at reservoir and temperature and pressure conditions). We found that in order to saturate the source rock to its adsorption capacity, a minimum 20% oil saturation threshold is needed. Therefore, in the 2D modeling, we set the oil migration threshold at 20% oil saturation before which oil expulsion does not take place. We also assumed 10% of the generated oil is retained within the kerogen. These assumptions enabled the model to retain and crack some of the oil so that retained gas can be better estimated.

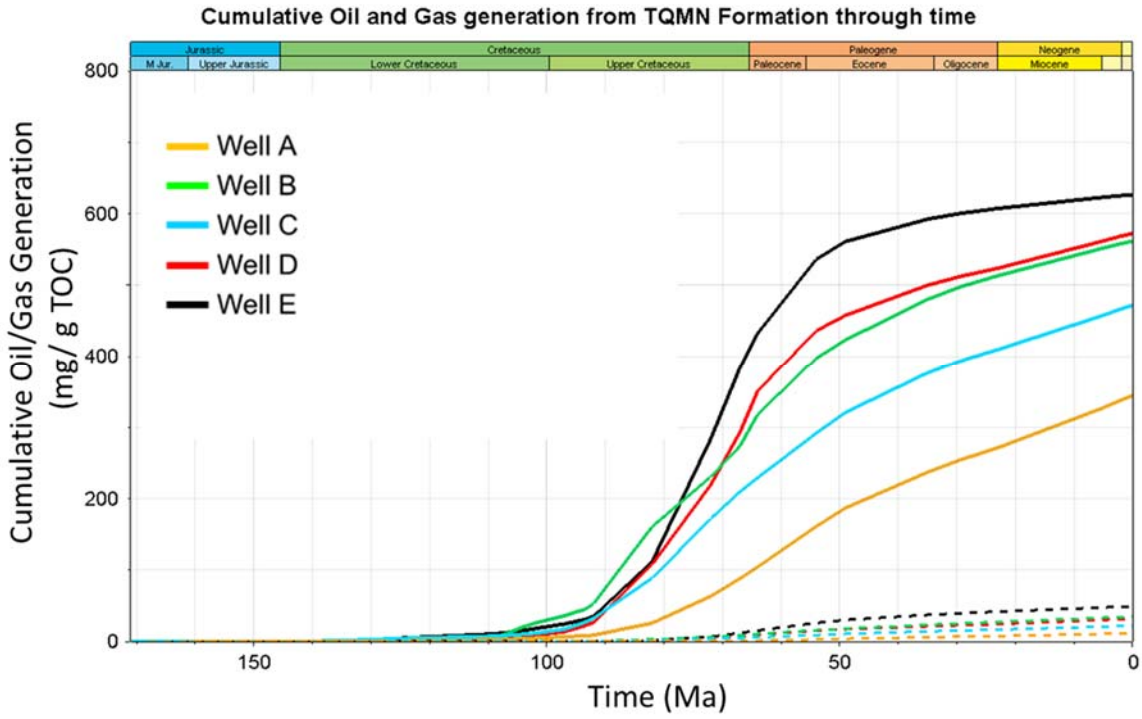

Figure 4-14 Cumulative hydrocarbon (oil and gas) generation from the TQMN formation at five well locations. Solid lines depict oil generation and dashed lines depict gas generation. Maximum cumulative generation took place at location of Well E where the TQMN formation has the highest maturity

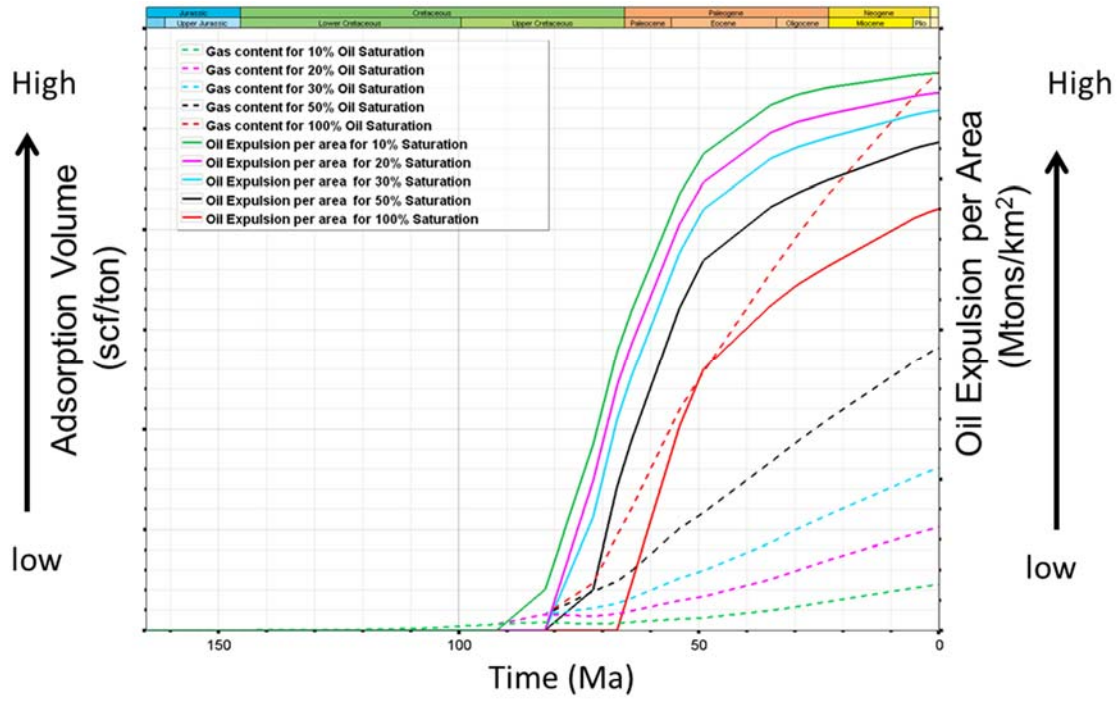

Figure 4-15 A modeling results for oil expulsion threshold versus present-day gas content for TQMN Formation at location of Well E. For the model to predict the gas adsorption capacity of the formation obtained from experiment (utilizing reservoir pressure and temperatures), minimum 20% oil saturation is required. Lower assumptions of oil expulsion threshold will lead to gas under-saturation in the modeling results. See text for discussion.

4.5.3 Estimation of Gas Content in TQMN Source Rock

Modeling results on estimated gas content variation along section A–A' is shown in Figure 4-16. Oil saturation threshold for oil migration was set at 20%; below this saturation level, the oil resides inside the source rock and cracks to gas at higher temperatures. Accordingly, the TQMN source rock contains higher amount of gas at location of Well E than that of Well D. The gas content is calculated to be the lowest at location of Well C. The amount of gas (free and adsorbed) that can be expected within the TQMN source rock should be equal to or higher than the gas adsorption capacity. As shown at location of Well E and Well D, where the maturity is sufficient for gas generation as shown in Figure 4-14, TQMN source rock's gas saturation is equal to or higher than its gas adsorption capacity.

Considering free gas that may accumulate within the intergranular pore space (where the rock is sufficiently self-sealing and/or adjacent rocks are impermeable), gas content may even be higher. At location of Well C, due to lower maturation level, TQMN source rock is shown to be gas under-saturated with respect to gas adsorption capacity at subsurface temperature and pressure conditions. At locations of Well A and C, where the TQMN is at peak oil generation maturity, we suggest that TQMN source rocks have high potential for unconventional oil resource. Field operations and testing of hydrocarbons in these wells have enabled us to accumulate some critical data such as Gas Oil Ratio (GOR) and API of the produced hydrocarbons. Modeling results on GOR along section A–A' are shown in Figure 4-17. Along this cross section, the GOR is predicted to be higher for areas of wells D and E, which is in full agreement with the maturity and production data.

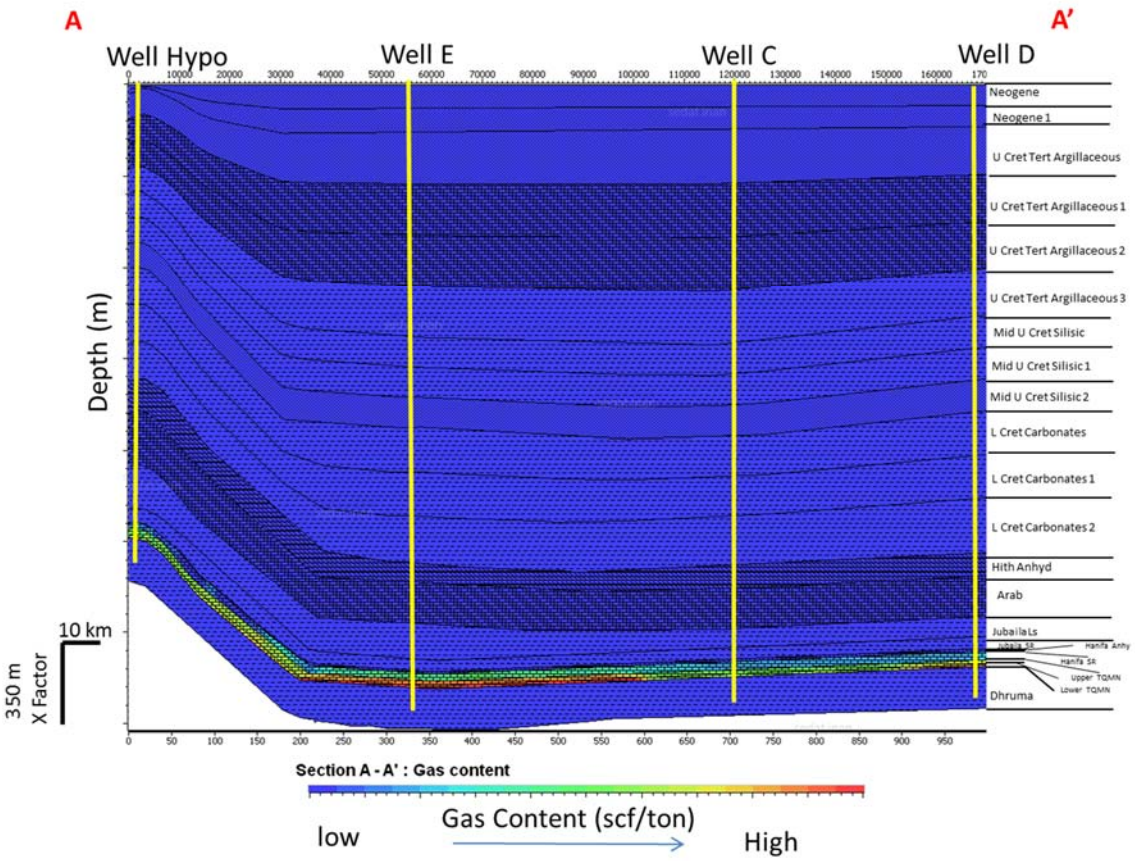

Figure 4-16 Gas potential estimates for the TQMN formation along section A–A'. Oil expulsion threshold is assumed to be 20% oil saturation; below this threshold saturation, it is assumed that oil cannot escape the source rock and thus cracks to gas. As expected from maturity distribution, gas potential is higher in location of Wells E and D compared to that of location of Well C. See text for discussion

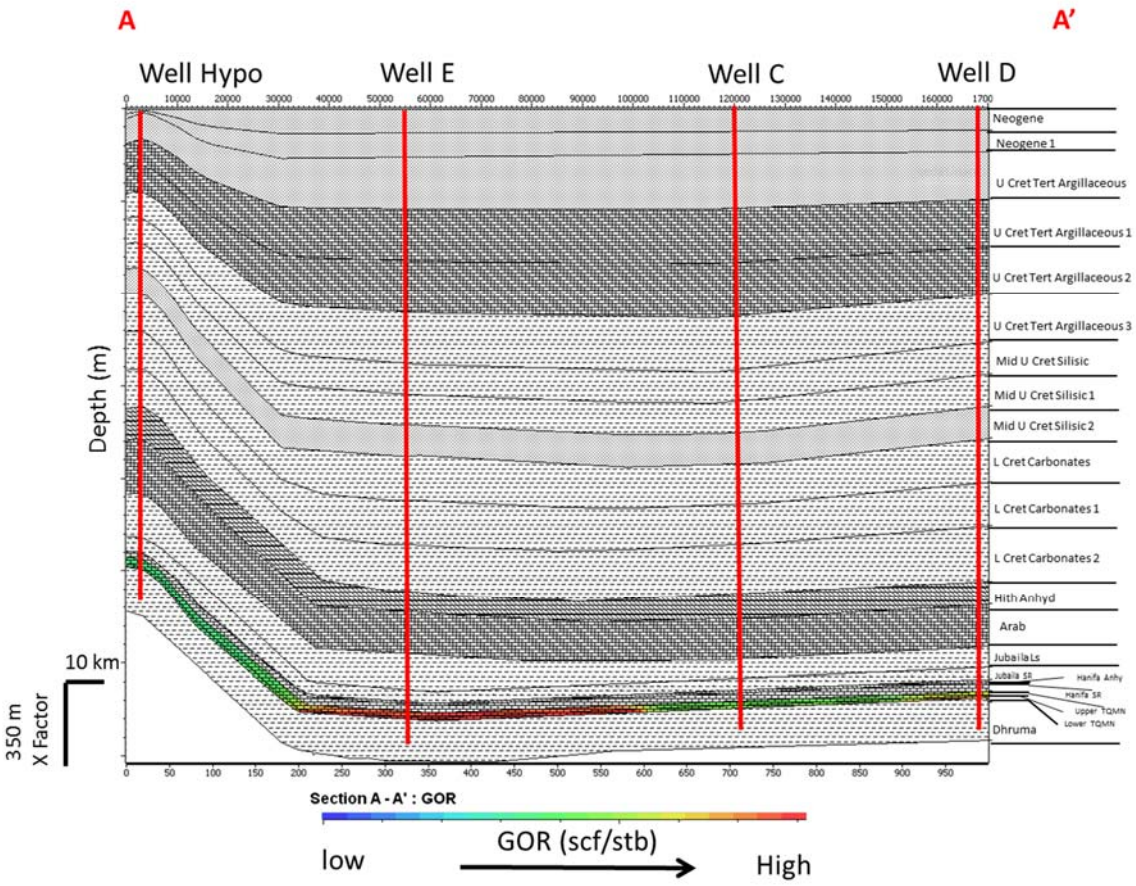

Figure 4-17 Gas Oil Ratio (GOR) calculated for the TQMN formation along section A–A'. GOR is predicted to be higher for areas of wells D and E in agreement with the maturity and production data. See text for discussion

4.6 Conclusion

Main conclusions of this study are:

- Thermal maturity of the TQMN source rocks show significant lateral variations (from 0.80 to 1.25% VRE; roughly equivalent to peak oil generation to wet gas generation window) despite relatively small differences in paleo-burial and present-day burial depth.

- Calibrated Basin modeling study suggests that the spatial thermal maturity variations of the Tuwaiq Mountain (TQMN) source rocks in the Jafurah Sub-Basin are attributed to spatial variation of the thermal regime in the basin.
- In warmer parts of the basin (≥28 °C/km), higher heat flow modeling input was required to predict past and present-day temperatures and maturities. Higher heat flow values were incorporated in the model by increasing basal heat flow. Higher basal heat flow is most likely due to more acidic basement rocks; contributing higher radiogenic heat.
- In warmer (e.g., high subsurface temperature gradient (≥28 °C/km)) of the Jafurah Sub-Basin, the TQMN source rocks are within late oil generation to wet gas generation window. In relatively cooler (≤28 ° C/km) parts the Basin, the TQMN source rocks are at peak oil generation window.
- The modeling results suggest that TQMN source rocks started generating oil at about 100 Ma and they reached the peak oil generation at about 70 Ma, and at present, they are at wet gas generation window in warmer (≥28 °C/km) northern and eastern part of the Jafurah Sub-Basin. The central and southwestern parts of the basin are cooler, and here, the TQMN source rocks are within the peak oil generation maturity window.
- The warmer parts of the basin have higher gas potential for the TQMN source rocks compared to cooler parts of the Basin.
- For proper modeling and estimations of gas content in source rocks, some advanced modifications in basin modeling parameters are necessary. For example, variations of the oil saturation threshold is necessary until a gas saturation level equal to or

higher than the gas adsorption capacity of the source rock is obtained, otherwise, modeling will lead to overestimation of the oil migration out of the source rock and thus amount of the oil that can be cracked to gas, and thus amount of eventual gas content, will be underestimated.

- Following our basin modeling study, we note that collection of more subsurface temperature data will be necessary in the future to better estimate the maturity and gas potential of the TQMN source rocks in the Jafurah Basin.

4.7 References

AbuAli, M.A., Littke, R., 2005. Paleozoic petroleum systems of Saudi Arabia: a basin modeling approach. GeoArabia 10, 131–168.

AbuAli, M.A., Franz, U.A., Shen, J., Monnier, F., Mahmoud, M.D., Chambers, T.M., 1991. Hydrocarbon generation and migration in the Paleozoic sequence of Saudi Arabia. Society of Petroleum Engineers, SPE 21376, 345–356.

AbuAli, M.A., Rudkiewicz, J.L., McGillivray, J.G., Behar, F., 1999. Paleozoic petroleum system of Central Saudi Arabia. GeoArabia 4, 321–335.

Al Duhailan, M.A., Ahmed, A.S., Al Hakami, A.M., Leyva, I.F., 2016. Little-Known Differences in Tuwaiq Mountain Petroleum Generation: Implications for Different Unconventional Resource Play Fairways. Unconventional Technology Conference proceeding by SPE, pp. 1–3 (August, 2016 San Antonio, Texas USA).

Alexander, T., Baihly, J., Boyer, C., Clark, B., Waters, G., Jochen, V., Le Calves, J., Lewis, R., Miller, C.K., Thaeler, J., Toelle, B.E., 2011. Shale gas revolution. Oilfield Review 23, 40–55.

Al-Husseini, M.I., 1997. Jurassic sequence stratigraphy of the western and southern. Arabian Gulf: GeoArabia 2, 361–382.

Ayres, M.G., Bilal, M., Jones, R.W., Slentz, L.W., Tartir, M., Wilson, A.O., 1982. Hydrocarbon habitat in main producing areas, Saudi Arabia. AAPG Bull. 66, 1–9.

Behar, F., Vandenbroucke, M., Tang, Y., Marquis, F., Espitalié, J., 1997. Thermal cracking of kerogen in open and closed systems: determination of kinetic parameters and stoichiometric coefficients for oil and gas generation. Org. Geochem. 26, 321–339.

Cantrell, D.L., Nicholson, P.G., Hughes, G.W., Miller, M.A., Bhullar, A.G., Abdelbagi, S.T., Norton, A.K., 2014. Tethyan petroleum systems of Saudi Arabia. In: Marlow, L., Kendall, C., Yose, L. (Eds.), Petroleum Systems of the Tethyan Region. AAPG Memoir Vol. 106, pp. 613–639.

Carrigan, W.J., Cole, G.A., Colling, E.L., Jones, P.J., 1995. Geochemistry of the Upper Jurassic Tuwaiq Mountain and Hanifa Formation petroleum source rocks of Eastern Saudi Arabia. In: Katz, B.J. (Ed.), Petroleum Source Rocks. Springer-Verlag, New York, pp. 67–87.

Chalmers, G.R., Bustin, R.M., Power, I.M., 2012. Characterization of gas shale pore systems by porosimetry, pycnometry, surface area, and field emission scanning electron microscopy/transmission electron microscopy image analyses: Examples from the Barnett. Woodford, Haynesville, Marcellus, and Doig units: AAPG Bulletin 96, 1099–1119. http://dx.doi.org/10.1306/10171111052.

Chen, H.H., 1995. Kinetic models of hydrocarbon generation from Jurassic source rocks, Arabian Basin, Eastern Province. Aramco Internal Report: ARI 340-93/03-I-R4 (27 pages).

Cole, G.A., Carrigan, W.J., Colling, E.L., Halpern, H.I., Al-Khadhrawi, M.R., Jones, P.J., 1994. The organic geochemistry of the Jurassic petroleum system in Eastern Saudi Arabia. Can. Soc. Petrol. Geol. Mem. 17, 413–438.

Curtis, J.B., 2002. Fractured shale-gas systems. AAPG Bull. 86, 1921–1938.

Droste, H.H.J., 1990. Depositional cycles and source rock development in an empiric intraplate form basin, the Hanifa Formation of the Arabian Peninsula. Sediment. Geol. 69, 281–296.

Gasparik, M., Bertie, R.P., Gensterblum, Y., Ghanizadeh, A., Krooss, B.M., Littke, R., 2014. Geological controls on the methane storage capacity in organic-rich shales. Int. J. Coal Geol. 123, 34–51.

Hakami, A., Ellis, L., Al-Ramadan, K., Abdelbagi, S., 2016. Mud gas isotope logging application for sweet spot identification in an unconventional shale gas play; a case study from Jurassic carbonate source rocks in Jafurah Basin, Saudi Arabia. Mar. Pet. Geol. 76, 133–174. http://dx.doi.org/10.1016/j.marpetgeo.2016.05.003.

Hantschel, T., Kauerauf, A.I., 2009. Fundamentals of Basin and Petroleum Systems Modeling. Springer-Verlag, Berlin (476 pages).

Hao, F., Zou, H., Lu, Y., 2013. Mechanisms of shale gas storage: implications for shale gas exploration in China. AAPG Bull. 97, 1325–1346.

Heller, R., Zoback, M., 2014. Adsorption of methane and carbon dioxide on gas shale and pure mineral samples. J. Unconv. Oil Gas Resour. 8, 14–24.

İnan, S., Yalçın, M.N., Mann, U., 1998. Expulsion of oil from petroleum source rocks: Inferences from pyrolysis of samples of unconventional grain size. Org. Geochem. 29, 45–61.

İnan, S., Goodarzi, F., Schmidt Mumm, A., Arouri, K., Qathami, S., Ardakani, O.H., İnan, T., Tuwailib, A.A., 2016. The Silurian Qusaiba hot shales of Saudi Arabia: An integrated assessment of thermal maturity. Int. J. Coal Geol. 159, 107–119. http://dx.doi.org/10.1016/j.coal.2016.04.004.

İnan, S., Hakami, A., AbuAli, M., 2017. A Petroleum System and Basin Modeling Study of Northwest and East-Central Saudi Arabia: Effect of Burial History and Adjacent Rock Lithology on the Gas Potential of the Silurian Qusaiba Shales. AAPG Memoir # 114: Petroleum Systems case Studies (in press).

Jacob, H., 1989. Classification, structure, genesis, and practical importance of natural solid bitumen ("migrabitumen"). Int. J. Coal Geol. 11, 65–79.

Arvie, D.M., Brenda, L.C., Floyd, H., Breyer, J.T., 2001. Oil and Shale Gas from the Barnett Shale, Ft. Worth Basin, Texas. AAPG National Convention, June 3–6, 2001, Denver, CO American Association of Petroleum Geologists Bulletin 85 (2001). 13 ((Supplement), A100).

Jarvie, D.M., Hill, R.J., Ruble, T.E., Pollastro, R.M., 2007. Unconventional Shale-Gas Systems: The Mississippian Barnett Shale of North-central Texas as One Model for Thermogenic Shale-Gas Assessment: AAPG Bulletin, 91, 475–499. http://dx.doi.org/10.1306/12190606068.

Konert, G., Afifi, A.M., Al-Hajri, S.A., Droste, H.J., 2001. Paleozoic stratigraphy and hydrocarbon habitat of the Arabian plate. GeoArabia 6, 407–442.

Lindsay, R.F., Khan, S., Dhubeeb, A., Davis, R., 2014. Unconventional Jurassic Carbonate Source Rocks, Saudi Arabia. International Conference & Exhibition, September 14–17, 2014, Istanbul, Turkey. AAPG article # 90194.

Love, A.H., 1982. Kerogen-isolation method; a study with kerogen data from sedimentary rocks. USGS Open-File Report, pp. 82–891 (21 pages).

Mann, U., Hantschel, T., Schaefer, R.G., Krooss, B., Leythaeuser, D., Littke, R., Sachsenhofer, R.F., 1997. Petroleum migration: mechanisms, pathways, efficiencies and

numerical simulations. In: Welte, D.H., Horsfield, B., Baker, D.R. (Eds.), Petroleum and Basin Evolution. Springer, Heidelberg, pp. 397–515.

Milliken, K.L., Rudnicki, M., Awwiller, D.A., Zhang, T., 2013. Organic matter-hosted pore system, Marcellus Formation (Devonian), Pennsylvania. AAPG Bulletin 97, 177–200. http://dx.doi.org/10.1306/07231212048.

Montgomery, S.L., Jarvie, D.M., Bowker, K.A., Pollastro, R.M., 2005. Mississippian Barnett Shale, Fort Worth Basin, north-central Texas: Gas-shale play with multi-trillion cubic foot potential. AAPG Bull. 89, 155–175.

Murris, R.J., 1980. Middle East stratigraphic evolution and oil habitat. AAPG Bull. 64, 597–618. Orr, W.L., 1986. Kerogen/asphaltene/sulfur relationships in sulfur-rich Monterey oils. Org. Geochem. 10, 499–516.

Pepper, A.S., Corvi, P.J., 1995. Simple kinetic models of petroleum formation. Part III: Modelling an open system. Mar. Pet. Geol. 12, 417–452.

Petersen, H.I., 2006. The petroleum generation potential and effective oil window of humic coals related to coal composition. Int. J. Coal Geol. 67, 221–248.

Pollastro, R. M., 2003, Total petroleum systems of the Paleozoic and Jurassic, greater Ghawar uplift and adjoining provinces of central Saudi Arabia and northern Arabian-Persian Gulf: U.S. Geological Survey Bulletin 2202-H, 100p.

Romero-Sarmiento, M.F., Rouzaud, J.N., Bernard, S., Deldicque, D., Thomas, M., Littke, R., 2014. Evolution of Barnett shale organic carbon structure and nanostructure with increasing maturation. Org. Geochem. 71, 7–16.

Sandvik, E.I., Young, W.A., Curry, D.J., 1992. Expulsion from hydrocarbon sources: the role of organic absorption. Org. Geochem. 19, 77–87.

Schlumberger, PetroMod© Version 2013.1 and Version 2014.1 User Guide, Aachen, Germany. Schoenherr, J., Littke, R., Urai, J.L., Kukla, P.A., Rawahi, Z., 2007. Polyphase thermal evolution in the Infra-Cambrian Ara Group (South Oman Salt Basin) as deduced by maturity of solid reservoir bitumen. Org. Geochem. 38, 1293–1318.

Sharland, P.R., Archer, R., Casey, D.M., Davies, R.B., Hall, S.H., Heward, A.P., Horbury, A.D., Simmons, M.D., 2001. Arabian Plate Sequence Stratigraphy: GeoArabia Special Publication 2. Gulf PetroLink, Bahrain 371 pages.

Stainforth, J.G., Reinders, J.E.A., 1990. Primary migration of hydrocarbons by diffusion through organic matter networks, and its effect on oil and gas generation. Org. Geochem. 16, 61–74.

Sweeney, J.J., Burnham, A.K., 1990. Evaluation of a simple model of vitrinite reflectance based on chemical kinetics. AAPG Bull. 74, 1559–1570.

Tissot, B.P. Welte, D.H., 1984. Petroleum Formation and Occurrence. Springer-Verlag, Berlin 699 pages.

Yalcin, M. N., Littke, R., Sachsenhofer, R.F., 1997. Thermal history of sedimentary basins. In: Welte, D.H., Horsfield, B., Baker, D.R. (Eds.), Petroleum and Basin Evolution. Springer, Heidelberg, pp. 71–167.

Zhang, T.W., Ellis, G.S., Ruppel, S.C., Milliken, K., Yang, R.S., 2012. Effect of Organic Matter Type and Thermal Maturity on Methane Adsorption in Shale-Gas Systems: Organic Geochemistry, 47, 120–131.

Ziegler, M.A., 2001. Late Permian to Holocene Paleofacies evolution of the Arabian plate and its hydrocarbon occurrences. GeoArabia 6, 445–504.

CHAPTER 5

Tuwaiq Mountain Reservoir Characterization

Characterization of Carbonate Mudrocks of the Jurassic Tuwaiq Mountain Formation, Jafurah Sub-Basin, Saudi Arabia: Implications for Unconventional Reservoir Potential Evaluation

Ahmed Hakami [a,*], Ahmed Al-Mubarak [a], Khalid Al-Ramadan [b], Clay Kurison [a], Ivan Leyva Poveda [a]

[a] Saudi Aramco, Exploration Organization, 31311, Dhahran, Saudi Arabia
[b] Petroleum Engineering and Earth Science College, King Fahad University of Petroleum and Minerals

Published Paper in Journal of Natural Gas Science and Engineering May, (2016) 1-20

(ELSEVIER)

Abstract

Organically rich mud rocks are currently targeted for unconventional oil and gas exploration and development in many places around the world, including Saudi Arabia. The Jurassic Tuwaiq Mountain Formation in the Jafurah Sub-Basin located east of the giant Ghawar oil field is the primary focus of this paper. The formation has been divided into 3 Tiers possessing varying reservoir qualities. Of these Tiers, the bottom Tier 1 possesses

the most excellent shale gas characteristics such as high total organic content (TOC), low clay content and high hydrocarbon saturation. The formation of interest is also in the proper maturity window for hydrocarbon generation and relatively shallow, making it attractive for an economic unconventional shale gas play. To expedite shale gas development in Saudi Arabia, a phased de-risking strategy has been implemented. The strategy consists of four phases; exploration, appraisal, pilot and development. Three wells, representing the first unconventional reservoir exploration wells drilled in the Jafurah Sub-Basin have been selected for this study. The wells were drilled vertically, cored and logged. Wells were then sidetracked with 5,000 ft horizontal laterals and stimulated through multistage hydraulic fracturing. All stimulated wells flowed gas and condensate to surface. This paper summarizes, with examples, a workflow for characterizing the Tuwaiq Mountain Formation as a potential unconventional liquid rich gas play. Crucial to this, is the development of a reservoir quality predictive model for acreage grading, sweet spot identification and fracturing stage selection. This methodical approach is applicable to the evaluation of any emerging unconventional play.

5.1 Introduction

The Jurassic Tuwaiq Mountain Formation in the Jafurah Sub-Basin is a potential world-class unconventional play. This formation is the primary source for Jurassic conventional oil reservoirs in Saudi Arabia including Ghawar, which is the most prolific oil field in the world (Cole et al., 1994, and Carrigan et al., 1995). The Jafurah Sub-Basin (Figure 5-1) spreads over a large area equivalent in size to the Eagle Ford play in South Texas. The

unconventional exploration program in the Jafurah Sub-Basin started a few years ago targeting the Tuwaiq Mountain Formation. Wells A, B and C marked the first Saudi Arabian unconventional wells drilled and hydraulically fractured with proppant placement in such an ultra-tight carbonate rock. These wells were drilled as part of the exploration phase of the de-risking strategy. The initial flowback results indicated the potential of a promising unconventional resource play. Accurate assessment of unconventional plays requires the integration of key multidisciplinary variables. Understanding the reservoir and completion parameters including but not limited to organic matter richness, clay type and content, intra-kerogen porosity, matrix porosity, brittleness, reservoir pressure, natural fractures, and hydrocarbon saturations are critical to the proper evaluation and ultimately, the success of developing a play. This paper presents a workflow in which a structured approach was followed to characterize the Tuwaiq Mountain unconventional shale gas play. The workflow involves the integration of geoscience and engineering data into a predictive model for sweet spot identification. The geological, geochemical and petrophysical data were used to guide the characterization of Tuwaiq Mountain reservoir properties. The geomechanical and production data were used to validate the efficiency of the stimulation treatments and production potential of the play.

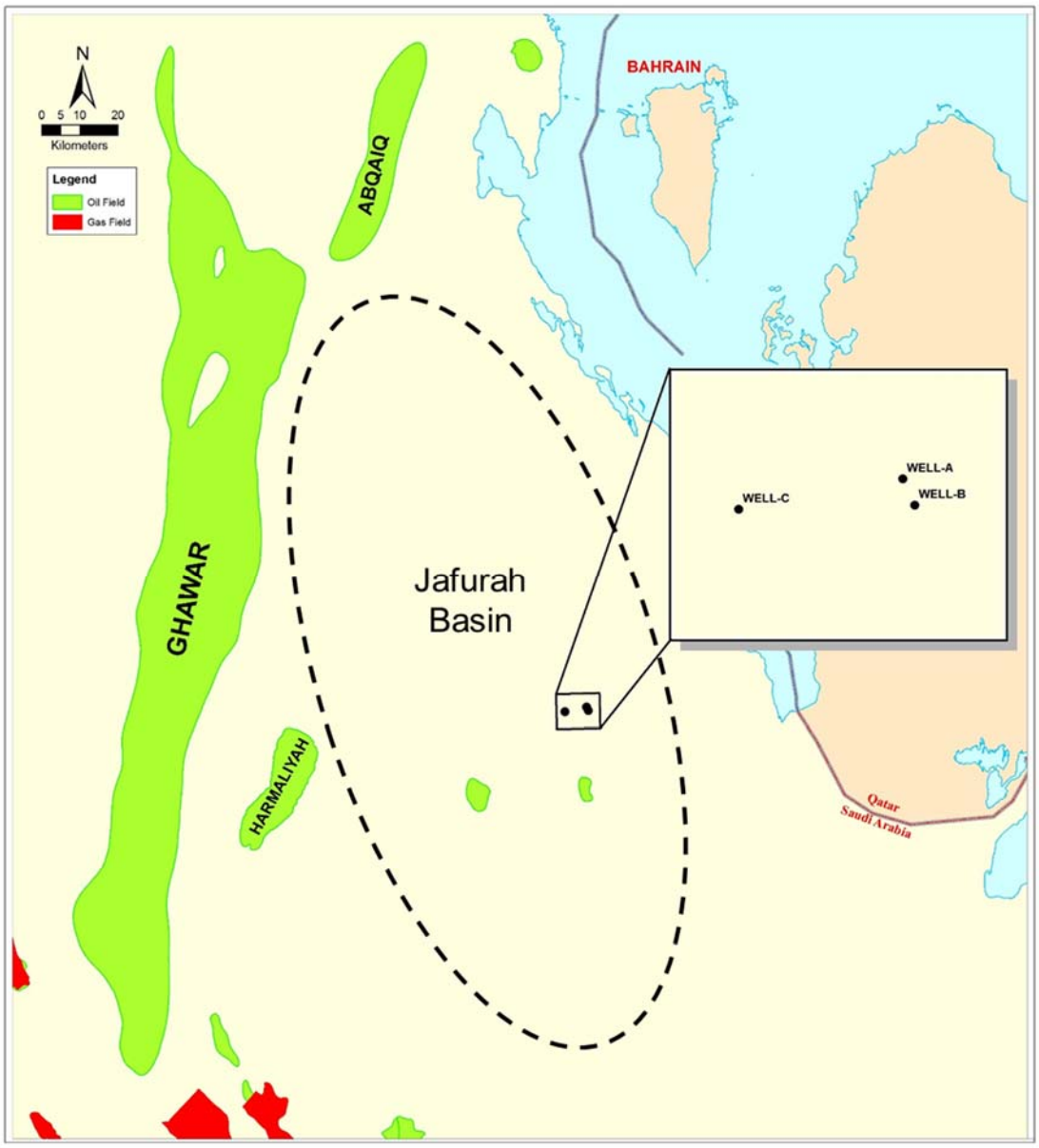

Figure 5-1 Location map of the study area, showing the Ghawar giant oil field in Saudi Arabia, the approximate outline of Jafurah Sub-Basin (dashed black line), and the three wells used in the study.

5.2 Unconventional Resource De-risk Strategy

Successful development of unconventional resources requires a paradigm shift from the process for developing conventional oil and gas resources. Conventional plays require a few exploration and delineation wells to determine the presence, volume and deliverability of hydrocarbons so that a development plan can be implemented. Unconventional plays require a considerable number of wells to define the area but an order of magnitude higher number of development wells to be drilled due to the lower productivity and rapid decline of such plays (Holditch, 2006). A phased de-risking strategy was implemented by Saudi Aramco to evaluate the unconventional resources within the Kingdom. The work is being conducted by a multidisciplinary asset team working together in a more collaborative and well integrated environment. As illustrated in (Figure 5-2), the de-risking strategy is divided into four phases with each having certain expectations: Exploration, Appraisal, Pilot and Development. The focus for each phase is shifting between reservoir data collection and analysis, increasing expected ultimate recovery (EUR) and cost reduction:
In the exploration phase, the focus is on **data collection** to assist in answering a simple question: Is there a hydrocarbon resource base? Critical reservoir parameters are also collected to ensure the play is in the optimum maturity window for hydrocarbon generation.

Once the play is confirmed, the appraisal phase begins by drilling a number of offset wells to delineate the area and to determine whether sufficient hydrocarbon-in-place exists to make the area worthy of further evaluation. In this phase, the focus shifts towards **Feasibility of Access and Understanding Well Recovery** by understanding the initial drilling and completion challenges with an overall goal of operational feasibility.

Next comes the pilot phase, where several wells will be drilled to tune technologies to the unconventional reservoir, optimize lateral length, and adjust fluid and proppant volumes to increase the EUR per well. In this phase, the focus is firmly on **maximizing the EUR**, while **reducing the cost** of drilling and unit cost of fracturing stimulation by streamlining logistics, pad drilling and simultaneous operations. Another focus of this phase is repeatability and scalability so set economic benchmarks can be used to understand how economic the play will be. Last is the development phase where the focus will be on large-scale producibility and profitability through improved execution facilitated by a manufacturing mode framework.

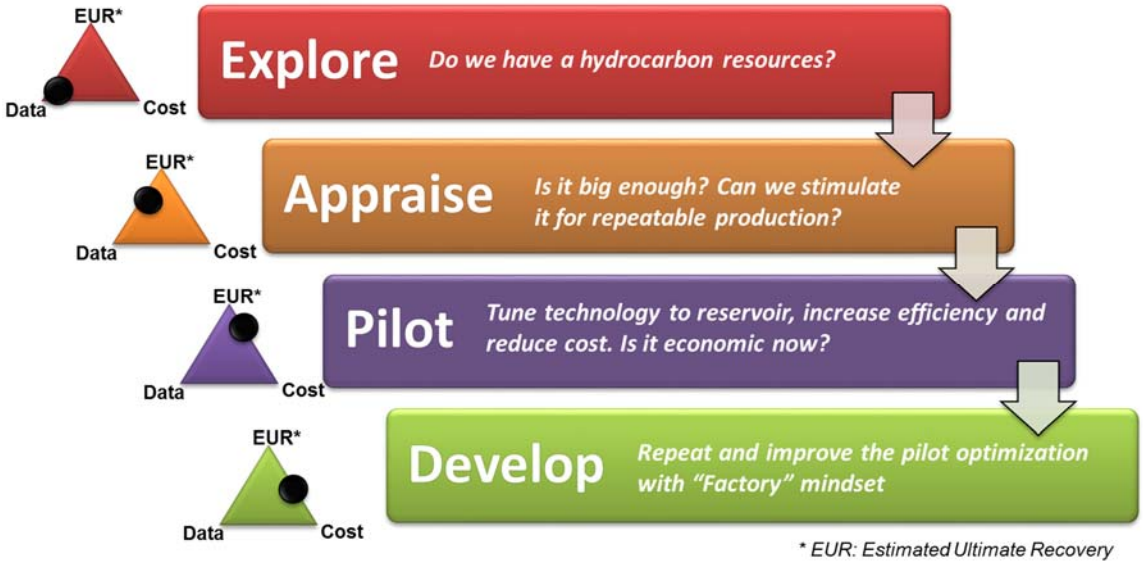

Figure 5-2 Saudi Aramco's de-risking strategy for unconventional gas development. The strategy is divided into four phases where certain expectations are targeted for each phase. The black dot in the colored triangles shows the focus for each phase between reservoir data collection, increasing EUR and cost reduction

5.3 Data and Methods

A comprehensive formation evaluation and data acquisition program was implemented to acquire a wealth of core and well-log data from the three wells used in the study. The coring program was designed to collect enough core samples across the Tuwaiq Mountain Formation in the study area to allow for detailed petrophysical and geochemical analyses. The wireline logging program was designed to collect complete log datasets to assist in petrophysical modeling.

5.3.1 Coring and Analysis

The exact cored intervals were determined through correlation with historical conventional offset wells. While drilling, coring points were picked by utilizing near-bit measuring-while-drilling gamma ray (MWD GR) to minimize depth errors. The coring process ensured that the entire Tuwaiq Mountain section and some portions of overlying and underlying formations were covered. This coring technique allowed the capture of transitions across formations and eliminated the risk of missing the zone of interest. In addition, these short cored intervals in the overlying and underlying formations provided valuable sedimentological insight to the depositional history and information critical for fracture growth behavior. Part of the cores were preserved and sent to laboratories for detailed petrophysical analyses (Figure 5-3); the core measurements include porosity, permeability, density and fluid saturation using the Gas Research Institute (GRI) methodology (Luffel et al., 1996). RockEval pyrolysis, LECO® and Petrography were utilized to identify source rock intervals, assess their quality (generative potential), and

their thermal maturity. X-ray diffraction (XRD) and scanning electron microscopy (SEM) were also utilized to identify rock composition and morphology.

Figure 5-3 A schematic illustrating the technique in which the core from the study wells have been divided. The top 2 feet of core are conventionally processed using basic analysis. Whereas the bottom 1 foot of core is preserved and sent for advanced analyses

5.3.2 Wireline Logging

The wireline logging program for each well includes calipers, spectral gamma ray, sonic, resistivity, resistivity image, density, photoelectric logs, neutron porosity and vertical seismic profile (VSP). A magnetic resonance imaging (MRI) measurement was also acquired to estimate total and effective porosities, and bound fluid volumes. As magnetic resonance is less sensitive to kerogen volume, combining bulk density and elemental spectroscopy data provides accurate kerogen volume estimation (Hook et al., 2011). The elemental spectroscopy tool was also deployed to refine mineral fractions and to measure the total organic content (TOC) associated with Tuwaiq Mountain. Resistivity and acoustic image logs were run across the target section for wellbore stability, stress orientation and natural fractures analysis.

5.3.3 Enabling Applications and Software

Modeling and data integration (e.g. *Petrel*®)

Log processing and petrophysical analysis (e.g. *TechLog*®)

Operational geology and geosteering (e.g. *OpenWorks* ®)

The software packages of choice were selected for their efficiency and data transfer compatibility. (Figure 5-4) summarizes the workflow that was followed for the Tuwaiq Mountain Formation play evaluation.

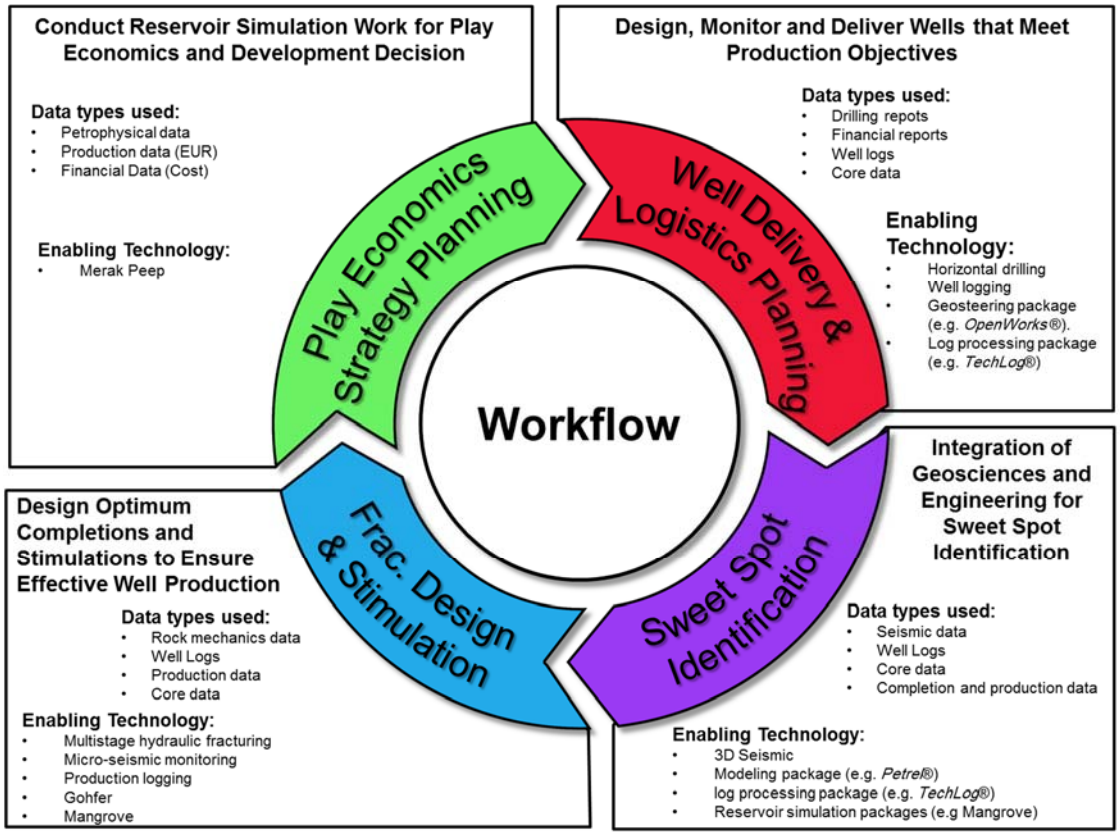

Figure 5-4 A Workflow for unconventional play evaluation.

5.4 Tuwaiq Mountain Prospectivity, Results and Discussion

5.4.1 Source Rock Richness and Maturation

Total organic carbon across the Tuwaiq Mountain Formation tends to be cyclical, probably due to fluctuations in relative sea level (Carrigan et. al., 1995). This cyclicity can be easily recognized from well logs such as the density (Figure 5-5). Therefore, the Tuwaiq Mountain Formation is subdivided into three tiers. Tier 1, at the base, represents the most organic-rich interval. Tier 2 represents the intermediate source rock quality, while Tier 3 represents the lean source rock sitting right below the Hanifa Formation. *RockEval* pyrolysis analysis was performed on approximately 200 core samples collected from three wells (Well A, Well B and Well C). Organically enriched (TOC > 1%) intervals occur throughout the Tuwaiq Mountain Formation source rock intervals as shown in (Figure 5-6) which shows the distribution of TOC by Tier. Tier 1 source rock facies have an average TOC of 7.4% and maximum values as high as 13.2%, which together represent excellent source rock potential. Tier 2 source rock facies show an average TOC of 5.9% and maximum values as high as 14.3%. Tier 3 source rock facies show lean source rock facies with an average TOC of 3.2% and maximum of 8.9% (Table 5-1). In the stratigraphic cross section in Fig. 8, the thickness of these source rock facies is relatively constant between the three wells used in the study. Though the identified Tiers show varying reservoir quality, collectively, they provide a good mass of hydrocarbon resources.

Thermal maturity is one of the most important parameters used in the evaluation of source rock generative potential. Several methods exist that may estimate the maturity level of a source rock (Jarvie et al., 2001). Vitrinite reflectance (%Ro) optical method (Tissot and

Welte, 1984) is one of the most accepted and accurate method for determining organic maturity. Vitrinite is a type of maceral that originates from the woody tissue of higher plants. In cases where no vitrinite is available, or rare, as in the case in carbonate depositional environments, reflectance of solid bitumen or other vitrinite-like macerals is used, with resulting measurements converted to a normalized 'equivalent' reflectance value (VRo- eq). Solid bitumen reflectance has been used successfully in Lower Paleozoic rock and in younger rocks with no or scarce vitrinite (Jacob, 1989; Schoenherr et al., 2007; Petersen et al., 2013). Alternatively, organic matter type and maturity may also be assessed using Rock Eval or other pyrolysis techniques. In this paper, present day thermal maturity was measured and calculated for all samples using both Rock Eval and solid bitumen optical reflectance techniques.

The average Tmax value for Tier 1, Tier 2 and Tier 3 is 475 °C correspond to the maturity window of late wet gas window (Figure 5-7). This suggest that all tiers exhibit similar hydrocarbon maturity window. Jarvie's conversion formula (Equation 1) was used to calculate VRo - eq from Tmax data (Jarvie et al., 2001). This formula was developed based on Ro and Tmax data correlation from Barnett shale, and has been used extensively in basins worldwide. VRo-eq was calculated to be 1.39% using Jarvie's conversion formula.

$$VRo - eq\ (\%) = 0.018\ X\ Tmax(°C) - 7.16 \quad \text{.....Equation 1}$$

Maturity was also validated by vitrinite equivalent (VRo-eq), estimated from reliable bitumen reflectance (BitRo) using Jacob's conversion formula (Equation 2), Jacob, 1989.

$$VRo - eq\ (\%) = 0.618\ X\ BitRo(\%) + 0.4 \quad \text{..... Equation 2}$$

(Figure 5-8) shows the bitumen reflectance measurements histogram and images of a representative Tuwaiq Mountain polished section of a core sample. In general, measured samples are rich in organic content and consist of solid bitumen having various forms, co-deposition with carbonate grains, and in association with framboidal pyrite in some cases. A network of amorphous bituminite and traces of inertnite were also observed in the matrix. No primary vitrinite was found in the tested samples. The mean BitRo of the bitumen reflectance for sample 09 is 1.62%, based on 22 readings, and the VRo-eq was calculated to be 1.4% using the Jacob's conversion formula. This value is very comparable with VRo-eq calculated from Tmax (1.39%) using Jarvie's conversion formula. Both maturity calculation methods indicate that the Tuwaiq Mountain organic matter is mature and in the late wet gas window of hydrocarbon generation.

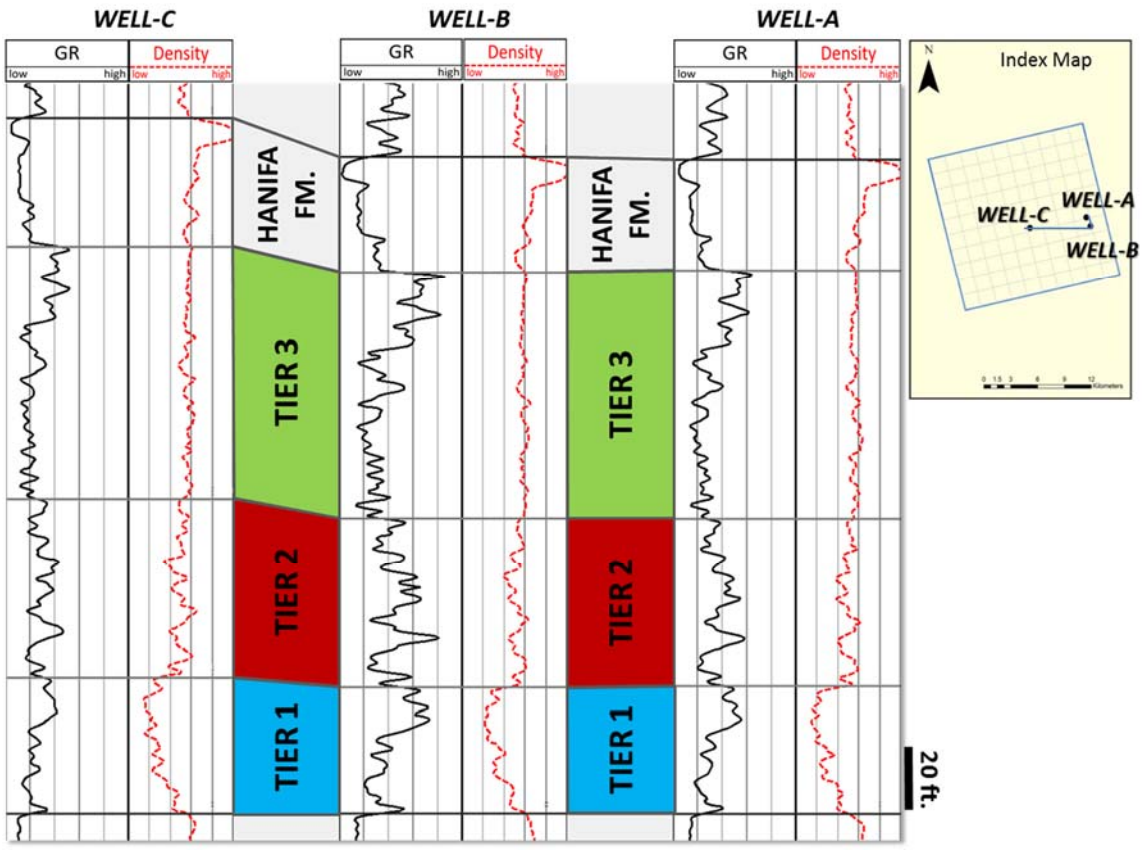

Figure 5-5 Stratigraphic cross section between the three wells used in the study. The cyclicity within Tuwaiq Mountain Formation can be easily recognized from well logs, such as for density, and so the Tuwaiq Mountain Formation is subdivided into three Tiers (Tier 1, Tier 2 and Tier 3).

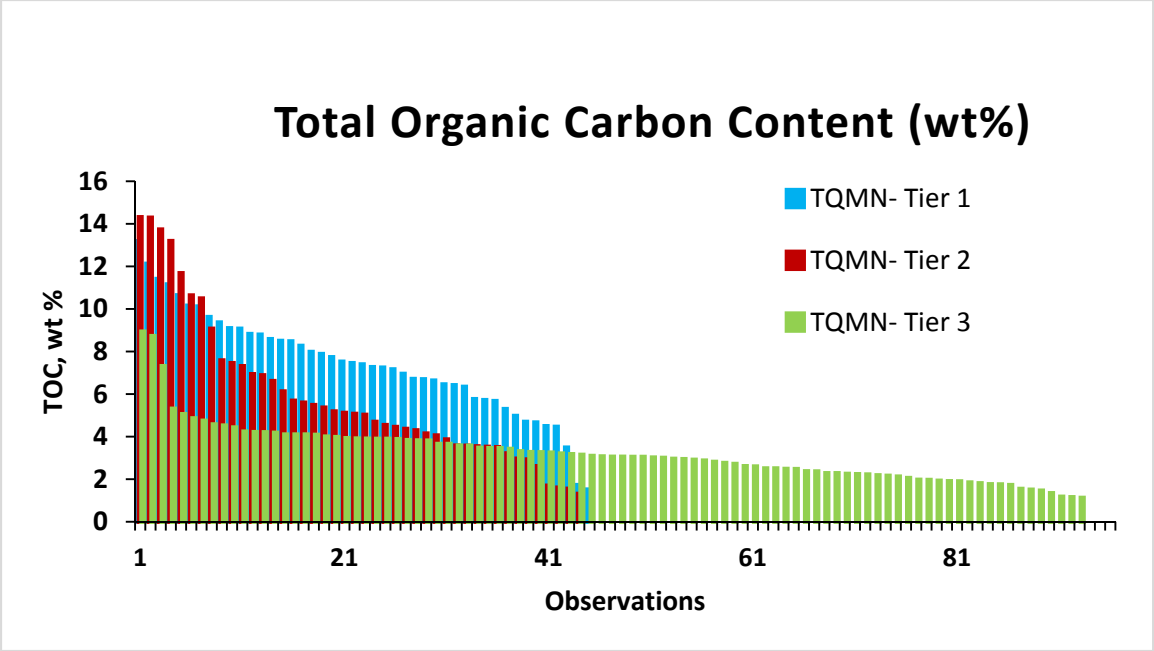

Figure 5-6 Distribution of the TOC content of the Tuwaiq Mountain Formation by tiers.

Table 5-1 Average geochemical properties for the Tuwaiq Mountain Formations Tier 1, Tier 2 and Tier 3 are based on the three wells used in the study.

Geochemical Attributes		Tuwaiq Mountain Formation		
		Tier 1 (45 Samples)	Tier 2 (44 Samples)	Tier 3 (93 Samples)
Total Organic Carbon Content (Wt. %)	maximum	13.2	14.3	8.9
	minimum	1.5	1.3	1.1
	average	7.4	5.9	3.2
S1 Pyrolysis Yield (Free Hydrocarbon) (mg HC / g rock)	maximum	12.0	8.4	4.3
	minimum	0.8	0.7	0.1
	average	5.7	4.1	2.2
S2 Pyrolysis Yield (Remained Potential) (mg HC / g rock)	maximum	14.4	14.4	8.7
	minimum	0.6	0.6	0.8
	average	7.4	5.2	2.7
Hydrogen Index (S2*100/TOC)	maximum	130.8	117.3	111.1
	minimum	56.5	52.1	45.1
	average	100.2	86.4	82.4
T_{max} (ºC)	maximum	481.2	479.7	480.6
	minimum	471.0	461.1	463.0
	average	476.3	474.4	474.3

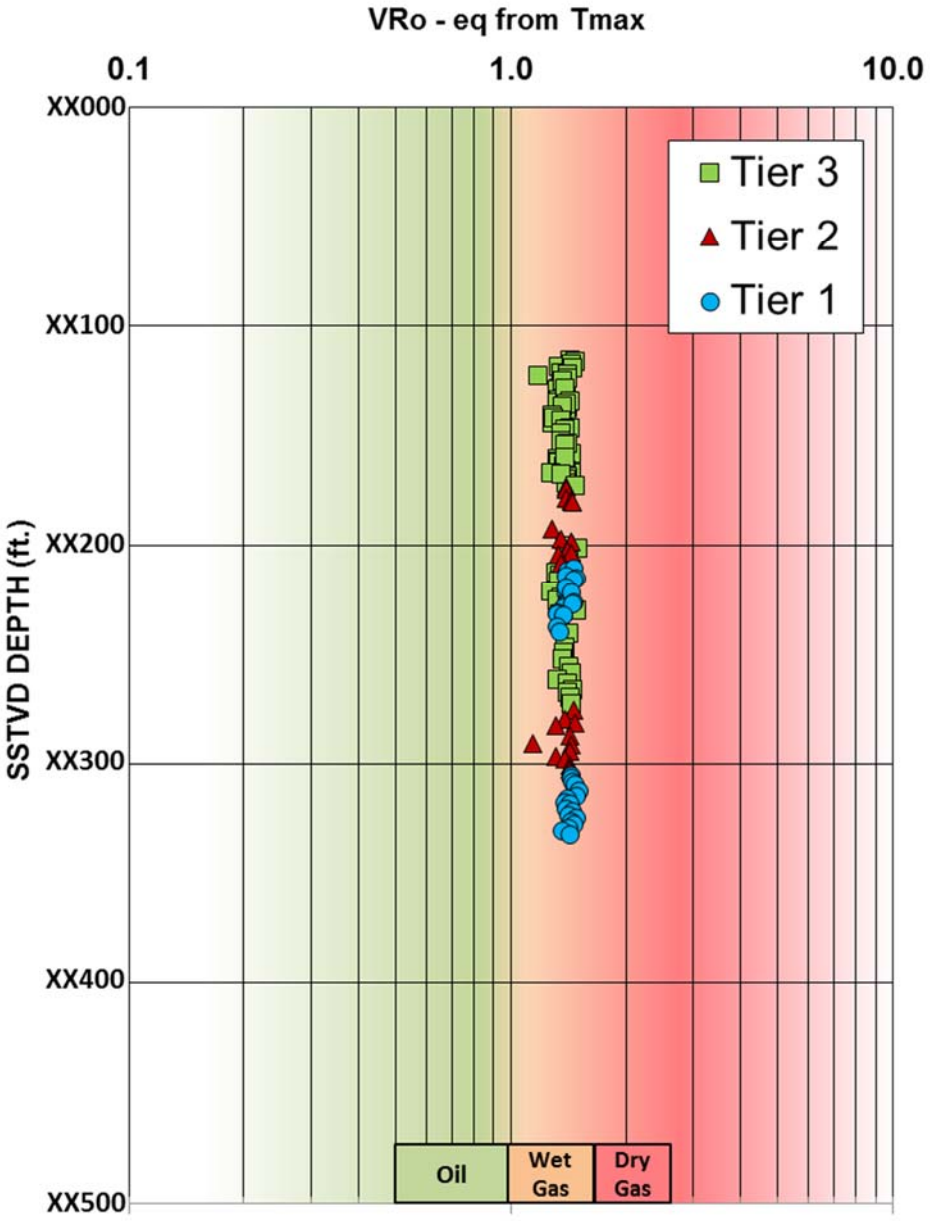

Figure 5-7 Vitrinite reflectance equivalent calculated from Tmax using Jarvie's conversion formula. The profile indicates a late wet gas maturity window for Tier 1, Tier 2 and Tier 3

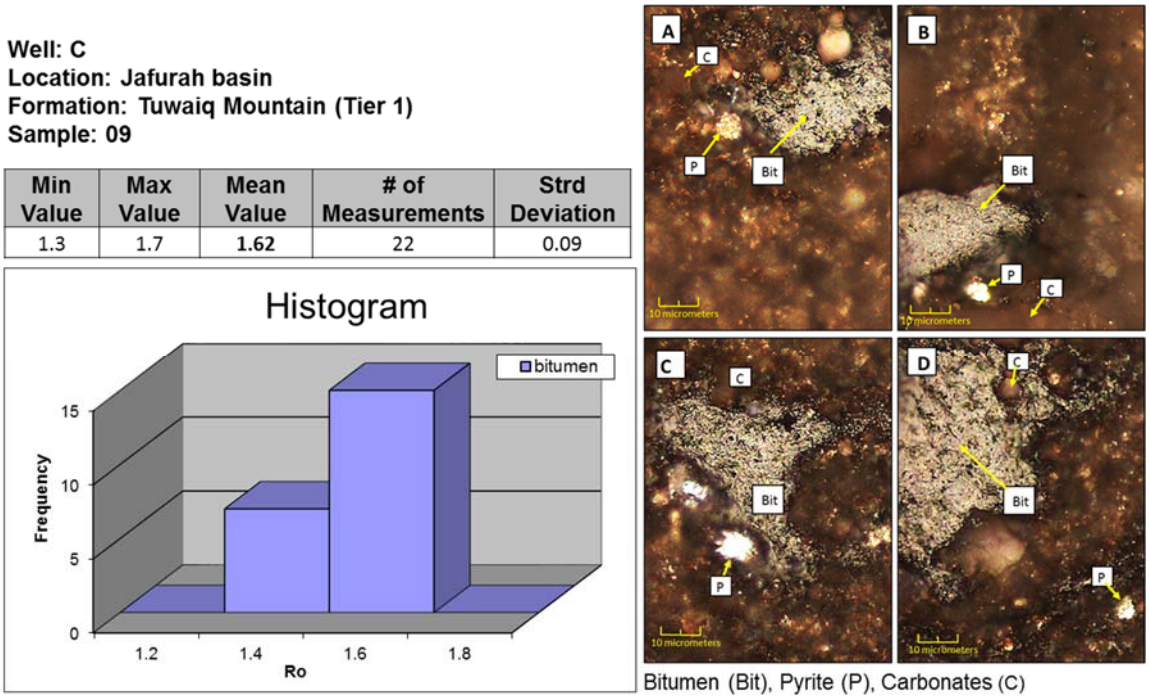

Figure 5-8 Bitumen reflectance measurements (histogram and images) of a representative Tuwaiq Mountain core sample. VRo-eq was calculated to be 1.4% using Jacob's conversion formula.

5.4.2 Mineralogical Composition

The Tuwaiq Mountain Formation is composed of thinly laminated wackestone and peloidal dark packstone. Based on XRD measurements from cores, calcite is the dominant component (Table 5-2). The calcite distribution ranges from 59% to 89% by volume and averages 74%. Dolomite occurs in low amounts and ranges from 1% to 30% with average of 11%. The quartz content is relatively low, ranging from 1.7% to 5% with a 3% average. The total clay content is extremely low, ranging from 2.8 to 7.6% with averages of 5% with illite and Kaolinite predominant. The low volume of clays was also supported by the low water saturation in the matrix of the rock measured in the laboratory. The high brittle calcite content along with the low ductile clay content makes Tuwaiq Mountain Formation the

ideal lithology for hydraulic fracturing stimulation. (Figure 5-9 shows illustrations of Tuwaiq Mountain Formation whole rock and clay mineralogy. The rock classification for the ternary plot is based on Helena et al., (2012) classification for organic mudstones based on bulk mineralogy.

Table 5-2 XRD summary data of bulk and clay mineralogy of the Tuwaiq Mountain Formation Tier 1, Tier 2 and Tier 3.

				Whole Rock XRD																Clay Mineral XRD					
Well	Sample Type	Sample No	Formation/Member	illite_mica	illite-smectite	kaolinite	chlorite	quartz	alkali_feldspar	plagioclase	calcite	dolomite	siderite	pyrite	anhydrite	baryte	gypsum	Halite	Total	illite	illite-smectite	smectite	kaolinite	chlorite	Total
Well-A	Plug Trim	1	Tier 3	2.0	1.6	1.6	1.1	2.6	0.6	1.6	80.7	2.6	0.7	0.9	2.6	0.3	0.5	0.7	100	36.81	32.40	-	29.70	1.09	100
Well-A	Plug Trim	2		1.8	1.8	2.1	1.4	1.8	0.9	1.5	74.4	10.3	0.8	0.7	0.7	0.3	0.7	0.7	100	36.97	30.25	-	31.36	1.42	100
Well-A	Plug Trim	3		1.0	1.1	1.0	0.6	2.2	0.5	1.0	75.3	12.0	0.6	0.4	3.2	0.3	0.2	0.5	100	33.46	30.89	-	35.05	0.60	100
Well-A	Plug Trim	4		1.3	1.2	0.9	0.5	2.1	0.4	0.9	64.9	22.4	0.6	0.7	2.8	0.3	0.3	0.8	100	33.57	36.93	-	28.99	0.51	100
Well-B	Plug Trim	1		1.6	1.6	1.4	0.8	2.3	0.8	1.2	86.8	1.0	0.6	0.5	0.3	0.2	0.3	0.7	100	33.93	27.65	-	37.65	0.77	100
Well-B	Plug Trim	2		1.6	1.4	1.2	0.8	4.6	0.8	1.2	68.7	15.6	0.7	1.3	0.6	0.3	0.4	0.8	100	34.88	29.89	-	34.41	0.82	100
Well-B	Plug Trim	3		1.6	1.4	1.2	0.7	3.6	0.7	1.0	65.8	20.1	0.7	0.7	1.3	0.3	0.4	0.8	100	41.84	33.47	-	24.00	0.70	100
Well-B	Plug Trim	4		1.8	1.6	1.4	0.8	3.1	0.7	1.6	81.9	3.9	0.7	0.8	0.3	0.3	0.4	0.9	100	35.07	29.08	-	35.04	0.81	100
Well-C	Plug Trim	1		1.8	1.4	1.4	0.8	3.0	0.7	1.3	84.6	2.3	0.6	0.7	0.3	0.2	0.4	0.7	100	33.69	27.51	-	38.02	0.78	100
Well-C	Plug Trim	2		1.8	1.4	1.4	0.8	3.0	0.7	1.3	84.6	2.3	0.6	0.7	0.3	0.2	0.4	0.7	100	36.94	30.78	-	31.49	0.78	100
Well-C	Plug Trim	3		1.9	1.3	1.6	1.0	2.3	0.8	1.0	78.3	5.9	0.7	0.9	2.6	0.4	0.6	0.9	100	34.06	29.81	-	35.15	0.98	100
Well-C	Plug Trim	4		1.4	1.4	1.5	0.9	1.9	0.6	1.2	85.8	2.1	0.7	0.4	0.6	0.3	0.3	0.8	100	35.13	29.58	-	34.39	0.91	100
Well-A	Plug Trim	5	Tier 2	1.8	1.6	1.4	0.9	2.2	0.7	1.2	83.1	3.2	0.7	0.6	1.2	0.3	0.4	0.8	100	36.07	27.49	-	35.59	0.85	100
Well-A	Plug Trim	6		1.5	1.4	1.2	0.7	2.3	0.5	1.4	82.7	4.3	0.6	0.6	1.6	0.2	0.4	0.8	100	35.03	24.37	-	39.92	0.68	100
Well-A	Plug Trim	7		2.3	1.7	2.3	1.3	4.4	1.0	1.6	74.1	4.8	0.7	1.6	2.4	0.5	0.5	0.8	100	32.87	28.58	-	37.27	1.27	100
Well-A	Plug Trim	8		2.1	1.9	1.6	0.9	3.3	0.9	2.0	75.7	6.2	0.7	1.5	1.3	0.4	0.5	0.9	100	32.59	32.59	-	33.88	0.95	100
Well-B	Plug Trim	5		1.8	1.6	1.5	0.9	2.1	0.6	1.1	68.9	16.2	0.6	1.2	1.9	0.4	0.4	0.8	100	64.58	16.14	-	18.42	0.86	100
Well-B	Plug Trim	6		1.2	1.1	0.7	0.6	2.2	0.5	0.9	72.7	10.4	0.6	0.5	7.5	0.3	0.2	0.7	100	37.01	28.47	-	33.94	0.58	100
Well-B	Plug Trim	7		1.4	1.1	1.8	0.0	3.1	0.6	0.8	85.1	2.3	0.6	0.7	1.1	0.3	0.2	0.8	100	33.47	26.77	-	39.76	-	100
Well-B	Plug Trim	8		2.1	1.5	2.4	0.0	4.8	0.9	1.5	61.8	19.3	0.8	2.4	0.5	0.4	0.6	0.9	100	29.62	27.55	-	42.83	-	100
Well-C	Plug Trim	5		1.7	1.2	1.8	0.0	2.0	0.7	1.2	71.9	15.1	0.8	1.1	0.9	0.4	0.3	0.9	100	33.79	28.16	-	38.05	-	100
Well-C	Plug Trim	6		1.8	1.3	3.2	0.0	3.6	0.7	1.1	59.1	23.6	0.7	1.0	2.5	0.3	0.4	0.8	100	33.11	29.43	-	37.46	-	100
Well-C	Plug Trim	7		1.1	1.1	1.3	0.0	2.6	0.5	1.1	65.7	22.9	0.8	1.0	0.6	0.6	0.2	0.7	100	32.38	35.98	-	31.64	-	100
Well-C	Plug Trim	8		1.3	1.0	1.0	0.0	1.7	0.7	1.0	76.9	12.9	0.7	0.8	0.7	0.4	0.2	0.8	100	33.03	29.04	-	37.93	-	100
Well-A	Plug Trim	9	Tier 1	2.0	1.5	1.1	0.0	3.1	0.8	1.3	71.9	13.9	0.8	1.0	1.1	0.5	0.3	0.8	100	35.57	31.27	-	33.16	-	100
Well-A	Plug Trim	10		2.0	1.3	1.5	0.0	3.6	0.8	1.4	71.2	14.6	0.6	1.1	0.4	0.4	0.3	0.8	100	43.04	26.90	-	30.06	-	100
Well-A	Plug Trim	11		0.9	0.6	1.3	0.0	3.3	0.4	0.8	88.9	2.2	0.4	0.4	0.1	0.1	0.2	0.4	100	36.52	29.22	-	34.26	-	100
Well-B	Plug Trim	9		1.5	0.9	1.3	0.0	2.9	0.7	1.6	80.2	7.8	0.6	0.9	0.4	0.3	0.2	0.7	100	36.32	25.94	-	37.74	-	100
Well-B	Plug Trim	10		1.3	1.0	1.1	0.0	3.5	0.7	1.3	76.2	11.9	0.6	0.9	0.3	0.3	0.2	0.9	100	36.53	32.14	-	31.33	-	100
Well-B	Plug Trim	11		1.3	1.6	1.8	0.0	3.8	0.9	1.5	66.5	16.2	0.8	1.0	3.2	0.4	0.4	0.7	100	35.37	25.26	-	39.37	-	100
Well-C	Plug Trim	9		1.0	0.8	1.5	0.0	3.0	0.6	0.9	59.0	30.1	0.5	0.7	0.8	0.3	0.2	0.7	100	31.23	27.82	-	40.95	-	100
Well-C	Plug Trim	10		1.3	0.9	2.5	0.0	3.1	0.5	0.9	66.3	5.1	0.7	1.4	15.9	0.4	0.5	0.5	100	79.14	7.91	-	12.95	-	100
Well-C	Plug Trim	11		1.9	1.5	2.6	0.0	4.6	1.0	1.4	61.6	17.9	0.8	2.1	2.5	0.8	0.4	0.8	100	35.32	37.25	-	27.43	-	100
			Max	2.3	1.9	3.2	1.4	4.8	1.0	2.0	88.9	30.1	0.8	2.4	15.9	0.8	0.7	0.9		79.1	37.3		42.8	1.4	
			Min	0.9	0.6	0.7	0.0	1.7	0.4	0.8	59.0	1.0	0.4	0.4	0.1	0.1	0.2	0.4		29.6	7.9		12.9	0.5	
			Average	1.6	1.3	1.6	0.5	3.0	0.7	1.2	74.3	11.0	0.7	0.9	1.9	0.3	0.3	0.8		37.2	28.7		33.6	0.9	

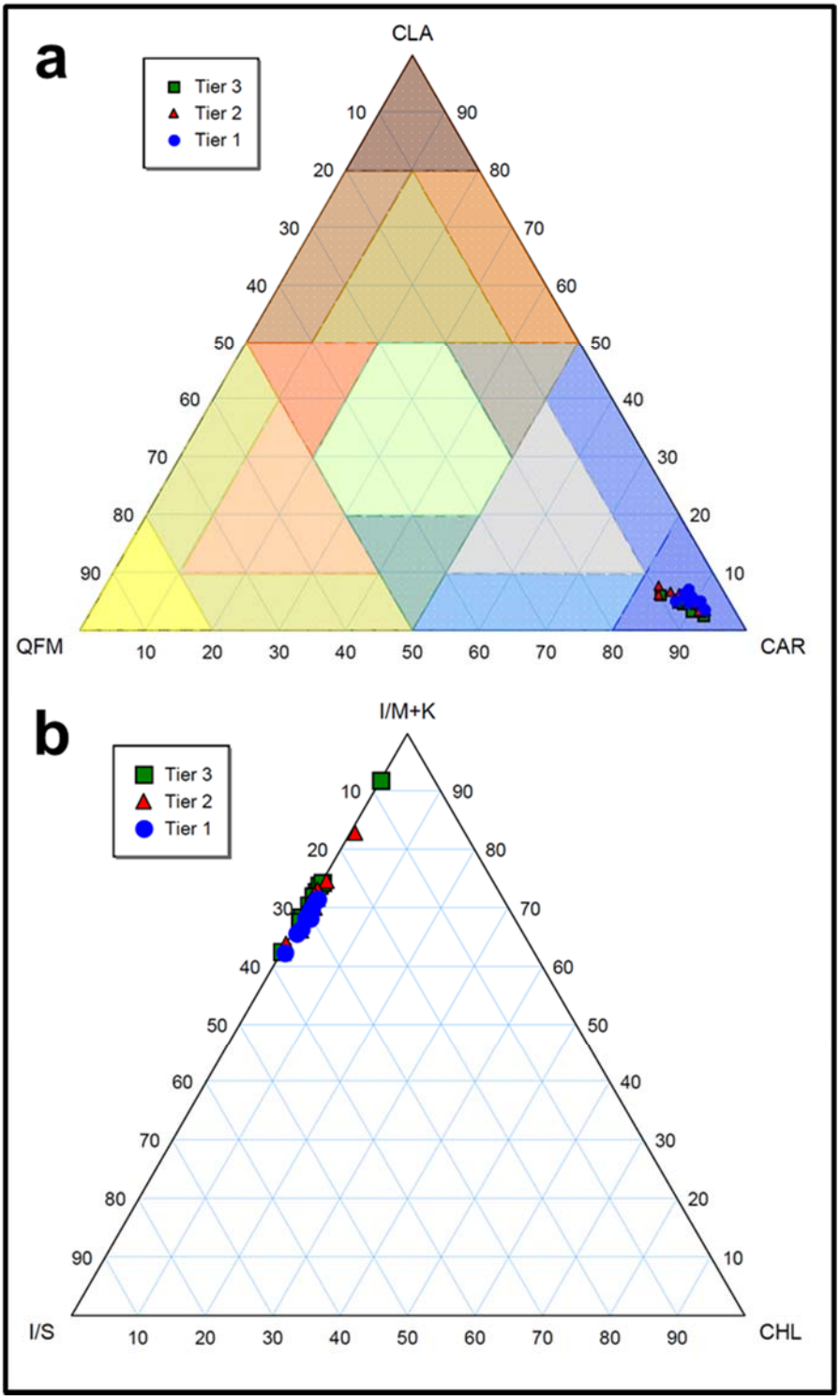

Figure 5-9 Ternary plots of Tuwaiq Mountain Formation Tier 1, Tier 2 and Tier 3 whole rock (a) and clay mineralogy (b) XRD data. The rock classification for the bulk mineralogy is based on Helena et al., (2012) classifications for organic mudstones.

5.4.3 Petrophysical Properties

All wireline logs acquired from the vertical wells have been calibrated using core data from the same wells. Applying these calibrations is necessary to validate the quality of the log data, as well as providing proper constraints for geo-cellular modeling and sweet spot identification. Figure 5-10 illustrates a representative and well calibrated petrophysical model for Tuwaiq Mountain Formation at Well C. Figure 5-11 shows multi-well histograms of some reservoir properties (e.g., TOC, SW, K and Porosity).

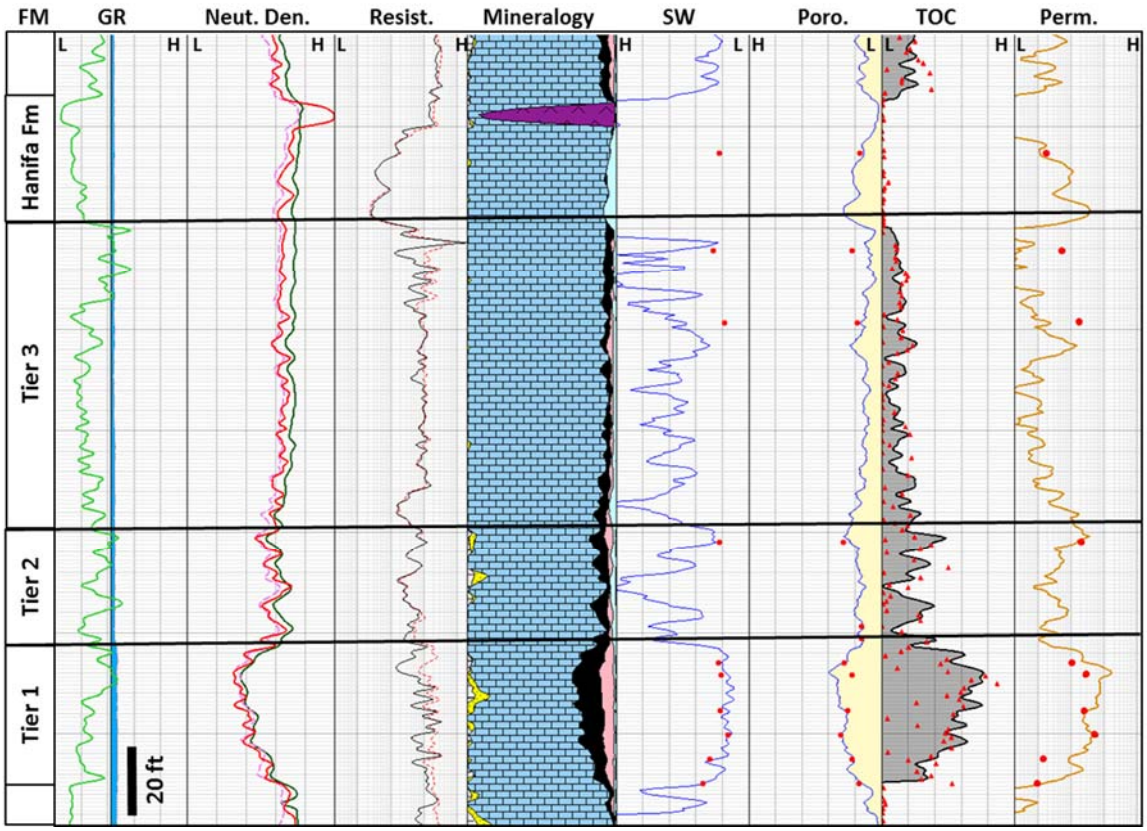

Figure 5-10 Tuwaiq Mountain Formation petrophysical model (Well C). Red dots are the core calibration points.

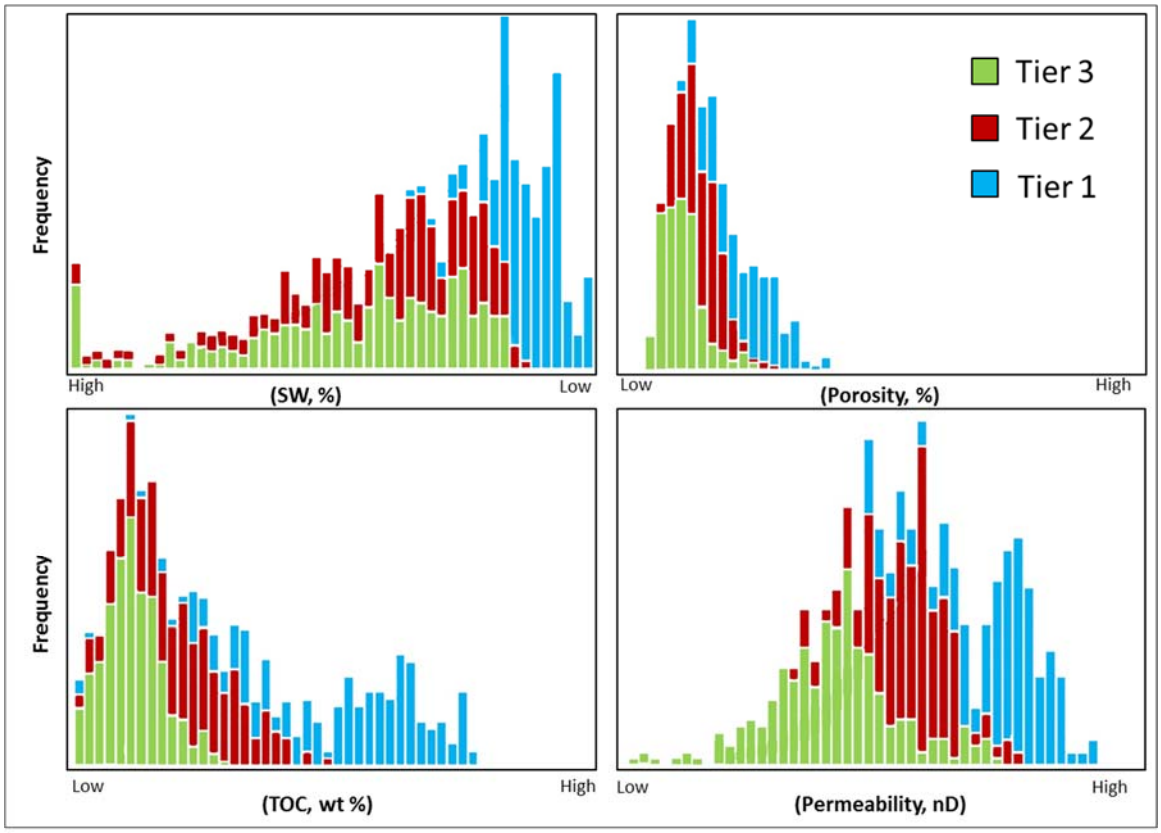

Figure 5-11 Multiwell histograms of TOC, water saturation (SW), matrix permeability (k) and porosity for Tuwaiq Mountain Formation Tier 1, Tier 2 and Tier 3.

The acquired nuclear magnetic resonance (NMR) data is of critical importance since other porosity logs (density, neutron and sonic) are heavily affected by the combined effect of kerogen and fluids; NMR data provide a robust estimation of porosity. The estimation of formation water saturation is very challenging. Available equations were built and calibrated for conventional reservoirs and there are no appropriate equations for unconventional resource rocks. The water saturation equation parameters a, m and n (Archie, 1952) are unknown; and the formation water salinity, as it is not necessarily similar to regional conventional aquifers in the area. Water saturation from GRI lab data has been used to establish a model for saturation, and at the same time to calibrate the

formation water saturation obtained based on resistivity logs. GRI data results from reference wells show a very good trend relating absolute permeability to total porosity (Figure 5-12). It is worth mentioning here that the GRI permeability measurement uses crushed samples of the core. The permeability values from this technique can be affected by the grain size and test conditions, which eventually could provide higher permeability estimates. As in other plays, additional methods such as pulse decay are predicting lower than what was initially determined using GRI technique. With that being said, we are considering in the near future analyzing selected samples for permeability measurement using pulse decay for comparison. It is worth mentioning also that we do not see any indication that permeability measurement whether high or low would have any effect on other results (e.g., TOC, SW, and Porosity). These attributes were derived independently from permeability values. For example, the water saturation was derived based on resistivity logs and matched with GRI saturation. TOC was estimated based on modified Schmoker equation using bulk density from log. This was also validated by TOC data obtained from core analyses. The porosity was extracted from NMR and other porosity logs, and then was calibrated with core porosity. Deriving permeability from well logs was done in a number of steps. First, a porosity–GRI permeability relationship based on core data (Figure 5-12) was derived resulting in permeability equation 3. Using the earlier calibration between core and log porosity, the determined equation was used to calculate permeability from porosity logs in wells with no core data.

$$K\,(mD) = 10^{-7} \times Porosity\,(\%)^{\,3.6622} \quad \text{..... Equation 3}$$

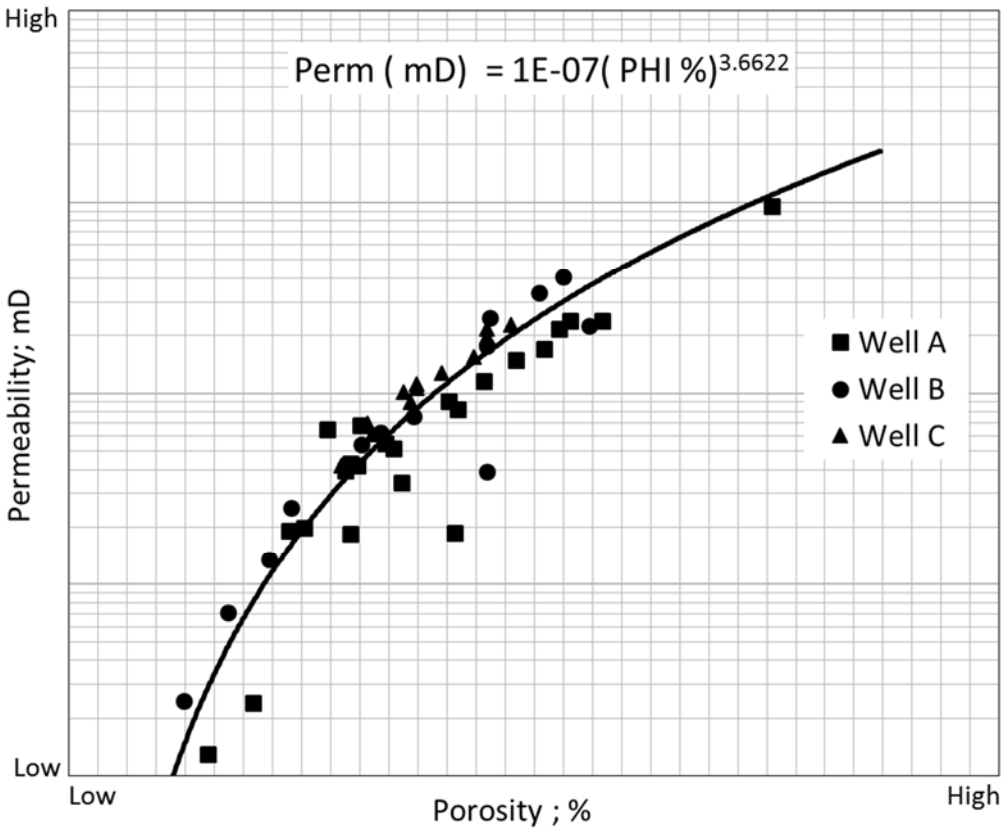

Figure 5-12 Tuwaiq Mountain Formation porosity and permeability relationship based on core data.

As illustrated by the petrophysical model in (Figure 5-10 and Figure 5-11), Tier 1 was found to be the optimum target for the lateral well placement. This is due to its high TOC, high maturity, low clay content, low water saturation, high porosity and high gas saturation. Subsequently, all three wells were sidetracked to drill 5,000 ft horizontal laterals into Tier 1 for multistage hydraulic fracture stimulation to evaluate the reservoir's maximum potential.

Scanning electron microscopy was used to characterize the pore types of the Tuwaiq Mountain Formation. As illustrated in (Figure 5-13), nanopores are common in the internal texture of the organic matter. This type of porosity has been well described by Pommer

and Milliken (2015) and it is the dominant pore type in shale gas plays like the Eagle Ford. SEM images reveal a moderately to well-connected organic pore system in the matrix of the Tuwaiq Mountain Formation. The shapes of the pores are mostly irregular polygonal to spherical with predominant pore sizes less than 1µm (84% distribution) and the remaining fraction has micro pores greater than 1 µm. As a result, the pore network in the Tuwaiq Mountain play will be controlled by the abundance, distribution, and the thermal maturation levels of the organic matter. It is noted that the pores show no evidence of compaction, and it is reasonable to conclude that the dominate calcite framework is very strong in not permitting organic matter or pore compaction.

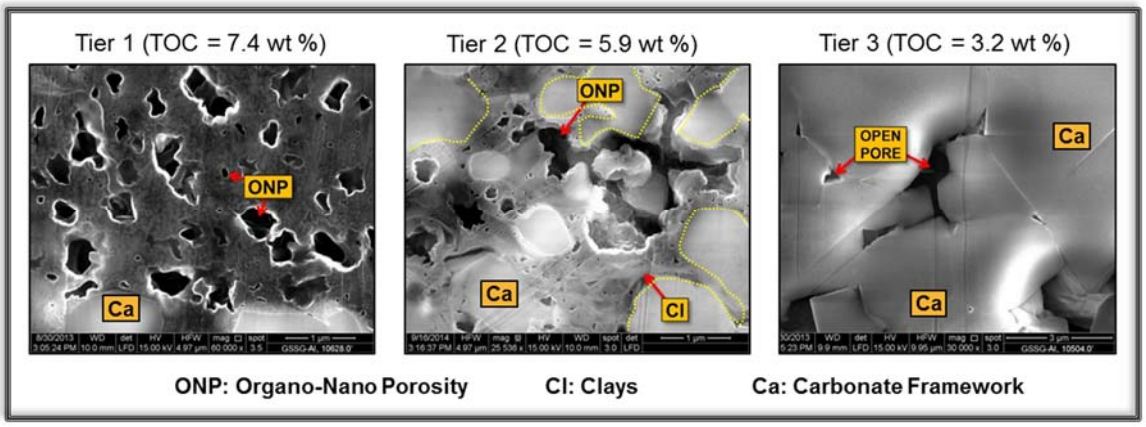

Figure 5-13 SEM images illustrating the distribution of the organo-porosity, with Tier 1 showing the highest organic porosity occurrence.

5.4.4 Total Organic Carbon (TOC) Content Estimation

As described in section 6.2, Mineralogical Composition, the Tuwaiq Mountain Formation is predominantly composed of carbonate with low percentages of detrital material (clay and silica) in addition to organic matter. An accurate estimate of the TOC represents an important factor in the process of formation evaluation. TOC is usually measured in the

laboratory from vertical/sidewall cores and cuttings using *open-system pyrolysis and/or LECO® instruments*. There are different methods that have been used to estimate TOC (e.g., TOC calculation from logs).

5.4.1.1 TOC Estimation from Well Logs

In this study, a modified Schmoker equation (Schmoker et al., 1983) was proven to provide the best estimation of TOC from logs. Equation 4 uses bulk density from logs in g/cm^3, and provides a calculated TOC value reported in wt%. This method was also validated when compared with TOC measured from core plugs. The relationship between calculated and measured TOC is very close (Figure 5-14) with an average correlation coefficient of 0.85. In addition, an elemental spectroscopy log was acquired in all three wells to characterize the mineralogy of Tuwaiq Mountain source rock and to enhance the accuracy of petrophysical results. This tool also captures the amount of total carbon in the formation and so the amount of TOC present in the formation can be derived

$$TOC\ (\%) = \frac{154.497}{\rho_b\ (\frac{g}{cm3})} - 57.261 \quad \text{..... Equation 4}$$

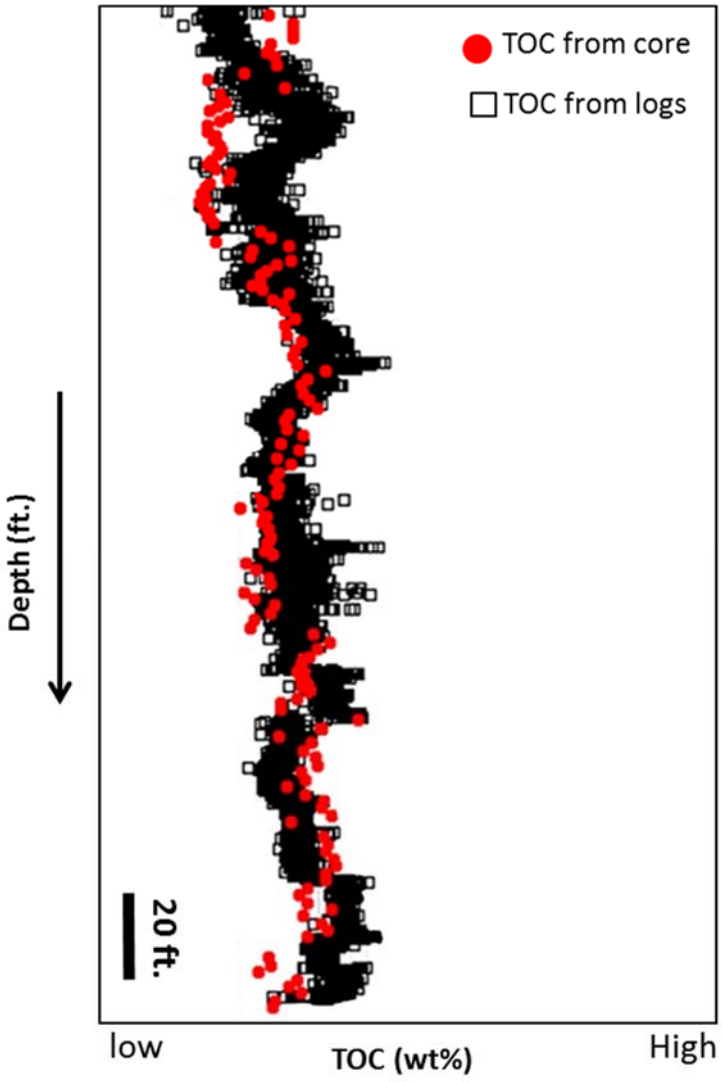

Figure 5-14 TOC calibration plot.

5.5 Reservoir Quality Lateral Continuity Prediction

To advance any unconventional resource play towards the pilot and development phases, a robust understanding of the geology and reservoir quality must be established. Since the Tuwaiq Mountain Formation is extensive and exhibits a high degree of reservoir heterogeneity both vertically and laterally, a reservoir quality prediction model was created to address this challenge, and aid in understanding the lateral continuity of specific reservoir parameters for initial acreage grading, well stacking and optimum well placement.

5.5.1 TOC Quality Prediction from Seismic

Seismic data were used to check for the lateral continuity of the target horizon. Prestack 3D seismic data was evaluated and conditioned to improve the amplitude variation with offset (AVO) response. AVO simultaneous prestack inverted volumes such as acoustic impedance (AI), shear impedance (SI), and density volumes were generated. A good correlation between high TOC and low acoustic impedance from seismic was observed at the well scale (Figure 5-15). This relationship was extrapolated to existing 3D seismic data to generate seismic inverted TOC map for TOC prediction. A blind test was conducted to validate the level of accuracy of TOC prediction from seismic. The results were very encouraging which increase the confidence in the model. For example, well C was positioned based on low acoustic impedance data, which suggests that the Tuwaiq Mountain Formation Tier 1 at this location would exhibit about 8 wt % TOC (Figure 5-16). This was then validated by TOC measurement obtained from core samples retrieved from well C. The Rock-Eval data suggests an average of 8.5% TOC for Tier 1 at well C;

showing strong correlation between both maps (Figure 5-16). Additional appraisal wells are being drilled to calibrate the seismically derived TOC for lateral reservoir continuity. This seismic attribute product is being used to help with well placement and acreage grading.

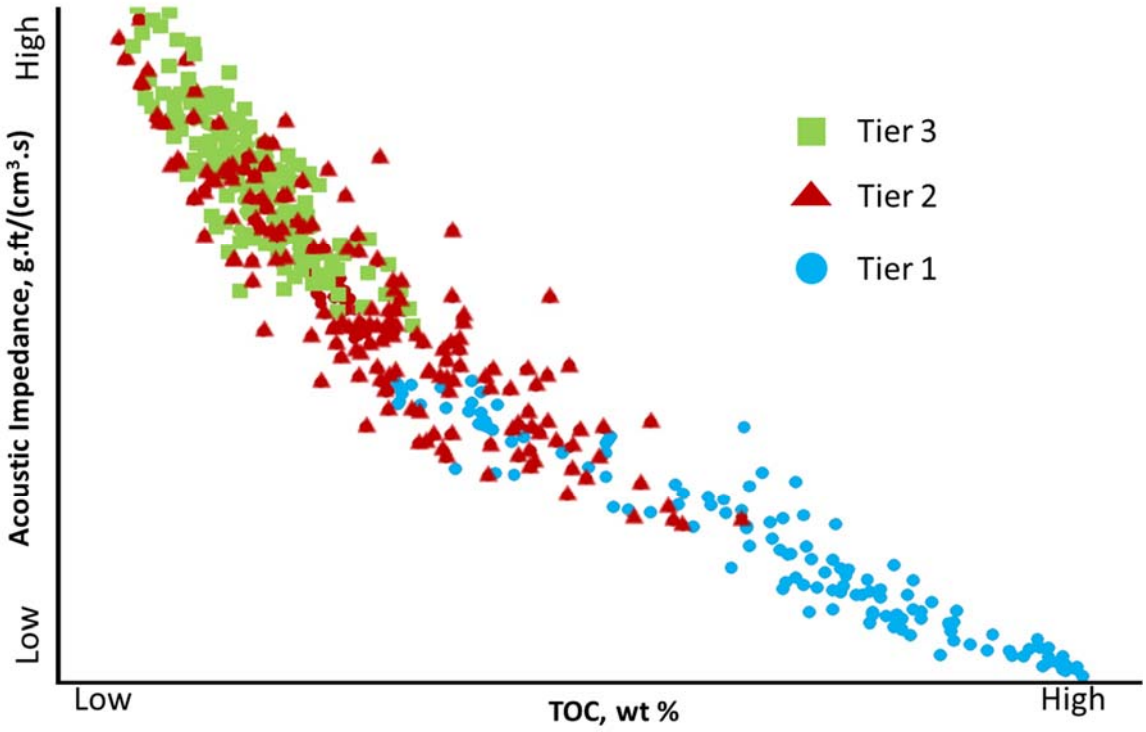

Figure 5-15 Cross plot showing close relationship between acoustic impedance and measured TOC. Low AI correlates to higher TOC values

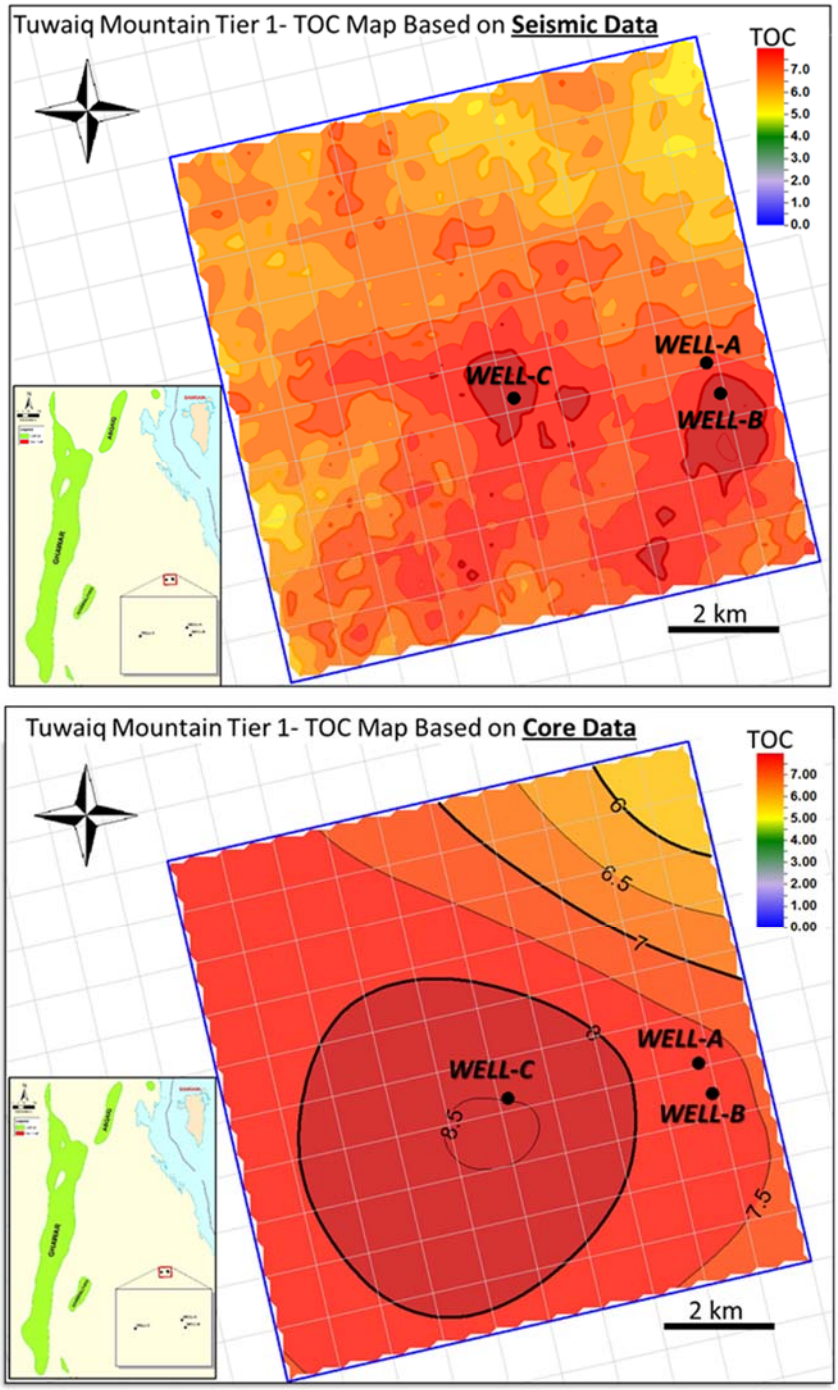

Figure 5-16 Comparison of a seismic inverted TOC map for Tuwaiq Mountain Formation Tier 1 versus a TOC map based on measured well data for the same horizon.

5.5.2 Thickness Prediction from Seismic

Zero offset vertical seismic profile (VSP) acquired in the first vertical exploration well (Well A) was used to establish a well to seismic tie. This relationship was then propagated across the area of interest to map thickness of the target zone. (Figure 5-17) shows the close relationship between reservoir thicknesses predicted from seismic versus thickness from well data.

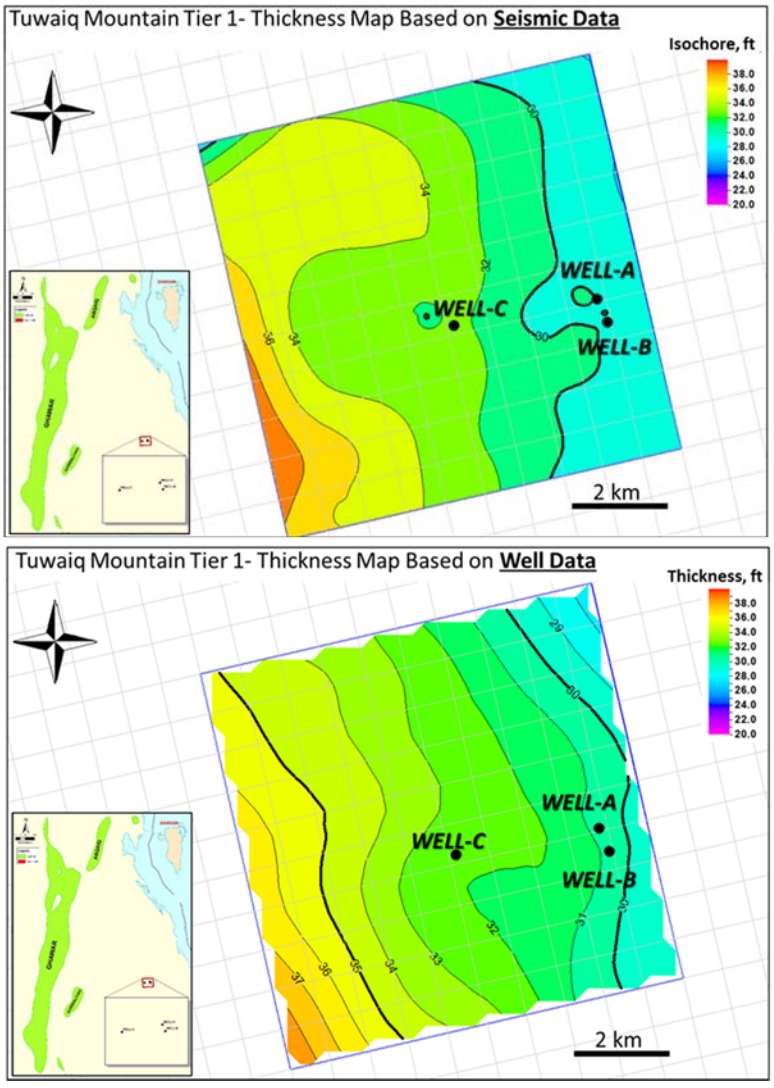

Figure 5-17 Tuwaiq Mountain Formation (Tier 1) thickness map based on wells and seismic inverted data.

5.5.3 Discrete Petrophysical Properties

A Neural Net algorithm was then applied to the existing petrophysical results, creating a number of discrete rock type classes across the Tuwaiq Mountain Formation. The Neural Net algorithm is an estimation model that creates a specific number of classes based on input log curves. The algorithm will cross correlate all input curves to develop a relationship that can identify discrete classes. The user has the ability to constrain the number of output classes. For this study, porosity, bulk density, gamma ray, and TOC were used as the main inputs for the Neural Net algorithm. Certain cut-offs were applied for each of these properties. While cut-offs can widely vary within the oil and gas industry, the following values were determined suitable to characterize the Tuwaiq Mountain. Hydrocarbon saturation of 45% or higher, porosity of 7 p.u. or higher, and TOC of 3 wt% or higher. The algorithm produced between seven to nine discrete classes that provide clearly defined intervals within the Tuwaiq Mountain. (Figure 5-18) shows the output classes that were defined across the target interval.

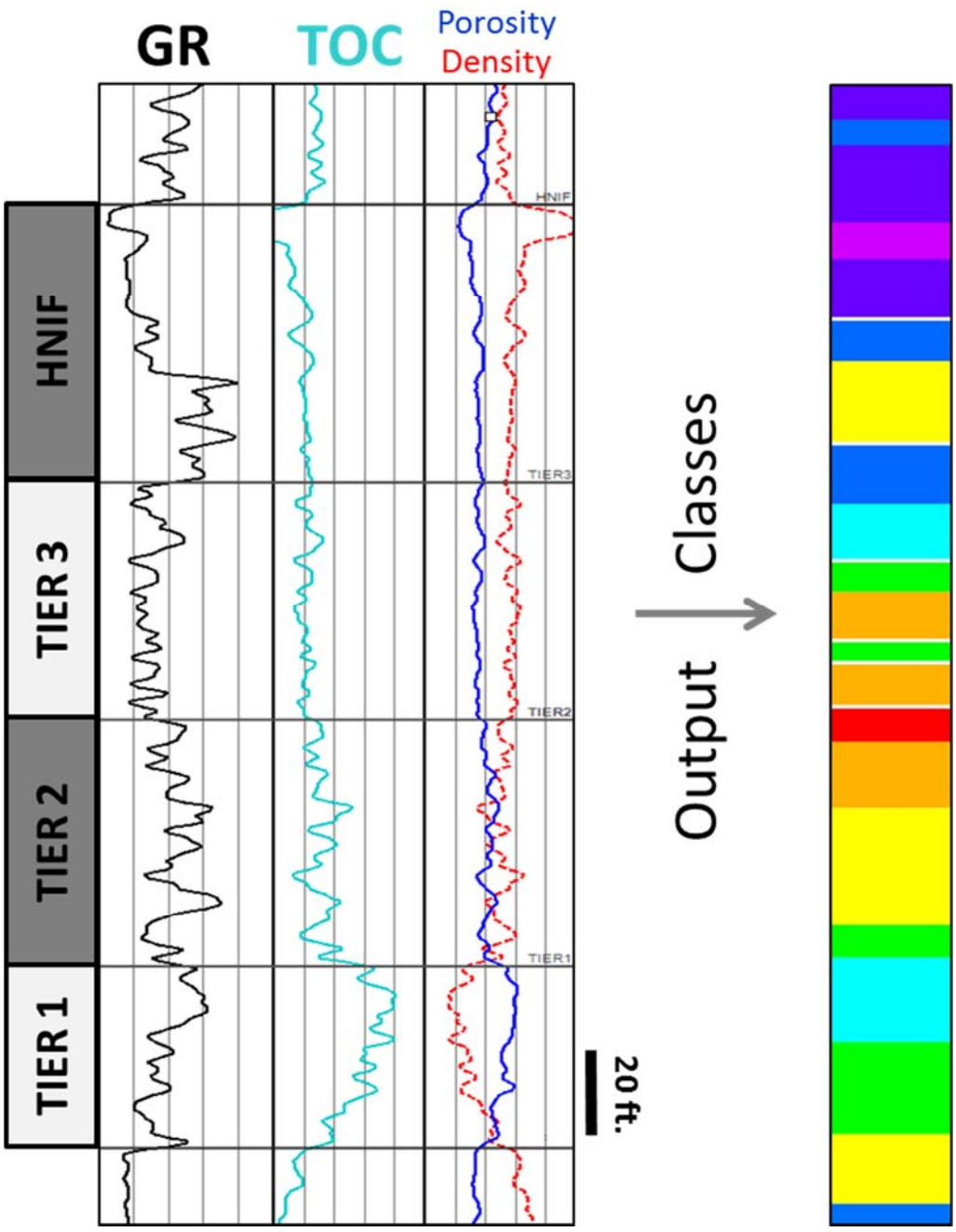

Figure 5-18 A sample output for the Neural Net algorithm across Tuwaiq Mountain Formation. Nine output classes are represented here based on inputs from gamma ray, porosity, density, and TOC.

5.5.4 Petrophysical Reservoir Properties Prediction

A 3D geo-cellular model was developed for prediction of the Tuwaiq Mountain reservoir properties. The geo-cellular framework was built using seismic and well information with a high resolution grid size both in vertical and lateral directions. Based on the distribution of the reservoir properties, the model incorporated 3 zones (Tier 1, Tier 2 and Tier 3). Up scaled petrophysical well logs were the main input for the different reservoir properties modelled. Geostatistical data analysis was used for each zone; and based on our current knowledge of the basin evolution, a major direction – NNW-SSE – was used for the variogram analyses. Sequential Gaussian Simulation was the main algorithm used for the process of modeling the reservoir properties. Co-kriging modeling trend was used for certain reservoir parameters like PHI and TOC, where a positive correlation has been established from the data set. Petrophysical facies were also modeled using the Sequential Gaussian Indicator algorithm.

In this study, hydrocarbon saturation, porosity, TOC, and brittleness were modeled to define sweet spots within the basin. Figure 5-19 shows an example of two reservoir properties that were modeled across the Tuwaiq Mountain Formation. Taking in consideration other reservoir parameters (e.g., SW, K), the model clearly shows that Tier 1 toward the base of the model exhibits the highest reservoir quality parameters. This data is consistent with the petrophysical model developed from the well data. As more appraisal wells are drilled, the model will be tested further and updated where change is needed.

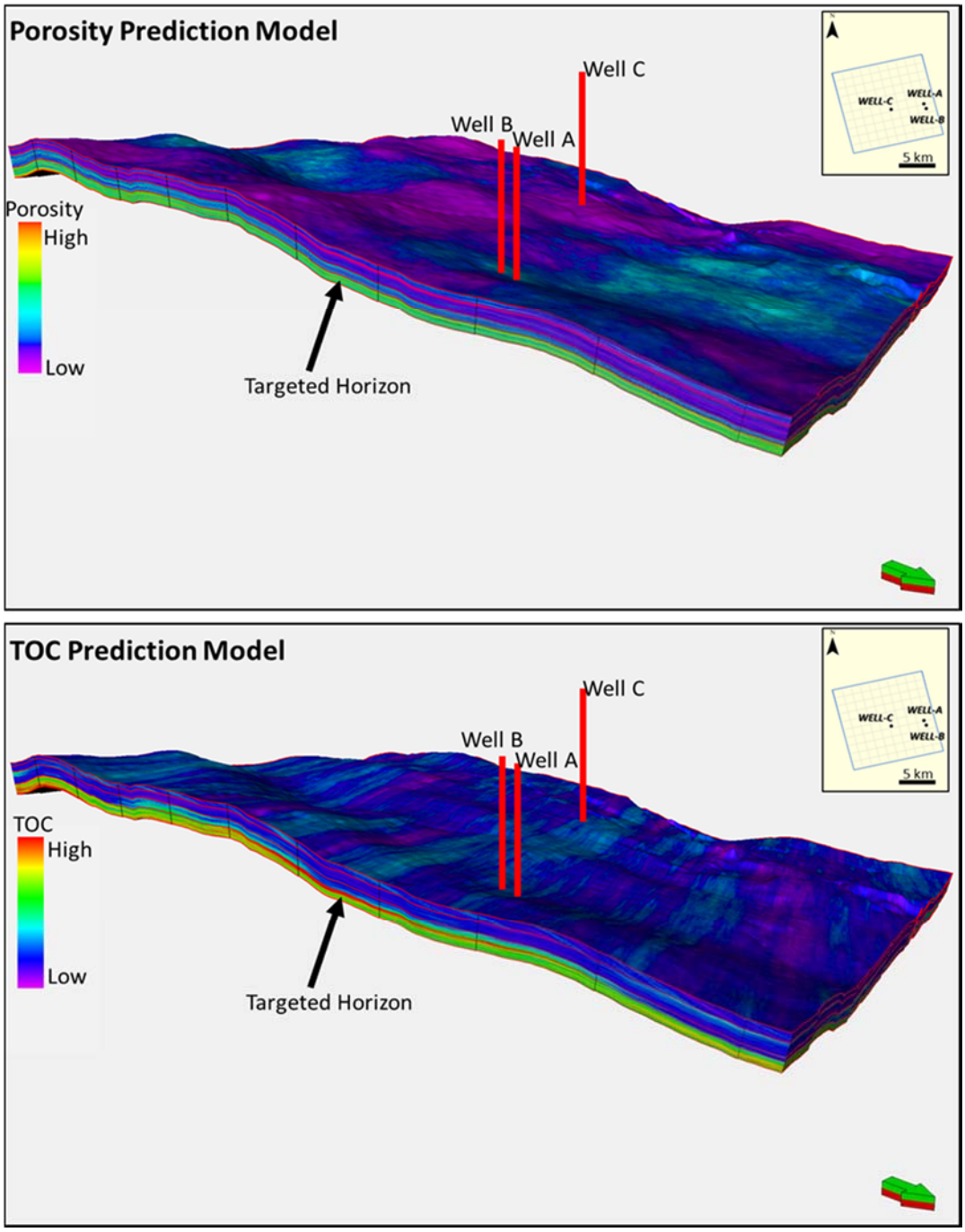

Figure 5-19 Reservoir quality prediction models for porosity and TOC. This model was built based on seismic data and three wells. However, additional appraisal wells are being drilled to fine tune the model

5.6 Drilling Operations

To economically develop this resource play, a combination of geosteering horizontal wells through target sections and multi-stage hydraulic fracture stimulations must be performed to maximize reservoir contact. A successful completion in these wells is directly related to the successful well placement across the target zone. To ensure proper well placement, a number of logging while drilling (LWD) can be utilized. Several logging tools have proven beneficial in geosteering and guiding drilling operations specifically in horizontal wells. Distinctive log signatures or profiles must be first established to be able to identify the appropriate logging suite to use while drilling.

5.6.1 Well Planning

To minimize error and uncertainty when drilling the first few wells in a frontier area, a vertical/horizontal well combination should be used. Drilling the vertical well will provide valuable information and insight to the geological behavior in the area. In addition, the wireline logs acquired in the vertical hole would be used as a robust control point to plan the horizontal well. After drilling the vertical well and identifying the target zone, cement plugs are placed to plug and abandon, and a sidetrack from the vertical hole is initiated. A curved section is drilled after which the horizontal well is then placed properly in the target zone.

5.6.2 Well Placement-Geosteering

As part of the initial stages of drilling horizontal wells in an unconventional reservoir, clear guidelines about log signatures and profiles need to be defined. Typically, organic-rich source rock exhibit high gamma ray signatures indicative of the reducing depositional environment. Given the subtle gamma ray differences in the zone of interest, geosteering with such a curve was found to be difficult (Figure 5-20). It is due to such characteristics that drilling horizontal wells in unconventional reservoirs is a great challenge. To overcome these challenges, a broader outlook must be adopted and different relationships between reservoir characteristics and log signatures must be properly understood. The organic-Tuwaiq Mountain Formation shows strong invers relation between organic content and bulk density, as mentioned in section 5.4.1.1.

While geosteering, density and density image logs were considered the best guiding tools for proper well placement. Figure 5-21 emphasizes the sensitivity of the density log to the slightest stratigraphic or lithologic variation in the Tuwaiq Mountain, while gamma ray, resistivity, and porosity remain almost unaffected.

Ultimately, to properly place the wells in the target zone, petrophysical modeling needs to be incorporated into drilling and geosteering operations. The established discrete classes developed from the Neural Net algorithm in the vertical wells, were simply applied to the horizontal well. While maintaining the same criteria in which these classes were created, this petrophysical modeling technique can be extrapolated throughout the horizontal section. This provides significant benefits in understanding the exact stratigraphic interval in which a well is being drilled. Slight change across the target zone will be immediately highlighted by the distinct color coding represented by the Neural Net classes. Figure 5-

22 shows an example well where the same discrete classification scheme was extrapolated across a horizontal well section. This provides an insight of the heterogeneity across the lateral section, which aids assessment of reservoir and completion quality, as well as stage by stage productivity.

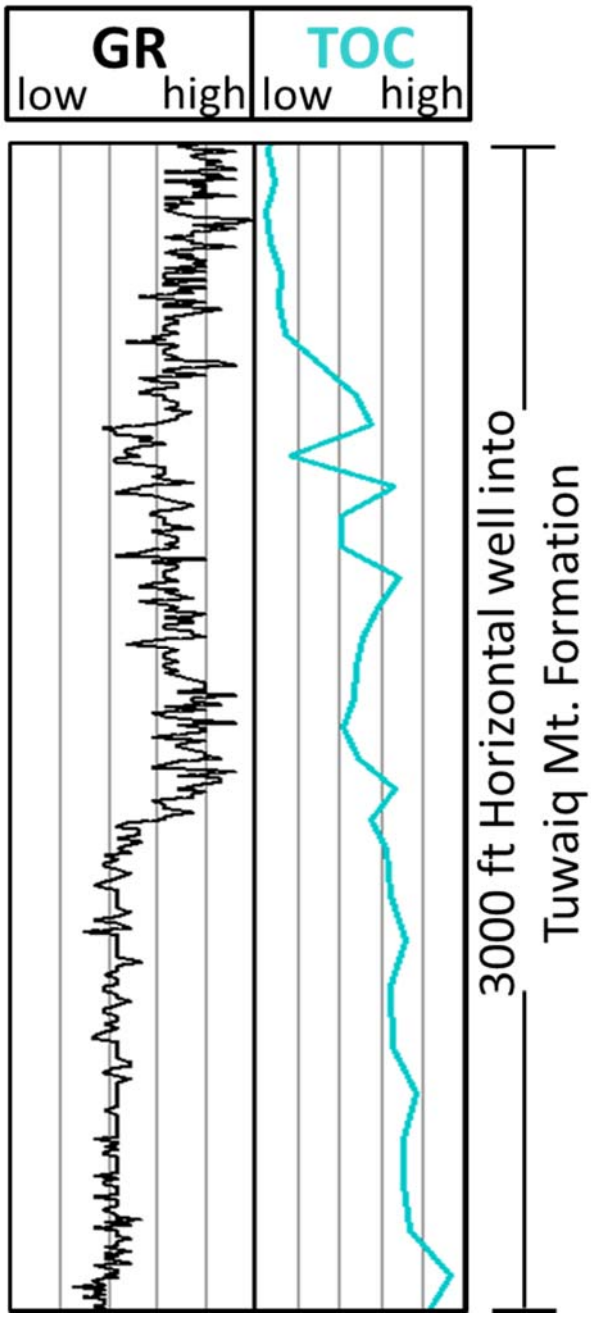

Figure 5-20 Sample log emphasizing the lack of a direct relationship between gamma ray and organic richness. This is a 3000 ft lateral into the Tuwaiq Mountain showing low gamma ray interval correlating to high TOC.

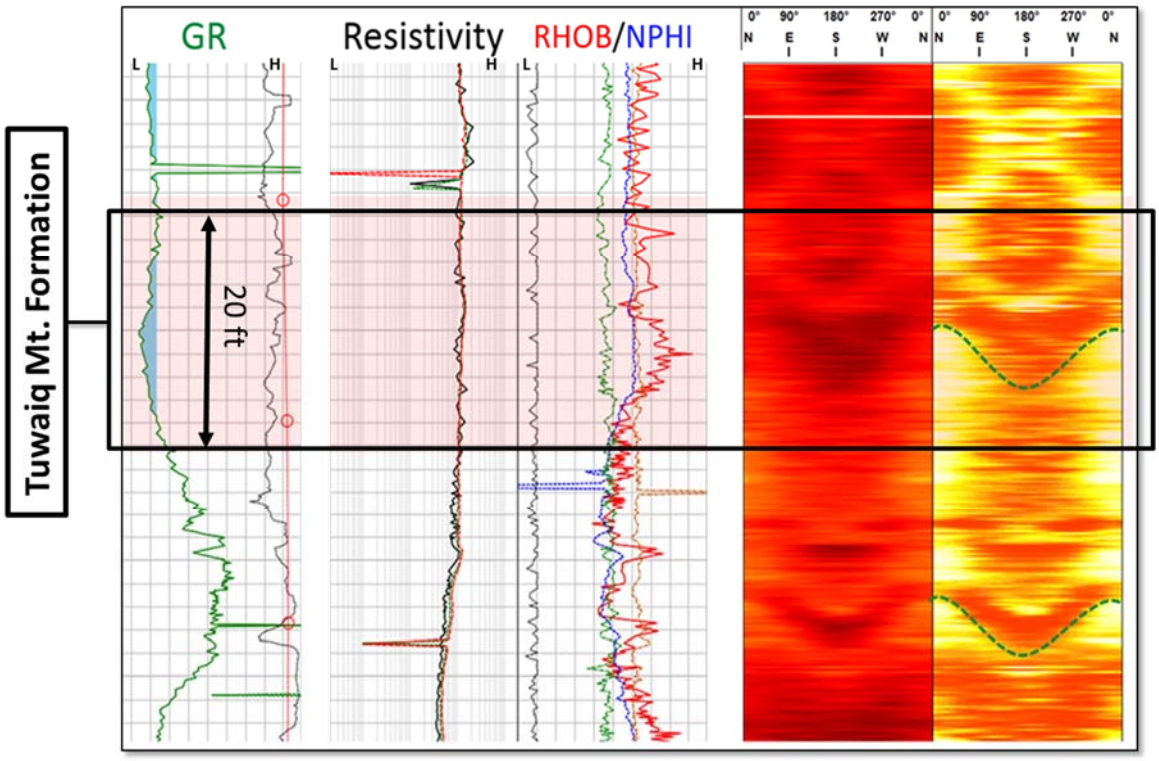

Figure 5-21 Real-time data transmission display showing GR, resistivity, bulk density, porosity and density image logs. The area shaded in light red shows clear density variation across the drilled horizontal interval, while minimal change is seen in the remaining log suite.

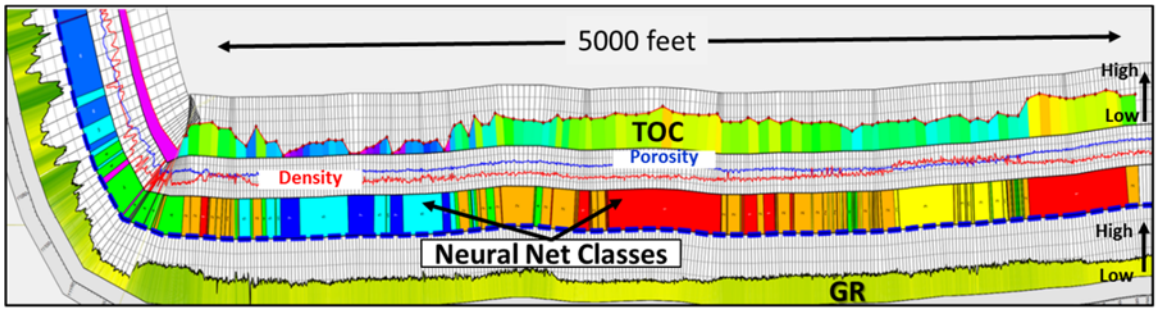

Figure 5-22 Sample horizontal well showing the extrapolation of the Neural Net classification previously discussed in section 6.3.1. The figure shows that the majority of the well was placed in zone classes 1 and 2 (red and orange consecutively).

5.7 Completion and Stimulation

Ultra-low permeability reservoirs require hydraulic fracturing to provide fracture surface area and pathways for hydrocarbon to flow. As a result, the success in all unconventional projects is driven largely by effective completion and stimulation of the reservoir. The geomechanical and production data are essential to validate the efficiency of the stimulation treatments

5.7.1 Geomechanical Properties

Understanding geomechanical properties of mudrocks is essential for optimum hydraulic fracturing treatments. Laboratory studies on the elastic and deformational mechanical properties of these mudrocks show that these rock exhibit wide range of mechanical properties and significant anisotropy reflecting their complexity on material composition and fabric (Sone, 2012). In this study, an anisotropic mechanical rock tests were performed on representative core samples from Tuwaiq Mountain Formation Tier 1. The data shows that this zone exhibit medium degree of anisotropy when compared to other highly argillaceous shales (Terratek Core Laboratories courtesy). The static Young's Modulus ratio Eh/Ev is about 1.65, whereas the static anisotropic Poisson ratio ν_h/ν_v is about 1.38 (Table 5-3). Also, the horizontal Young's Modulus and Poisson ratio are larger than the vertical properties, which is common in this type of rocks.

The average static Young's Modulus in the horizontal direction (Eh) is 4.81 Mpsi, whereas in the vertical direction (Ev) it shows a value of 2.92 Mpsi. For static Poisson ratio the rock exhibits 0.29 in the horizontal direction (ν_h) and 0.21 in the vertical direction (ν_v). Although the anisotropic mechanical tests for Tier 2 and Tier 3 core samples are not

available, we can expect lower values for static Young's Modulus in the horizontal direction and higher values in the vertical direction (Ev) as the soft material (Kerogene and Clay) content decreases in those zones. According to Sone and Zoback (2013) the static anisotropy for Young's Modulus (Eh/Ev) decrease as the soft material (Clay + Kerogene) content decreases. Figure 5-23 illustrates the influence of soft material (Clay + Kerogene) content on the static anisotropy Eh/Ev of various shale gas plays (Sone and Zoback, 2013). Data for Tuwaiq Mountain Formation Tier 1 is somehow comparable to Eagle Ford Play. The dynamic Young's Modulus for Tuwaiq Mountain Formation Tier 1 is larger than the static but for Poisson's ratio the static properties are larger than the dynamic (Table 5-3). The difference between static and dynamic mechanical properties is caused by the inelastic behavior of reservoir rocks and saturation conditions. Wide differences in the frequency and loading conditions of static and dynamic tests allow static tests to measure the elastic and inelastic deformation behavior of the rock, whereas acoustic measurements only capture the elastic deformation response (Yale and Jamieson, 1994).

Table 5-3 Summary of the anisotropic mechanical elastic properties of Tuwaiq Mountain Formation in Tier 1 at Wells A, B and C.

Mechanical Elastic Properties		Horizontal	Vertical	Horizontal/Vertical Ratio
DYNAMIC	Young's Modulus, Mpsi	6.26	5.10	1.23
	Poisson Ratio	0.30	0.16	1.88
STATIC	Young's Modulus, Mpsi	4.81	2.92	1.65
	Poisson Ratio	0.29	0.21	1.38

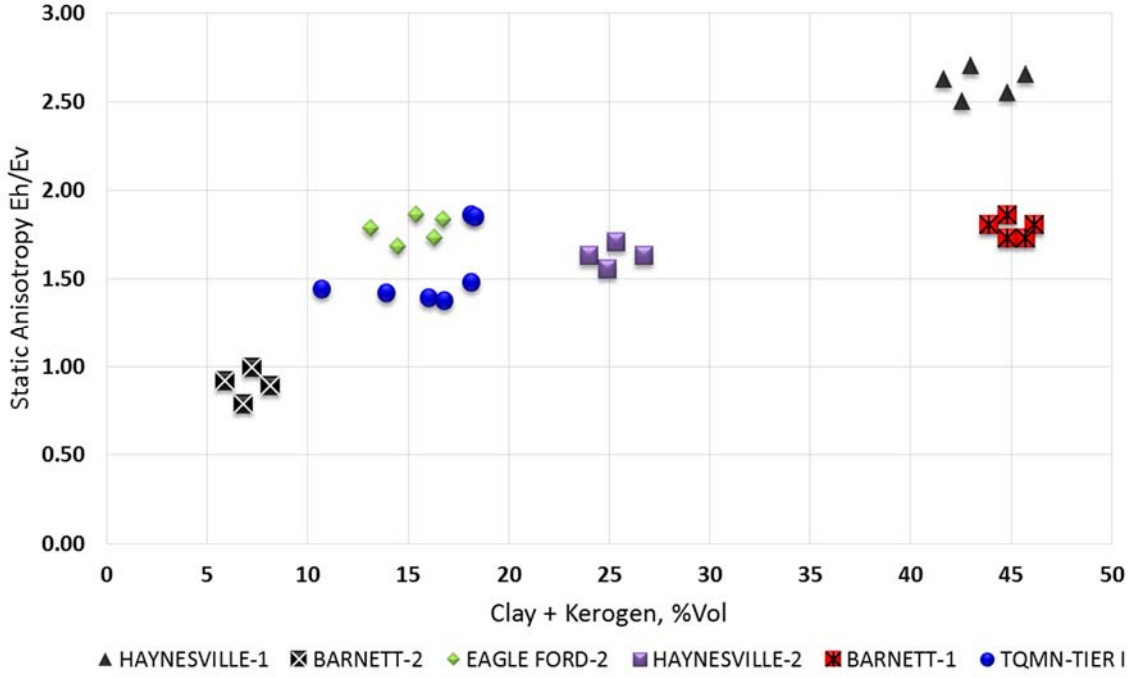

Figure 5-23 Influence of soft material (Clay + Kerogen) content on the static anisotropy Eh/Ev. Data for Tuwaiq Mountain Formation Tier 1 is shown in blue, whereas the other data were extracted from Sone and Zoback (2013).

5.7.2 Completion and Stimulation Strategy

The completion and stimulation approach followed in the initial Jafurah wells was much aligned with the de-risking strategy. In the exploration phase, wells A, B and C were drilled vertically, cored, logged, and cased. Then, two vertical stimulation stages were executed in well A for two reasons. First, to determine if proppant could be placed in a tight carbonate rock formation as this had not been yet proven in Saudi Arabia. The second objective was to confirm the maturity window of wet gas as predicted from basin modeling. Placement of proppant in Saudi Arabia's tight carbonate was very successful (Al-Mulhim et al., 2014). In addition, well A flowed gas and condensate. The diagnostic fracture injection test (DFIT) and the vertical well hydraulic fracturing stimulation experiments indicated that the Jafurah wells require high treating pressure with formation closure pressure in the range of 0.98 psi/ft to 1.05 psi/ft. This required the proper selection of wellheads, tubing, casing and liners to facilitate Tuwaiq Mountain high-pressure completions.

Wells A, B and C were then sidetracked with 5,000 ft horizontal laterals into Tier 1 of the Tuwaiq Mountain Formation, which possesses excellent shale gas characteristics. All laterals were drilled in the direction of the minimum principal horizontal stress (NNW). This allows for transverse hydraulic fractures across the wellbore to achieve maximum reservoir contact. Wells were completed with a 4½ inch production liner and 5½ inch tubing. This completion was selected to minimize friction pressure at higher fracturing pump rate (Al-Momin et al., 2015).

Different fracturing techniques were tested to investigate operational efficiency, cost and potential to maximize well performance. The four fracturing stimulation technologies

tested in the three lateral wells were slickwater, conventional crosslink gel, conventional crosslink hybrid and channel fracturing treatments. An average of 16 stages were placed in each well (Figure 5-24). The number of stages, stage spacing and number of clusters per stage were selected based on the integration of all engineering and geoscience data collected from the wells. A completion and reservoir properties driven cluster selection approach was used instead of a geometric design to optimize the stimulation design. (Table 5-4) summarizes the stimulation design applied in Wells A, B and C.

To maximize stimulation efficiency, a limited entry technique was utilized for multi-cluster stages: 2 feet of perforations with six shots per foot at 60° phasing, 0.3-0.4 inch entry hole per cluster and 2-4 clusters per stage for effective diversion. All fracturing treatments started with 6,000 gallons of pre-pad acid stage to breakdown the formation, manage near wellbore friction and reduce treating pressure, followed by linear gel and cross-linked gel in the pad and slurry stages (Al-Momin et al., 2015). During the initial stimulation trials, slickwater was found to be prone to high treating pressure and early screenouts. At least 98% of the treatments were placed with conventional crosslink, and channel fracturing treatments. Both stimulation treatments showed good contribution to the early production. High and medium strength proppants were used in most of the fracturing treatments to provide long term fracture conductivity. A pilot well having high strength and local low-strength proppants indicated that both proppants were competent to produce in early stage. The well has been placed on long term testing to assess if locally available low strength proppant provides adequate conductivity for the long-term production deliverability. The advantage of this is cost reduction which is one of the key parameters for the success of the pilot stage (Figure 5-2).

Table 5-4 Summary of stimulation design applied in Wells A, B and C.

Attribute	Applied Practice
Fracturing Techniques Tested	Slickwater, Conventional Crosslinked Gel, Hybrid and Channel designs
Average Number of stages	16
Fracturing treatment rate	40-70 bpm
Number of clusters	1-4
Cluster spacing	70-100 ft
Fluid per Cluster	1000-1400 bbls
Proppant per cluster	70,000- 90,000 lb
Maximum Proppant concentration	4.5 - 6 ppa
Proppant Type	40/70, 30/50, 20/40 ceramic proppant. Locally available low strength proppant in a dedicated well

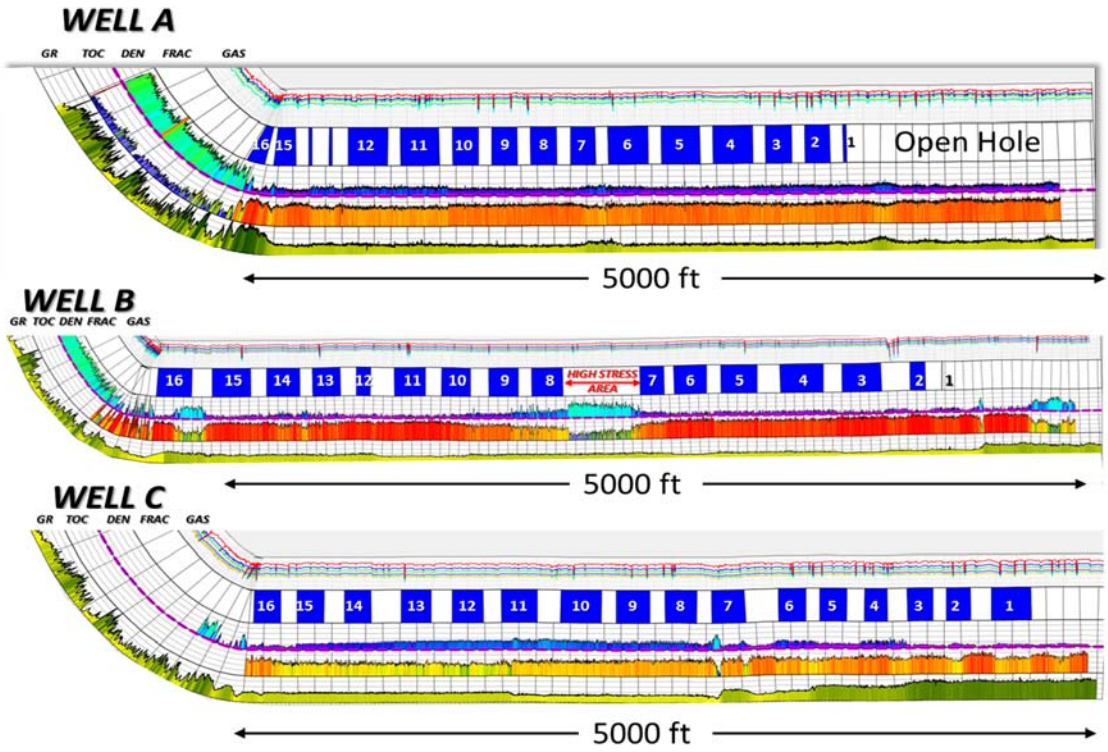

Figure 5-24 Three laterals well placed in Tier 1 highlighting the petrophysical properties and the stimulation design. All three wells show consistent reservoir quality with minor variability throughout the horizontal section.

To assess the efficiency of the fracturing stimulation treatments in the lateral sections, production logging (PLT) was undertaken after the initial flow back. The production log analysis showed that all stimulated stages and cluster for the three wells were contributing to the wells production (Al-Momin et al., 2105). It was also determined that stages stimulated by both conventional and channel fracturing stimulation contributed to production. Due to the few stages with slickwater treatments, it is not statistically possible to determine if those stages would have contributed to production when completed effectively. Wells flowed gas and condensate to surface at consistent initial flow rates. The flowback was for short period due to lack of surface facility and to comply with the gas flaring regulations. A modular early testing facility will be considered for extended flow back test (minimum 12 months) to allow for better EUR estimation. It is expected that most of the wells in Jafurah Sub-Basin will flow gas and condensate at varying CGRs values (<100 – >400 bbl/mmscf). Figure 5-25 illustrates an example of an initial flow data from one of the wells. Since these initial wells were completed with a conservative stimulation design, a completion benchmarking assessment based on fracturing stages/clusters, volume of proppant/fluid, type of proppant/fluid and length of lateral was undertaken. Normalizing the completion design size to analogs from the Eagle Ford play in Texas, it was shown that the initial flow rates for Wells A, B and C are comparable and the play has more potential if completion strategy is up scaled.

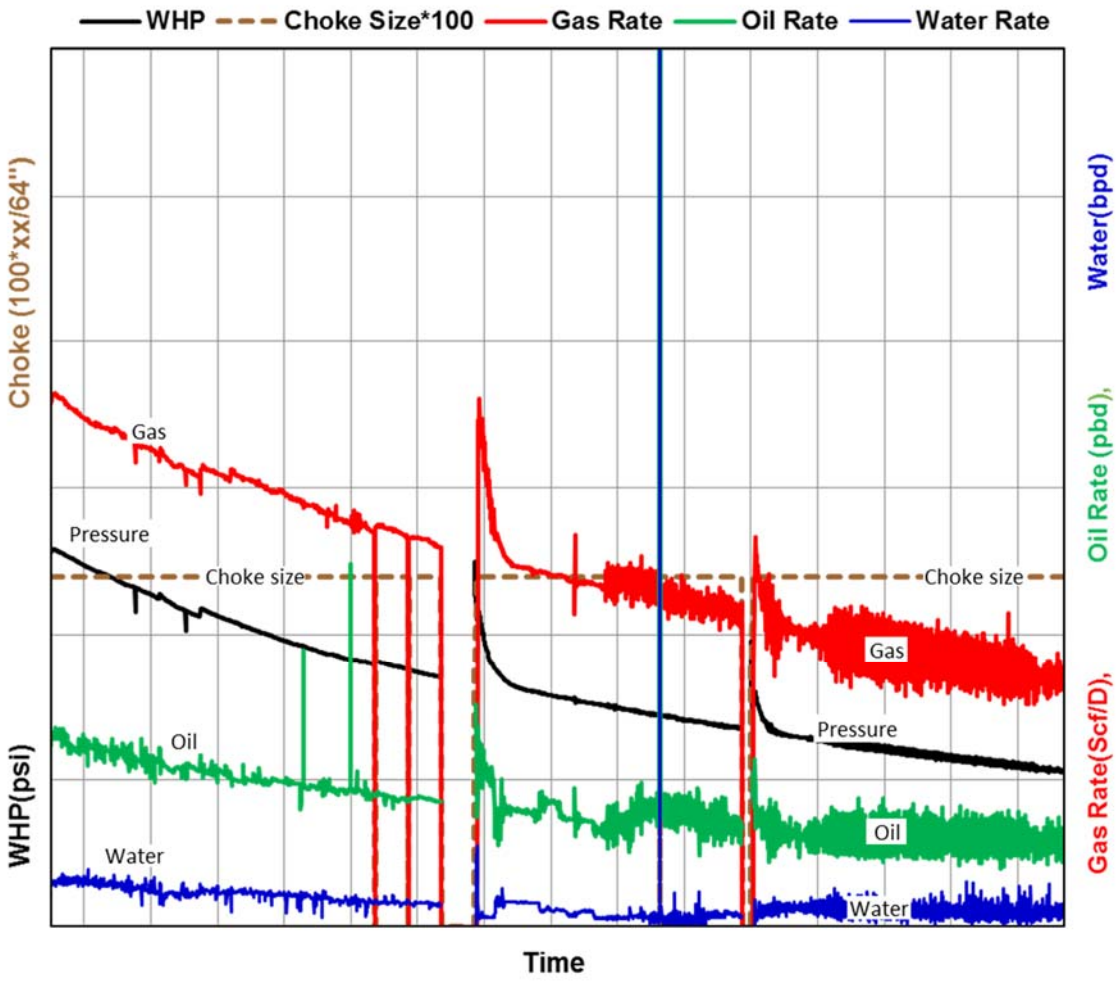

Figure 5-25 Flowback chart for well B (modified after Al-Momin et al., 2015).

5.8 Conclusion

- A successful phased de-risking strategy is being implemented to explore for unconventional hydrocarbon accumulation in the Jafurah Sub-Basin, Saudi Arabia. This basin spreads over a large area equivalent in size to the Eagle Ford play in South Texas.
- A comprehensive formation evaluation and data acquisition program was implemented to acquire a wealth of core and well-log data from the first three exploration wells.
- The Jurassic Tuwaiq Mountains Formation possesses good shale gas attributes, such as high TOC, low clay content, low water saturation, high porosity and high gas saturation. The three Tiers identified in the characterization show varying reservoir quality with Tier 1 having excellent attributes. Initial reservoir modeling indicates that all Tiers will be accessed by hydraulic fracture stimulation.
- A methodic reservoir quality prediction model was developed to help with initial appraisal well scoping, lateral target selection, effective well placement and geosteering operations.
- A number of appraisal wells are being drilled to delineate the Jafurah Sub-Basin boundary and to search for a dryer gas window.
- Intensive characterization of the rock and proper data integration facilitated the optimal lateral placement, stage selection and successful placement of the fracturing stimulation treatments. Since these initial wells were completed with a conservative stimulation design, a completion benchmarking assessment based on fracturing stages/clusters, volume of proppant/fluid, type of proppant/fluid and

length of lateral was undertaken. Normalizing the completion design size to analogs from the Eagle Ford play in Texas, it was shown that the initial flow rates for Wells A, B and C are comparable and the play has more potential if completion strategy is up scaled.

- A number of pilot wells are being planned to tune technologies and find the most efficient and cost effective drilling and stimulation recipe for the Jafurah unconventional play development.

5.9 References

Al-Husseini, M., 1997. Jurassic sequence stratigraphy of the western and southern Arabian Gulf: GeoArabia, v. 2, no. 4, p. 361-382.

Al-Momin A., Kurdi M., Baki, S., Mechkak K., Al-Saihati A., 2015. Proving the concept of unconventional gas reservoir in Saudi Arabia through multistage fractured horizontal wells. SPE Annual Technical Conference and Exhibition, September 28-30, 2015, Houston, Texas, USA, SPE-176844-MS.

Al-Mulhim, N.I., Al-Saihati, A.H., Hakami, A.M., Al-Harbi, M. and Asiri, K.S., 2014. First successful proppant fracture for unconventional carbonate source rock in Saudi Arabia. Presented at the International Petroleum Technology Conference, Kuala Lumpur, Malaysia, December 10-12, 2014, IPTC-17765.

Al-Sharhan, A.S., and Christopher, G., Kendall ST. C., 1986. Precambrian to Jurassic rocks of Arabian Gulf and adjacent areas: their facies, depositional setting, and hydrocarbon habitat. AAPG Bulletin, v. 70, no. 8, p. 977-1002.

Archie, G. E., 1952. Classification of carbonate rocks and petrophysical consideration: AAPG Bulletin, v. 36, no. 2, p.218-298.

Ayres, M. G., Bilal, M., Jones, R. W., Slentz, L. W., Tartir, M. and Wilson, A. O., 1982. Hydrocarbon habitat in main producing areas, Saudi Arabia: AAPG Bulletin, v. 66, p. 1-9.

Cantrell, D.L., Nicholson, P.G., Hughes, G.W., Miller, M.A., Bhullar, A.G., Abdelbagi, S.T., Norton, A.K., 2014. Tethyan petroleum systems of Saudi Arabia, Petroleum systems of the Tethyan region: AAPG Memoir 106, p. 613-639.

Carrigan, W. J., Cole, G. A., Colling, E. L., and Jones, P. J., 1995. Geochemistry of the Upper Jurassic Tuwaiq Mountain and Hanifa Formation petroleum source rocks of eastern Saudi Arabia, in B. J. Katz, ed., Petroleum Source Rocks: Springer-Verlag, New York, p. 67-87.

Cole, G. A., Carrigan, W. J., Colling E. L., Halpern, H. I., Al-Khadhrawi, M. R. and Jones, P. J., 1994. The organic Geochemistry of the Jurassic petroleum system in eastern Saudi Arabia, Canadian Society of Petroleum Geologists, memoir 17, p. 413-438.

Droste, H. H. J., 1990. Depositional cycles and source rock development in an epeiric intra-platform basin, the Hanifa Formation of the Arabian Peninsula: Sedimentary Geology, v. 69, p. 281-296.

Helena, G. D., Camron, M., and Richard, L., (2012). sCore: A Classification for Organic Mudstones based on bulk mineralogy. Presented at AAPG 2012 Southwest Section Meeting, Ft Worth, Texas, 19-22 May 2012. Search and Discovery Article # 40951, posted June 11, 2012.

Holditch, S. A., 2006. Tight gas sands, SPE Journal of Petroleum Technology 58 (6), p. 86–93 SPE-103356-MS.

Hook, P., Fairhurst, D., Rylander, E., Badry, R., Bachman, N., Crary, S., Chatawanich, K., and Taylor, T., 2011. Improved precision magnetic resonance acquisition; application to shale evaluation, SPE Annual Technical Conference and Exhibition, 30 October-2 November, Denver, Colorado, USA, SPE-164883-MS.

Jacob, H., 1989. Classification, structure, genesis, and practical importance of natural solid bitumen ("migrabitumen"): International Journal of Coal Geology, v.11, no 1, p.65-79.

Jarvie, D. M., Claxton, B. L., Henk, F., and Breyer, J. T., 2001, Oil and shale gas from the Barnett Shale, Fort Worth Basin, Texas: AAPG Annual Meeting Program, v. 10, p. A100.

Lindsay, R.F., Khan S., Dhubeeb A., Davis R., 2014. Unconventional Jurassic carbonate source rocks, Saudi Arabia. International Conference & Exhibition, September 14-17, 2014, Istanbul, Turkey, AAPG article # 90194.

Luffel, D. L., Guidry, F. K., and Curtis, J. B., 1996. Development of laboratory and petrophysical techniques for evaluating shale reservoirs: Gas Research Institute Final Report GRI-95/0496 (October 1986–September 1993), p. 301

Murris, R.J. 1980. Middle East stratigraphic evolution and oil habitat, AAPG Bulletin, v. 64, p. 597-618.

Petersen, H.I, Schovsbo, N. H., and Nielsen, A. T., 2013. Reflectance measurements of Zooclasts and solid bitumen in Lower Paleozoic shales, Southern Scandinavia: Correlation to vitrinite reflectance. International Journal of Coal Geology v. 114, p.1-18.

Pollastro, R. M., 2003. Total petroleum systems of the Paleozoic and Jurassic, greater Ghawar uplift and adjoining provinces of central Saudi Arabia and northern Arabian-Persian Gulf: U.S. Geological Survey Bulletin 2202-H, 100p.

Pommer, M., and Milliken, K., 2015. Pore types and pore-size distribution across thermal maturity, Eagle Ford Formation, southern Texas: AAPG Bulletin, v. 99, no. 9, p. 1713-1744.

Schoenherr, J., Littke, R., Urai, J.L., Kukla, P.A., Rawahi, Z., 2007. Polyphase thermal evolution in the Infra-Cambrian Ara Group (South Oman Salt Basin) as deduced by maturity of solid reservoir bitumen. Organic Geochemistry v. 38, p. 1293–1318.

Schmoker, J., and T. Hester, 1983. Organic carbon in Bakken Formation, United States portion of Williston Basin: AAPG Bulletin, v. 67, p. 2165-2174.

Sharland, P. R., Archer, R., Casey, D. M., Davies, R. B., Hall, S. H., Heward, A. P., Horbury, A. D., and Simmons, M. D., 2001. Arabian Plate sequence stratigraphy: GeoArabia Special Publication 2, Gulf PetroLink, Bahrain, 371 p

Sone, H., 2012, Mechanical properties of shale gas reservoir rocks and its relation to the in-situ stress variation observed in shale gas reservoir. A dissertation submitted to the department of Geophysics of Stanford University in partial fulfilment of PhD. SRB Volume 128, March 2012

Sone, H., and Zoback, M. D., 2013. Mechanical properties of shale-gas reservoir rock- part 1: Static and dynamic elastic properties and anisotropy: SEG, v. 78, no. 5, p. D381-D392.

Tissot, B. P. and Welte, D. H., 1984. Petroleum Formation and Occurrences, second edition. Springer Verlag Berlin Heidelberg New York Tokyo.

Yale, D.P., and Jamieson, W.H., 1994. Static and dynamic rock mechanical properties in Hugoton and Panoma fields, Kansas; SPE Mid-Continent Gas Symposium, 22-24 May 1994, Texas, USA, SPE-27939-MS.

Ziegler, M. A., 2001. Late Permian to Holocene paleofacies evolution of the Arabian Plate and its hydrocarbon occurrences: GeoArabia, v. 6, no. 3, p. 445-504.

CHAPTER 6

Tuwaiq Mountain Drainage Strategy

Coupling Geoscience and Fracture Modeling Data for Tuwaiq Mountain Well Spacing and Drainage Strategy

Ahmed Hakami [a] and Clay Kurison [a]

[a] Saudi Aramco, Exploration Organization, 31311, Dhahran, Saudi Arabia

Submitted to SPE Journal for Reservoir Evaluation and Engineering – Reservoir Engineering

Abstract

Ultra-low permeability reservoirs require hydraulic fracturing to provide fracture surface area and pathways for increasing production from horizontal wells. An optimal reservoir drainage strategy requires the determination of well counts to guarantee future production through an understanding of completion design and well spacing both of which are challenging to determine. The focus of this study is on the organic rich Jurassic Tuwaiq Mountain Formation in the Jafurah Sub-Basin of Saudi Arabia. The formation is being considered a potential world-class unconventional play owing to its excellent shale gas characteristics such as high total organic content, low clay content and proper maturity window for hydrocarbon generation. This study demonstrates how integration of outputs

from reservoir characterization can be integrated with multidiscipline data such as microseismic and hydraulic fracturing modeling to provide insights on drainage strategies. Based on this multidiscipline study, it was realized that fracture geometries and matrix permeability affect reservoir drainage strategies. Improper characterization of these parameters can lead to serious consequences on well productivity and optimal development of an unconventional resources field.

6.1 Introduction

Typical unconventional reservoir descriptions reported by industry depict source rocks as having 25 to 300 feet of net pay, porosities ranging from 3 to 12 percent, original reservoir pressures from 5,000 to 11,000 psi, and matrix permeability that ranges from 0.1nD to 2000nD. Due to the wide ranges in values for reservoir properties, it is a primary task to reduce this uncertainty so as to allow an optimum reservoir drainage strategy. In addition to this uncertainty, there exist multiple and dramatically different interpretations about hydraulic fractures that place the created fracture half-length between 50 and 1,500 feet. The dilemma is that wells should produce adequately and be spaced close enough together to maximize field recovery yet excessive tight spacing can decrease productivity of future wells.

6.2 Review of the Nature of the Unconventional Resource Flow

Reservoirs exhibit multiple flow regimes among them being bilinear, radial and linear. El-Banbi e al., (1998) indicated that many tight reservoir wells exhibited long-term linear Flow. Linear flow can be detected by -½ slope line in log-log plots of either pressure drop or production rate versus time. Another study of United State lower 48 tight reservoirs (Elliott et al., 2011) showed that most exhibit linear flow for long periods as detected by -½ slope line in log-log plots of production rate versus time. The explanation for this phenomenon was transient flow induced by long planar fractures in medium of ultra-low matrix permeability. El-Banbi et al., (1998) presented linear reservoir solutions in a form that can be used for a variety of models. Solutions for analyzing pressure and production rate data under constant rate or pressure flowing conditions were provided. The analytical solutions were adapted to different reservoir models including fractured wells and wells producing reservoirs with high permeability streaks. Considering a constant pressure solution allows computation of permeability (k) and flow area (A_c), using Equation 3 and 4 for gas and oil reservoirs respectively. Knowledge of reservoir fluid viscosity (μ), porosity (φ), compressibility (C_t), flowing pressure conditions (P_i, P_{wf}), reservoir temperature (T), real gas pseudo pressures at flowing conditions $m(p_i)$, $m(p_{wf})$, and formation volumetric factor (*B*) is required, m_{CPL} is the slope of 1/rate versus square root of time.

$$A_c\sqrt{k} = \frac{1262\,T}{[m(p_i) - m\,(p_{wf})]\sqrt{(\emptyset\mu c_t)_i m_{CPL}}} \quad \text{.....Equation 3}$$

$$A_c\sqrt{k} = \frac{125.1\,B\mu}{(P_i - P_{wf})\sqrt{\emptyset\ \mu\ \mathrm{C}_t m_{CPL}}} \quad \text{..... Equation 4}$$

Equations 3 and 4: Equations for linear flow at constant bottom hole flowing pressure in gas and oil wells (El-Banbi et al., 1998).

Flow regimes in the early production from Jafurah's Tuwaiq Mountain formation wells also exhibited a -½ slope trend when bottom-hole conditions approached constant flowing pressure as shown in Figure 6-1. As described above, this was the initial indication of linear flow.

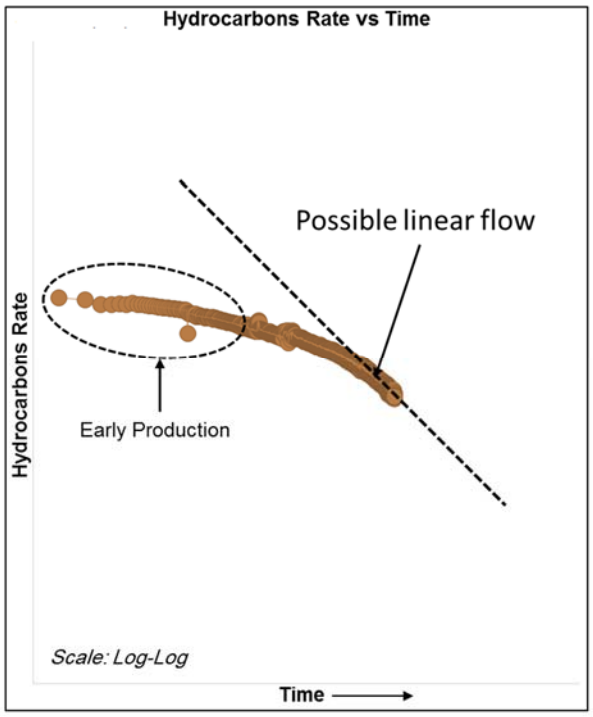

Figure 6-1 Depiction of linear flow in one of the initial wells.

The controlling parameters, permeability (k) and cross-sectional area to flow, A_c, cannot be separated without independent knowledge of one of the two. For the case of Tuwaiq Mountain wells, all have been hydraulically fractured. The initial simplified model to represent these wells is that of a planar fracture intersecting a low permeability matrix.

6.3 Review of Parameter Governing Linear Flow in Tuwaiq Mountain

An assessment of the key components of $\boldsymbol{A_c\sqrt{k}}$ is required to understand what will govern linear flow and for how long it will take. As indicated above, k represents the matrix permeability while for a simplified planar hydraulic fracture system, Ac is a product of fracture half-length, fracture height and number of hydraulic fractures.

6.3.1 Review of k, Permeability

An accurate measurement of tight rock permeability is challenging in both experimental and theoretical investigations because of complexities involved with modeling flow through nanoscale throats. The Gas Research Institute (GRI) methodology (Luffel et al., 1996) was used to measure permeability for core samples from Tuwaiq Mountain Formation. It is worth noting that the GRI measurement used crushed samples of the core. The results show a very good trend when absolute permeability is compared to total porosity (Figure 6-2). Equation 1 was developed to predict permeability values from logs in wells with no core data (Hakami et al., 2016).

$$K\ (mD)GRI = 10^{-7} \times Porosity\ (\%)^{3.6622} \quad \text{..... Equation 1}$$

For long, the industry has accepted optimistic permeability values (e.g. GRI) and also used the absolute values to rank emerging plays and engineer stimulation designs based on these results. Though the technique is widely used, validity of results has been questioned. Some of the common reasons about this inadequacy are lack of consistency among multiple

laboratories and the dependency of results on grain sizes of the crushed core. In addition, tests are usually not conducted at reservoir conditions and the approach tends to yield higher permeability estimates.

Alternative core plug based methods have been suggested to address GRI method uncertainties. Selected Tuwaiq Mountain samples were considered for pulse decay permeability measurements for comparison. This technique also allows the plugs to be subjected to stresses to account for reservoir conditions.

As illustrated in Figure 6-2, the Pulse decay measurements show at least an order of magnitude lower permeability values for the Tuwaiq Mountain Formation samples when compared to the GRI method results. Such data was critical in highlighting the potential of choosing the wrong matrix permeability value, which poses serious consequences on formulating an optimal reservoir drainage. Equation 2 was developed to predict Pulse decay permeability values from well logs in wells with no core data.

$$K\ (mD)\ PPD\ =\ 8 * 10^{-8} \times Porosity\ (\%)^{\ 3.3652} \quad \text{..... Equation 2}$$

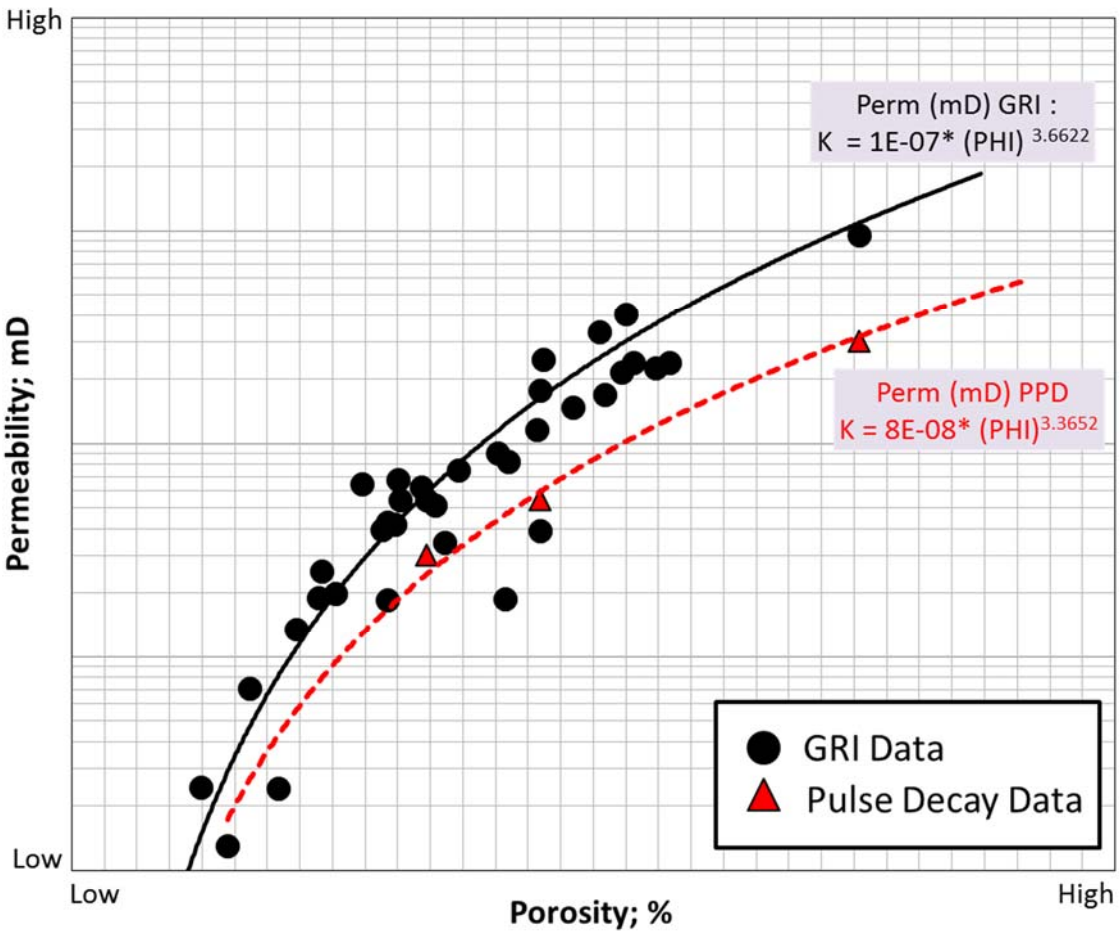

Figure 6-2 Tuwaiq Mountain Formation porosity and permeability relationship. Permeability was measured using two techniques: GRI and Pulse Decay methods.

In addition to the matrix permeability, natural fractures have been considered central to the economic production of tight reservoirs. Natural fractures have been reported as being critical for altering the system permeability of the formation. In this study, a characterization of Tuwaiq Mountain natural fractures was done to understand their impact on system permeability and hydrocarbon production. The role of these fractures in controlling productivity and influencing reservoir drainage strategies has been a topic for debate.

6.3.2 Natural Fractures and their Influence on System Permeability and Production

Micro-fractures are known to exist in source rocks because of tectonic settings and the hydrocarbon generation process. They have been attributed to enhancing the reservoir contact surface area if intersected as shown by Stalgorova et al., (2012). Based on the Tuwaiq Mountain formation evaluation, there is no indication of tectonic related natural fractures in Tuwaiq Mountain in the assessed wells. However, many micro-expulsion fractures in the Tuwaiq Mountain were observed in 20µm thin sections. Figure 6-3 shows representative 20µm thin sections w/red fluorescent dye impregnation of various Tuwaiq Mountain samples. These samples were selected to cover different maturity windows within the Jafurah sub-basin. Generally, source rock maturity increased from well X to Well E in Figure 6-3. All thin sections clearly show that expulsion micro fracture magnitude increases with the increase in maturity. Assessment of the natural fracture and rock images indicates that most of these micro-fractures are short and discontinuous. This indicates that their major contribution to production is obtained when intersected by a hydraulic fracture while those not in its close proximity or deeper in the matrix will not provide instant flow. This is different from reservoirs where existing extensive natural fractures might facilitate drainage of a larger reservoir area without stimulation or if done, with few hydraulic fractures.

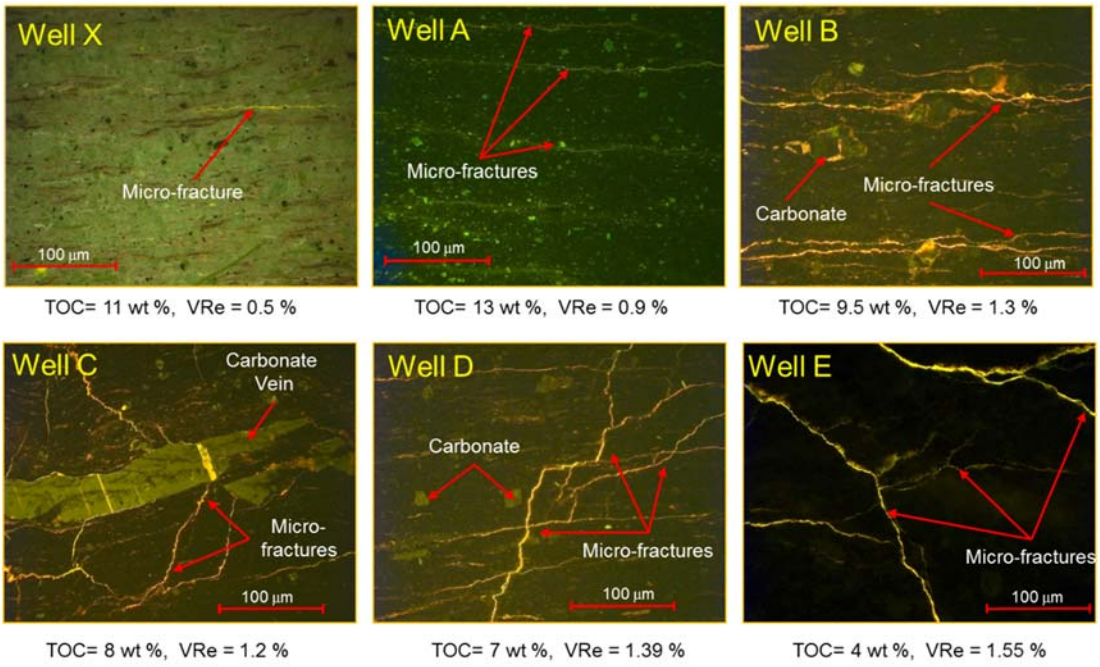

Figure 6-3 20µm Thin Section w/red fluorescent dye impregnation of representative Tuwaiq Mountain core samples. All images highlight the existence of natural fractures in the Tuwaiq Mountain but with various magnitude.

Though Tuwaiq Mountain hydrocarbon generation expulsion fractures are short and discontinuous, they might be an explanation for the higher initial production rate followed by steep decline. Figure 6-4 illustrates our understating of how early production volumes from intersected micro-fractures/natural fractures and instant matrix production flush leads to high initial flow rates. Figure 6-5 illustrates multiple hydraulic fractures intersecting with numerous, but discontinuous micro-natural fractures and the resulting increase in initial production.

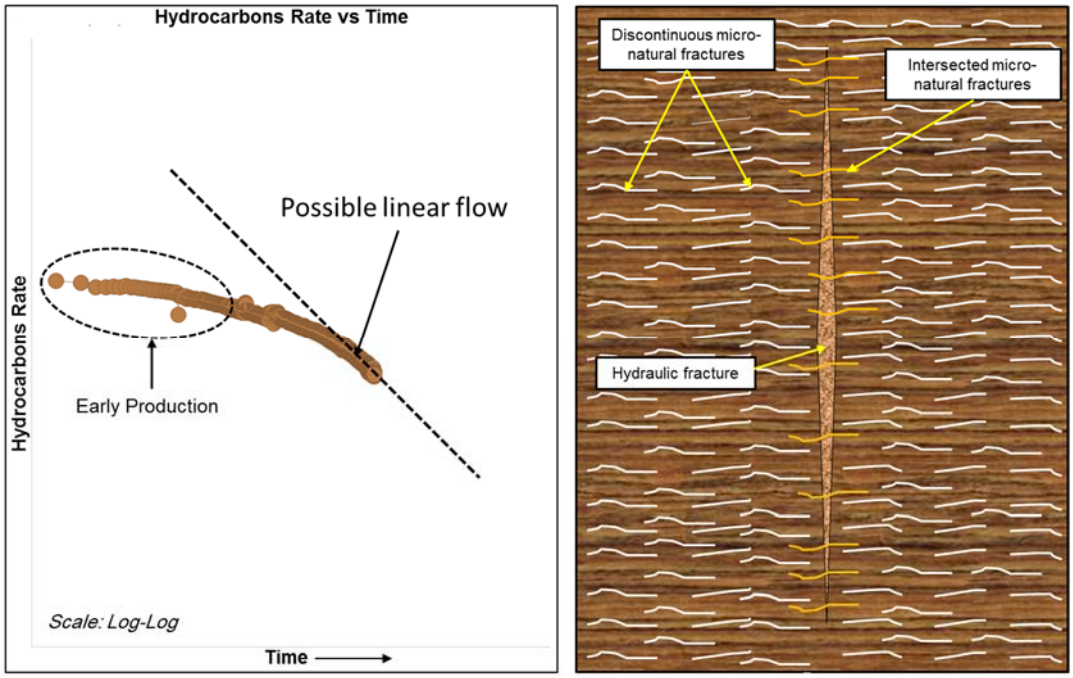

Figure 6-4 Depiction of linear flow in one of the initial wells (left). Early production commonly considered fracture flow and an interpretation of a hydraulic fracture interacting with numerous but discontinuous natural micro-fractures

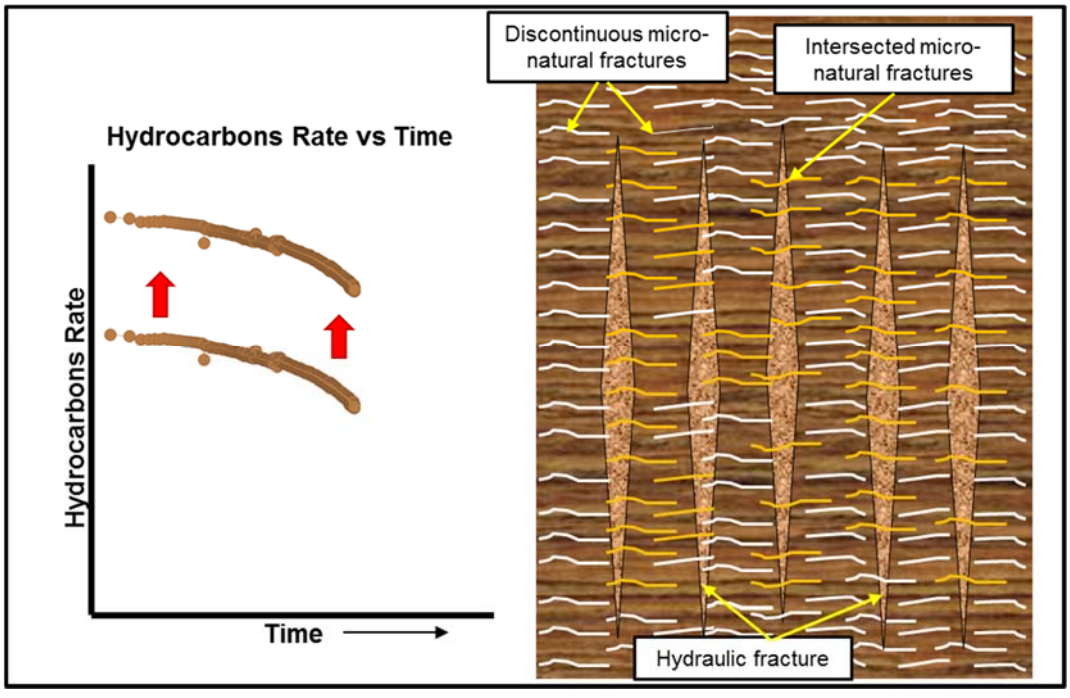

Figure 6-5 An interpretation of multiple hydraulic fractures interacting with numerous but discontinuous natural micro-fractures (Right). Impact on production rate (left).

6.3.3 Review of Ac, Flow Area

To describe a hydraulic fracture in the Tuwaiq Mountain formation, the initial simple model used comprises of a highly conductive fracture in low permeability matrix. Ac is a product of fracture half-length, fracture height and number of hydraulic fractures. Diagnostic Fracture Injection Tests (DFITs) were used to estimate instantaneous shut-in pressure (ISIP) gradient, closure pressure gradient, fracture closure time, injection fluid efficiency, and upper bound pore pressure gradient (Al-Mulhim et al., 2014). With the use the, well logs from vertical wells and anisotropic mechanical rock tests, geomechanical property attributes were derived and calibrated.

Based on the derived geomechanical model and stimulation treatment discussed in chapter 5, a hydraulic fracture half-length of 900 feet was obtained when DFIT representative fluid efficiency (90%+) and low leak off coefficient (0.00035 ft.min1/2) were used. For sensitivity purposes, use of larger values of formation leak off coefficient (0.0015 ft.min1/2) reduced the fracture half-length to 400 feet. Figure 6-6 illustrates outputs from a Tuwaiq Mountain formation-fracturing model with the same geomechanical profiles but different leak off coefficients.

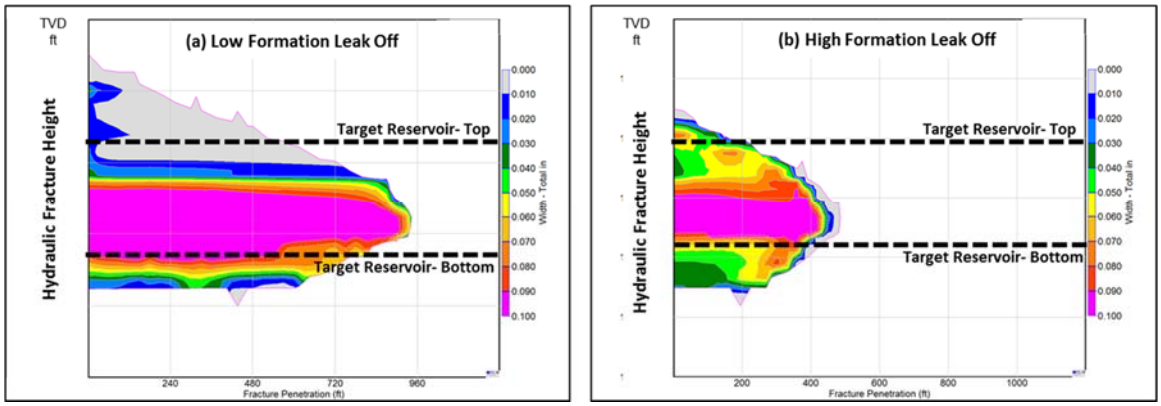

Figure 6-6 Variability in fracture geometry based on different model inputs. a) Low formation leak off coefficient shows a hydraulic fracture half-length of 900 feet; b) Larger formation leak off coefficient shows a hydraulic fracture half-length of 400 feet

The variability in modeled hydraulic fracture half-length and height as a result of uncertainty in property profiles and values poses challenges for completion optimization, and well spacing which are vital for a reservoir drainage strategy. Supplementary data sets were integrated with existing data and models to understand fracture geometry and drainage area.

6.4 Hydraulic Fracture Geometry Estimation from Microseismic

Microseismic monitoring of hydraulic fracturing stimulations in unconventional reservoir wells has improved understanding on geometries of created hydraulic fractures, adequacy of the completion hardware and provision of insights for field development planning. The most common and important attributes from a microseismic operation are fracture half-length, azimuth, height, and width (Warpinski et al., 1997), (Maxwell and Cipolla, 2011) all of which are key parameters for assessing reservoir contact. Fracture half-length is a dominant parameter for defining well spacing in field development. Figure 6-7 illustrates the acquisition set up for the first microseismic monitoring job in the Jafurah Sub-Basin. The operation consisted of monitoring several hydraulic fracturing stages in well A (horizontal) using a 20-level geophones array deployed in well B (a vertical monitoring well), located 250 meter from the treatment well. The distance from the bottom geophone of the monitoring array to the midpoint of the stimulated stages depth ranged between 1,506 ft to 2,305 ft. A total of 16 stages were planned for this well but during execution, 5 were skipped due to mechanical reasons. Of the 11 stages that were executed, seven underwent microseismic monitoring.

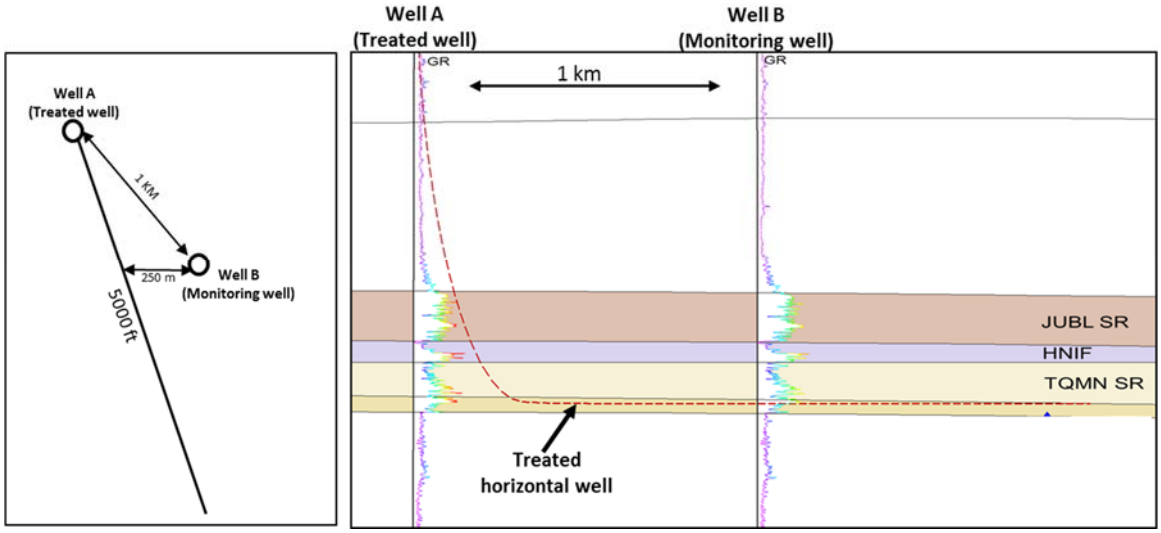

Figure 6-7 Acquisition set up for the first microseismic monitoring job in Jafurah Sub-Basin

The microseismic event locations for all the monitored stages are shown in Figure 6-8. Taking into consideration the bias resulting from the vertical monitoring well's location, microseismic results indicated that the observed height covered the target reservoir. All stages close to the monitoring well exhibited acoustic fracture half-lengths greater than 750 feet with Stage 6 having a maximum cloud extent of 830 feet as fracture half length. As a check on earlier fracture modeling attempts, matching the observed microseismic fracture geometry required DFIT representative low formation leak off coefficient and minimal adjustments to the stress profile. This geometry is similar to that predicted by fracturing model with low leak off coefficient.

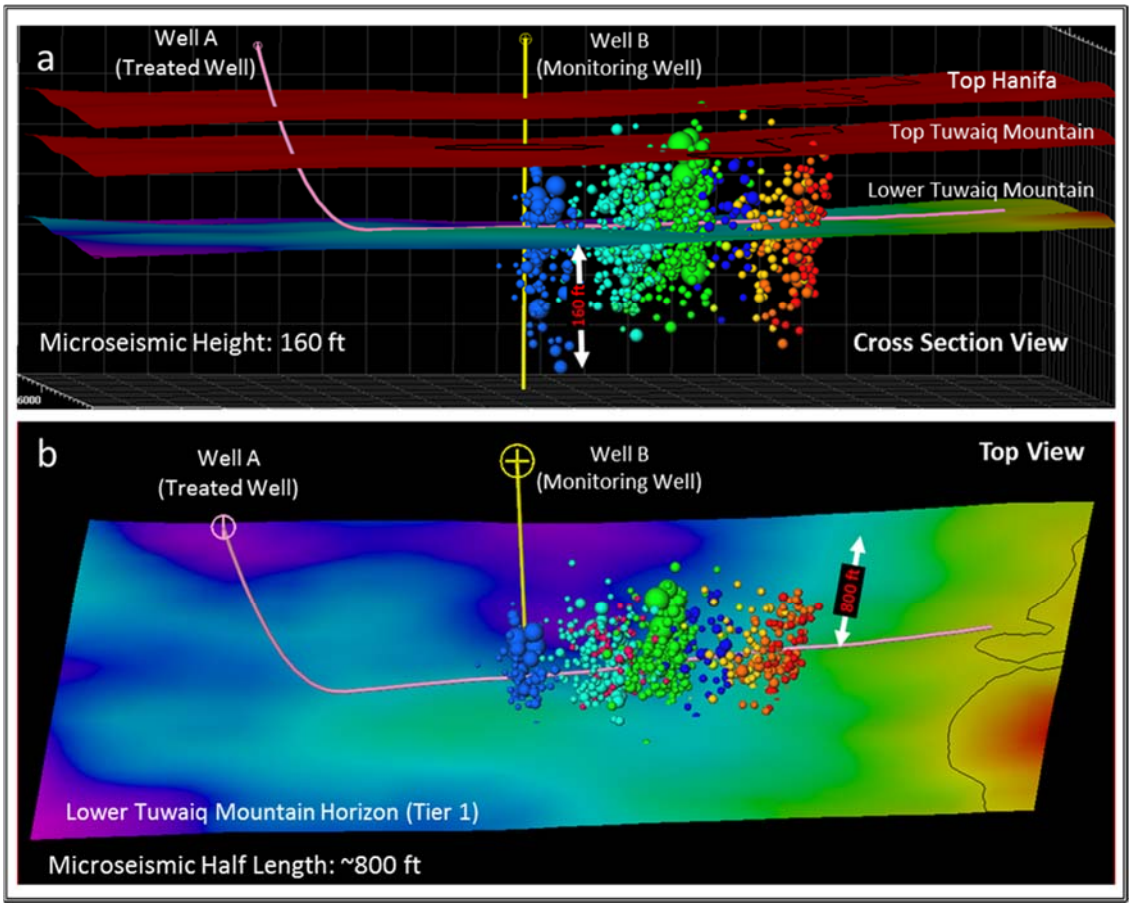

Figure 6-8 Microseismic events for all the monitored stages, a) cross section view showing maximum fracture growth height b) top view showing maximum fracture half-length of 800 ft.

6.4.1 Possible Interpretation of Microseismic Data

In spite of interpretations from fracture modeling, DFITs, and microseismic monitoring, multiple industry hypothesis still cast doubt on what is the producing portion of created hydraulic fractures. Fracture half-length has for long been described as having hydraulic and effective portions based on after-closure proppant concentration, hence generating multiple thoughts. This study has grouped the schools of thought into three categories as described below:

6.4.1.1 Short Hydraulic Fracture

This school of thought states that real hydraulic fractures are short and fracture geometries observed in microseismic monitoring comprise of acoustic portions as illustrated by Carl et al., (2014). Productive fracture half-length out of this hypothesis is usually estimated to be within 50 to 200 feet. Fracture modeling to match these geometries requires the use of high formation leak off coefficient, which are not representative of what is obtained from DFITs. Fracture half-length is this range can only be supported by using higher permeability as those determined from the GRI technique.

6.4.1.2 Long Hydraulic Fracture with Short Effective Portions

This is the most common line of thinking in the industry though its authenticity is still questioned. It indicates that fracture geometries observed in microseismic monitoring are real but comprise hydraulic portions without adequate conductivity or the initial conductive fracture undergoes decay. Productive fracture half-length out of this hypothesis is usually estimated to be within 50 to 400 feet. Douglas, et al., (2013) and Carl et al., (2014) present cases where this school of thought is verified. For the two theories above, the choice of

fracturing fluids to place the needed proppant is usually highly viscous cross-linked fluid systems. Subsequent to the need for high fracture conductivity, the theories place preference on high strength proppants pumped at high concentrations to maintain adequate fracture conductivity. Fracture half-length is this range can only be supported by using higher permeabilities as those determined from the GRI technique.

6.4.1.3 Long Hydraulic with Long Effective Portions

This line of thinking supports the belief that fracture geometries observed in microseismic monitoring are largely real and retain their deliverability even after fracture-closure. Productive fracture half-length out of this thought can range from 500 to at least 1,000 feet as illustrated by Mayerhofer et al., (2011) and Sardinha et al., (2014). This approach prioritizes creation of adequate hydraulic fracture surface area with large fluid volumes pumped in the form of slick water and hybrid systems other than traditional high viscosity crosslinks. Subsequent to the need for minimal fracture conductivity, the theory encourages low to medium amounts of low strength proppants pumped at low concentrations. Fracture half-length is this range can only be supported by using lower permeabilities as those determined from the pulse decay technique.

6.5 Reservoir Drainage Strategy: Optimization and Completion, Production and Well Space

Part of completion optimization involves maximizing individual recovery and determining well spacing. As noted from above, $A_c\sqrt{k}$ provides insights on fracture properties and matrix permeability. Figure 6-9 is a plot of average matrix permeability against fracture half-length doe a derived value of $A_c\sqrt{k}$ from Tuwaiq Mountain formation wells. The plot provides insights about measured permeabilities, modeled fracture geometries and microseismic geometries.

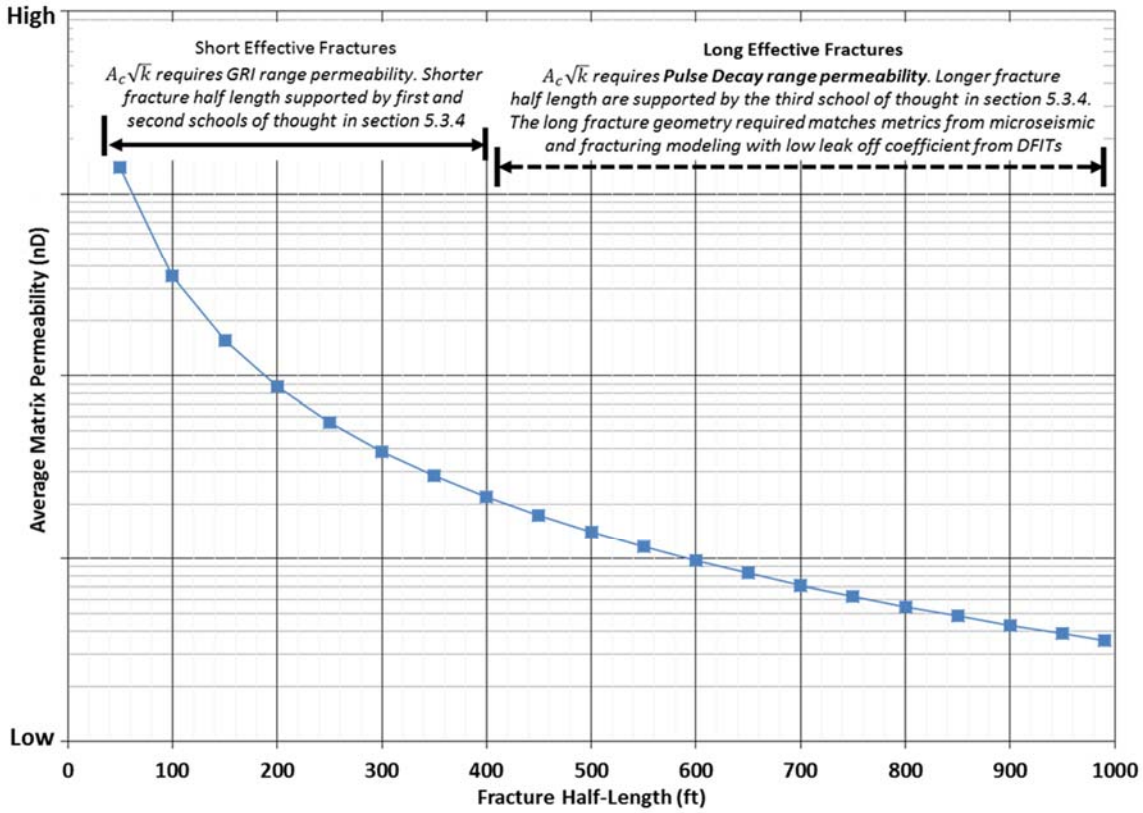

Figure 6-9 A sensitivity analysis of fracture half-length and permeability for Tuwaiq Mountain using a constant fracture height. The vertical scale for average matrix permeability is logarithmic.

Figure 6-10 illustrates how permeability and fracture geometry influence the stimulation approach and reservoir drainage strategies. In case of higher matrix permeability, the stimulation approach should deliver few short and highly conductive hydraulic fractures. If the permeability is very low, the stimulation's aim is to create a considerable number of fractures that are long but not necessarily possessing high conductivity.

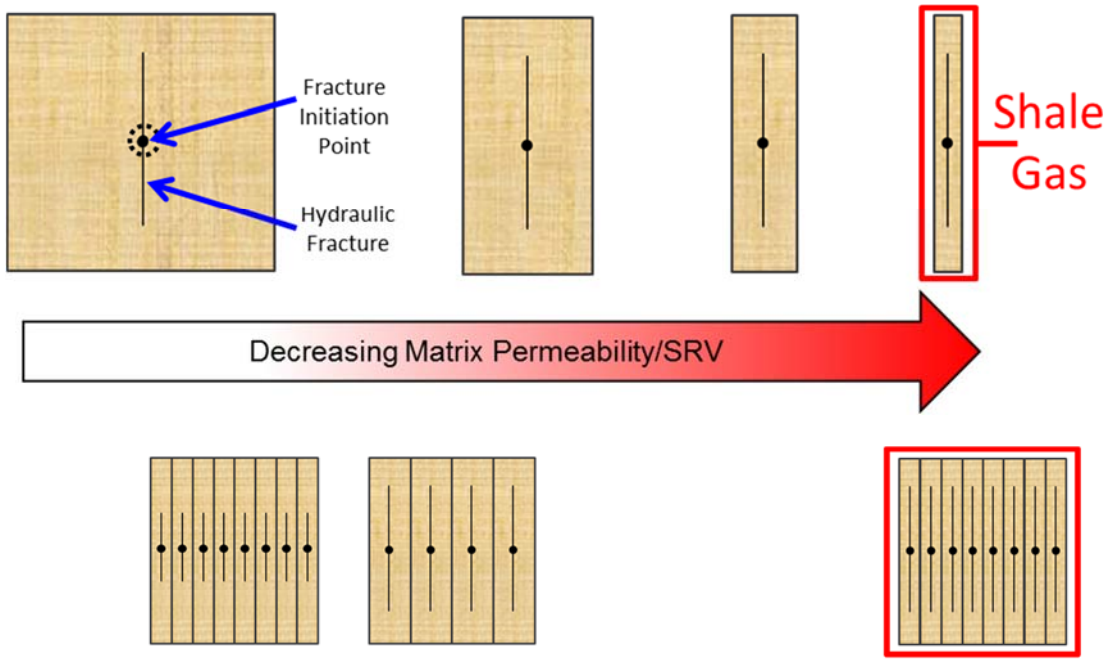

Figure 6-10 Top view illustrating the affect of matrix permeability on the stimulated reservoir volume (SRV).

6.5.1 Reservoir Drainage Strategy: Option 1

Based on microseismic geometries, pulse decay matrix permeability and fracture modeling with DFIT representative lower formation leak off coefficient, hydraulic fracture half-length of at least 800 feet was obtained for the Tuwaiq Mountain Formation. Given the long periods of transient or linear flow and reservoir pressure conservation in unconventional reservoirs, it is likely that the matrix permeability is also very low as in other proved unconventional reservoirs or as shown by pulse decay measurements. Coupled with the third School of thought about hydraulic fracture geometry, Figure 6-11 illustrates a development strategy based on what is discussed above.

Using 800 feet of fracture half-length for illustration purposes, horizontal wells would need to be spaced 1600 feet apart. Since the permeability in this case is very low, hydraulic fracturing stages would need to be tightly spaced. Each stage would require multiple perforation clusters that are densely spaced. To create the long fracture half-length required to drain the reservoir, large volumes of stimulation fluids would be needed to create the fracture geometry. Additional insight is provided in the third School of thought described earlier. Figure 6-11 illustrates tightly spaced fracturing stages with densely space perforation clusters.

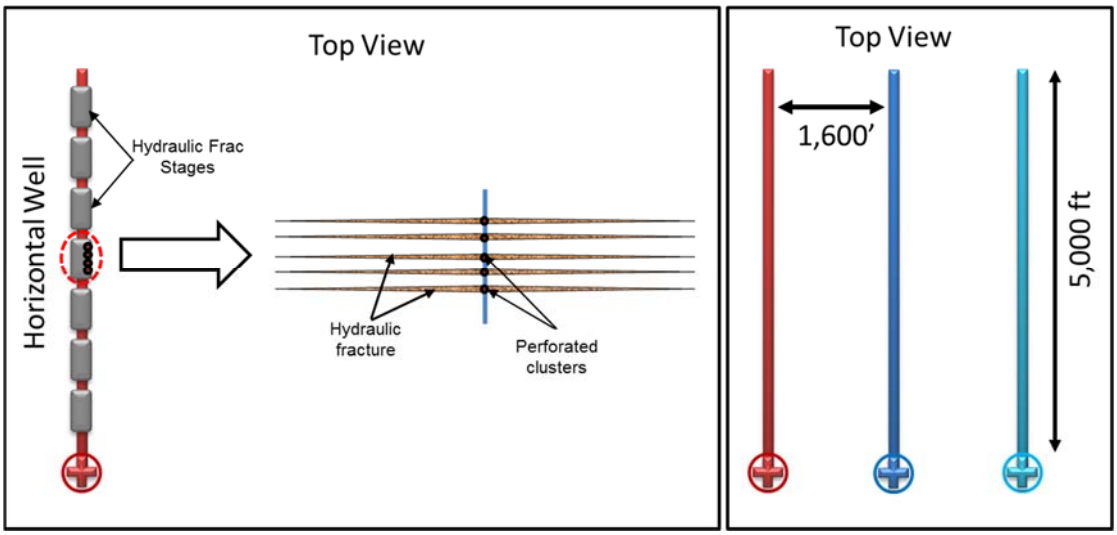

Figure 6-11 Left - A well with tightly spaced fracturing stages with densely space perforation clusters. Right - Widely spaced lateral wells.

Assuming 5,000 feet horizontal laterals are to be drilled, a 640 acres block would require 3 wells at a well spacing of 1600 feet as shown in Figure 6-11 on the right. The largest portion of the development budget would be for stimulation operations. This therefore calls for less development wells which results in less drilling capital but more emphasis on stimulation effectiveness. Since the drainage beyong the fracture is limited, increasing lateral length yields incremental production if proportional increase of stages is considered. However, consideretion of drilling and fracturing operational feasibility should be evlauted.

6.5.2 Reservoir Drainage Strategy: Option 2

Reservoir drainage strategies based on higher matrix permeabilities as those obtained from the GRI method require different considerations for hydraulic fracture geometry. As indicated above, GRI permeabilites are supported by the. Using 400 feet of fracture half-length for illustration purposes, horizontal wells would need to be spaced 800 feet apart. Since the permeability in this case is high, hydraulic fracturing stages would need to be spaced widely with fewer perforation clusters. To create the short and highly conductive fracture half-length required to maintain reservoir deliverability, less volumes of stimulation fluids but large amounts of proppant would be needed to create the fracture geometry. Additional insight is provided by the first and second schools of thought about hydraulic fracture geometry described earlier. Figure 6-12 illustrates a development strategy based on option 2.

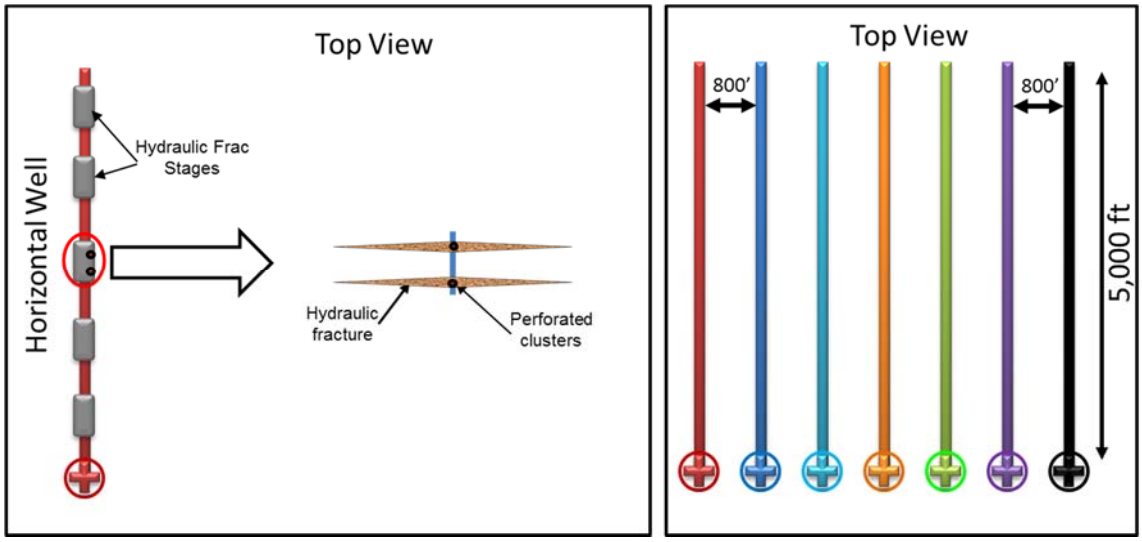

Figure 6-12 Left - A well with widely spaced fracturing stages with fewer perforation clusters. Right - Wells at low spacing between laterals.

Assuming 5,000 feet horizontal laterals are to be drilled, a 640 acres block would require 7 wells at a well spacing of 800 feet as shown in Figure 6-12 on the right. The largest portion of the development budget would be for capital expenditure for drilling operations. This therefore calls for more development wells which results in more drilling capital but less on stimulation effectiveness. An assessment on the impact of increasing well lateral length was done to understand the likely incremental production. For the case with higher matrix permeability, there is a lower optimum lateral length and number of stages contrary to the ultra-low permeability case. Additional lateral length or fracturing stages will not add much to overall long term production.

6.6 Implication for an Unconventional Reservoir Drainage Strategy

If the lower matrix permeability case as described in **Reservoir Drainage Strategy: Option 1** is representative, but the opposite is chosen, numerous drilled wells might be under stimulated, leading to low individual well recovery and deployment of too many rigs. However if the higher matrix permeability case as described in **Reservoir Drainage Strategy: Option 2** is representative, but the opposite is chosen, few wells will be drilled but might be over stimulated which leads to unnecessary completion cost. Efforts are in place to further characterize parameters that define the two **Reservoir Drainage Strategies** by creating dedicated field pilots in the Tuwaiq Mountain formation.

6.7 Conclusion

In this work, it has been demonstrated that there exist multiple and dramatically different interpretations and models on unconventional reservoir properties and drainage strategy. Conclusions reached in this study include:

- Integration of multidiscipline data to fully characterize the most probable fracture geometry and matrix permeability is critical as these impact completion optimization, individual well recovery and reservoir drainage strategy to be adopted.
- Assuming the wrong fracture geometry, matrix permeability and reservoir drainage model has consequences on optimal and economic development of an unconventional play.

- Reservoir drainage strategy scenarios for low and high ranges of matrix permeability illustrated. One interpretation hinges fracture design on contacting more fracture surface area requiring less development wells but more fracturing stimulation stages. The other scenario considers more development wells requiring more rigs but minimal fracturing stimulation stages. This work illustrates how the planar fracture reservoir model is more representative based on its reliance on microseismicity, fracture modeling, PPD permeability and DFIT results.
- History matched simulation models can assist in describing possible fracture geometries, matrix permeability and drainage areas. These scenarios can guide diligent data acquisition and expectations of test duration so uncertainties can be reduced by employing additional surveillance technologies and pilot design.
- The integration presented in this section aided the planning of completion trials and data acquisition strategy in field/pilot setups being implemented in the Tuwaiq Mountain Formation. It also showed the upside potential in reservoir productivity if drilling, stimulation and perforation designs are tailored accordingly.

6.8 References

Al-Mulhim, N.I., Al-Saihati, A.H., Hakami, A.M., Al-Harbi, M. and Asiri, K.S., 2014, "First Successful Proppant Fracture for Unconventional Carbonate Source Rock in Saudi Arabia," IPTC paper 17765, presented at the International Petroleum Technology Conference, Kuala Lumpur, Malaysia, December 10-12, 2014.

Carl Neuhaus, Mary Ellison, Cherie Telker, and Keith Blair, 2014, Drainage Estimation and Proppant Placement Evaluation from Microseismic Data. Society of Petroleum Engineers, SPE/EAGE European Unconventional Resources Conference and Exhibition, 25-27 February, Vienna, Austria, SPE-167685-MS.

Douglas Portis, Hector Bello, Mark Murray, Gervasio Barzola, Paul Clarke, and Katy Canan, 2013, Searching for the Optimal Well Spacing in the Eagle Ford Shale: A Practical Tool-Kit. Society of Petroleum Engineers, Unconventional Resources Technology Conference, 12-14 August, 2013, Denver, Colorado, USA. SPE-168810-MS.

El-Banbi, A.H., and Wattenbarger, R.A., 1998, Analysis of Linear Flow in Gas Well Production. Society of Petroleum Engineers, SPE: 10.2118/39972-MS.

Elliott Hough and Thomas McClurg, 2011, Impact of Geological Variation and Completion Type in the U.S. Bakken Oil Shale Play using Decline Curve Analysis and Transient Flow Character. Search and discovery article #40857, adapted from oral presentation at AAPG International Conference and Exhibition (ICE), Milan, Italy, October 23-26, 2011.

Luffel, D. L., Guidry, F. K., and Curtis, J. B., 1996. Development of laboratory and petrophysical techniques for evaluating shale reservoirs: Gas Research Institute Final Report GRI-95/0496 (October 1986–September 1993), p. 301

Hakami, A., Al-Mubarak, A., Kurison, C., Al-Ramadan, K., and Leyva Poveda, I., 2016, Characterization of Carbonate Mudrocks of the Jurassic Tuwaiq Mountain Formation, Jafurah Sub-Basin, Saudi Arabia: Implications for Unconventional Reservoir Potential Evaluation; Journal of Natural Gas Science and Engineering, vol. 33 (2016), p. 1-20.

Maxwell S.C., and Cipolla, C., 2011, What does Microseismic Tell Us About Hydraulic Fracturing?: Proceedings SPE Annual Technical Conference and Exhibition, October 30-November 2, 2011, Denver, Colorado, SPE paper 146932, p. 14.

Mayerhofer J.M., Neil A. S., James O.B., Kevin M.R., 2011, Integrating Fracture Diagnostics and Engineering Data in the Marcellus Shale. Society of Petroleum Engineers, SPE Annual Technical Conference and Exhibition, 30 October-2011, Denver, Colorado, USA. SPE-145463-MS.

Sardinha, M., Petr, C., Lehmann, J., Pyecroft, J. F., and Merkle, S., 2014, Determining Interwell Connectivity and Reservoir Complexity Through Frac Pressure Hits and Production Interference Analysis. Society of Petroleum Engineers. SPE: 10.2118/171628-MS.

Stalgorova, K., Mattar, L., 2013, Analytical Model for Unconventional Multifractured Composite Systems. Society of Petroleum Engineers. SPE: 10.2118/162516-PA.

Wattenbarger, R. A., and Alkouh, A. B., 2013, New Advances in Shale Reservoir Analysis using Flowback Data. Society of Petroleum Engineers. SPE: 10.2118/165721-MS.

CHAPTER 7

Conclusion

The Jurassic organic-rich Tuwaiq Mountain source rock in the Arabian basin has long been recognized as the principle source for conventional hydrocarbons trapped in the supergiant Jurassic reservoirs. Renewed interest in these rocks has revealed major gaps in our understanding of the Tuwaiq Mountain as a reservoir. This research work resulted in the following conclusions:

a) Based on a stratigraphic cross section correlation between wells used in this study, the Tuwaiq Mountain shows a uniform thickness (100 ft. – 150 ft.), whereas, the overlying Hanifa Formation displays various thickness between 50 ft - 200 ft. An interesting observation is the presence of source rock facies with high GR was seen within the bottom part of the Jubaila formation. The thickness of this source rock facies increases from 40 ft at well A to >200 ft. at Well E.

b) Based on detailed core description, six distinct lithofacies have been recognized within the Tuwaiq Mountain Formation, four of which are categorized as reservoir facies due to high organic content (TOC) ranging between 3 to 11wt, %.

c) One of the important parameter for determining a good shale gas reservoir is the clay content. Less clay is favorable for hydraulic frac stimulation. Tuwaiq Mountain Formation whole rock and clay mineralogy suggest that the kerogen is largely the second main component after calcite and the clay content in Tuwaiq Mountain Formation is a very low 3-5%.

d) The petrophysical analyses suggest that Tuwaiq Mountain Formation has petrophysical characteristics similar to successful shale gas plays in North America. The Tuwaiq Mountain Formation tends to be cyclical, probably due to fluctuations in relative sea level changes. This cyclicity can be easily recognized from well logs such as GR and density. Therefore, the Tuwaiq Mountain Formation is subdivided into three tiers. Tier 1, at the base, represents the most organic-rich interval. Tier 2 represents the intermediate source rock quality, while Tier 3 represents the lean source rock sitting right below the Hanifa Formation.

e) Predictive models for TOC estimation based on density log and seismic acoustic impedance were developed and tested. Both models show strong correlation between measured TOC and predicated values.

f) The basin modeling work suggests that the Jafurah basin is continuously subsiding and the present depths of the Tuwaiq Mountain Formation represent the maximum burial depths that the formation exposed to throughout the burial history. The modeling also shows an increase in geothermal gradient in the Jafurah Basin to east and north. The higher temperature gradient areas of the basin are interpreted to have higher basement heat flow. According to Saudi Aramco internal report by FrogTech, the variation in heat flow is related to different basement composition within Jafurah basin, (granitic vs. basaltic basement) with the granitic generating more radiogenic heat. The modeling results suggest that TQMN source rocks started generation at about 100 Ma, reached the peak oil generation at about 70 Ma, and wet gas generation window at present time in warmer (≥28 °C/km) parts of the basin (the northern and eastern part of the Jafurah Sub-Basin).

g) An integration of outputs from geoscience workflows with multidiscipline data such as microseismic and hydraulic fracturing modeling was conducted to characterize the Tuwaiq Mountain and to provide insights on drainage strategies. Results from this effort suggest that fracture half-length for Tuwaiq Mountain ranges between 400 ft and 800 ft, which can be used as initial considerations for field development planning.

Vitae

PERSONAL DATA

Name: Ahmed Mohammed Hussain Hakami

Birth date: March 29, 1974

Nationality: Saudi

Civil State: Married

Residence: Hajr District-6827

Dhahran 34253-5354

Saudi Arabia

Work: Exploration Organization

Unconventional Resources

P.O. Box 9581, Dhahran 313111

Saudi Aramco, Saudi Arabia

http://www.saudiaramco.com

E-mail: ahmed.hakami.2@aramco.com

ACADEMIC FORMATION

1992 - 1996: Bachelor degree in Geology

Faculty of Earth Sciences, King Abdulaziz University Jeddah-KSA

2002 - 2004: MSc Degree in Geology

Geosciences Department, University of Houston, USA

Title of the thesis: Petroleum geochemical analysis of the Triassic sequence of Central and Eastern Saudi Arabia.

2011 – 2016: PhD in Geology, King Fahad University of Petroleum and Minerals-Saudi Arabia. College of Petroleum Engineering and Geosciences

LANGUAGES

Arabic (first language)

English (fluent)

PROFESSIONAL EXPERIENCE

1996 – Present: Saudi Arabian Oil Company (Saudi Aramco)

1996 -1998 Wellsite Geologist: Mentoring Oil and Gas Drilling Wells

1998 - 2000 Explorationist: Prospect evaluation

2000 - 2002 Regional Geologist: Resources Assessments studies

2002 - 2004 Advance Degree Program, Houston, Texas, USA

2005 - 2006 Petroleum System Specialist

2006 - 2010 Geochemistry Unit Supervisor

2010 - 2011 Schlumberger Innovation Center, Salt Lake City, Utah, USA

2011 - 2012	Unconventional Gas Exploration
2012 - 2013	Northwest Area Exploration Department
2013 - 2015	Chief Explorationist, Jafurah and Rub Al-Khali Division
2015 - 2016	Residency program at KFUPM

PUBLICATIONS/ PRESENTATIONS

Ahmed M. Hakami, Kurt J. Marfurt and Saleh Al-Dossary, 2004. “Curvature Attribute and seismic interpretation: Case study from Fort Worth Basin, Texas, USA”. SEG Int'l Exposition and 74th Annual Meeting, Denver, Colorado, 10-15 October 2004 - SEG Proceeding.

A.M. Hakami, S.T. Abdelbagi, M.A. Abu-Ali, and A.S. Ahmed, 2005. "New Paleozoic and Mesozoic Petroleum Systems, Saudi Arabia". The International Petroleum Technology Conference held in Doha, Qatar, 21–23 November 2005.

Ahmed Al-Hakami, Peter Jenden, Andreas Fuhrman and Adry Bissada, 2007. Petroleum System Analysis of the Triassic Sequence in Central and Eastern Saudi Arabia. International meeting on Organic Geochemistry, IMOG, UK, Touky September 2007

Andreas Fuhrmann, **Ahmed M. Hakami**, Peter D. Jenden, Henry I. Halpern and Sami T. Abdelbagi, 2008. "Geochemical characterization of petroleum in Jurassic reservoirs south of Ghawar field, Saudi Arabia: Implications for the petroleum system". GeoArabia-Bahrain

Peter D. Jenden, **Ahmed M. Al-Hakami** and Pierre J.L. Van Laer b, 2010. "Stable carbon isotope geochemistry of Saudi Arabian natural gas". GeoArabia Conference-Bahrain March 8, 2010.

Roberto S. R., **Hakami A.**, Edelman1 E., Handwerger D., and Gathogo P, 2012. Improving Geologic Core Descriptions and Heterogeneous Rock Characterization via Continuous Profiles of Core Properties. SPWLA 53rd Annual Logging Symposium, June 16-20, 2012

Al-Mulhim, N.I., Al-Saihati, A.H., **Hakami, A.M.**, Al-Harbi, M. and Asiri, K.S., 2014, "First successful proppant fracture for unconventional carbonate source rock in Saudi Arabia," IPTC paper 17765, presented at the International Petroleum Technology Conference, Kuala Lumpur, Malaysia, December 10-12, 2014.

Hakami, A., Ellis, L., Al-Ramadan, K., and Abdelbagi, S., 2016. Mud gas isotope logging application for sweet spot identification in an unconventional shale gas play; A case study from Jurassic carbonate source rocks in Jafurah Basin, Saudi Arabia. Marin and Petroleum Geology 76 (2016) 133-174.

Hakami, A., Al-Mubarak, A., Kurison, C., Al-Ramadan, K., and Leyva Poveda, I., 2016, Characterization of Carbonate Mudrocks of the Jurassic Tuwaiq Mountain Formation, Jafurah Basin, Saudi Arabia: Implications for Unconventional Reservoir Potential Evaluation; Journal of Natural Gas Science and Engineering, doi:10.1016/j.jngse.2016.04.009. p. 1-20.

Ahmed Hakami and Sedat İnan, 2016. A Basin Modeling Study of the Jafurah Basin, Saudi Arabia: Implications for unconventional hydrocarbon potential of the Jurassic Tuwaiq Mountain Formation. Submitted to International Journal of Coal geology-accepted for publication

Al Duhailan M.A., Ahmed A. S.A.S., **Al Hakami A.M**. and Leyva I.F., Little-Known Differences in Tuwaiq Mountain Petroleum Generation: Implications for Different Unconventional Resource Play Fairways. Unconventional Technology Conference 2016, 1–3, (August, 2016 San Antonio, Texas USA).

Ahmed Hakami and Clay Kurison, 2016. Coupling Geoscience and Reservoir Engineering Perspectives in Optimization of Completions and Well Spacing: A Case Study from a Jurassic Unconventional Play in Saudi Arabia. Submitted to Journal of Petroleum Engineering-under review.

İnan, S., **Hakami, A.**, Abu Ali, M. in press 2017, A Petroleum System and Basin Modeling Study of Northwest and East-Central Saudi Arabia: Effect of Burial History and Adjacent

Rock Lithology on the Gas Potential of the Silurian Qusaiba Shales. AAPG Memoir no. 114: Petroleum Systems case Studies.

MEMBERSHIP IN SCIENTIFIC ORGANIZATIONS

1. American Association of Petroleum Geologists (AAPG)
2. European Association of Organic Geochemists (EAOG)
3. Dhahran Geosciences Society (DGS)
4. Society of Petroleum Engineering (SPE).